GEOLOGY AND ISOTOPE GEOCHEMISTRY OF THE SAMAIL OPHIOLITE COMPLEX, SOUTHEASTERN OMAN MOUNTAINS

Thesis by

ROBERT THEODORE GREGORY

In Partial Fulfillment of the Requirements

for the Degree of

Doctor of Philosophy

California Institute of Technology

Pasadena, California

1981

(submitted November 14, 1980)

Frontispiece: A 1:1,000,000 ERTS image of the southeastern Oman Mountains shows the location of the Ibra section of the Samail ophiolite. The dark area between Ibra and Muscat is the Samail peridotite, the predominant member of the ophiolite section. Jabal Hammah represents the southernmost and least deformed of the Hawasina nappes.

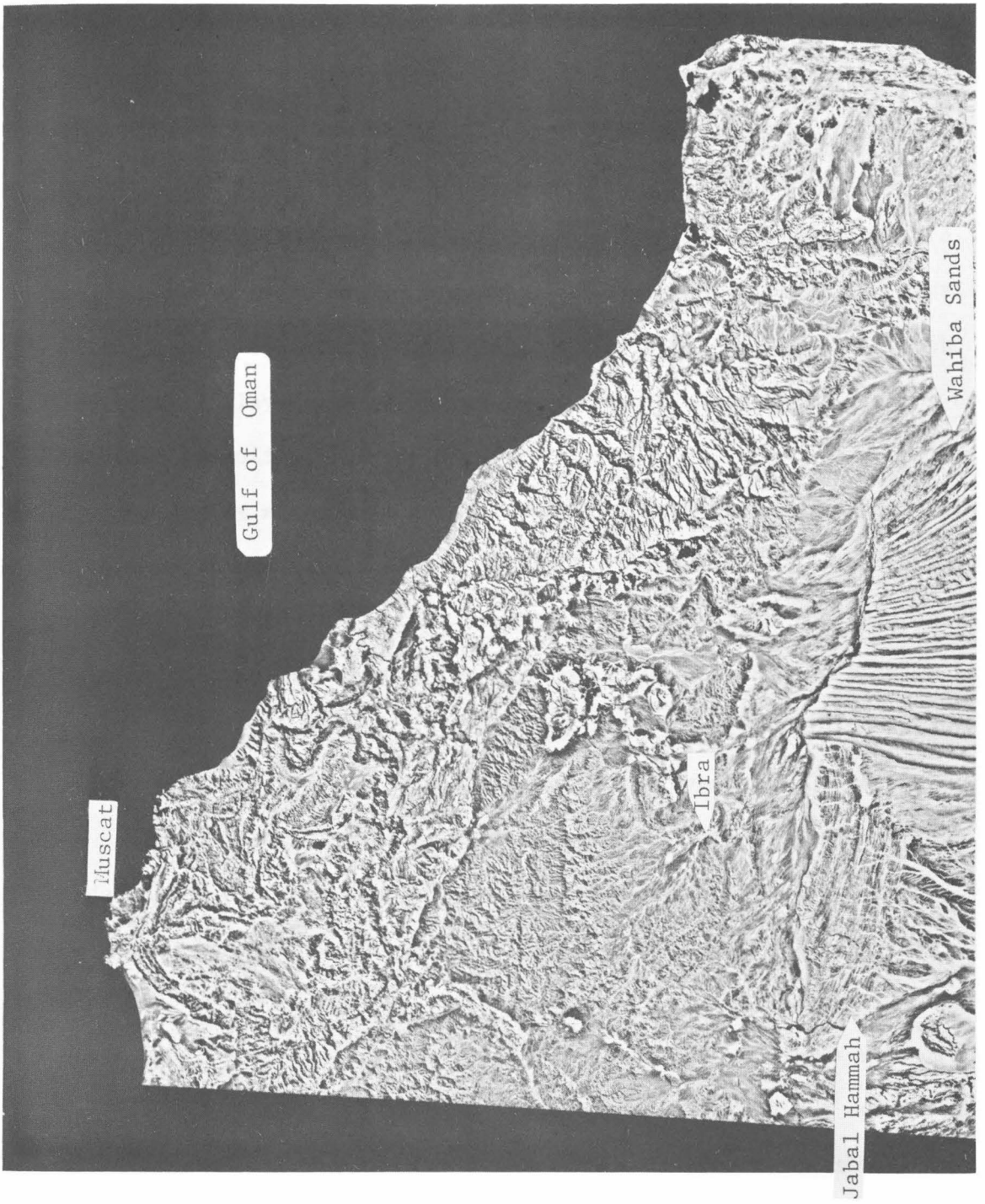
Muscat
Gulf of Oman
Ibra
Wahiba Sands
Jabal Hammah

ACKNOWLEDGEMENT

This thesis work has been accomplished with the help of many people. Hugh Taylor, Jr., as an instructor, sparked my interest in ophiolites and in stable isotopes, and, as a thesis advisor, gave me much independence, sprinkled with some good advice when it was needed. Robert G. Coleman, both as a colleague and a friend, taught me many things about field work, and life in the Middle East and elsewhere. I would like to thank all of the other Oman project members and particularly Cliff Hopson, John Pallister, Francoise Boudier, Malcolm McCulloch, and Edgar Bailey for discussions which increased my understanding of the Oman ophiolite.

During my stay at Caltech, I was fortunate to be a contemporary with some of the best students I have ever seen, too many to acknowledge separately. However, I would like to thank Bob Criss for help in all things isotopic, Bob Powell for his moral support and interest in the field aspects of the work, and Jim Quick for his timely discussions of peridotites and for his help during the first years at Caltech.

I would also like to acknowledge faculty members Thomas Ahrens, Arden Albee, Barclay Kamb, Heinz Lowenstam, Edward Stolper, and Gerald J. Wasserburg for their interest and support. Sam Epstein provided access to the mass spectrometer lab. Staff members John Coulson, Joop Goris, Mike Carr and Vic Nenow were of great help during the laboratory work. I wish to thank the Caltech Geology secretarial staff, especially Dorothy Coy and Susan McCurdy, for their assistance over the years.

Financial support during my stay at Caltech has been provided by the National Science Foundation, Continental Oil, and the Geological Society of America. The Caltech Division of Geological Sciences provided a vehicle for field work in Oman.

I would like to acknowledge Susan Hallquist for help in the final typing and editing of the manuscript and for her good spirit during our stay in Pasadena. My family was also a patient source of inspiration during my long stay at Caltech.

ABSTRACT

The Samail nappe, Oman, is a classic ophiolite complex consisting of a thick section (~12 km) of "depleted" peridotite tectonite, overlain by layered gabbro cumulates (~5 km) and high-level noncumulate gabbro (<1 km), followed by a 100% sheeted dike complex (~1.3 km), and capped by a series of highly altered pillow lavas (~0.5 km). The ophiolite stratigraphy is exposed in the Oman Mountains, an arid region covering over 15,000 km^2, with relief exceeding 2 km. In the first part of this thesis, the results of field mapping along a 20 X 125 km strip from Muscat to the Wahiba Sands are presented forming the foundation for the isotopic work reported in the second part of the thesis.

The upper mantle and oceanic crustal sections preserve a partial record of the events that occurred in the dynamic spreading environment underying the Hawasina Ocean, a portion of the Tethys Seaway. The Samail peridotite section records a history of partial melting, plastic flow, and reaction with transitory melts. Ascending melts reacted with the harzburgite wall-rocks leaving behind dunite (at all depths in conduits with high melt/ rock), and olivine orthopyroxenite, websterite, clinopyroxenite, and gabbro (from deeper-to-shallower levels in conduits with low melt/rock). The entire peridotite section was affected by pervasive upper mantle deformation during its ascent, and a basal harzburgite-dunite zone may represent the boundary of the originally vertical conduit that fed both melts and peridotite to the Samail ridge system. The supply of melt was sufficient to produce an "open system" magma chamber that achieved a steady state with respect to cumulus phases; orthopyroxene saturation was rarely attained in the gabbro section. Crystal accummulation predominantly occurred from

the bottom upward. Because the high-level gabbro intrudes >90% of the overlying dike complex, both the diabase dikes and pillow lavas are interpreted to have been intruded close to the ridge-axis and to be comagmatic with the cumulate gabbro section. The thin, heterogeneous high-level gabbro preserves a record of many piecemeal stoping events occurring in a chamber roof environment that was mechanically unstable. Plagiogranite commonly occurs near the gabbro-diabase contact; field evidence and $^{18}O/^{16}O$ relationships demonstrate that the plagiogranites either form by partial melting of stoped blocks of hydrothermally altered roof rock, by extreme differentiation of a hydrous tholeiitic magma strongly modified by exchange and dehydration of such stoped blocks. The data suggest that the magma chamber was open both at the bottom and the top, and thus, MOR basalts are not considered to be primary, unmodified melts of the mantle.

The shallow-level magma chamber (<3 km below the seafloor) was the heat engine that drove convective seawater circulation through joints and fractures in the overlying section of diabase and basalt and simultaneously in the gabbro underlying the "wings" of the funnel-shaped chamber. Both stable ($^{18}O/^{16}O$ and D/H) and radiogenic (Sm/Nd and Rb/Sr) isotope systems were used to investigate the characteristics of the hydrothermal system. The Sm/Nd system was virtually unaffected by seawater-hyrothermal hydrothermal alteration and crystallization ages were obtained from plagioclase and pyroxene separates on single gabbro samples. Measured $\delta^{18}O$ values in whole-rocks, $2.5<\delta^{18}O<19.6$, from the oceanic crustal section are typically depleted in the lower parts of the section, and enriched in the upper parts, relative to the primary magmatic value of 5.7 ± 0.2. Also, the initial $^{87}Sr/^{86}Sr$ ratios vary from 0.7030 to 0.7065 increasing upward. The large variations in $\delta^{18}O$ and $^{87}Sr/^{86}Sr$ are clearly the result of seawater hydro-

thermal alteration, demonstrating that large amounts of heated seawater (T>500°C) penetrate deep into oceanic layer three as far down as the oceanic Moho. Mineral-mineral $\delta^{18}O$ systematics (e.g. plagioclase-clinopyroxene) have been used to demonstrate isotope disequilibrium caused by this subsolidus hydrothermal exchange, to ascertain the primary $\delta^{18}O$ values of the gabbro and plagiogranite reservoirs, to estimate relative exchange rates between minerals, to deduce the $\delta^{18}O$ changes occurring in the hydrothermal fluids at various levels within the crust, and to differentiate between the effects of closed and open system hydrothermal exchange in natural systems.

The ^{18}O redistribution within the oceanic crust was systematic, with whole-rock $\delta^{18}O$ increasing from a minimum $\delta^{18}O = 3.7$ in the cumulate section about 1-2 km below the gabbro-diabase contact to values as high as 19.6 in the pillow lava section. A mass-balance calculation for the entire oceanic crustal section indicates that, the net change over the whole oceanic crustal section was zero implying that seawater also did not change and thus the seawater-oceanic crustal system was at some steady-state during the late Cretaceous. Modeling of the circulation extrapolated to the world-wide ridge system suggests that the $\delta^{18}O$ of seawater is <u>controlled</u> by the hydrothermal interactions, and will be buffered to within 1 per mil of its present-day value as long as global spreading rates exceed 1 km^2/yr.

TABLE OF CONTENTS

LIST OF FIGURES

LIST OF TABLES

CHAPTER 1

INTRODUCTION

The purpose of this thesis is to present the results of a geologic and geochemical investigation of the Samail Ophiolite Complex, probably the largest and best-exposed ophiolite complex on Earth. Field, petrologic, and isotopic data presented here will suggest that the Samail ophiolite originated at a spreading center in the Tethyan Sea in a dynamic environment. This ophiolite complex has a size comparable to that of the Sierra Nevada batholith and because of its high relief and its exposure in an arid region, it is even more amenable to geologic investigation than the other large ophiolites, such as Papua, New Guinea [Davies, 1968] and Bay of Islands, Newfoundland [Smith, 1958]. It should be remembered during the following discussion that the preservation of these larger ophiolite sheets in the geologic record requires an unusual sequence of events; nevertheless, although these ophiolites represent anomalous features in the history of the Earth, they are extremely important because they provide virtually unique opportunities to study an integrated section through the oceanic crust and upper mantle.

The following discussion will largely focus upon processes that occur at oceanic spreading centers. An underlying assumption is that the Samail ophiolite is representative of some kind of oceanic crust. Although the emplacement of the ophiolite upon the Arabian continental margin was certainly an anomalous geologic event, the processes which resulted in the formation of this slice of oceanic crust were not. Whether the Samail ophiolite represents an open ocean basin or a marginal basin, or whether it represents fast or slow spreading, are still subjects of much debate (as they are for any ophiolite complex). However interesting the above debate is, the discussion of geologic setting does not affect the major conclusions resulting from

data presented here, except perhaps to modify some of the numerical values that pertain to the scale or rate of certain geologic processes.

The field work which is the foundation of this thesis occurred over three consecutive winters from 1977 through 1979. Two of the field seasons were conducted as part of a team involved in a joint National Science Foundation--U.S. Geological Survey Project on the Oman Mountains, led by C.A. Hopson and R.G. Coleman. This was originally conceived as a two-part project: 1) to produce a 1:100000 geologic map across the Oman Mountains from Muscat to the Wahiba Sands [see Frontispiece], and 2) to use the geologic map as a basis for several interdisciplinary studies on the ophiolite section such as geophysical studies (gravity and magnetics), geochemical studies (rare-earth elements, isotopic studies), petrologic studies, and geochronological studies. The first field season was primarily devoted to geologic mapping and sample collecting (my time was equally divided between the peridotite and the oceanic crustal section). The second field season was primarily devoted to more detailed geologic traverses (1/3 time on a peridotite traverse with R.G. Coleman and F. Boudier and 2/3 time on the oceanic crustal section, part of which was in collaboration with J.S. Pallister and C.A. Hopson), together with further sample collecting, using the preliminary geochemical data as a guide to the zones that required more detailed study. The third field season (1979) was conducted entirely by myself without the other project members, just prior to attending the International Ophiolite Symposium in Cyprus. The major task of this last field season was to fill-in some gaps in the 1:100000 map, to complete a traverse through the gabbro, to map the distribution of hydrothermal veins as a function of depth, and to return to the

Dasir plagiogranite area for more detailed mapping and sample collecting. In summary, total field time was partitioned in the following manner: peridotite, 2.5 months; oceanic crustal rocks, 2.5 months; Dasir plagiogranites, 1.5 weeks; and Hawasina, Maestrichtian, and basal metamorphic rocks, 1 week.

The following discussion is organized around three papers which have been accepted for publication in the Journal of Geophysical Research as part of a special issue on the Samail ophiolite, scheduled to appear early in 1981. This volume will also include the colored version of the Muscat-Ibra transect 1:100000 map (Bailey, et al., 1981). Unfortunately, the map is not available for inclusion in this thesis. Chapter 2 of this thesis, the geology of the Samail ophiolite, represents a paper that I co-authored with C.A. Hopson, R.G. Coleman, J.S. Pallister and E.H. Bailey. Coleman and I served as co-editors and produced the final manuscript from a considerably longer first-draft produced by all of the authors. The ideas presented therein represent a fragile consensus concerning most of the field facts and their interpretation. In chapter 3, I have added new material and expanded upon some of the ideas presented in the jointly-authored geology article, including some preliminary studies on the peridotite carried out in cooperation with R.G. Coleman and F. Boudier.

Chapter 4 of this thesis presents the results of oxygen isotope studies of the Samail ophiolite, elaborating upon a paper co-authored with H.P. Taylor, Jr. Chapter 5 represents a paper co-authored with M.T. McCulloch, G.J. Wasserburg and H.P. Taylor, Jr. that discusses Nd-Sr-O systematics within the Samail ophiolite.

Chapter 6 of this thesis discusses the effects of hydrothermal alteration within the oceanic crust upon the oxygen isotopic composition of the oceans through geologic time and essentially represents the last half of the forthcoming article in Journal of Geophysical Research co-authored with H.P. Taylor, Jr. The buffering of the oxygen isotopic composition of the oceans by hydrothermal circulation in the oceanic crust was proposed by Muehlenbachs and Clayton [1976], and the sixth chapter extends and re-evaluates work of Muehlenbachs and Clayton in light of the new isotopic data obtained in the present study.

CHAPTER 2

GEOLOGY ALONG THE MUSCAT-IBRA TRANSECT, SOUTHEASTERN OMAN MOUNTAINS

2.1 INTRODUCTION

Work on the Samail ophiolite was designed as a multidisciplinary study of a selected section through the ophiolite. The main emphasis of this chapter is to provide a geologic setting for the 20 x 125 km transect through the ophiolite and its associated basement and cover rocks.

The geologic mapping of the transect at a scale of 1:100,000 was carried out in two field seasons, January-March 1977 and January-March 1978. The main emphasis of our work was to provide an accurate description of the stratigraphy, structure, petrology, chemistry, and age relations within the Samail ophiolite. The central focus of this discussion will be on the 1:100,000 map (Bailey et al., 1981). The reader will no doubt perceive some inconsistencies in our interpretation, but with such a large and diverse group, it was not always possible to arrive at a consensus.

Ophiolites are now generally recognized as ancient pieces of oceanic crust and uppermost mantle [Coleman, 1977]. Most ophiolite complexes, due to the vagaries of emplacement, are generally dismembered during obduction and preserved only as small blocks exposed along major fault zones. In contrast, the almost undeformed Samail ophiolite complex, located in the Oman Mountains, Sultanate of Oman, crops out in a magnificently exposed desert region exceeding 15,000 km^2 with approximately 2 km of relief.

Early (pre-1970) geologists [Lees, 1928; Hudson et al., 1954; Morton, 1959; Hudson and Chatton, 1959; Hudson, 1960; Tschopp, 1967; Wilson, 1969; Greenwood and Loeny, 1968] divided the Oman Mountain rock units into four groups (Figure 2-1):

1. Autochthonous group consisting of pre-Permian basement rocks overlain by a thick (~10 km) section dominated by shallow continental shelf carbonates--the Hajar Supergroup, mid-Permian to Cenomanian. The Hajar Supergroup is characteristic of the eastern continental margin of Arabia and the Zagros fold belt of Iran [Coleman, 1981];
2. The Hawasina Group, a sequence of deeper water limestone, radiolarian chert, and shale, deposited contemporaneously with the Hajar Group;
3. The Samail ophiolite, a thick allochthonous sequence of peridotite, gabbro, diabase, pillow lava and associated pelagic sedimentary rocks (Cretaceous);
4. Shallow-water marine limestone, locally conglomeratic, of latest Cretaceous to Middle Tertiary age, which are transgressive over the previous allochthonous rock units including the ophiolite.

All of the workers listed above would undoubtedly agree on the major rock units. They would, however, disagree as to the timing and allochthonous nature of the Hawasina Group and of the Samail ophiolite. Lees [1928] originally proposed that both the Hawasina Group and the Samail ophiolite were in thrust contact over the Hajar Group, with the Samail rocks representing the highest pre-Tertiary tectonic member of the Oman Mountains. In contrast, Morton [1959] proposed that both the Samail and the Hawasina were autochthonous due to the concordant nature of the contacts between Hawasina and underlying Hajar Group and between the Samail ophiolite and Hawasina Group.

Figure 2-1. ERTS image of the Muscat-Ibra transect with major geologic units plotted. See opposite page for explanation of units. Cross-section modified from 1:100,000 map (Bailey et al., 1981).

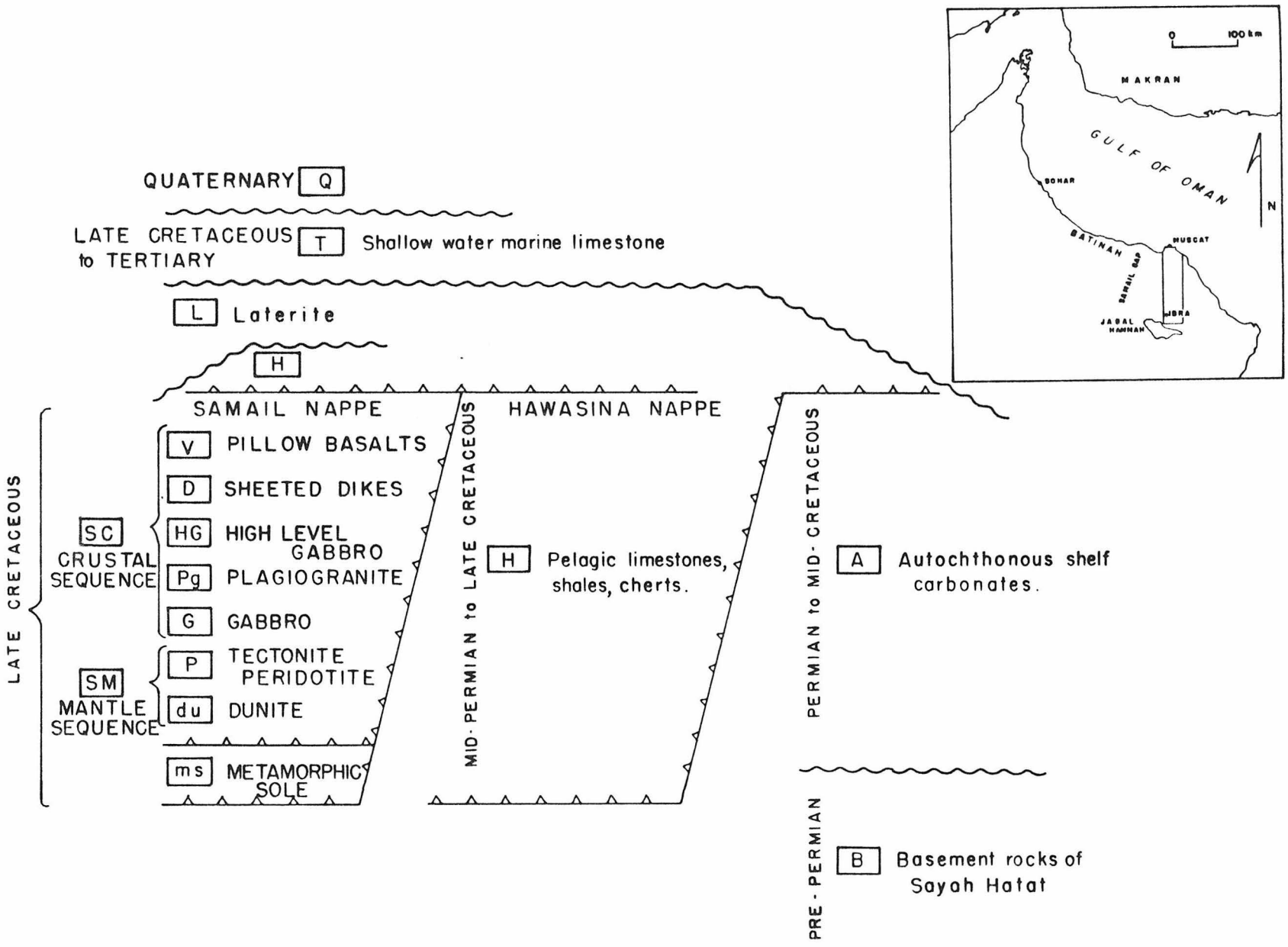
QUATERNARY Q
LATE CRETACEOUS to TERTIARY T Shallow water marine limestone
L Laterite
H
SAMAIL NAPPE
HAWASINA NAPPE
LATE CRETACEOUS
SC CRUSTAL SEQUENCE
V PILLOW BASALTS
D SHEETED DIKES
HG HIGH LEVEL GABBRO
Pg PLAGIOGRANITE
G GABBRO
SM MANTLE SEQUENCE
P TECTONITE PERIDOTITE
du DUNITE
ms METAMORPHIC SOLE
MID-PERMIAN to LATE CRETACEOUS
H Pelagic limestones, shales, cherts.
PERMIAN to MID-CRETACEOUS
A Autochthonous shelf carbonates.
PRE-PERMIAN
B Basement rocks of Sayah Hatat
0 100 km
MAKRAN
GULF OF OMAN
SOHAR
BATINAH
MUSCAT
SAMAIL GAP
IBRA
JABAL HAMMAH
N

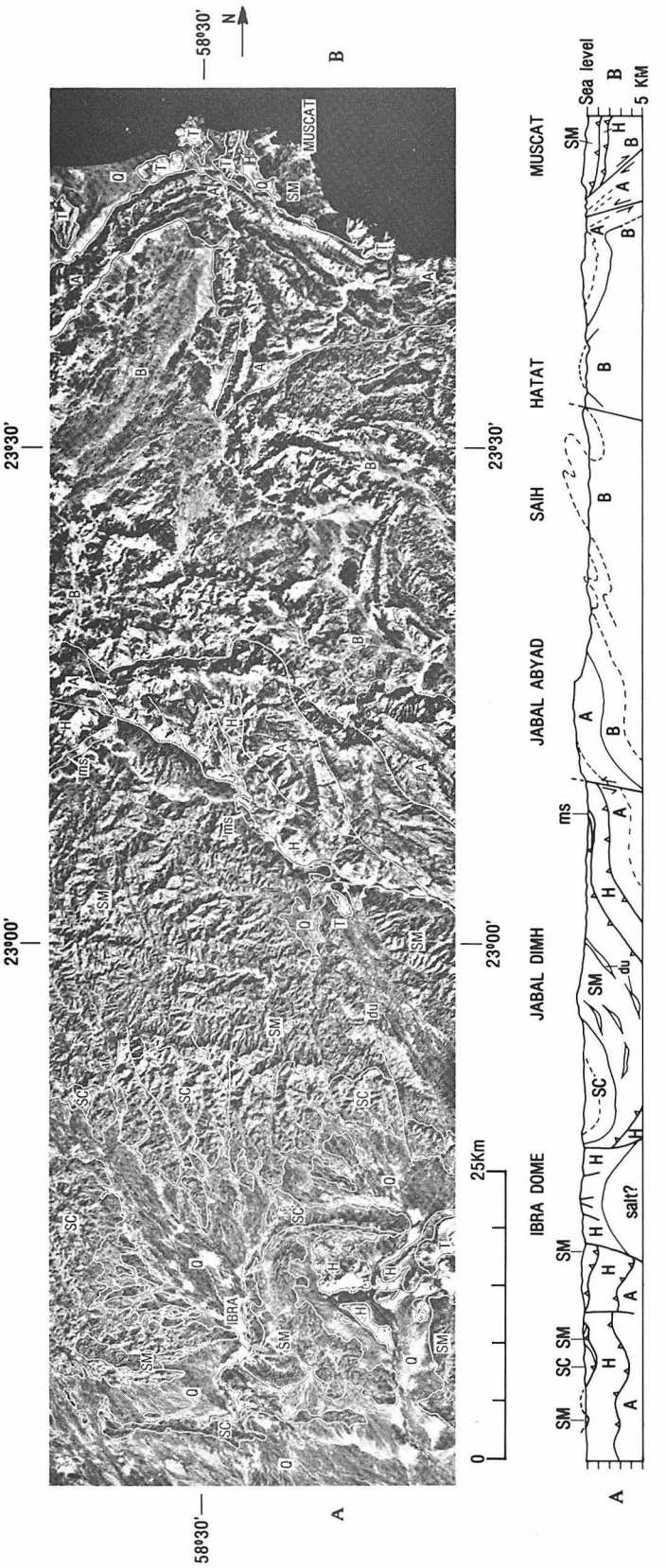
58°30'
N
B
23°30'
23°00'
MUSCAT
IBRA
SC
SM
Q
T
H
A
B
ms
du
0
25Km
A
IBRA DOME
JABAL DIMH
JABAL ABYAD
SAIH
HATAT
MUSCAT
Sea level
5 KM
salt?

Recent work on the Oman Mountains has thrown the weight of geologic evidence in favor of Lees [Glennie et al., 1974; Glennie et al., 1973; Reinhardt, 1969; Allemann and Peters, 1972]. This later work has singled out the Samail ophiolite as a prime area for the study of ancient sea-floor processes because (1) the complete ophiolite stratigraphy is comparable in thickness to geophysical estimates of typical oceanic crustal layers; (2) its size insures continuity both parallel and perpendicular to presumed paleospreading directions; (3) post-emplacement plutonism or regional metamorphism has not occurred within the Oman Mountains, and (4) excellent exposures occur throughout the mountain range. For all of these reasons, the Samail ophiolite is an ideal area to investigate an intact piece of oceanic crust and upper mantle in terms of its structure, petrology, geochemistry, geochronology, and geophysics.

2.2 OPHIOLITE STRATIGRAPHY

2.2.1 General Overview

As described above, the Samail ophiolite has a classic ophiolite "stratigraphy" consisting in the Ibra region of (from bottom-to-top): (1) tectonized peridotite (9 to 12 km thick), predominantly harzburgite with abundant dunite; (2) layered gabbro (3 to 5 km thick) generally with a narrow (~0.5 km) zone of two-phase olivine + chromite cumulates at the base, overlain by several kilometers of three-phase cumulates: olivine + clinopyroxene + plagioclase; megascopic features such ratio layering, size layering, and orientation of cumulus phases, particularly plagioclase and clinopyroxene, result in a sedimentary outcrop appearance of the layered gabbros; (3) high-level gabbro, a

thin (<1 km) regionally mappable unit of isotropic noncumulus gabbro with extremely variable texture and proportions of phases; the high-level gabbros are more fractionated than the cumulates and may differentiate to plagiogranite; (4) sheeted diabase dike complex (1.0 to 1.6 km thick) consisting of virtually 100 percent sheeted dikes, all intensely affected by hydrothermal alteration; and (5) pillow lavas (~500 meters thick) which crop out as erosional remnants near the axis of the Ibra Valley syncline (Figure 2-2).

The following section presents a more detailed description of each of the ophiolite units and associated rocks. Because the geology is inseparable from the other special studies, some of the major conclusions of the petrology, geochemistry, geochronology, and geophysical studies are previewed here with reference made to the special study in each case. We acknowledge the work of our collaborators in formulating synthesis of the geology described below.

2.2.2 Structural Environment of the Ophiolite

The Samail ophiolite nappe in the Muscat-Ibra region has been emplaced upon the thick autochthonous Permian to Cretaceous shelf carbonate section that characterizes the Arabian Peninsula. The pre-Permian basement structure underlying the shelf carbonates and exposed in the Sayah Hatat window (Figure 2-1) consists of isoclinally folded quartz-mica schist and greenstone that trend NNE. Thrust over this schist and greenstone are the Amdeh quartzite and Hijam dolomite which have a northward overturning and vergence. This package of pre-Permian rocks contains no major granitic intrusions and represents a period of Paleozoic metamorphism and deformation unknown on the rest of the Arabian Peninsula.

Figure 2-2. Geologic map of the Wadi Tayin-Ibra area, southeastern Oman Mountains. Map symbols for Samail ophiolite units: P, peridotite tectonite member, mainly harzburgite and subordinate dunite; G, layered gabbro member, chiefly ol-cpx gabbro but includes cumulus dunite at the base and minor melagabbro and wehrlite layers higher up; HG, high-level gabbro, chiefly hypidiomorphic (non-cumulus) gabbro and minor diorite; includes a lower zone of cumulus but non-layered transitional gabbro; Pg, plagiogranite, small bodies near top of the plutonic suite; D, sheeted dike member, chiefly diabase, dominant strike of sheeting indicated by line pattern on map; V, volcanic mamber, mafic pillowed and massive lava, minor breccia and sparse mafic dikes. Other rock units: metamorphic rocks at base of peridotite, chiefly amphibolite, quartzite (metachert), greenschist and phyllite; H, Hawasina nappe (Permian or Triassic to Late Cretaceous), chiefly clastic limestones, radiolarian chert, and melange; A, Hajar Super group (middle Permian to Late Cretaceous), chiefly shelf carbonates; T, Maestrichtian and Tertiary sedimentary rocks, including reworked laterite, conglomerate, sandstone, and shallow water limestone. Quaternary deposits are represented by unpatterned areas. Standard geologic symbols apply except for the bracket symbol, which is used to indicate cumulus layering.

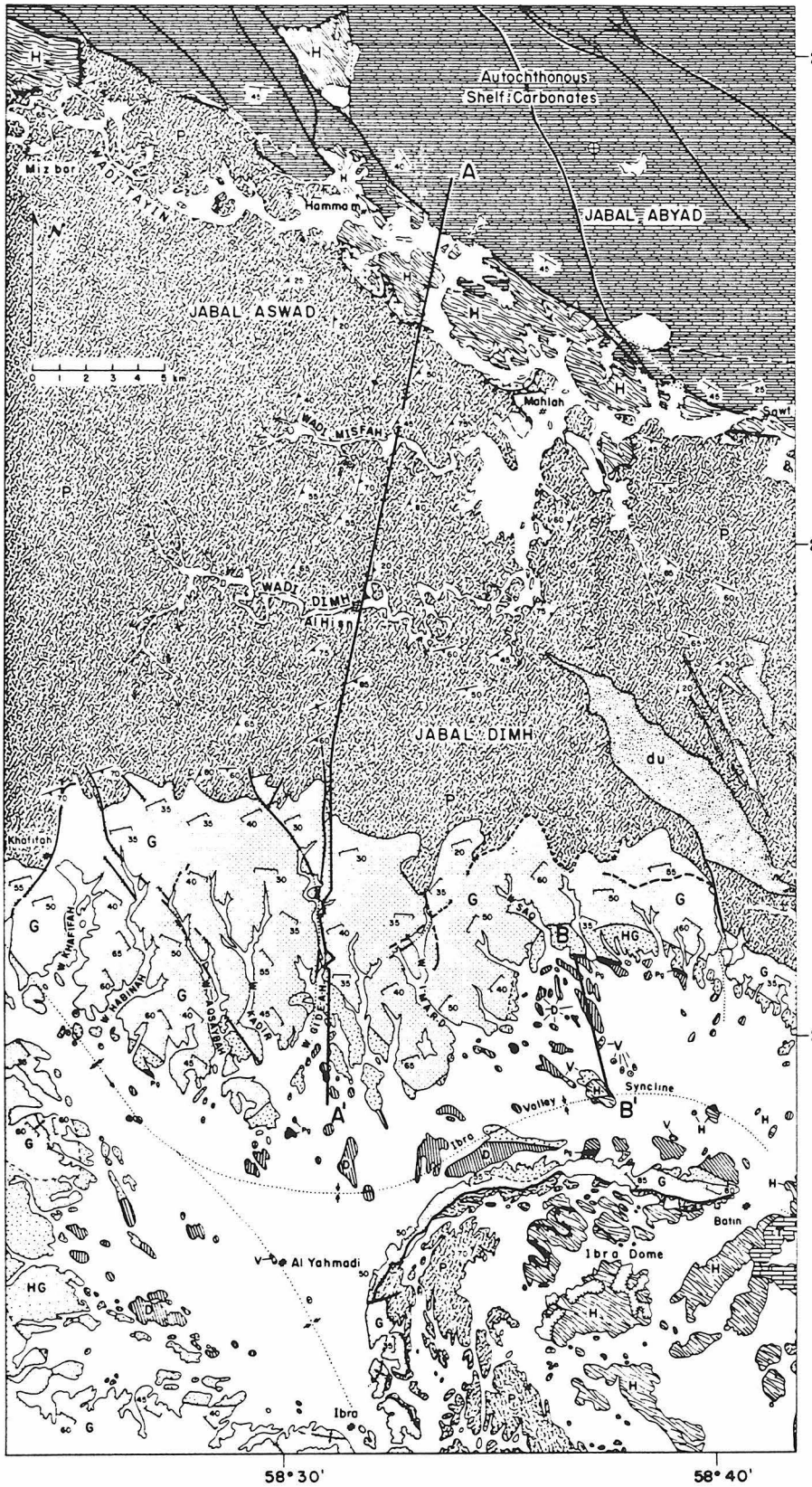
Autochthonous
Shelf Carbonates
JABAL ABYAD
JABAL ASWAD
JABAL DIMH
WADI TAYIN
WADI MISFAH
WADI DIMH
Mizbar
Hamma m
Mahlah
Sawi
Khatifah
Al Yahmadi
Ibra
Ibra Dome
Batin
Syncline
Valley
A
A'
B
B'
23°10'
23°00'
22°50'
58°30'
58°40'
0 1 2 3 4 5 km

The platform sedimentary rocks deposited above these basement rocks form a broad arch that extends across the Sayah Hatat window (Figure 2-1). On the south, just north of Wadi Tayin, these rocks are 4-4 1/2 km thick and form the south flank of the arch with a WNW axis generally dipping south 55°. On the north flank of the Sayah Hatat window, the platform sedimentary rocks are nearly 4 km thick and dip steeply to the north. However, on the north flank, the lowest part of the platform rocks are tightly isoclinally folded with nearly flat axial planes. Units within the carbonate section appear to have been slightly metamorphosed, producing folded schistose members cut by WNW trending normal faults, and later deformed into the broad Sayah Hatat upwarp.

Underlying the Samail ophiolite are the Hawasina allochthonous units which have undergone various degrees of dismemberment and which grade into melanges (Figure 2-3). To the south of Ibra in the Jabal Hammah area, these pelagic units still retain their original stratigraphy, but they are imbricated by a sequence of steeply dipping faults. In the Wadi Tayin area, however, the Hawasina units under the Samail ophiolite form both melange units and imbricated faulted blocks of coherent rock, whereas in the Muscat-Ruwi area, the Hawasin underlying the Samail ophiolite consists of 100 percent melange.

The rocks at the base of the Samail ophiolite provide the critical field evidence for the ophiolite emplacement. Preserved contacts reveal metamorphic sequences consisting of narrow garnet amphibolite zones in contact with mylonitic peridotite [Boudier and Coleman, 1981]. The mineral assemblages reflect rapid changes in metamorphic grade downward away from the peridotite contact. However, within metamorphic

slabs, discontinous changes in grade suggest internal structural discontinuities [Ghent and Stout, 1981]. Where the original contact is not preserved, the peridotite rests directly on a melange consisting of Hawasina sedimentary rocks, and blocks of amphibolite, greenschist, and serpentinized peridotite. At these latter contacts, the peridotite shows more serpentinization, and mutual tectonic elements with the serpentinized peridotite and melange are not found. The present basal contact of the Samail ophiolite appears to be a thrust that cuts across the section, reaching the layered gabbros to the south (Figures 2-1 and 2-2).

As shown by Boudier and Coleman [1981], the peridotite member of the Samail ophiolite shows high-stress mylonitic textures at the base, and the structures of the narrow amphibolite zone at the base probably formed simultaneously in the same stress field. A spinel lineation dipping slightly to the southwest parallels isoclinal fold axes of primary banding in the harzburgite. This deformation is consistent throughout the section and is considered to be imprinted on the peridotite as an upper-mantle process near a spreading ridge. No field evidence was found to indicate that the peridotite member was repeated by imbricate thrust faults [Boudier and Coleman, 1981].

The contact between the overlying cumulate section and the deformed peridotite shows lateral continuity and is assumed to represent an ancient mantle-crust boundary within the Tethyan Sea (Figure 2-3). The assumption that this boundary marked a horizontal plane within the Tethyan Sea also provides a datum plane for post-detachment deformation of the Samail ophiolite nappe. The contact between the cumulus layered sequence and peridotite is offset by normal vertical faults that trend

Figure 2-3. A composite columnar section constructed from stratigraphic data along section lines A-A' and B-B', Figure 2-2. Letter symbols for rock units are the same as in Figure 2-2. Additional symbols are: GM, GMW, zones of interlayered olivine gabbro, melagabbro-wehrlite within the main layered gabbro; W, zone of wehrlite at top of the cumulus gabbro; TG, transitional gabbro composed of cumulus, but non-layered gabbro. In the peridotite tectonite, diagonal lines depict layering and foliation trend, stippled bodies depict concordant and discordant dunite bodies, and unpatterned dikes are pyroxenite and gabbro dikes. Position of the "petrologic moho" [Gass and Smewing, 1973] in the column is inferred to be the gradational contact between cumulus dunite and the tectonite harzburgite-dunite. The "seismic moho" is placed at the contact between cumulus dunite and gabbro.

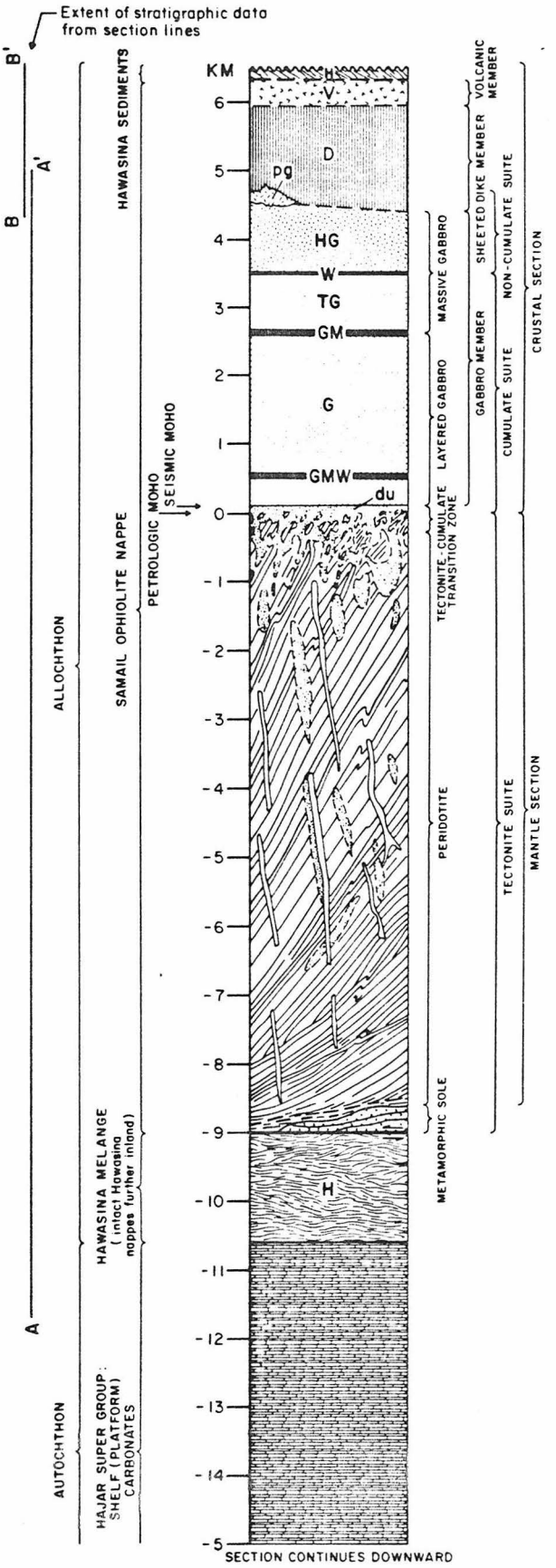
Extent of stratigraphic data from section lines
B'
B
A'
A
KM
6
5
4
3
2
1
0
-1
-2
-3
-4
-5
-6
-7
-8
-9
-10
-11
-12
-13
-14
-5
V
D
pg
HG
W
TG
GM
G
GMW
du
H
SEISMIC MOHO
PETROLOGIC MOHO
SECTION CONTINUES DOWNWARD
HAWASINA SEDIMENTS
ALLOCHTHON
SAMAIL OPHIOLITE NAPPE
HAWASINA MELANGE (intact Hawasina nappes further inland)
AUTOCHTHON
HAJAR SUPER GROUP: SHELF (PLATFORM) CARBONATES
METAMORPHIC SOLE
PERIDOTITE
TECTONITE - CUMULATE TRANSITION ZONE
LAYERED GABBRO
MASSIVE GABBRO
VOLCANIC MEMBER
SHEETED DIKE MEMBER
GABBRO MEMBER
CUMULATE SUITE
NON-CUMULATE SUITE
TECTONITE SUITE
CRUSTAL SECTION
MANTLE SECTION

in a northerly direction. These normal faults cannot be traced beneath the peridotite or above the cumulate rocks and may represent pre-emplacement deformation, although post-obduction movement is present along these same faults. Low-angle thrust contacts between layered gabbros and peridotite are exposed around the Ibra dome and in the mountains west of Ibra. Relations between the massive high-level gabbro and cumulate gabbro require N-to-NW trending normal faults that may also be a result of pre-emplacement deformation. Non-systematic open folding within the Samail nappe appears to be unrelated to units above or below the nappe and suggests prethrust folding.

The base of the sheeted dike unit is basically conformable with the cumulate layers within the Samail ophiolite but the individual dikes are not all normal to the layering in the cumulate section. These dikes now exhibit a regional N-NW trend that may be related to a fossil spreading center in the Tethyan Sea (Figure 2-2).

Exposures of pillow lavas are too sparse in the transect to provide detailed structural data, but their mapped pattern shows that they overlie the sheeted dikes. Interbedding of pelagic sediments with these pillow lavas could not be confirmed in this area.

Tilting of the Samail ophiolite southward either during detachment or emplacement in the Late Cretaceous may have given rise to extensive erosion. The apparent absence of ophiolite clastic debris in the Late Cretaceous shelf and platform sedimentary rocks suggests that some of the erosion of the ophiolite may have taken place prior to its emplacement onto the continental margin. The occurrence of residual laterite on eroded members of the Samail ophiolite indicates subaerial exposure during or after its emplacement. Reworking of the laterite and its

deposition upon Hawasina and autochthonous carbonate units also suggests a second stage of erosion after emplacement. Deformation of shallow-water Tertiary limestone transgressive on top of the Samail ophiolite northeast of Ibra takes the form of circular basins that may represent collapse due to salt tectonics. Exposures of the Samail ophiolite in and around Ibra suggest that a WNW-trending broad syncline whose axial trace is 6 km north of Ibra was later disturbed by uplift of the Ibra dome cored by Hawasina rocks (Figures 2-1 and 2-2).

Prominent WNW normal faults are present across the section and offset both the Samail ophiolite and the Tertiary limestones. In Wadi Tayin, a WNW fault dipping 45° -60° to the south offsets the detachment thrust and Hawasina down to the south. A parallel, steeply dipping, WNW fault 4 km south of Ibra offsets the Samail ophiolite and rocks have been dropped down on the south side. A similar WNW fault may form the NE boundary of the Sayah Hatat where the rocks are down on the north side.

2.2.3 Peridotite Member (map symbols P)

The peridotite member of the Samail ophiolite occurs in three separate areas: (1) Muscat-Mutrah peridotite occupies the shoreline at the northern end of the transect and consists mainly of peridotite with only minor gabbro and volcanic rocks; (2) Wadi Tayin-Jabal Dimh peridotite forms the base of a continuous section of the Samail ophiolite from pillow lavas, sheeted dikes, layered gabbros, into peridotites; and (3) Ibra dome area peridotites form discontinuous and somewhat dismembered units that have been deformed after emplacement [Bailey et al., 1981]. The peridotite is the dominant rock type of the exposed Samail ophiolite and makes up about 60 percent of its surface exposures.

Peridotites form dark colored badlands consisting of rugged topography characterized by sharp ridges and steep-walled gorges. Weathering of the peridotite develops a rough irregular surface caused by differential weathering of serpentinized peridotite and more resistant joint sets filled with magnesite, hydromagnesite, and clinochrysotile.

The peridotite consists of two main rock types----harzburgite and dunite. Harzburgite is by far the most predominant rock type, consisting of olivine Fo_{90-91} (~74 percent), orthopyroxene En_{90-91} (~24 percent), and spinel (~2 percent). Clinopyroxenes are only rarely present and appear to be chromium diopsides. A section studied in detail through this peridotite reveals that the banded harzburgite is chemically depleted in incompatible elements and that its major- and minor-element chemistry does not vary with depth [Boudier and Coleman, 1981]. The olivine in the discordant and concordant dunites is usually Fo_{90-91} and is accompanied by spinel (2-3 percent) and varying amounts of orthopyroxene and clinopyroxene.

The harzburgite and dunite are pervasively serpentinized with lizardite, clinochrysotile, brucite. Estimates on the average degree of serpentinization for the harzburgite is 62 percent, and that for the dunite is 81 percent. It is difficult to establish the degree of serpentinization for the total thickness of these peridotites. However, the deeper exposed parts of the peridotites in deeply incised wadis appear to be less serpentinized than the surface samples. Throughout the peridotites, the occurrence of springs containing calcium hydroxide water gives rise to the development of mortar beds cemented by carbonates that are formed by dispersion of Ca^{2+}-rich water from springs into

CO_3^{2-}-rich water flowing within the Wadi bottoms [Barnes and O'Neil, 1971]. These waters are considered to be the product of present-day serpentinization of the peridotite.

The peridotite tectonite exhibits a banded [1/] appearance that grades into massive zones in certain areas. This banding consists of concentrations of orthopyroxene-rich zones, 3 to 10 cm thick, interbanded with olivine-rich zones (Figure 2-5). The banding exhibits consistent and systematic trends, as does the spinel lineation. The spinel lineations slightly plunging to the SW, parallel isoclinal fold axes in the primary banding of the harzburgite. Microfabrics [given in Boudier and Coleman, 1981] indicate that the main harzburgite mass has undergone a high-temperature, low-stress subsolidus deformation. Deformation flowlines and sense of shear can be related to asthenosphere flow away from a former spreading ridge in the now vanished Tethyan Sea [Boudier and Coleman, 1981].

Dunite has two distinct habits within the peridotite: (1) concordant dunite that is conformable to the banding and has also undergone the high-temperature low-stress deformation; and (2) discordant dunite that forms large (3 × 10 km) to small (10 × 10 cm) bodies cross-cutting the banded peridotite (Figure 2-1).

The concordant dunite is most abundant near the basal contact of the peridotite where it forms bands as much as several meters thick and may make up more than 50 percent of the basal peridotite. This concordant dunite is present throughout the peridotite, but above the base (~2.5 km), it usually consists of less than 15 volume percent

---

1/ We prefer to use the term "band" here rather than "layer" because layers can be confused with original magmatic cumulate layers.

Figure 2-4. Photograph of amphibolite near the contact with tectonite peridotite west of Mahlah. The amphibolites are strongly foliated with planes of foliation defined by compositional layering of plagioclase and amphibole. Epidote-rich veins cross-cut the amphibolite, which is retrograded to greenschist.

Figure 2-5. Photograph of banded tectonite harzburgite with orthopyroxene-rich bands (the lighter colored bands). The banding parallels the spinel foliation in this outcrop exposed in Wadi Nah, 2 km east of Al Hisn.

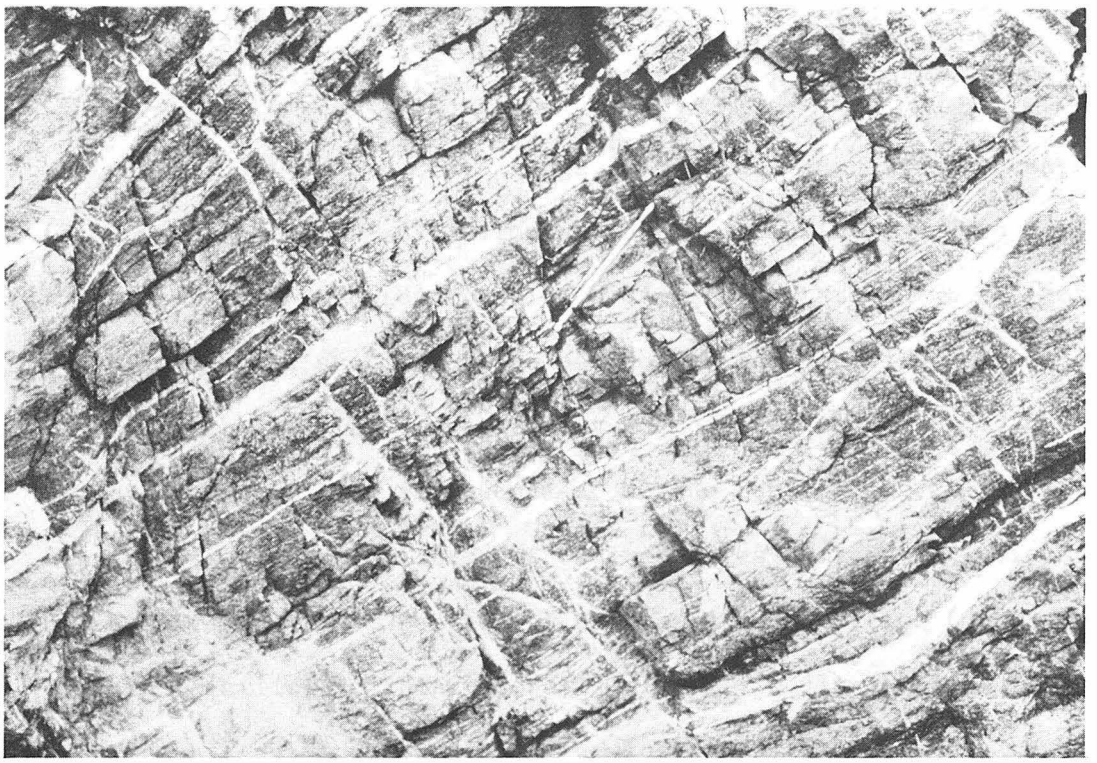

Figure 2-4

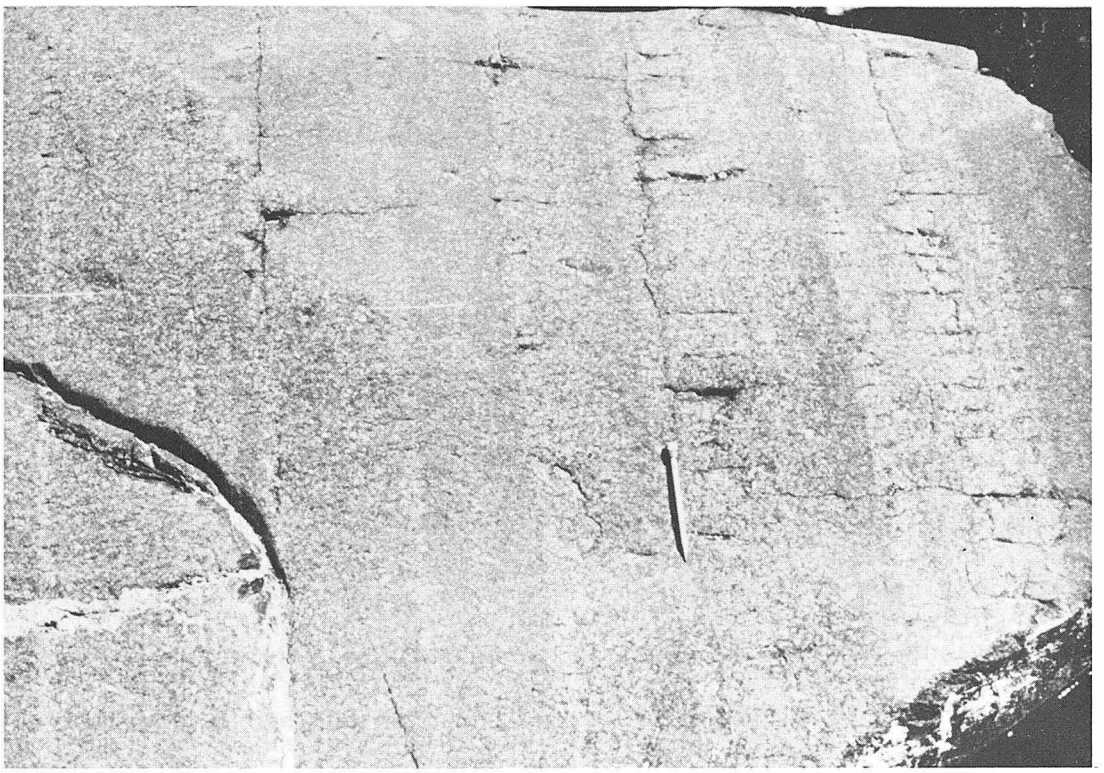

Figure 2-5

of the peridotite. Boundaries between the concordant dunite and harzburgite are commonly diffuse, grading one into the other over a distance of several centimeters.

Discordant dunite forms large, elongate, low-relief exposures (3 × 10 km maximum size) having sharp contacts with the main peridotite mass. The discordant dunite bodies occur throughout the entire 9 to 12 km-thick section of the peridotite and generally are elongated to the northwest. Although grossly discordant, these bodies commonly exhibit a fabric that is concordant to the regional harzburgite fabric. Many of the discordant dunite bodies contain inclusions of harzburgite and, near the top of the peridotite section (upper 3-4 km), contain poikilitic clinopyroxene and locally holly-leaf plagioclase. Petrographic evidence such as adcumulus and heteroadcumulus textures, xenoliths, size-sorting, and straight grain boundaries support a cumulate origin for some of the uppermost mantle dunite.

Both field evidence (see below) and supporting experimental studies [Green et al., 1979] show that orthopyroxene does not appear on the liquidus surface of any of the parent melts for the overlying cumulates. Therefore, harzburgite could not have been in equilibrium with ascending igneous melts, and harzburgite-melt contacts become reaction boundaries. At these contacts, either harzburgite melted incongruently, leaving behind residual dunite and chromium spinel, or olivine plus chromite precipitated from the melt as crystal cumulates that isolated harzburgite from the melt. Deformed chromitites with cumulate texture associated with discordant dunites deep (~8 km below the gabbro contact) within the tectonite section support a working hypothesis that the discordant dunites occupy fossil conduits through which parental melts ascended.

Websterite dikes, both deformed and undeformed, are present in the peridotite in small amounts. The deformed websterite dikes are concentrated in the lower third of the peridotite, whereas the undeformed websterite dikes are present throughout the peridotite. Undeformed gabbro dikes are found mainly in the upper two-thirds of the peridotite. The bulk composition and mineralogy of the discordant dunite, websterite dikes, and gabbro dikes suggest that these bodies represent fractionation products of magmas that had passed through the harzburgite.

The discordant dunite, being the most abundant, resulted from the flow crystallization of olivine from picritic tholeiite that may be parental to the overlying cumulate. The gabbro and websterite represent fractional crystallization products of a more evolved liquid or a completely different liquid derived from a different part of the mantle [Boudier and Coleman, 1981].

The peridotite thickness in the Wadi Tayin-Jabal Dimh area, coupled with thickness of overlying oceanic crustal section, give the approximate maximum depth into the mantle represented by the base of the peridotite. To estimate the mantle thickness, we have assumed a 35° dip for the cumulate-peridotite contact at the top and a similar dip at the base of the peridotite. Internal structural consistency within the peridotite and the absence of repeated low-angle thrusts suggest that the peridotite outcrop area represents the original slice of oceanic lithosphere detached and emplaced on the Arabian continental margin (Figure 2-1). Therefore, it is estimated that 9-12 km of upper mantle is represented in the Wadi Tayin-Jabal Dimh peridotite. With

the addition of the oceanic crustal section at most 8 km thick, a lithostatic pressure approaching 6 kb may have been exceeded at the base of the peridotite.

2.2.4 Peridotite-Gabbro Transition Zone

The peridotite-gabbro transition is a mappable heterogeneous zone, that marks the transition from uppermost mantle rocks (harzburgite and dunite) characterized by tectonite fabric to oceanic crustal rocks represented by cumulate ultramafic rocks and gabbro and lacking any tectonite fabric.

The contact between gabbro cumulates (interlayered gabbro, wehrlite, and dunite) and tectonite peridotite is usually clear-cut in the field because the cumulate rocks crop out and weather differently than the underlying tectonite peridotites. This contact is particularly striking on the ERTS image shown in Fig. 2-1 and 3-12. The major controversy concerning the peridotite-gabbro transition zone is the distribution and significance of the dunite bodies below the mappable contact.

The transition zone from peridotite tectonite to dunite cumulate must represent the base of a magma chamber, presumably under an oceanic spreading center where primary melts were being expelled from plastically upwelling asthenosphere. Mixtures of depleted mantle residuum (harzburgite) and cumulus magmatic olivine (dunite) characterize this gradational contact. Ascending primary melts that form within the mantle at depths greater than the level of exposure fractionate olivine (Fo_{91} ± chrome spinel) as they move upward through the peridotite and continue to do so when they first enter the magma chamber. Trails of dunite left by the ascending primary melts are now represented by

discordant dunite that occurs over most of the peridotite sequence. Subsolidus deformation is superimposed upon the harzburgite and the enclosed discordant dunite, presumably as the upper mantle flowed away from the spreading ridge. Where the discordant dunite merges into the overlying zone of massive dunite, it is difficult to distinguish a boundary between discordant dunite in the harzburgite and cumulate dunite at the base of the magma chamber. Continued fractionation of olivine within the magma chamber, augmented by magma mixing, brings melt composition to the point at which olivine-clinopyroxene-plagioclase crystallize, forming wehrlite, picrite, and gabbro cumulates above the earlier formed basal dunite cumulates.

Variations in the basal cumulus stratigraphy along strike can be explained by interactions between fractionated magma in the chamber and pulses of primary melt from the mantle. All the hypothetical processes above took place in a tectonically active setting (mid-ocean spreading center), resulting in strong penecontemporaneous subsolidus deformation of the peridotite and the discordant dunite that represented earlier channelways of the rising primary melts. Soft sediment style of deformation, retention of igneous textures, and diapiric movement of olivine cumulates in the lower cumulate section, indicate that the lower cumulate section was still partly mushy from the presence of intercumulus melts and reacted quite differently to the stresses at the spreading center than did the underlying tectonite peridotite. The absence of similar structures in the upper parts of the layered gabbro section indicates that this style of deformation in the lower cumulates is restricted to or near the spreading ridge.

The complex subsolidus and plastic deformation in the transition zone appear to record the effects of diapiric movement of fractionating primary melts through depleted harzburgite and the accumulation of the lower cumulates upon a conveyor belt of constantly deforming depleted peridotite within the zone of high heat flow at a spreading center.

2.2.5 Gabbro Member

The gabbro of the Samail ophiolite forms two regionally mappable units: cumulate gabbro ("G") and high-level gabbro ("HG") that were first described by Reinhardt [Glennie et al., 1974]. The two-fold division of the gabbro developed by Reinhardt was maintained during geologic mapping in the Ibra region (Figures 2-2 and 2-3).

On the north limb of the Ibra Valley syncline along Jabal Dimh, the peridotite-gabbro contact is at the crest of the range 500-800 meters above the alluvial plain. Topography in the layered gabbro is controlled by: (1) the layering attitude of the cumulate gabbro, and (2) joint sets nearly normal to the layering planes which are commonly lined by hydrothermal veins. Near the base of the cumulate gabbro, hydrothermal veins are less abundant, and the ridges parallel the strike of the layering but are serrated where prominent joint and fracture sets occur. Higher in the gabbro section, the topographic relief decreases, and wider valleys occupy zones altered by prominent hydrothermal activity. The high-level gabbro occurs in isolated hills (with 50 meters relief) whose distribution is also controlled by differential erosion of the highly fractured, hydrothermally altered areas.

2.2.5.1 Layered Gabbro (map symbol "G")

Most of the gabbro in the Ibra region belongs to the layered gabbro unit. Five measured stratigraphic sections show a range in thickness of 2.6 - 5.5 km. The layered gabbro unit is composed chiefly of cumulate olivine-clinopyroxene-plagioclase. Ultramafic cumulates (<300 m thick) typically occur at the base of the cumulate section although ultramafic cumulates recur at higher stratigraphic levels in several of the sections. Cumulate layers range in thickness from millimeter to meter scale (Fig. 2-6). The layers are defined by variation in the relative abundance and/or grain size (~1 to 5 mm) of the three primary cumulus phases. Virtually all of the layered gabbros have a strong planar lamination created by elongate plagioclase and clinopyroxene lying parallel to layering planes. Adcumulate textures are predominant, although heteroadcumulate textures with poikilitic clinopyroxene are locally present, especially in the ultramafic layers.

Individual layers are discontinous along strike on scales varying from a few meters for thin, small-scale layers to several hundred meters for thicker meter-size layers (Fig. 2-6). Distinctive ultramafic-mafic layer sets have been traced for as much as 5 km along strike. Layering has a uniform dip over large areas in Jabal Dimh although locally it is gently folded. No obvious intrusive contacts or layer discordance associated with separate, crosscutting gabbroic plutons have been recognized in our 30 km-wide map strip.

Figure 2-6. Cumulus layering is shown on two different scales: in Fig. 2-6a, a large dunite lens (the dark band) is continuous for several hundred meters. This cumulate dunite layer is found close to the contact between Samail peridotite (in the foreground) and the layered gabbro section, and in Fig. 2-6b, clinopyroxenite "troughs" on cm scales. Individual clinopyroxenite lenses are continuous from a ~15 centimeters to several meters and this distinctive cumulate horizon is continuous for over a kilometer along strike.

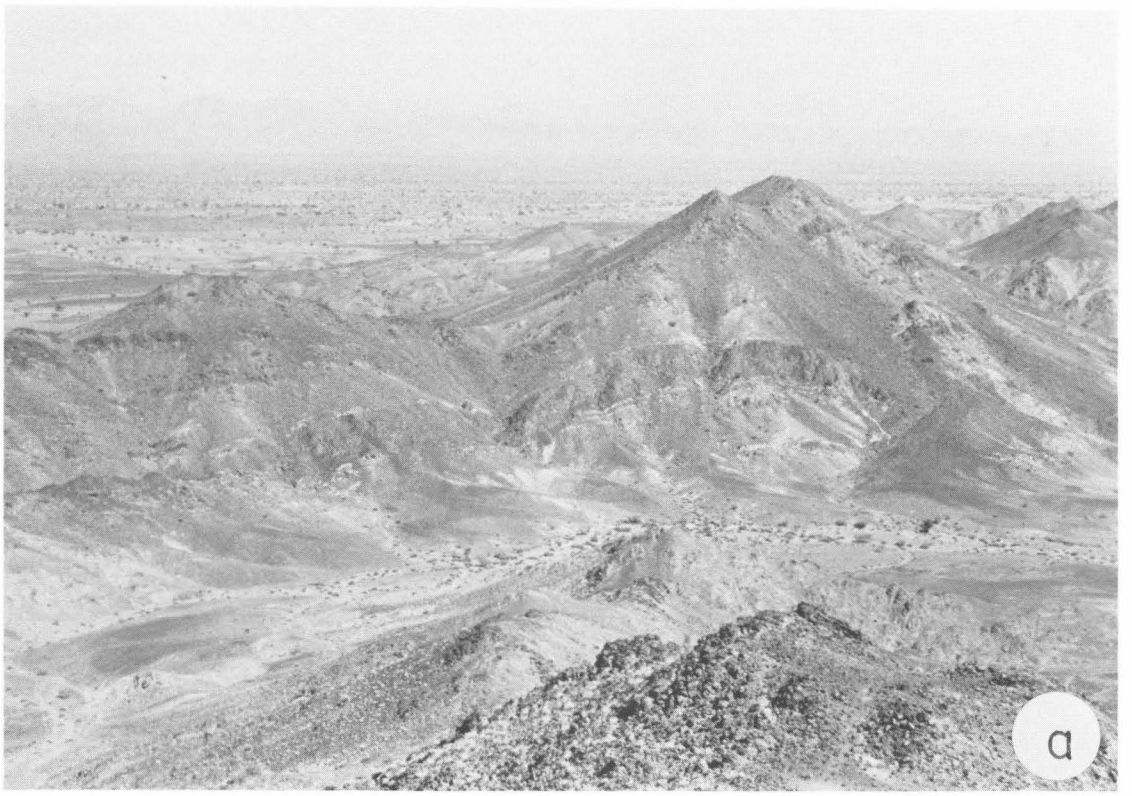
a


b

The sequence of rock types exposed in each stratigraphic section through the layered gabbro reveals the order of crystallization of the magma. Olivine and Cr-spinel are the early liquidus phases and form the early basal cumulus dunites. Clinopyroxene and plagioclase appear nearly simultaneously, forming gabbro interlayered with dunite and wehrlite. Cumulus gabbro is always present within a few hundred meters of the gabbro-peridotite contact, and in some places, it rests directly on harzburgite with no intervening dunite or wehrlite. Olivine, clinopyroxene, and plagioclase continue as cumulus phases throughout the layered section and show cryptic compositional variations. Occasional ultramafic intervals that repeat the crystallization sequence mark reversals in the cryptic variation trends of the cumulus minerals. Cryptic variation trends may also reverse with no concomitant association of ultramafic cumulates [Pallister and Hopson, 1981]. Orthopyroxene is never a cumulus phase in layered gabbros of the Ibra section, although it is present as a post-cumulus phase in the uppermost cumulates near Wadi Gideah.

The crystallization sequence in the gabbro, combined with the occurrence of abundant discordant dunite in the underlying peridotite, indicates that the parental melt was crystallizing olivine and spinel during its ascent to the magma chamber. Upon entering the chamber, the parental melt mixed with melts already crystallizing plagioclase, olivine and clinopyroxene. This mixing moved the parental melts to the three-phase cotectic where the magma reservoir remained while pl-cpx-ol crystallization from the bottom upward built an average of ~4 km of cumulates (Fig.2-7). Conversely, the addition of new pulses of

primitive melt throughout the period of crystal fractionation prevented differentiation of the chamber magma to the four-phase ol-opx reaction point. The absence of the four-phase reaction point implies that crystallization was buffered at the three-phase cotectic by repeated influx of new magma. Furthermore, any diabase dike or pillow basalt tapped from this "steady-state" magma chamber cannot be primary unfractionated melt of the mantle.

As expected from the field relations (the general absence of the ol-opx reaction), the range in mineral composition from the layered gabbro is quite limited relative to that found in differentiated (single magma pulse), continental layered gabbros [Pallister and Hopson, 1981]. Microprobe analyses of the cumulate phases from three sections show the following compositional ranges: olivine, Fo_{69-90}; plagioclase, An_{62-95}; clinopyroxene, (En_{40-54}, Fs_{4-16}, Wo_{37-49}), which can be related to systematic cryptic variations [Pallister and Hopson, 1981].

2.2.5.2 High-level Gabbro (map symbol HG)

The high-level gabbro is equivalent to the hypabyssal gabbro of Reinhardt [Glennie et al., 1974] and to "isotropic gabbro" of Hopson and Pallister [1978, 1979]. The high-level gabbro varies in thickness (<1 km) and always occurs as a sandwich horizon between overlying sheeted dike complex and underlying layered gabbro (Figures 2-2 and 2-3). The high-level gabbro is in intrusive contact with the dike complex. The contact, where observable, is sharp and roughly "parallels" other major lithologic boundaries within the ophiolite. The contact between layered gabbro and high-level gabbro is typically gradational, although

locally high-level gabbro (and sometimes plagiogranite) intrudes downward into the layered gabbro.

Texturally and lithologically, the high-level gabbro is complex with extreme variability exhibited down to meter scale. Generally, the coarser grained and/or more differentiated members cross-cut finer grained, more mafic members. The finer grained rocks are usually plagioclase-clinopyroxene-Fe-Ti oxides ± olivine ± orthopyroxene and hornblende gabbro, whereas the coarser grained rocks are typically plagioclase-hornblende ± clinopyroxene ± Fe-Ti oxides ± quartz gabbro and diorite.

The high-level gabbro does not exhibit cumulus textures and is texturally variable on the scale of a thin section. Primary minerals are strongly zoned. Plagioclase in the high-level gabbro is zoned from An_{75} to An_{35}. Compositions of the cores of plagioclase crystals approach the more-calcic plagioclase compositions of underlying cumulates. Plagioclase crystals commonly exhibit a sharp change in An content from labradorite to andesine, possible correlated with hornblende coming in on the liquidus. Although the high-level gabbro is hydrothermally altered, exhibiting uralite replacement of both pyroxene and hornblende and talc replacement of olivine, reconstruction of the crystallization sequence is possible using petrographic evidence and field relations. Olivine + clinopyroxene + plagioclase are the first liquidus phases similar to the underlying cumulus gabbro. In places, the olivine-orthopyroxene reaction is reached, and orthopyroxene replaces olivine on the liquidus. More commonly, primary magmatic hornblende replaces clinopyroxene as shown by clinopyroxene inclusions in many hornblendes. Hornblende and Fe-Ti oxide crystallization drives the remaining melt toward the plagiogranite end member.

Figure 2-7. Photograph of layered gabbro illustrating ratio phase layering on cm to m scales in an outcrop exposed near the mouth of W. Imard, approximately 500 m below the contact with high-level gabbro. The darker layers (10-30 cm thick) are thinner and more olivine-rich than the more plagioclase-rich layers. Graded phase layering is visible in the right-hand of the photograph.

Figure 2-8. Photomicrograph of plagiogranite illustrating graphic intergrowths of quartz and albite intersertal to tabular grains of turbid plagioclase.

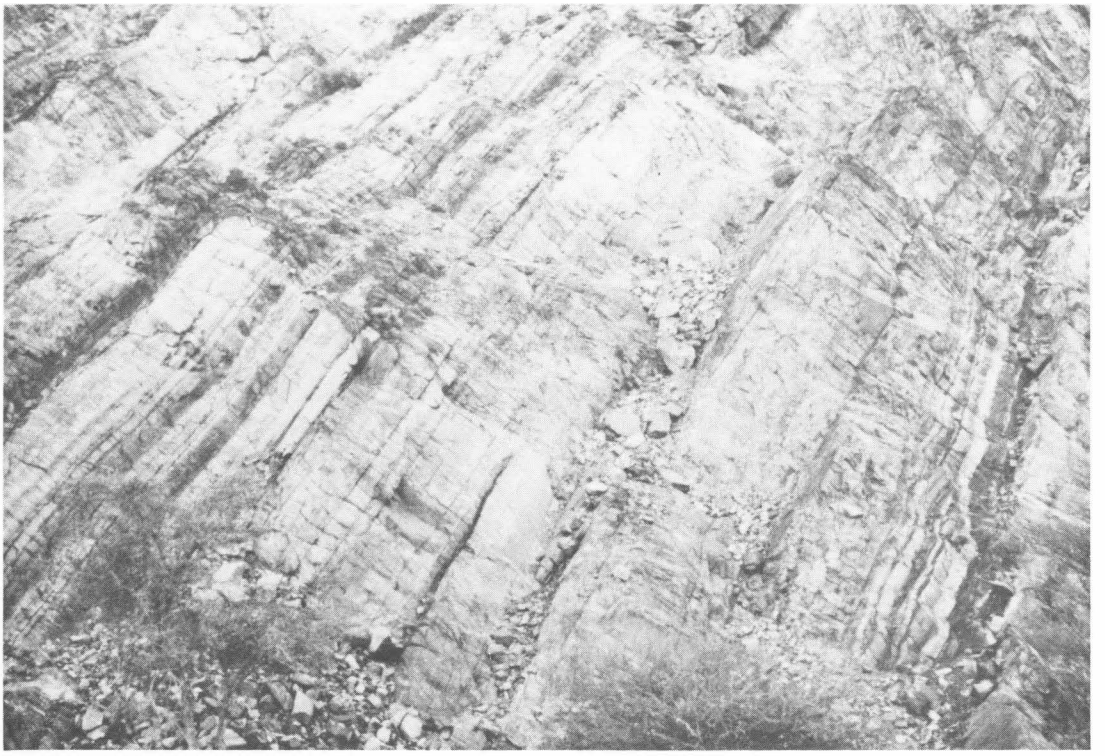

Figure 2-7

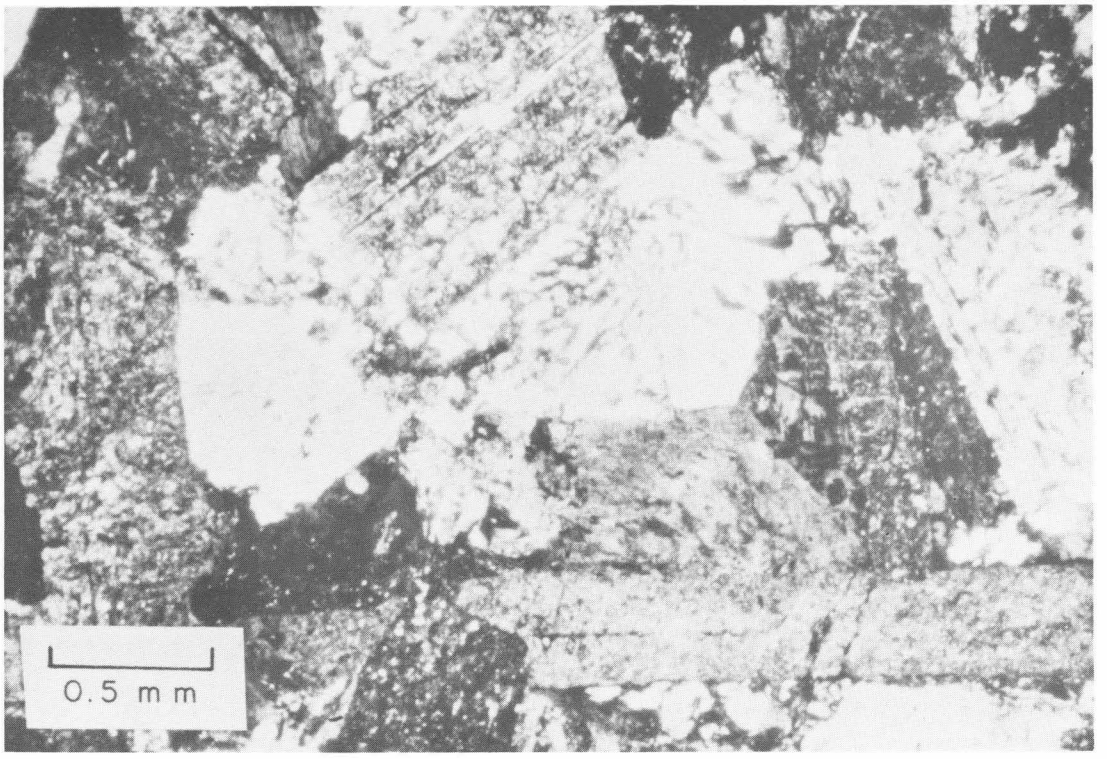

Figure 2-8

2.2.6 Plagiogranite (map symbol Pg)

Plagiogranite commonly occurs as thin sills (<1 km^2 × 50 m) sandwiched between gabbro and dike complex rocks although volumetrically it is insignificant in the Ibra area (Figures 2-2 and 2-3). End member albite granite may occur anywhere in the high-level gabbro sections either as dikes coming from above or as small irregular bodies formed in-situ. Dikes derived from underlying plagiogranite bodies are locally abundant in the sheeted dike complex, and locally are cross-cut by other diabase dikes. The end member rock has a color index <10 percent, modal quartz <30 percent, and zoned plagioclase An_{10-60}. Potassium feldspar is conspicuously absent even from myrmekitic intergrowths of feldspar and quartz [Coleman and Donato, 1979] (Figure 2-8). Hornblende, magnetite, and minor biotite, usually altered to chlorite, are the primary mafic phases.

The complex intrusive relations between texturally and compositionally different high-level gabbro, plagiogranite, and diabase dikes suggest that the roof of the magma chamber was a dynamic, unstable feature throughout crystallization history of the underlying cumulates. The ratio of layered cumulate rocks to high-level gabbro (~4) supports this conclusion. The constant piecemeal stoping and reworking of the roof by intrusion of magma from below resulted in the thin high-level gabbro section and also provided access of seawater into the melt. The common occurrence of hydrothermally altered inclusions of metadiabase and microgabbro within plagioclase and high-level gabbro [Gregory and Taylor, 1981] suggests that water from these roof-rock inclusions locally hydrated the remaining melt driving it to hornblende saturation. Crystallization of low-silica phases such as hornblende

and magnetite under hydrous conditions promotes crystallization to a plagiogranite end member. In addition, extraction of the low-melting fraction (plagiogranite) from stoped blocks leaving behind hornblende-magnetite-labradorite hornfels also produced plagiogranite while the underlying chamber was still relatively unfractionated. This has been observed locally in the Ibra high-level gabbro section, and spectacularly at Dasir (near northeast end of the Samail gap [Gregory and Taylor, 1981]. The field relations suggest that all of the plagiogranite observed in the upper parts of the Ibra oceanic crustal section was generated in-situ either by partial melting of the roof rocks or by extreme differentiation of a hydrous tholeiitic melt.

2.2.7 Sheeted Dike Complex (map symbol D)

The sheeted dike complex is a mappable unit with a consistent stratigraphic position; it overlies high-level gabbro and penetrated upward into, and locally fed pillow lava (Figures 2-2; 2-3; 2-9). The dike complex is composed of nearly 100 percent parallel to subparallel diabase and basalt dikes (Figure 2-10). The absence of other wallrock indicates that pre-existing dikes were host to each subsequent parallel intrusion, except near the contact of the complex where septa of high-level gabbro (lower contact) and pillow lava (upper contact) occur. Although geometrically simple (parallelism), the internal intrusive relations revealed by chill-margin facing directions, and petrographic variation are far from simple. Multiple intrusion in the same planar orientation has resulted in dike-splitting. One sided dikes are separated from their mates by variable numbers of younger dikes, which commonly are also split.

Figure 2-9.

a) Photograph of sheeted dike complex that shows a set of half-dikes which have only a single chill margin. The arrows point to the unchilled part of the dike; the dike orientation here is N/S with chill margins developed on the east side and half-dike width of ~ 1 meter.

b) Sheeted dikes are exposed approximately 5 km west of Al Yahamdi. Note the screen of plagiogranite on the left-hand side of the photograph. Long axis of the photograph is approximately 5 meters.


a

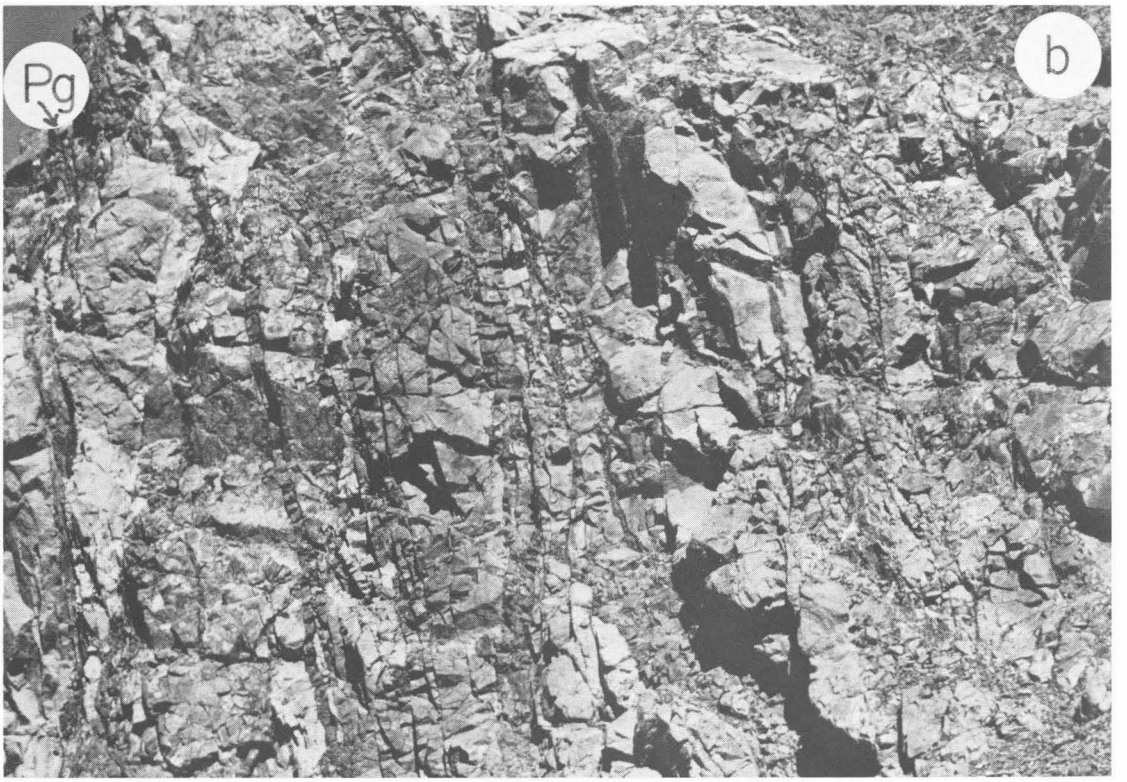
Pg
b

Figure 2-10. The diabase-gabbro contact is a sharp discontinuity, where most (>90 percent) of the dikes are truncated along a sharp intrusive boundary with the high-level gabbro. Exposure 2-9a is found along the Ibra-Muscat road between Al Yahamdi and Khafifah towards the western edge of the map strip. Exposure 2-9b is found just west of Batin (see Figure 2-2) on the north flank of the Ibra dome. The contact is overturned and dips to the south.


a

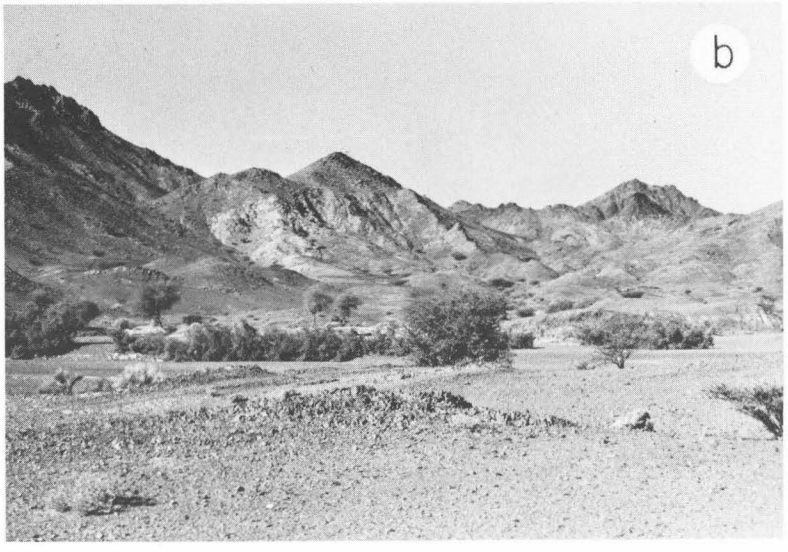
b

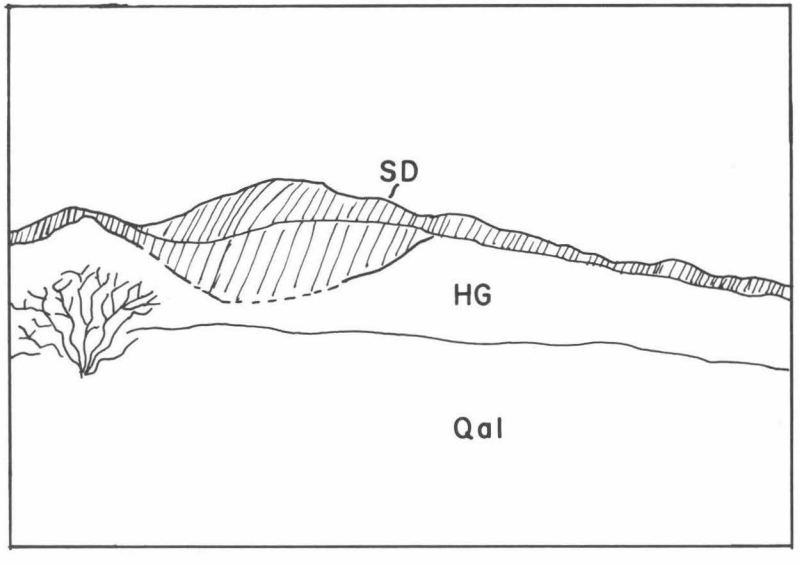
SD
HG
Qal

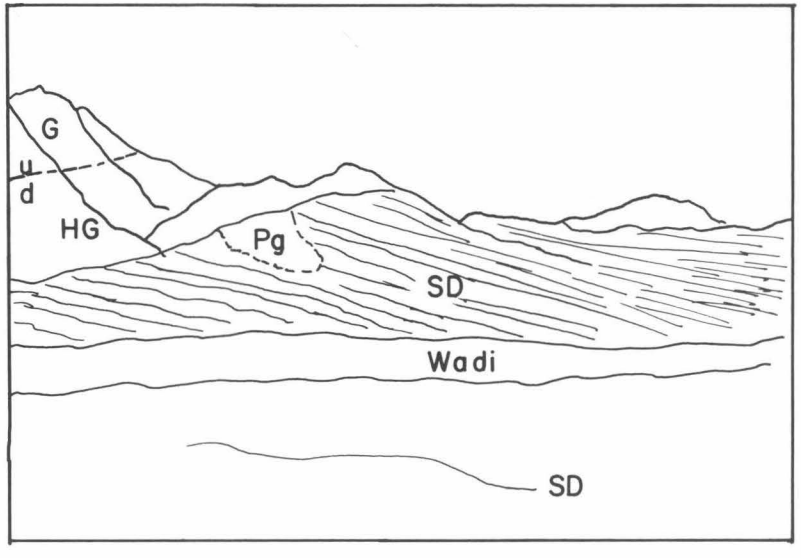
G
u
d
HG
Pg
SD
Wadi
SD

Although local domains of sheeted dike exposure are consistent, a structural analysis of the Ibra valley sheeted dikes reveals considerable variation in corrected domain attitudes. These attitude divergences between individual dike domains suggest that perhaps all the original dike attitudes may not have been vertical or that post-injection block faulting near the paleo-ridge has disturbed the initial geometry. However, it is possible to establish a NNW (345° ± 10) regional dike trend for the Ibra valley sheeted dikes, indicating a possible paleo-ridge axis orientation.

The sheeted dike complex is discontinuously exposed in the foothills of the mountains that rim the Ibra Valley, and in erosional remnants surrounded by alluvium, both in the valley floor and in the region south of Ibra (Figures 2-1 and 2-2). More than 30 km of exposure roughly perpendicular to the strike of the dikes is represented in the Ibra Valley. However, individual outcrops tend to be elongated parallel to the dike strike such that continuous exposures across strike are usually limited to less than 100 m.

The estimated stratigraphic thickness of the dike complex is 1.2 - 1.6 km as measured in cross sections constructed through the crustal section of the ophiolite in the central Ibra Valley and Jabal Dimh Figure 2-3).

The contact of the sheeted dike complex with the underlying high-level gabbro is characterized by an abrupt transition from ~100 percent dikes to massive high-level gabbro over a distance of only a few tens of meters. The high-level gabbro is intrusive against the base of the sheeted dike complex, truncating most (>90 percent) of the dikes along a sharp intrusive boundary. Some of the dikes penetrate

Figure 2-11. Photograph of sheeted dikes showing the absence of wallrock and contacts of dike against dike from an outcrop located 6 km northwest of Ibra near the contact between diabase dike complex and high-level gabbro.

Figure 2-12. Photomicrograph of pillow basalt containing microphenocrysts of plagioclase, clinopyroxene, and olivine which is the same assemblage that crystallizes as cumulus phases in the underlying layered gabbro. The plagioclase and olivine grains are pseudomorphed by secondary minerals.

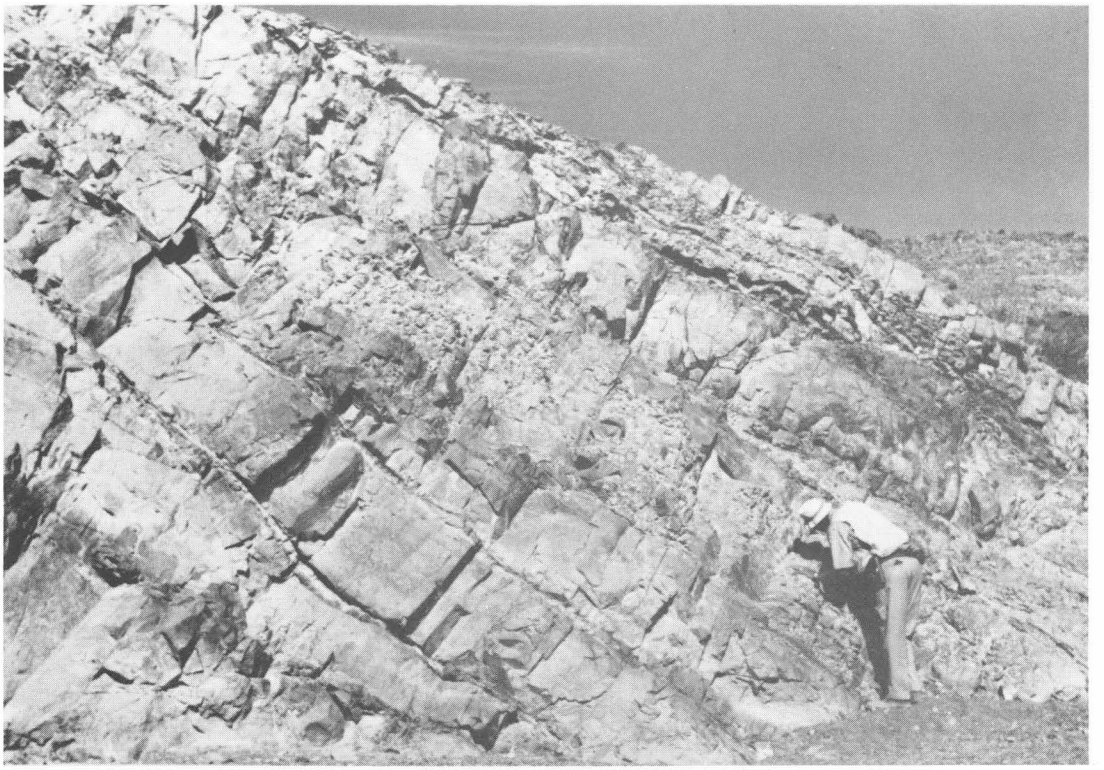

Figure 2-11

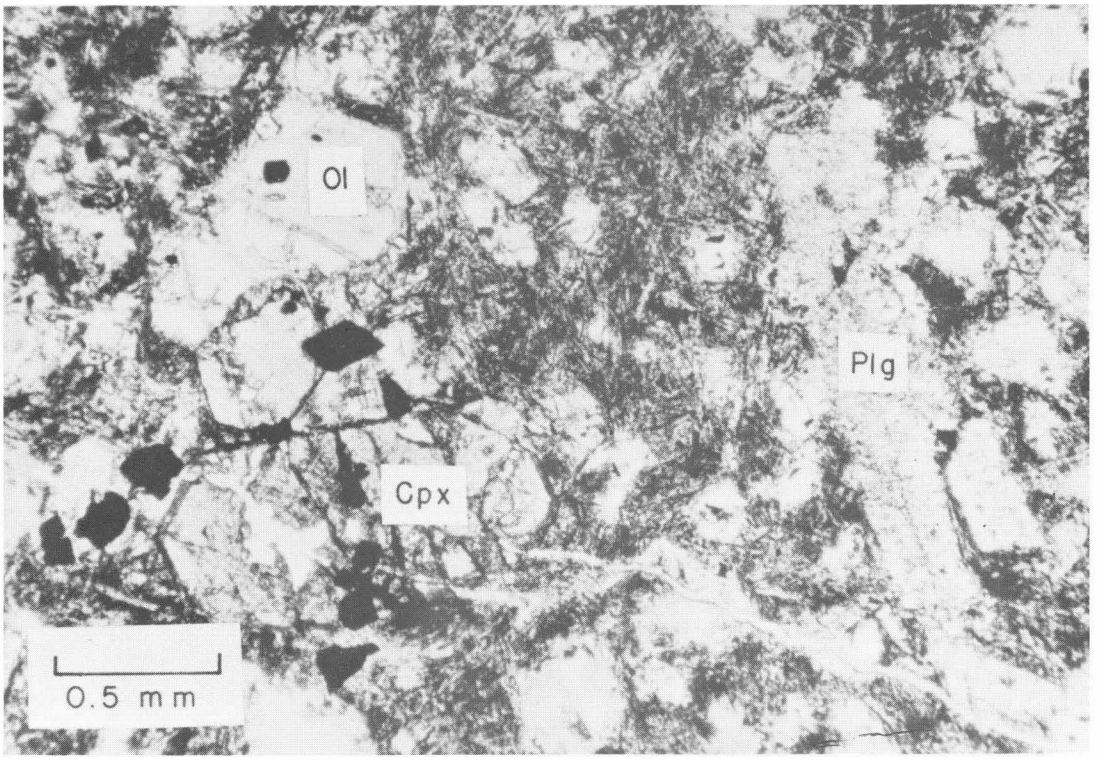

Figure 2-12

into the high-level gabbro, but they decrease in abundance rapidly downsection, and none has been traced into the cumulus gabbro. These relations indicate that most, but not all, of the dikes of the sheeted complex predate high-level gabbro crystallization, and virtually all either predate or originated from the magma above the cumulates crystallizing at the base of the chamber. Although most dikes are cut off by the high-level gabbro, the presence of some dikes penetrating into the latest stage differentiates indicates that the complex is composite with respect to dike age. Inclusions from the cumulates have not been observed in the sheeted dike complex, and only a single plagiogranite inclusion has been observed. Conversely, diabase inclusions are common in many plagiogranite and diorite bodies that occur along the contact of the dike complex with the high-level gabbro.

The upper contact of the dike complex with pillow lava is exposed in only a few localities in the Ibra Valley (Figure 2-2). Outcrops of ~100 percent dike rock are separated by only a few tens of meters from pillow lava containing few dikes. Therefore, the upper contact of the sheeted complex is considered to be an abrupt transition.

A range in composition and grain size exists between individual dikes. Most dikes are medium- to fine-grained aphyric uralite metadiabase. Olivine-clinopyroxene-plagioclase, and clinopyroxene-plagioclase phyric metadiabases have also been observed. Rare plagiogranite dikes are present in the complex, but are usually associated with nearby plagiogranite sills or irregular intrusive bodies along the contact of the high-level gabbro with diabase.

The diabase is hydrothermally altered, exhibiting zeolite- to upper-greenschist-facies assemblages with metamorphic grade increasing downward. Donato and Coleman [1977] report pervasive hydrothermal alteration in the basalt, diabase, and some gabbro from the Samail ophiolite and have related this to sea-floor hydrothermal metamorphism. Fractures produced by cooling of the diabase dikes results in permeability patterns that produce local variations in hydrothermal alteration. The absence of Tertiary post-emplacement plutonism and regional metamorphism, coupled with a consistency of alteration assemblages, indicates that the observed alteration records sea-floor metamorphism.

Whole-rock major-element analyses of diabase dikes show high H_2O, CO_2, Na_2O, and SiO_2: low CaO; and variable but generally high Fe_2O_3/FeO relative to primary values for ocean-ridge basalts probably as a result of alteration. In spite of the pervasive hydrothermal alteration, however, these chemical analyses for most major elements closely reflect the rocks' original igneous characteristics. Normative calculations of the diabase chemical analysis when plotted on several classification schemes are found to be tholeiitic [unpublished U.S.G.S. data]. Comparison of selected element ratios from diabase analyses definitely show their affinity toward oceanic ridge basalts [Pallister and Knight, 1981].

Using observed Mg/Fe^{+2} ratios in diabase as an indication of the liquid composition derived from the underlying magma chamber, calculated liquidus olivine compositions (Fo_{79-89}) agree with the olivine cumulate compositions (Fo_{69-89}) in the underlying cumulate gabbros and provide petrologic evidence of cogenetic origin for the diabase and layered gabbro.

2.2.8 Volcanic member (map symbol V and SC)

Basaltic volcanic rocks (<700 meters thick) are exposed discontinuously over 23 km^2 in the core of the Ibra Valley syncline between Yahamdi and Batin and are also exposed at the southern end of the map strip in Wadi Bu Taymah [see Bailey et al., 1981]. The volcanic member crops out in low hills or is exposed in pediments and thus is the most poorly preserved member of the ophiolite stratigraphy in the southeastern Oman Mountains. As a result of its sparse distribution, the volcanic member has received little attention beyond initial mapping, and limited petrographic and isotopic work [Gregory and Taylor, 1981: McCulloch et al., 1981].

The volcanic rocks are all intensely altered, yet original igneous features have been preserved on all scales. Pillow lavas along with massive flows and pillow breccias are preserved in the best exposures. In hand specimen, the basalts are aphyric and vesicular and most vesicles are lined or filled with secondary minerals (primarily calcite). Sparsely microvesicular pillow rims suggest a deep-water origin [Moore, 1975; Moore and Schilling, 1973]. In thin section, the basalts are generally microphyric preserving delicate igneous textures such as quench and variolitic textures.

The most conspicuous feature of the Samail volcanic rocks is the pervasive effect of hydrothermal alteration in zeolite or lower greenschist facies on all of the rocks. Inferences of igneous paragenesis are based upon textural arguments, as no primary minerals (with the exception of clinopyroxene) are preserved. Original acicular plagioclase grains are replaced by turbid albite. Olivine has not been observed in any of the rocks, and we interpret its absence as a

consequence of the pervasive recrystallization and not due to the primary crystallization sequence. On textural grounds (Figure 2-12), the basalts were crystallizing along two- or three-phase cotectics at the time of eruption matching the stage of fractionation of the magmas that produced the underlying cumulus gabbros [Pallister and Hopson, 1981], which suggests a cogenetic origin for the volcanic member and underlying gabbro cumulates of the Ibra section. We find no evidence for a basalt-andesite-rhyolite fractionation series, which is characteristic of a stratigrapically higher "off-axis sequence" of lavas in northern Oman [Alabaster et al., in press; Smewing, in press].

2.3 ROCKS ASSOCIATED WITH THE SAMAIL OPHIOLITE

2.3.1 Metamorphic Rocks (map symbol ms)

Narrow, discontinuous zones of metamorphic rocks are present along the base of the peridotite in the mapped transect, particularly in the Wadi Tayin area (Figures 2-1, 2-2, and 2-3). These metamorphic rocks previously have been described by Alleman and Peters [1972] and Glennie et al., [1974] and are now considered to be related to oceanic detachment of the ophiolite [Woodcock and Robertson, 1977; Ghent and Stout, 1981]. The actual basal contact of the peridotite is irregular and, within Wadi Tayin, measured dips are to the south and locally are 30° to 50° to the south. Vertical post-metamorphic diabase dikes intrude the peridotite as well as the metamorphic rocks along the base. None of these dikes extend into the underlying Hawasina melange or autochthonous carbonate rocks. In the Wadi Tayin area, the metamorphic rocks consist of an amphibolite 100 meters thick right at the peridotite contact (Figure 2-4) that contains discontinuous piedmontite-

bearing quartzite layers a few meters thick. Below the amphibolite, another 100 meters of greenschist underlies the amphibolite, and this then grades into Hawasina sediments that are only slightly metamorphosed. Discontinuous zones of garnet-clinopyroxenite less than 2 m thick, occur at the peridotite contact. These high-grade rocks show polyphase deformation and early partial retrogression with recrystallization to greenschist, followed by cataclastic fabrics with no recrystallization. In contrast, the greenschist generally shows only one phase of recrystallization and deformation suggesting a dynamic, discontinuous metamorphism. Estimates of temperatures by using Kd distribution coefficients of garnet and pyroxene suggest maximum temperatures of metamorphism of 660 to 700°C with pressures probably less than 2 kb [Ghent and Stout, 1981].

The metamorphic gradient is steep from the peridotite contact down through the amphibolite into the greenschist, where the metamorphic rocks appear to grade into or are faulted against unmetamorphosed sedimentary and volcanic rocks. The presence of amphibolite blocks in the melange as well as dikes cutting the metamorphic sequence and peridotite suggests that the metamorphism is pre-emplacement [Cakir et al., 1978]. Retrograde metamorphism in the garnet-clinopyroxene amphibolites as well as development of low-temperature rodingite assemblages by Ca-metasomatism along the peridotite contact indicates post-metamorphic retrogression. It is assumed that the highest grade rocks were tectonically transported the greatest distance and that the lower grade rocks were successively incorporated into the aureole as the peridotite was thrust over progressively cooler rocks [Ghent and Stout, 1981]. The diabase dikes cutting the metamorphic

rocks and peridotites along Wadi Tayin are oceanic tholeiites that were intruded after the initial oceanic detachment of the Samail ophiolite and before its obduction onto the Arabian continental margin [Pallister, 1981].

2.3.2 Hawasina Group (map symbol H) [2/]

The allochthonous Hawasina Group as described by Lees [1929] and mapped by Glennie et al. [1974] with the Oman Mountains is an imbricated assemblage of thin nappes consisting chiefly of marine sedimentary rocks. The Hawasina allochthon is tectonically sandwiched between the Samail ophiolite nappe above and the autochthonous sequence of middle Permian to Late Cretaceous shelf carbonates (Hajar Supergroup) below (Figures 2-1, 2-2, and 2-3). The Hawasina sedimentary rocks consist chiefly of shallow-water to deep-water clastic limestone, including limestone turbidite and slide breccias, quartz sand-bearing clastic limestone and minor quartzite, fine lithoclastic limestone thinly interbedded with radiolarian chert, radiolarian ribbon chert with shaly partings, and minor thinly-laminated shale and marl. Locally Hawasina marine sedimentary rocks are interlayered with minor (<50 m thick) basaltic volcanic rocks including pillow lava, massive flows, tuff, and volcanic breccia. Hawasina deposition spans the interval from Permian or Triassic to middle Cretaceous (Cenomanian), contemporaneous with the autochthonous Hajar Supergroup [Glennie et al., 1974].

[2/] Geographic names not appearing in Figures 2-1 or 2-2 can be found on the geologic map [Bailey et al., 1981].

The Hawasina Group is discontinuously exposed within our transect in six areas, and their approximate sizes from south to north are: (1) south of Wadi Bu Taymah, Jabal Hammah (>1000 km^2 mostly beyond our map area), (2) Wadi Bu Taymah (150 km^2), (3) Ibra dome (100 km^2), (4) Ibra syncline (25 km^2), (5) Wadi Tayin (100 km^2), and Ruwi (25 km^2). The exposures over this 125-km transect show south to north changes in lithology and structural style as the Hawasina is mapped from in front of the Samail nappe back beneath it. To document these changes, six areas are described, beginning at the south.

South of Wadi Bu Taymah, in Jabal Hammah, is a large expanse of the Wahrah Formation of Late Triassic to middle Cretaceous age described by Glennie et al. [1974]. The Wahrah consists chiefly of red radiolarian chert, calcareous mudstone, and fine-grained limestone turbidite displaying graded beds, sole marks, and ripple marks. The nearly perfect exposures across this belt show tight, easterly trending folds with wavelengths of 1-2 km. The average thickness of the Wahrah is estimated by Glennie as 185 m, but it has been thickened by imbrication to several times this figure; thus, continuous outcrop width of the formation now reaches 25 km. All strata are intact and melange with either exotic limestone blocks (see below) or volcanic rocks are not developed.

Extending west, from Mudayrib and Ad Dariz in Wadi Bu Taymah, is a belt containing more than 50 isolated hills of Hawasina rocks consisting of roughly equal amounts of limestone and ribbon chert with subordinate sections of both conglomerate that contains blocks of white limestone, and volcanic rocks (pillow basalt, tuff, and breccia). Radiolaria from the chert indicate ages of Valangian to Cenomanian.

The white limestone blocks contain abundant shallow-water fauna of crinoids, corals, and heavy-shelled bivalves that suggest late Paleozoic (Permian) deposition for the sediments from which the blocks were derived. The erratic distribution of the resistant hills and the occurrence of pillow basalt and exotic limestone contrasts strongly with the continuous exposures of Hawasina on Jabal Hammah to the south. In thrust contact overlying the Hawasina in a single outcrop near Mudayrib [see Bailey et al., 1981] is gabbro from the Samail nappe.

Hawasina rocks are next exposed 12 km northeast of Ibra in the core of the Ibra dome (Fig. 2-13). At Jabal Hamrah, the following sequence is exposed: a chaotic melange with blocks of red chert, minor limestone, ophicalcite, quartzite, quartz-mica schist, basaltic breccia, and rare harzburgite which is followed by an intact section, >75 m thick, consisting of basaltic breccia at its base overlain by 10 m of deep red fissile shale, and limestone conglomerate that grades into 30 m of thick-bedded white limestone containing scattered crinoids and corals similar to those described in Wadi Bu Taymah. A stratigraphically intact section of tightly folded clastic limestone and limestone turbidite of the Ibra Formation (Triassic-middle Jurassic [Glennie et al., 1974]) surrounds the central core of the Ibra dome represented by Jabal Hamrah. The Ibra Formation is thrust over a thick section of thinbedded red radiolarian chert and locally abundant red limestone designated by Glennie et al. [1974] as the Halfa Formation (Triassic to Lower Cretaceous). Although both the Ibra and Halfa formations are tightly folded, they appear to be stratigraphically intact. Approaching the peridotite contact, outcrops of chert become phyllitic, although it is not clear whether the phyllites represent metamorphic equivalents of

Figure 2-13. Hawasina Group

a) The contact between the autochthonous Hajar Group and the allocthonous Hawasina is exposed in Wadi Al Mai'din near the south end of the Samail Gap (see Fig. 4-1). Sediments directly beneath the thrust belong to the Muti Fm. (Campanian to Maestrichtian) [Glennie et al., 1974] and Hawasina Group sediments directly above the thrust are Jurassic in age. The Hawasina section shown is approximately 100 meters thick.

b) A Permian exotic block exposed at Jabal Hamrah (~4 km in diameter) exposed in window through the Samail thrust.

c) A 30m-long block of recumbently folded ribbon chert exposed in Hawasina melange 2.5 km southeast of Mahlah in Wadi Tayin.

d) Thrust contact between Samail peridotite and Hawasina melange west of Mahlah in Wadi Tayin. The contact is overturned and dipping about 65 degrees to the south. No thermal metamorphism is associated with this contact.

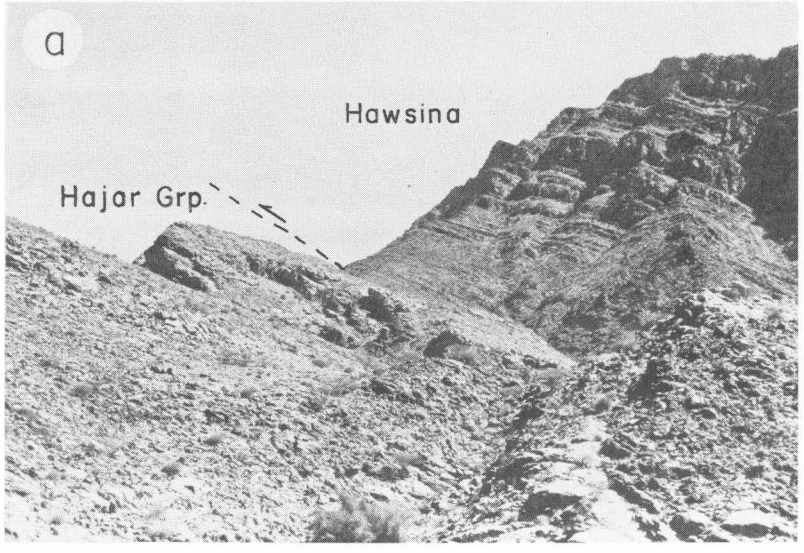
a
Hawsina
Hajar Grp.


b


d

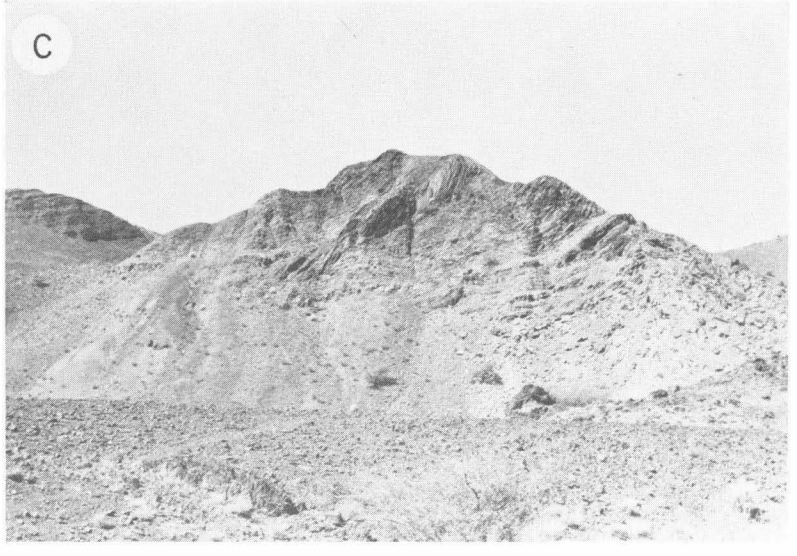
c

the thrust slices of Halfa and Ibra formations seen elsewhere in the dome or transported metamorphic slabs of different Hawasina formations.

Along the axis of the Ibra syncline about 3 km north of the center of the Ibra dome, discontinuous exposures of Hawasina consist chiefly of red chert, sandy limestone containing Halobia and microfossils of Triassic age, metaquartzite, and piedmontite-mica schist. These rocks all clearly overlie the Samail ophiolite and, because they are older, are presumed to be in fault relation.

At Wadi Tayin, Hawasina is sandwiched between the overlying Samail ophiolite nappe and the underlying autochthonous carbonate sequence (Hajar Supergroup) exposed on Jabal Abyad (Figure 2-1). The largest area of Hawasina rocks is a belt that extends 20 km east from Hammam to Sawt; other isolated areas lie northwest of Mizbar and in Wadi Hamdah (Figure 2-2). Hawasina is bounded on both sides by faults. Transported slabs of amphibolite- and greenschist-facies rocks derived from basalt, Mn-rich chert, and argillite protoliths occur locally along the contact between the Hawasina and the peridotite, but elsewhere unmetamorphosed Hawasina rocks underlie the peridotite.

The Hawasina shows a change in structural style from west to east along the length of Wadi Tayin. West of Mizbar, beyond our map area, intact Hawasina formations are stacked in several thrust sheets [Glennie et al., 1974], but towards the east, intact units become dismembered and grade into melanges. East of Mahlah (Figure 2-2), the Hawasina is almost entirely tectonic melange. The melange consists of blocks that abut against other blocks with little or no matrix between them such as shale or serpentinite (Figure 2-12 and 2-13). Stratigraphically intact remnants continuous as blocks up to several hundred

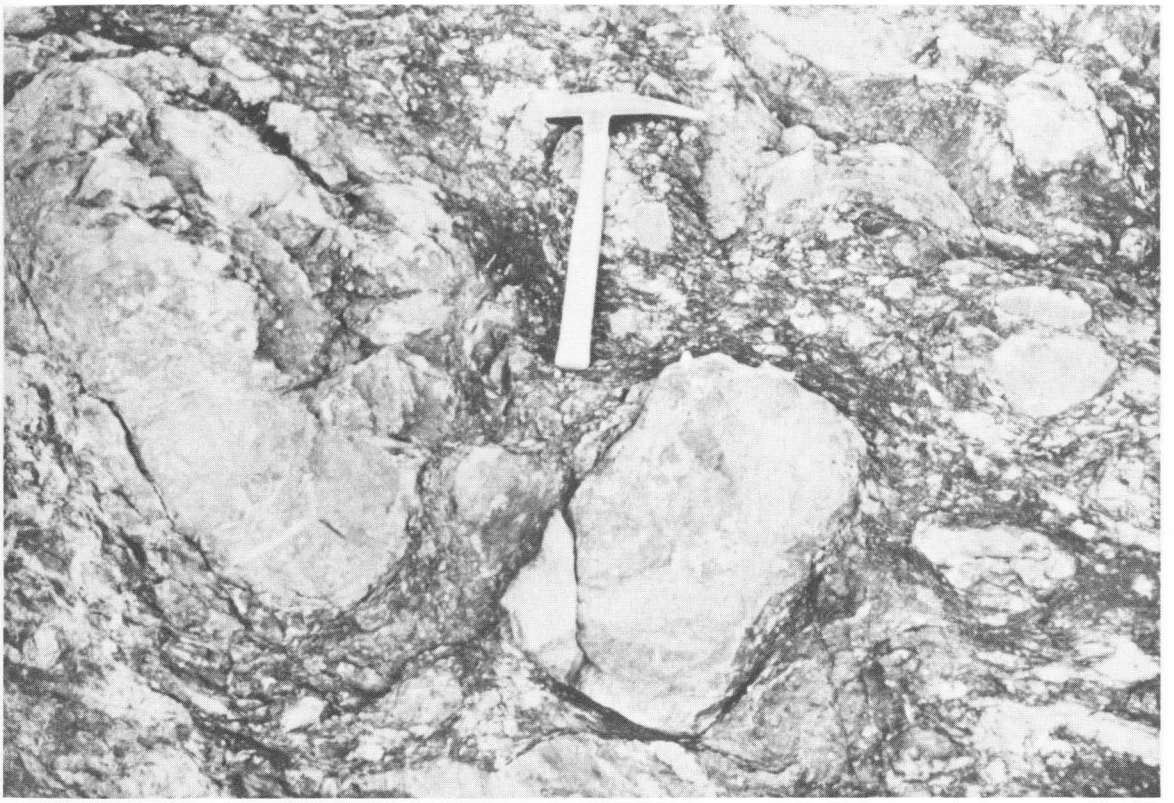

Figure 2-14. Photo of Hawasina melange consisting of limestone blocks within a matrix of shale and smaller broken fragments of chert, shale, and limestone.

meters locally grade through partly disrupted (broken) formation into melange with only native block assemblages. More commonly, the melange also contains blocks that are exotic with respect to the formations on either side, which indicates that mixing on large scales has occurred along these melange zones.

Melange blocks within the Wadi Tayin area are composed chiefly of Hawasina sedimentary rock types including clastic limestone of continental slope and rise facies [following Glennie et al., 1973], radiolarian cherts of Late Triassic to Early Cretaceous age [Tippit, pers. comm.], and subordinate shales of abyssal facies. Additional melange-block lithologies include: (1) volcanic, plutonic, and ultramafic rocks of the ophiolite suite, (2) trachyte and biotite diabase foreign to the ophiolite suite, (3) amphibolite, phyllite, and piedmontite-bearing quartzite, and (4) dark ophicalcite consisting of calcite mixed with serpentine, iron oxide, and chromite.

The northernmost occurrence of Hawasina is found in a small area extending from Ruwi to the coast. The rocks are faulted against calc-schist of the underlying autochthon and against overlying Samail peridotite. This small Hawasina remnant is entirely melange consisting of approximately equal amounts of ophiolitic rocks and abyssal sedimentary rocks (chert, shale, and minor limestone). The Hawasina melange at Ruwi represents disrupted oceanic crust and distal Hawasina sedimentary rock types are rare.

In summary, progressive changes in the Hawasina allochthonous unit along the Muscat-Ibra transect, from in front of the Samail nappe on the south to more than 100 km back beneath it to the north, are as follows: (1) The Hawasina changes from a tectonically thickened

sequence of imbricated thrust slices in front of the ophiolite (Jabel Hammah; Wadi Bu Taymah: [see Glennie et al., 1974 and Bailey et al., 1981]) to somewhat thinner, more disrupted sequences going back beneath the ophiolite. (2) Imbricated formations of the Hawasina in front of the nappe are stratigraphically intact, but disrupted strata and melange becomes proportionally greater beneath the Samail to the north. The Hawasina is entirely a melange at Ruwi (farthest north near Muscat) and along eastern Wadi Tayin and Wadi Khabbah (farthest east). (3) Clastic limestone (including turbidites) of the continental slope, and rise facies (Wahrah Formation and Hamrat Duru Group of Glennie et al., 1974] predominates on the south and farther west, but diminishes and gives way to mainly radiolarian chert and shale of abyssal facies (especially Halfa Formation) to the north. However, abundant Wahrah Formation was mapped by Glennie et al. [1974] along the Batinah coast north and west of the transect beyond the Samail Gap. (4) Ophiolitic rocks are not found in the imbricated Hawasina strata south of the Samail nappe, whereas volcanic rocks become progressively more abundant in the Hawasina toward the north underneath the ophiolite along the transect. However, since the association of pillow lavas, tuffs, and volcanic breccia with exotic Permian limestone blocks within the Hawasina is quite common, a conclusion relating the volcanic blocks to the Samail ophiolite is not warranted without other corroborating evidence. (5) The Hawasina melanges are mainly block-against-block (autoclastic) melanges with very little matrix. They appear to have formed by tectonic disruption and mixing of Hawasina map units, oceanic crust and mantle rocks, and minor metamorphic rocks such as those at the base of the Samail nappe (Fig. 2-13 and 2-14). No serpentine matrix melange has been

observed along our transect such as those described by Gansser [1974] and Saleeby [1977]. (6) Hawasina melange locally occurs on top of the ophiolite in the center of the Ibra syncline. The age relations, with the older rocks on top, suggest a tectonic contact.

These features within the Hawasina provide some constraints upon the emplacement of the Samail and Hawasina nappes. The facies progression within the Hawasina from predominantly clastic limestone (including slide breccia and turbidite) on the south and west (beyond our transect) to mainly abyssal radiolarite and volcanic debris on the north and east supports the paleogeographic interpretation of Glennie et al. [1974] that the continental margin lay to the southwest and abyssal plain and ocean ridge to the northeast during the Jurassic and Cretaceous. This facies change and the deformational gradient increasing to the north and east are suggestive of different styles of emplacement during the closing of the Hawasina ocean basin.

In the south and west beyond the front of the Samail nappe, tectonic melange is virtually absent. Where the contact between intact continental slope facies and underlying autochthon is exposed, Triassic to Lower Cretaceous rocks are thrust over Upper Cretaceous rocks [Glennie et al., 1974]. No penetrative deformation or thermal metamorphism is associated with this event. In contrast, in areas to the north (along the transect), tectonic disruption and mixing of distal Hawasina units underlying the ophiolite resulted in melanges. The melanges also exhibit no penetrative deformative or thermal overprint except in the contact metamorphic rocks that developed in the first stages of oceanic detachment.

The times of metamorphism and melange formation for units beneath the Samail nappe give a clue to the order of tectonic stacking. The garnet amphibolite was the first rock to be tectonically welded to the base of the ophiolite nappe during its detachment about 90 m.y. ago, followed by tectonic accretion of the lower-grade metamorphics about 85-79 m.y. ago as the nappe moved over Hawasina sediments [Lanphere, 1981; Coleman, 1981, Ghent and Stout, 1981]. The unmetamorphosed Hawasina nappes were then progressively accreted to the front of the advancing Samail nappe and carried back beneath it, the highest Hawasina slice being accreted first and the lower ones progressively later. Last to be accreted was the structurally lowest Hawasina unit, represented in Wadi Tayin by the shaly-matrix melange just above the Hawasina-autochthonous limestone (Wasia Group) contact. This melange formed from limey muds (Muti Formation) deposited in front of the Samail nappe during Campanian and early Maestrichtian time [Tippit, personal communication], plus ophiolitic and Hawasina blocks which slip into these muds from the advancing nappe front, followed by tectonic melanging as the nappe moved over this sedimentary mixture. This melanging marks the final stage of nappe movement, for by late Maestrichtian time the Samail and Hawasina nappes were covered unconformably by autochthonous shallow-water sediments. The progressive downward accretion of the metamorphic slices followed by the unmetamorphosed Hawasina nappe units suggests that the thrusting and telescoping began on the flank of the ocean ridge and then migrated progressively toward the Arabian continental margin.

An unanswered question concerning the emplacement of the Samail and Hawasina nappes is: (1) whether the process was continuous from the time of the initial detachment during the Turonian up to the final movement in the early Maestrichtian, or (2) whether a hiastus existed for approximately 10-15 m.y. between the initial oceanic detachment and its associated dynamothermal metamorphism and the final "cold" emplacement.

2.3.3 Maestrichtian-Tertiary (map symbol T)

The highest stratigraphic unit exposed in the southeastern Oman mountains unconformably overlies the eroded Samail ophiolite and all other rock groups. This unit is characterized by deposition of reworked laterite, interbedded with conglomerate and rare siltstone at the base, going up into crossbedded sandstone (all pre-Tertiary), and finally capped by transgressive shallow-water marine limestones (Maestrichtian to Oligocene) (Figures 2-1 and 2-2). Locally, residual laterites are developed directly upon the peridotite (Fanjah, Wasit, An Niba, and Mahlah). The Maestrichtian depositional surface crosscuts ophiolite stratigraphy and these relations suggest that significant folding, uplift, and erosion had occurred prior to the deposition of the Maestrichtian.

The laterite, conglomerate, and sandstone sections (30-150 m thick) are most commonly observed where the Maestrichtian section overlies the Samail ophiolite or, in some areas, Hawasina melange. The formation is lithologically similar to the Qahlah Formation [Glennie et al., 1974] and contains the Amqat Laterite Member [Glennie et al., 1974]. Both Lees [1929] and Glennie et al., [1974] have assigned a Maestrichtian age to these clastic rocks underlying the shallow-water limestone.

The thickness and stratigraphy of the Maestrichtian rocks vary from place-to-place, and these rocks crop out only in limited exposures so that detailed regional reconstruction of their original extent and continuity is difficult. Where the Late Cretaceous to Paleocene stratigraphy is preserved, it is clear that there was a period of widespread formation of laterite, mainly on the eroded Samail ophiolite. It is not clear whether the laterite had formed on non-ophiolitic rocks. Variability in the sections over short distances coupled with many local unconformities suggests that Maestrichtian deposition occurred in a tectonically active period. The laterites are interpreted as products of subaerial tropical weathering of the Samail ophiolite which requires significant uplift (>5 km) and concomitant erosion of the ophiolite prior to the laterite-forming event. Late Campanian to Maestrichtian rocks of the Juweiza Formation [Glennie et al., 1974] contain clasts of basic igneous rocks. The Juweiza Formation is found in the subsurface to the northwest of the Oman Mountains and is a thick sequence (>3 km) of flysch that overlaps the time of laterite formation. The presence of these clasts in the Juweiza suggests independently that the Samail ophiolite and Hawasina Group had been uplifted by the time of laterite formation and were shedding debris into a restricted basin southwest of the Oman Mountains.

Conglomerate interbedded with the reworked laterite contain clasts which are predominantly rounded quartzite, gray limestone, friable sandstone, chert, and rare peridotite. The carbonate, chert, and sandstone clasts may be derived from the Hawasina Group. Conglomerate containing Hawasina clasts was deposited on eroded ophiolite, and Hawasina olistostromes conformable to pelagic sediments also occur in

depositional contact on top of the Samail pillow lavas (northern Oman, Tippit and Pessagno, 1979). These facts suggest a source for Hawasina debris which does not exist in the present tectonic stacking of the Oman Mountains where the Samail ophiolite is the uppermost structural unit. Furthermore, synchronous deposition of Maestrichtian age rocks in three places containing Hawasina and Samail debris--Juweiza Formation in a basin beyond the front of the advancing nappes, the Hawasina melange resting directly on top of the autochthon in Wadi Tayin [Tippit, personal communication], and Qahlah Formation unconformably overlying Samail peridotite--requires that the final motion of the Samail nappe can be no older than Maestrichtian.

The final movement of the nappe is significantly younger than the time of oceanic detachment (~90 m.y., Lanphere, 1981) inferred from K-Ar ages of amphibolite beneath the Samail peridotite near Mahlah. Our inferences concerning the Maestrichtian are tentative, as they are based upon mapping in our area and paleontology from similar rocks over widely spaced areas. Further detailed mapping of the distribution both in time and space of the Maestrichtian formations may reveal information critical in understanding the details of nappe emplacement in the Oman Mountains.

2.4 SUMMARY

1. The peridotite section represents the uppermost mantle during the Late Cretaceous and records a history of mantle deformation of two kinds: (a) deformation under subsolidus conditions associated with the spreading axis environment, and (b) deformation associated with detachment in the oceanic environment prior to emplacement upon the

Arabian continental margin. This second deformation is contemporaneous and is related to the contact "freight train" metamorphic slabs exposed discontinuously along the basal thrust contact. The foliation in the metamorphic slabs is roughly concordant to the axial plane foliation of the basal isoclinally folded dunite-harzburgite layers. The detachment deformation occurred initially at very high temperatures because garnet amphibolite is preserved near contacts between peridotite and metamorphic slabs. Pressures at the base of the slab can be estimated using the combined thickness of the gabbro and the peridotite sections. The peridotite section near Ibra has not been repeated by folding or thrusting because large dunite bodies (Wadi Wushad) are not folded (Figure 1), and predetachment dike assemblages preserve a regionally mappable plagioclase stability boundary. Using a conservative thickness of the mantle section (12 km) and crustal section (6 km), the lithostatic pressure at the time of initial detachment was on the order of 6 kb.

2. The peridotite section records a history of melt separation and migration through the upper mantle. Harzburgite represents the depleted residuum of upper mantle melting events. At exposed levels, the harzburgite is not in equilibrium with the parental melts of the oceanic crust, because enstatite never appears on the liquidus of those melts. Dunite, therefore, represents either further depleted residuum resulting from continued partial melting or cumulates (now subsquently deformed) produced by fractional crystallization of olivine from ascending melt bodies within the harzburgite. The relative importance of the two processes has not been established and is significant, as it has bearing upon the initial composition of the ascending melts.

3. Coalescence of the cumulate dunite bodies (now both deformed and undeformed) in the uppermost part of the mantle section (<1 km below the gabbro) marks the transition from the mantle regime dominated by subsolidus deformation (mantle flow) to the lower oceanic crustal regime dominated by crystallization of cumulate gabbro.

4. All of the peridotite section is affected by a post-emplacement low-temperature serpentinization event that cross-cuts all other peridotite structures. The low-temperature nature of serpentinization is supported by the pervasive undeformed cubic fracture set that controls delicate mesh and web structures of the serpentine assemblage chrysotile, lizardite, brucite, and magnetite and the presence of low-temperature Ca-hydroxide springs within the peridotite with a chemistry controlled by the conversion of peridotite to serpentinite.

5. The combined stratigraphy of the gabbro section and limited range of mineral compositions require multiple injections of melt into the magma chamber where accumulation occurs upward from the bottom. The high-level gabbro represents crystallization that occurred at the top of the chamber. The high-level gabbro is in intrusive contact with the majority of overlying diabase dikes and is more differentiated than the underlying cumulates. These relations suggest that the high-level gabbro crystallized away from the central spreading ridge axis area. The field relations all point to the existence of a funnel-shaped magma chamber similar in cross-section to the larger layered continental gabbro intrusions.

6. Plagiogranite is common, although it is not significant volumetrically. It occurs predominantly at the diabase-gabbro contact and is the result of both extreme fractional crystallization and

partial melting of the chamber roof. The occurrence of abundant angular inclusions of hydrothermally-altered diabase in the plagiogranites and its flat, sheet-like morphology attest to mobilization after generation in situ.

7. The sheeted diabase dike complex formed in a region of 100 percent extension over the entire Ibra area and throughout the entire Oman Mountains. The only modern analog is the mid-ocean spreading environment. Most (>90 percent) of the dike complex pre-dates the crystallization of the high-level gabbro and plagiogranite, which indicates that dikes were fed by the part of the magma chamber affected by periodic replenishment.

8. The dike complex is composite with respect to both its intrusive and sea-floor hydrothermal alteration history.

9. The thin (~500 m) volcanic section consists of massive and pillowed submarine lavas, now pervasively altered by low-temperature oceanic hydrothermal activity. The lavas are chiefly microphyric basalts whose microphenocrysts assemblages can be related to the same stage of magma fractionation as that of the Samail cumulus gabbro.

10. Hydrothermal alteration is pervasive throughout the entire oceanic crustal section and is detectable mineralogically along fractures in the cumulate gabbro and mineralogically in the high-level gabbros, diabases, and pillow lavas.

11. Initial detachment of the ophiolite occurred while the base of the peridotite was still hot in a oceanic environment in the Turonian (~90 m.y.).

12. Latest motion on the Samail thrust is tentatively no older than Maestrichtian (71-65 m.y.).

13. The Hawasina Group displays a deformational gradient from south to north changing from a tectonically thickened thrust sequence to thinner more disrupted melange assemblages northward. Oceanic detachment of the still hot Samail nappe (~90 m.y.) produced a thin metamorphic sole of Hawasina rocks at the base of the nappe. Whether the southward movement of the Samail and Hawasina nappes was continuous or discontinuous onto the Arabian continental margin is unresolved. However, we know the final movement occurred in early Maestrichtian time.

CHAPTER 3

FIELD PETROLOGY OF THE SAMAIL OPHIOLITE: MELT-ROCK INTERACTIONS WITHIN THE UPPER MANTLE AND OCEANIC CRUST

3.1 INTRODUCTION

This chapter is divided into two parts unified by the common theme of melt-rock interactions. However, these melt-rock interactions occurred in two drastically different environments: 1) the peridotite, because it everywhere underlies the oceanic crustal section, had to be a zone through which transitory melts passed and where the integrated overall melt-rock ratio was relatively low (<0.5--the ratio of crustal section to peridotite section), and 2) the crustal magma chamber roof where hydrothermally altered diabase and gabbro were in contact with originally anhydrous tholeiitic basalt magma. Based on the geology discussed in Chapter 2, the chamber-roof was apparently a mechanically unstable zone, and this led to considerable piecemeal stoping of the overlying roof rocks, and H_2O was thus added to the high-level gabbro magma as the stoped blocks were dehydrated. In this environment, the melt-rock ratio (between the stoped blocks and melt) was much greater than one. In this first part of the chapter, the peridotite section will be discussed in terms of crosscutting relationships between the host-rock harzburgite and bodies of dunite, orthopyroxenite, websterite, and gabbro. In the second part of the chapter, the characteristics of the crustal magma chamber will be discussed in some detail, particularly with respect to the nature of the chamber roof and the origin of the discontinuous bodies of plagiogranite that are found at the roof contact.

3.2 GENERAL DESCRIPTION OF THE PERIDOTITE SECTION

3.2.1 Overview

The Samail peridotite exposed between Wadi Tayin and the crest of Jabal Dimh crops out over an area exceeding 700 km^2 within the map area. Over the entire Oman Mountains, peridotite (exposed over 9000 km^2) is the predominant member of the Samail ophiolite sequence. In order to place the enormous size of the Samail peridotite into perspective, the total areal extent of five of the best documented peridotites of North America is approximately 3,000 km^2, with the Trinity peridotite [Quick, 1981] contributing 2,100 km^2 to that figure. The Burro Mountain peridotite [Loney et al., 1971], with less than 15 km^2, can be contained within the area of a single large dunite body shown in Figure 3-1. In addition to its enormous size, the Samail peridotite can be studied in the context of the total geologic setting, a perspective not easily attained elsewhere.

The purpose of this section is to utilize the geologic setting of the peridotite in order to interpret its gross features as the result of partial melting, plastic flow, and reaction with the ascending melts that produced the overlying oceanic crustal section, all of which occurred at a depth of 100 km or less in the upper mantle. The discussion presents the results of 2.5 months of field mapping, and is an expansion of Section 2.2.3 of Chapter 2 and the work of Boudier and Coleman [1981]. The results presented here are preliminary and represent the formulation of a working hypothesis which will be tested during future work on the peridotite in collaboration with R.G. Coleman and F. Boudier.

3.2.2 Stratigraphic thickness

The Samail ophiolite peridotite section exposed along the Ibra transect is a 9 to 15 km thick terrane with a polymetamorphic history indicating more than one period of deformation and mineral crystallization. The section is not homogeneous, and heterogeneities are marked by changes in style of deformation, distribution of dunite both vertically and along strike, and mineral assemblages in dikes. This peridotite "stratigraphy" is consistent with the interpretation that the peridotite section is a single thrust sheet that has not been imbricated in any way.

The thickness of the peridotite section is difficult to ascertain for the following reasons: 1) The present-day basal thrust discontinuity truncates ophiolite stratigraphy with the thrust surface rising to the southeast. This observation precludes using the basal thrust contact attitude for establishing stratigraphic thickness. 2) Extrapolating the dip of the gabbro-peridotite section over horizontal distances exceeding 20 km must be done with caution because recent gentle east-west folding may be difficult to detect in the harzburgite section, whose foliation has a northerly trend and dips steeply. Nevertheless, the presence of a basal harzburgite-dunite sequence, a mappable plagioclase-in (occurrence of gabbro) boundary, and extremely large, NW-trending discordant bodies of dunite all suggest that folding and/or repetition by thrusting is not a serious problem (Figure 3-1).

Using approximately a 50° dip for the section east of Wadi Wushad gives a calculated thickness of peridotite close to 12 km. For the west side of the map area, a dip of approximately 35° gives a peridotite thickness approaching 15 km. A traverse through the village

Figure 3-1. Maps showing distribution of crosscutting dunite, gabbro and pyroxenite bodies and foliation within the tectonite peridotite section. This figure is from Boudier and Coleman [1981] and is based upon Bailey et al. [1981]. Notice that discordant dunite bodies trend predominantly northwesterly. Gabbro dikes are absent in the lower third of the tectonite section.

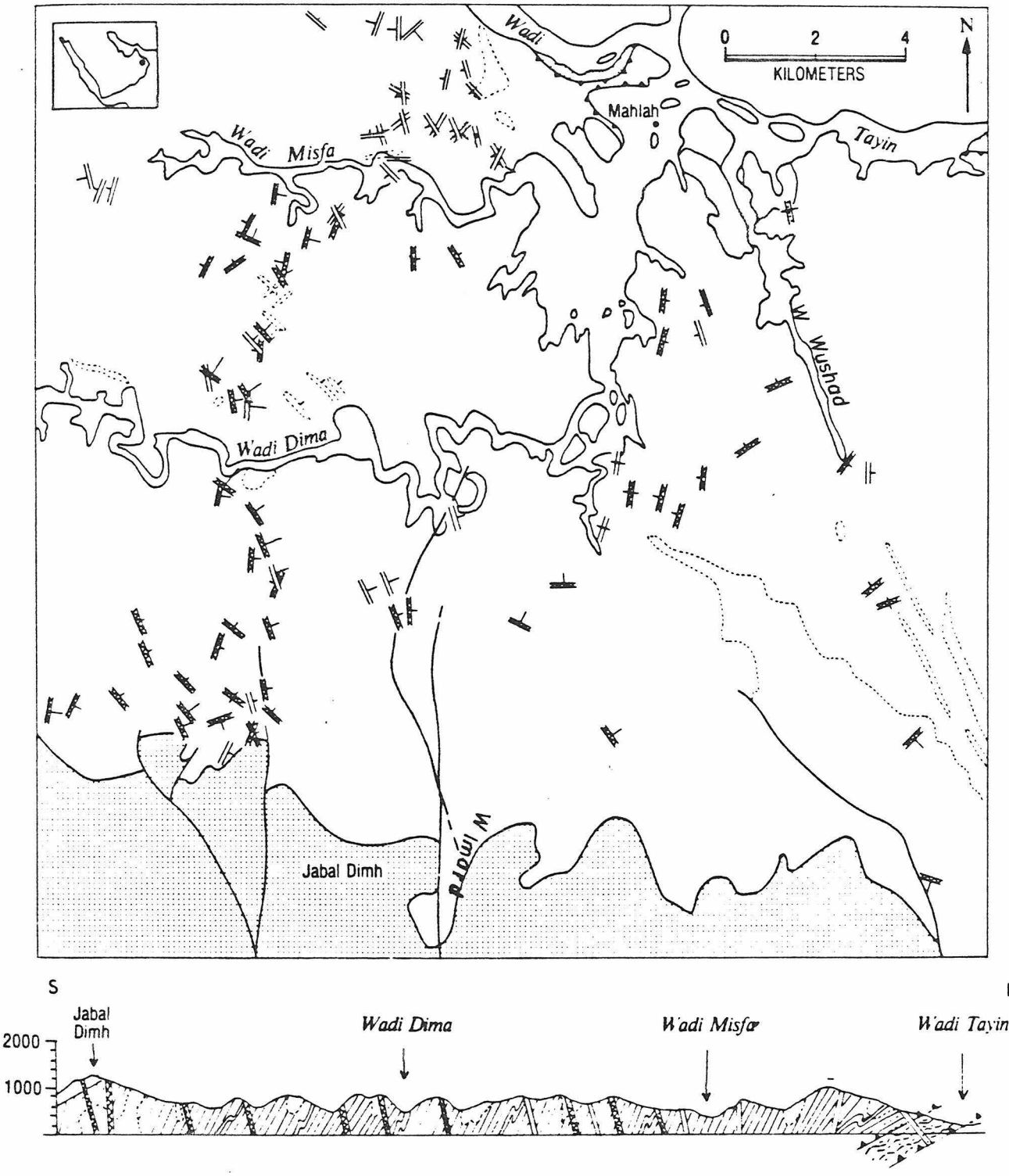
Wadi
0 2 4
KILOMETERS
N
Mahlah
Wadi Misfa
Tayin
W Wushad
Wadi Dima
W IMOTA
Jabal Dimh
S
N
Jabal Dimh
Wadi Dima
Wadi Misfa
Wadi Tayin
2000
1000

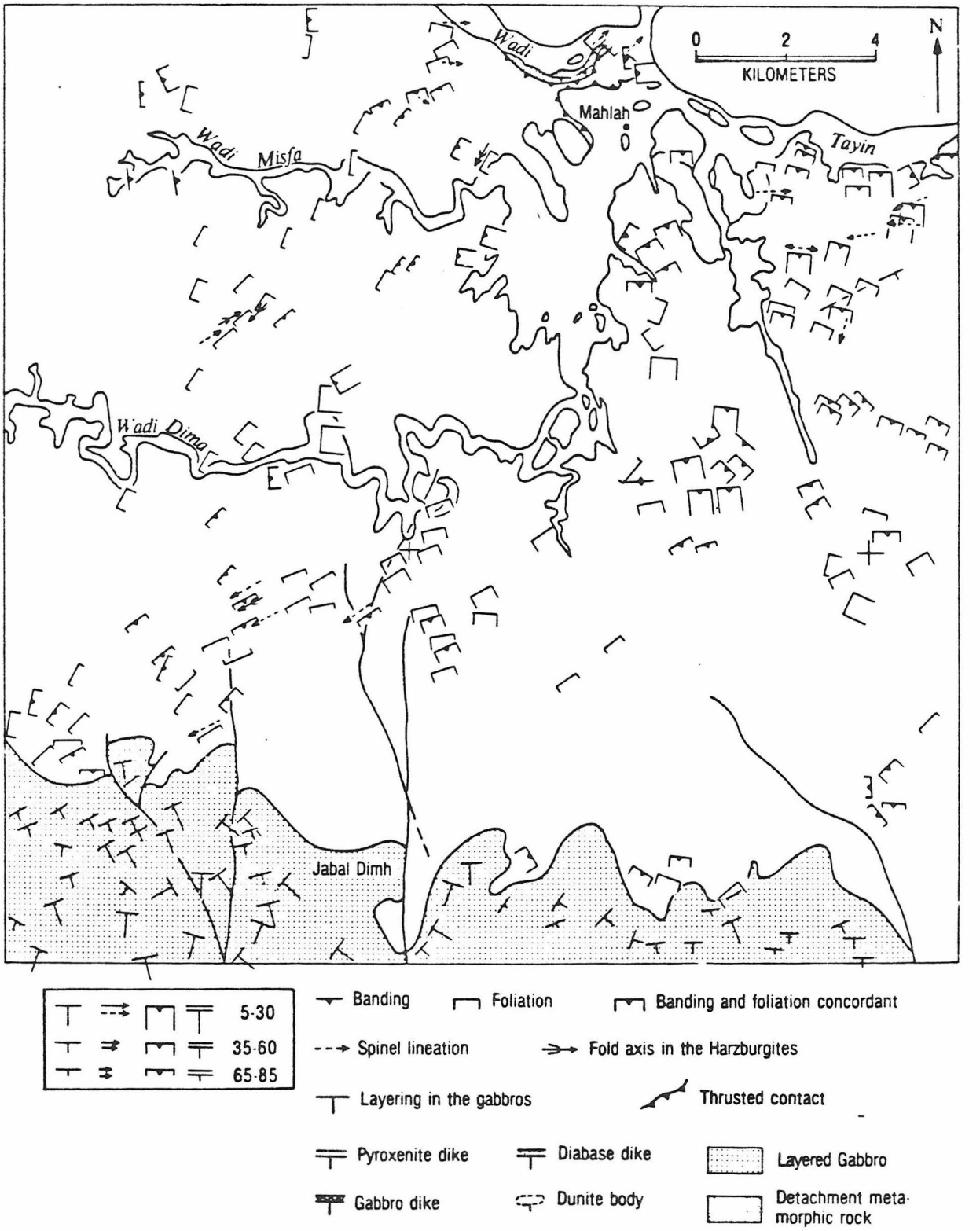
0 2 4
KILOMETERS
N
Wadi
Mahlah
Wadi Misfa
Tayin
Wadi Dima
Jabal Dimh
5-30
35-60
65-85
Banding
Foliation
Banding and foliation concordant
Spinel lineation
Fold axis in the Harzburgites
Layering in the gabbros
Thrusted contact
Pyroxenite dike
Diabase dike
Layered Gabbro
Gabbro dike
Dunite body
Detachment metamorphic rock

of Mahalah to Wadi Imard gives a minimum thickness of approximately 9 km. Assuming a uniform 8 km thickness of overlying oceanic crust, the 5 kb isobar is exceeded in most traverses. Pressure information calculated by stratigraphic arguments constrains the approximate position of the cotectics along which the melts (whose crystallization products produced the crosscutting features described below) crystallized.

3.2.3 Basal harzburgite-dunite zone

The basal zone of the peridotite is an isoclinally folded harzburgite-dunite layered sequence (up to approximately 4 km thick) where all structures have been transposed into the foliation plane. Locally at its base, the isoclinally folded peridotites are mylonites [Boudier and Coleman, 1981] and are in contact with the high-temperature metamorphic aureole rocks (Fig. 3-2a) described in detail by Ghent and Stout, [1981]. The mylonitization is interpreted as being related to the initial stages of detachment of the Oman ophiolite under high deviatoric stress between 1 and 2 kb. The fabric in the peridotite mylonite is concordant to the fabric in the underlying amphibolite and piedmontite-bearing quartzite [Boudier and Coleman, 1981]. In addition, both the transport direction and sense of shear are the same for the basal peridotite and the metamorphic aureole rocks [Boudier and Coleman, 1981]. However, most of the isoclinally folded harzburgite-dunite section is not a mylonite, suggesting that mylonitization was superimposed over previously folded rocks. Upward in the section, the intensity of deformation and transposition decreases and through a gradational contact over several hundreds of meters, the basal section gives way to the more massive harzburgite.

Figure 3-2.

a) Contact between harzburgite-dunite mylonite and garnet amphibolite exposed 1.5 km north of Mahlah along Wadi Tayin. White pods (15cm-long axis) of rodingite are discontinuously present along the contact suggesting more than one stage of movement.

b) Phyllites exposed ~125 meters below the amphibolite-peridotite contact. A sharp discontinuity of metamorphic grade going from amphibolite to low-grade phyllite suggests a tectonic break between the phyllite and the amphibolite.

c, d) Isoclinally folded harzburgite-dunite section near the base of the Samail thrust. Harzburgite interlayered with dunite has the same modal mineralogy as the overlying massive harzburgite suggesting that metamorphic differentiation was not important in the formation of these rocks.

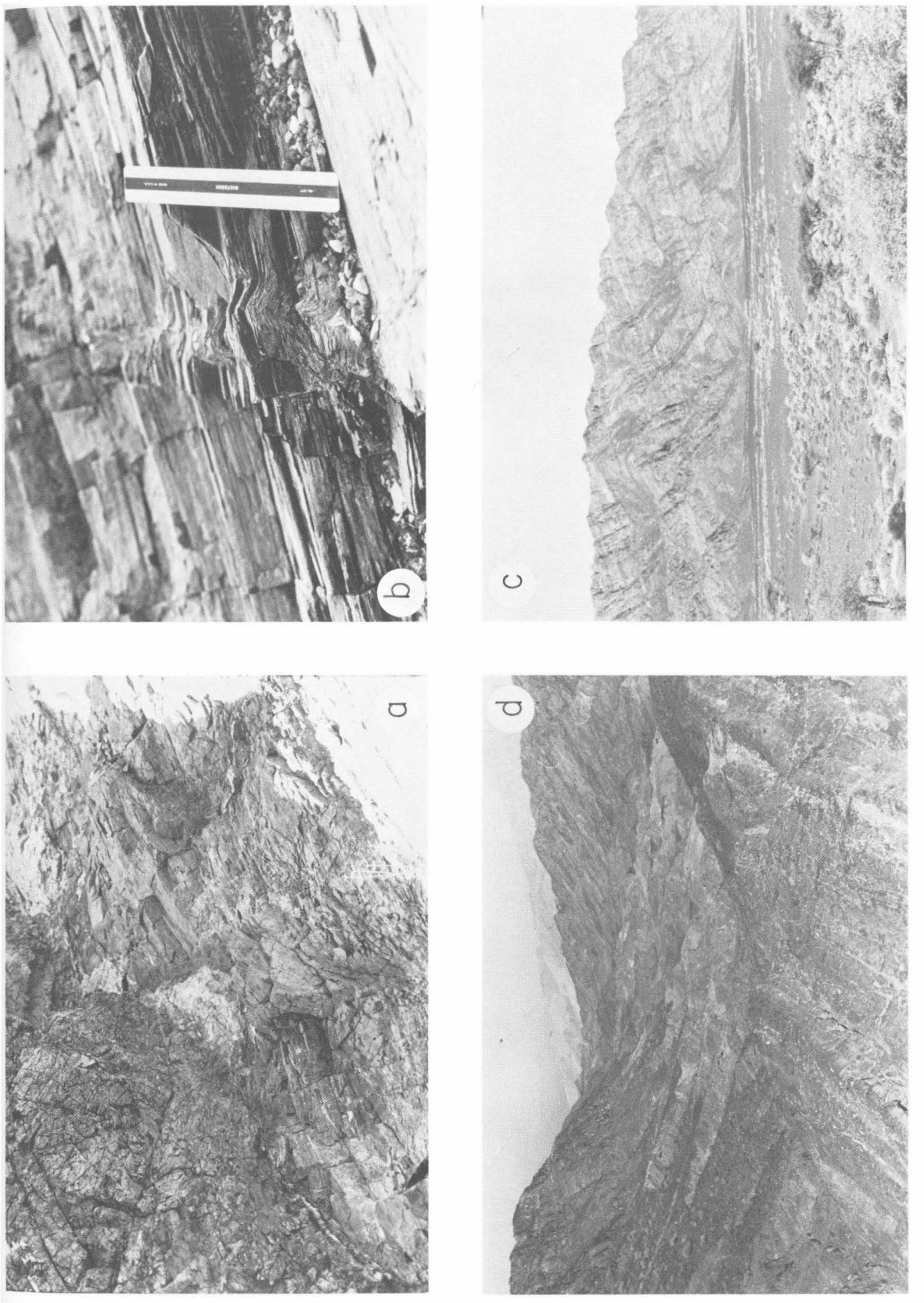
a
b
c
d

3.2.4 Concordant dunite, orthopyroxenite, and websterite within the harzburgite

Harzburgite is the most common rock type within the Samail peridotite. Its composition is shown on the forsterite-diopside-quartz plane of the quaternary system that also includes plagioclase (Fig. 3-7). Clinopyroxene is rarely present and modal olivine >orthopyroxene>>spinel. The harzburgites are uniform chemically with both the olivine and orthopyroxene exhibiting a narrow range of composition (Fo_{90-91}; En_{90-91} [Boudier and Coleman, 1981]). A tectonite fabric is developed in all of the harzburgite and, with the exception of mylonitic zones at the base, this suggests deformation under low deviatoric stress and at high temperature [Boudier and Coleman, 1981]. Throughout the harzburgite section, the layers of dunite and orthopyroxenite are isoclinally folded, with axial planes parallel to the spinel foliation (Figure 3-3). These features represent at least the second oldest features recognizable in the harzburgite (the first event being the formation of the harzburgite itself). If the layers were originally crosscutting, their orientation has been transposed by subsequent deformation. Neither the dunite (ol + chr) nor the orthopyroxenite (opx + ol + sp) bands have enstatite- or olivine-rich walls, and the modal mineralogy of the host harzburgite is no different than that of the overlying massive harzburgite, suggesting that metamorphic differentiation and hydrothermal alteration [Himmelburg and Loney, 1973; Dungan and Ave Lallemont, 1977] are not as important as magmatic processes in the origin of these bands. Their origin is attributed to deeper mantle processes which will be discussed below.

Figure 3-3.

a) Isoclinally folded dunite layer in a massive harzburgite cliff ~ 150m high near the head of Wadi Khafifah.

b) Isoclinally folded websterite dike near Wadi Misfah crosscutting harzburgite tectonite.

c) Discordant dunite dike with a chromite layer crosscuts the harzburgite whose foliation parallels the edge of the scale. Note olivine grains within the crosscutting dunite dike are elongated parallel to the foliation. The gabbro dike shows no preferred mineral orientation and cuts the harzburgite foliation at a higher angle than the dunite dike.

d) Discordant gabbro dike south of Wadi Misfah exhibits a lineation parallel to spinel lineation.

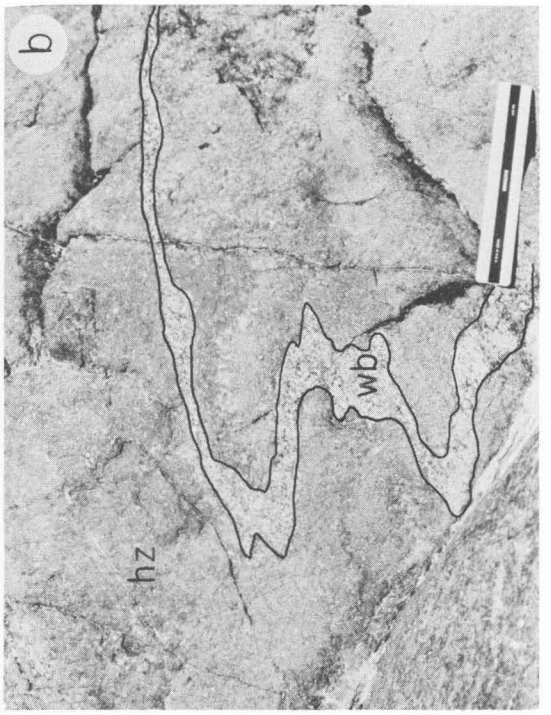
b
hz
wb

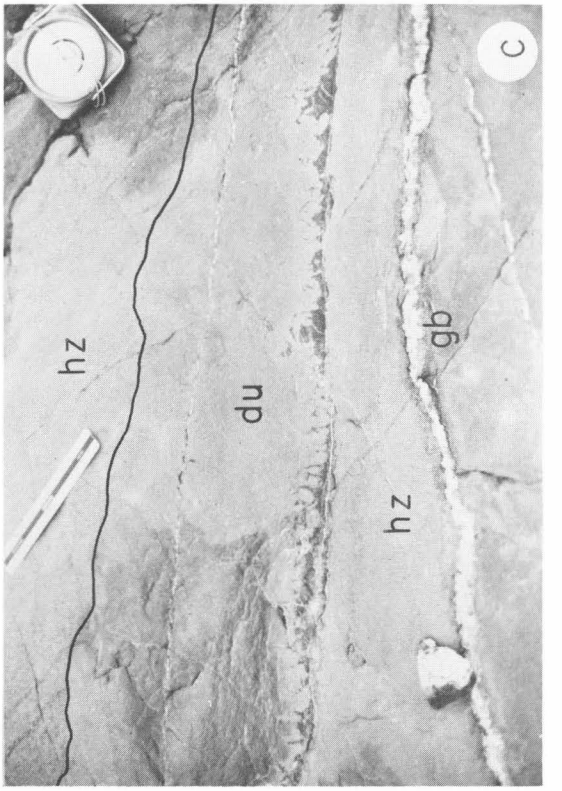
c
hz
du
hz
gb


a


d

Between the top of the basal zone and the appearance of the gabbro dikes that crosscut the harzburgite, websterite occurs as isoclinally folded layers that typically thicken at the hinges of the folds (Fig. 3-3b). Although the websterite is isoclinally folded, no tectonite fabric was observed in the field, suggesting that it crystallized from a melt phase that was present during the deformation. Moving upward in the section towards the horizon where gabbro dikes appear, the isoclinally folded websterite dikes decrease in abundance, and discordant websterite dikes appear. These discordant dikes commonly follow conjugate fracture sets. Mineralogically and chemically [R.G. Coleman, pers. com.], there is no difference between the concordant and discordant websterites. The chemical similarity of the two kinds of websterite dikes and their crosscutting relation to the earlier-formed orthopyroxenite bands and dunite layers suggests that the last deformation in the isoclinally folded zone at the base of the ophiolite occurred at its present structural level of exposure and probably post-dates the formation of the concordant dunite and orthopyroxenite layers occurring in the upper part of the peridotite section.

3.2.5 Discordant features within the harzburgite

Crosscutting the harzburgite above the top of the isoclinally folded basal zone, are discordant dunites (cm to km scale), websterites (cm scale), and gabbros (cm scale). The gabbro dikes are confined to the upper two-thirds of the section and the websterites become less abundant once the plagioclase-bearing dikes appear. All of these discordant bodies, regardless of their size, occupy conjugate fracture sets with the larger (up to km size) dunite bodies preferring the NW orientation (Figure 3-1). Inasmuch as all of the discordant bodies occupy one

Figure 3-4.

a) Large discordant dunite body (~10m thick) east of Wadi Wushad approximately 4 km south of Wadi Tayin. This dunite body contains abundant partially-dissolved inclusions of harzburgite.

b) Dunite-harzburgite banding exposed about 3 km west of Al Hisn. The layering here is concordant to the foliation defined by spinel crystals.

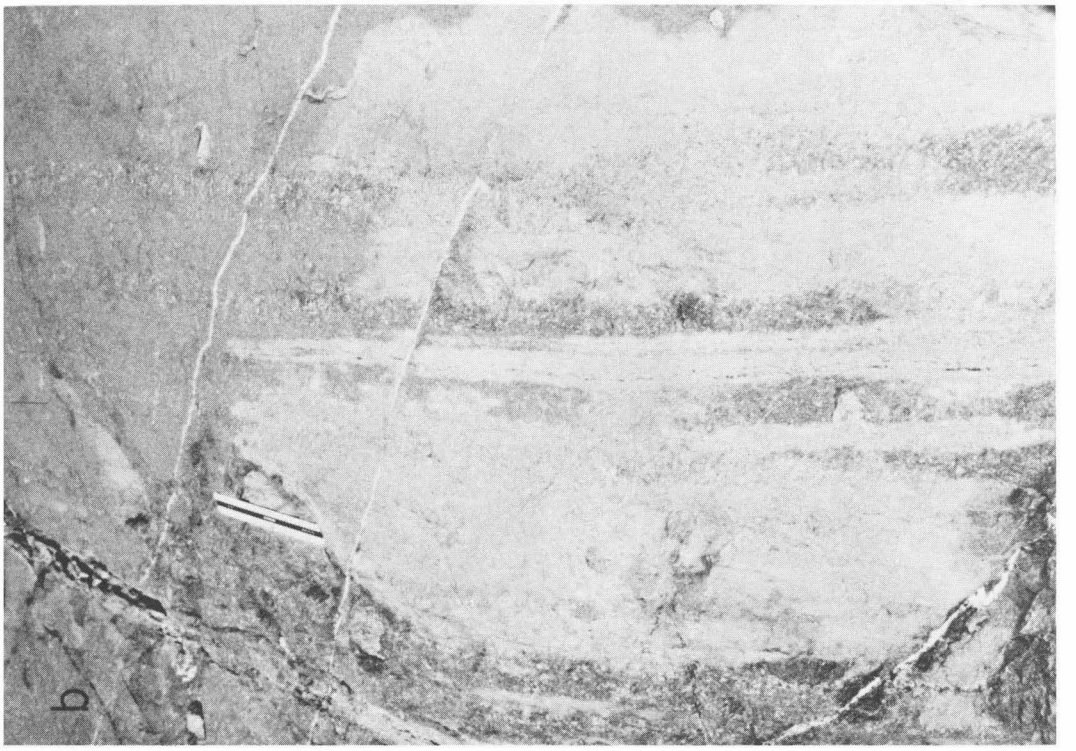
b

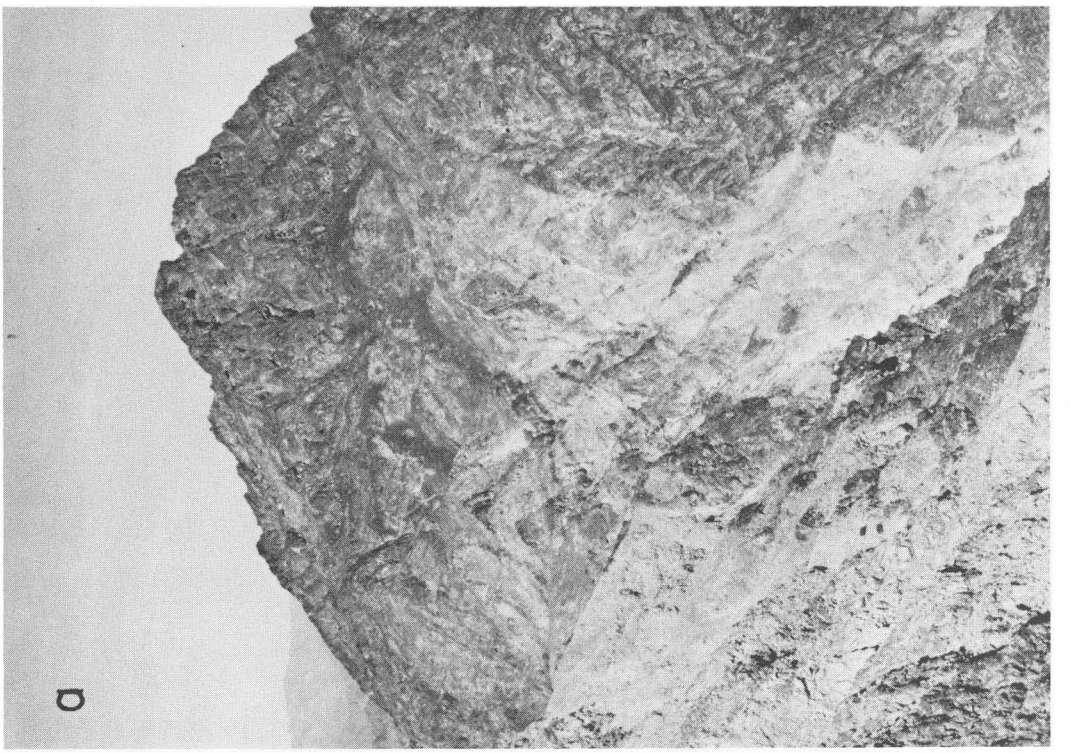
a

Figure 3-5.

a) Northern terminus of the largest discordant dunite body that crops out near the eastern boundary of the map strip. Notice dikes of dunite streaming into the surrounding harzburgite.

b) Discordant dunite body exposed along the traverse between Wadis Misfah and Dima. Small shows of chromite were associated with this dunite body approximately six kilometers below the peridotite-gabbro contact.

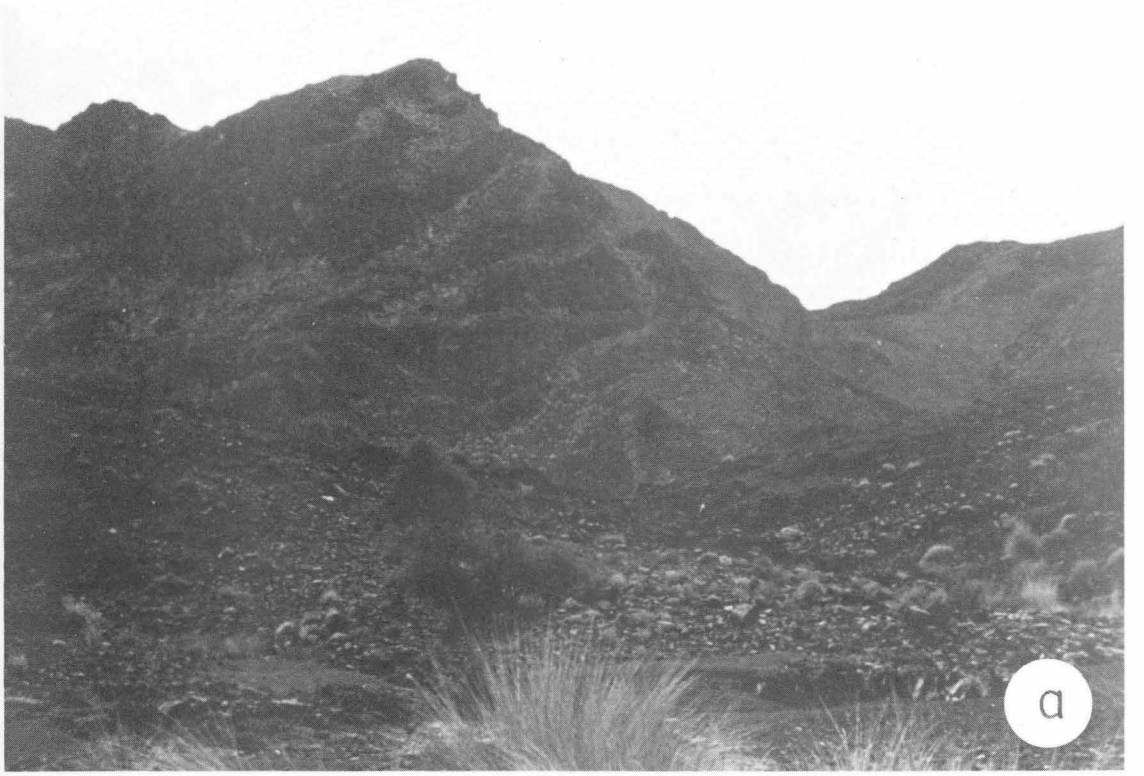
a


b

of the conjugate sets, they are interpreted to have formed at their present structural level of exposure at pressures less than 5 kb. Subsequent to their formation, uniform deformation affecting harzburgite rotated the discordant bodies to their present orientation relative to the peridotite-gabbro contact, with the earliest-formed bodies exhibiting the greatest amount of rotation towards the harzburgite foliation [Boudier and Coleman, 1981].

3.3 DISCUSSION OF THE FIELD DATA

3.3.1 Relation between harzburgite and oceanic crustal melts at low pressure

The crosscutting and concordant features discussed above and summarized in Table 3-1 can be interpreted when two facts are considered: 1) orthopyroxene is never an early cumulus phase in the overlying cumulate gabbros and is virtually absent in the southern Oman Mountains, and 2) orthopyroxene drops off the liquidus of tholeiites in experimental studies [Stolper, 1980, and Green et al., 1979] at pressures less than 10 kb [Figure 3-6]. Combining the field observations and corroborating experimental work requires that all contacts between harzburgite and the ascending melts (which produced the overlying cumulates) are boundaries where magmatic reactions occur. Because the melt and harzburgite are not in equilibrium, the reaction relationship between liquid and wall-rock results in some combination of crystal accumulation in the dike and dissolution of orthopyroxene in the harzburgite (incongruently at low pressures probably less than 5 kb [Stolper, 1980] and by direct solution into the melt at higher pressures). The various structural

TABLE 3-1 CROSSCUTTING RELATIONS IN THE SAMAIL PERIDOTITE

Rock type	Scale	Foliation	Remarks	Mineralogy	Relative Age*
diabase	m	discordant	rare,also cuts metamorphic aureole underlying Samail thrust		5
basal mylonite	m to ?	concordant to foliation in contact aureole	dies out up section before top of hz-du zone		4
gabbro	cm	discordant	conjugate dikes	ol,cpx,plag±sp opx,cpx,plag±sp	3c
clinopyroxenite	cm	discordant	conjugate dikes	cpx,ol	3b
websterite	cm to m	discordant	conjugate dikes	cpx,opx,sp,ol	3b
dunite	cm to km	shape of bodies invariably discordant; internal foliation concordant to discordant	occupy conjugate dike sets; plag types near the top of the peridotite section	ol,sp; ol,sp±cpx±plag	3b
websterite	cm	corcordant with no tectonite fabric	often concentrated at the hinges of folds	cpx,opx,ol, sp	3a
orthopyroxenite	cm	concordant	isoclinally folded	opx,ol,sp	2
dunite	cm to 10m	concordant	isoclinally folded	ol,sp	2
harzburgite	km	tectonite fabric	concordancy of all other features measured relative to harzburgite foliation	ol,opx,sp	1

*Rock types showing the same number designation are mutually crosscutting or virtually the same age. The lower case letter indicates which rock type would be more likely found crosscutting the other rock types under the same number category.

elements in the peridotite can be related to melts moving up through the upper mantle using a quaternary system and projecting from plagioclase onto the plane diopside-olivine-silica [Quick, 1981]. In many respects the concepts employed in the analysis of water-rock interactions (see Chapter 4) can be employed in magma-rock interactions. In the following section, aspects of magma-rock interactions in the upper mantle are discussed in qualitative terms, and thus represent preliminary ideas which must be tested by further field observations.

3.3.2. Experimental constraints on the composition of melts parental to tholeiites

Experimental work [Green et al., 1979 and Stolper, 1980] has shown that the four-phase saturation point (ol-opx-cpx-melt) is very sensitive to pressure [Figure 3-6]. As in the model oxide system [see Kushiro, 1979], and recently confirmed for the natural system, the ol-opx peritectic line moves away from the silica corner and crosses the diopside-enstatite join becoming a cotectic line which continues to move towards the diopside-olivine join with increasing pressure. Thus, in reverse, melts in equilibrium with harzburgite at high pressure become olivine-saturated at low pressure. Parental liquids capable of fractionating to the 1 atmosphere cotectic compositions exhibited by tholeiites are required to be picritic [O'Hara, 1968; Green et al., 1979; Stolper, 1980].

On the projection from plagioclase (Figure 3-7), undepleted lherzolite (pyrolite of Ringwood, [1966]) and harzburgite both plot near the olivine-enstatite join close to the olivine corner. A straight line connects residual harzburgite, lherzolite (pyrolite), and initial melt; the composition of the melt lies at the apex of a 3-phase triangle connecting olivine, orthopyroxene, and melt (Figure 3-7). The bulk

Figure 3-6

a) Phase relations for the system plagioclase-diopside-forsterite-silica using the projection method of Walker et al. [1979]. The 1 atm liquid lines of descent are from Walker et al. [1979]. For pressures other than 1 atm, the four-phase points are from Stolper [1980]. The cotectic lines are schematically sketched between the experimentally determined multiple saturation points and calculated eutectic points for the olivine-orthopyroxene system.

b) On the same diagram from Stolper [1980], the field of MORB is outlined by the dot pattern. Each dot represents an analysis from the catalogue of Walker et al. [1979]. The triangles represent data from the Samail ophiolite diabases [Pallister, 1981]. The liquidus relations were determined by Stolper [1980].

a)

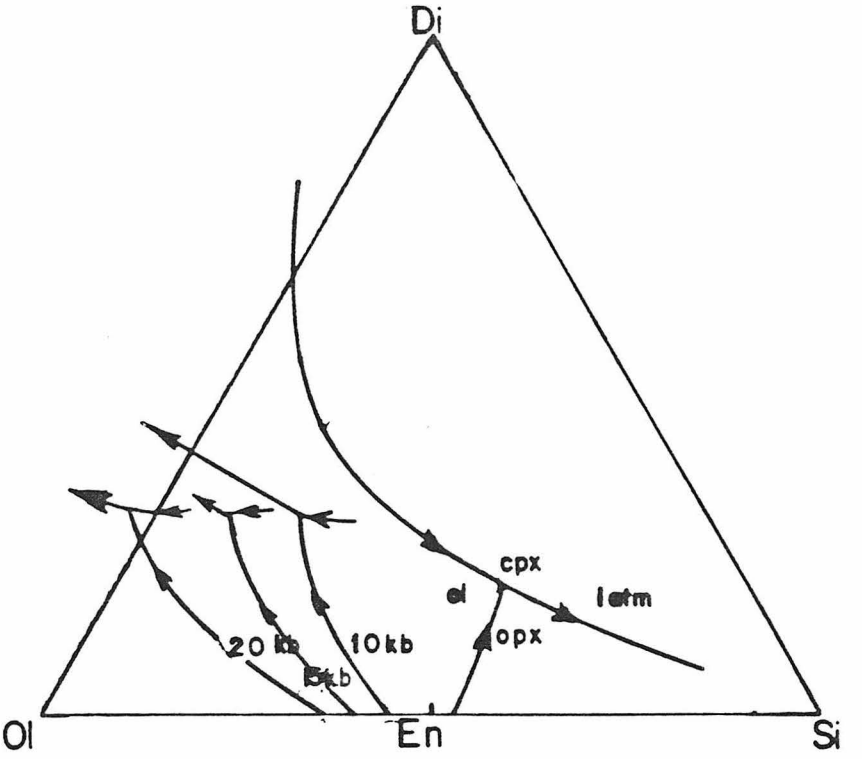
Di
cpx
ol
1 atm
opx
20 kb
10 kb
5 kb
Ol
En
Si

b)

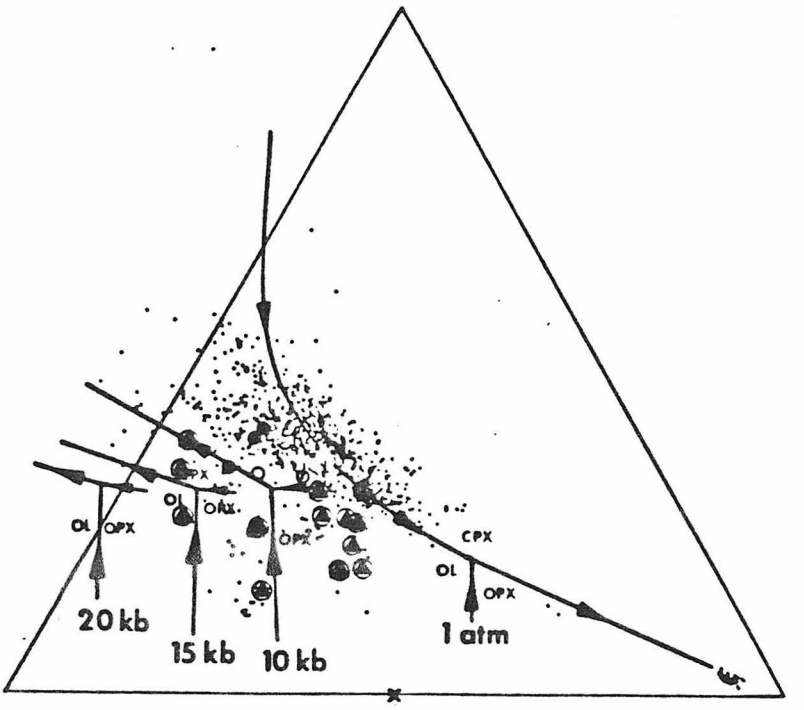
OL
OPX
20 kb
15 kb
10 kb
CPX
1 atm

composition of the system is closer to the harzburgite composition because melting of less than 30% is needed to produce tholeiites. If lherzolite is typical of the mantle from which melts parental to tholeiite are extracted, then tie-lines connecting harzburgites, lherzolites, and melts generate a field where melt separation last occurred (Figure 3-7). Realizing that the experimental work in this region of phase space is not extensive, the pressure of last equilibration of harzburgite with melt phase had to occur at $10<P<20$ kb. Therefore, the experimental work to date corroborates the field interpretation that the harzburgites in Oman were never in equilibrium with the melts that produced the overlying oceanic crustal section at any level in the present-day exposure (at $P<6$ kb).

3.3.3 Early ("higher pressure") concordant bodies in harzburgite

The concordant dunites and enstatite-rich layers can be explained by early "high" pressure crystallization in either the two-phase (olivine-melt) field or along the olivine-orthopyroxene cotectic. Upon separation of melt from harzburgite, the melt rises up through previously depleted harzburgite. As pressure is lowered, the four-phase field moves towards the diopside-silica join. Initially the melt and harzburgite are near the same temperature. If the melt-to-rock ratio is small, the harzburgite reacts with the melt and moves toward the olivine corner, while the melt moves to the olivine-orthopyroxene cotectic producing the orthopyroxene-rich concordant layers within the massive harzburgite (Fig. 3-8). Because of the curvature of the cotectic lines towards the orthopyroxene composition (Fig. 3-7), cumulates produced from crystallization along the ol-opx cotectic have a high modal

Figure 3-7. Melting relations between pyrolite, harzburgite and the 3 ϕ saturation field as determined by Stolper [1980]. The apex of the 3 ϕ triangle connecting orthopyroxene-olivine-melt moves from left-to-right as pressure decreases. Assuming an initial source composition of pyrolite [Ringwood, 1966] and harzburgite compositions from Oman leads to the plausible conclusion that melt segregation in the Samail ophiolite probably occurred at depths exceeding 30 km.

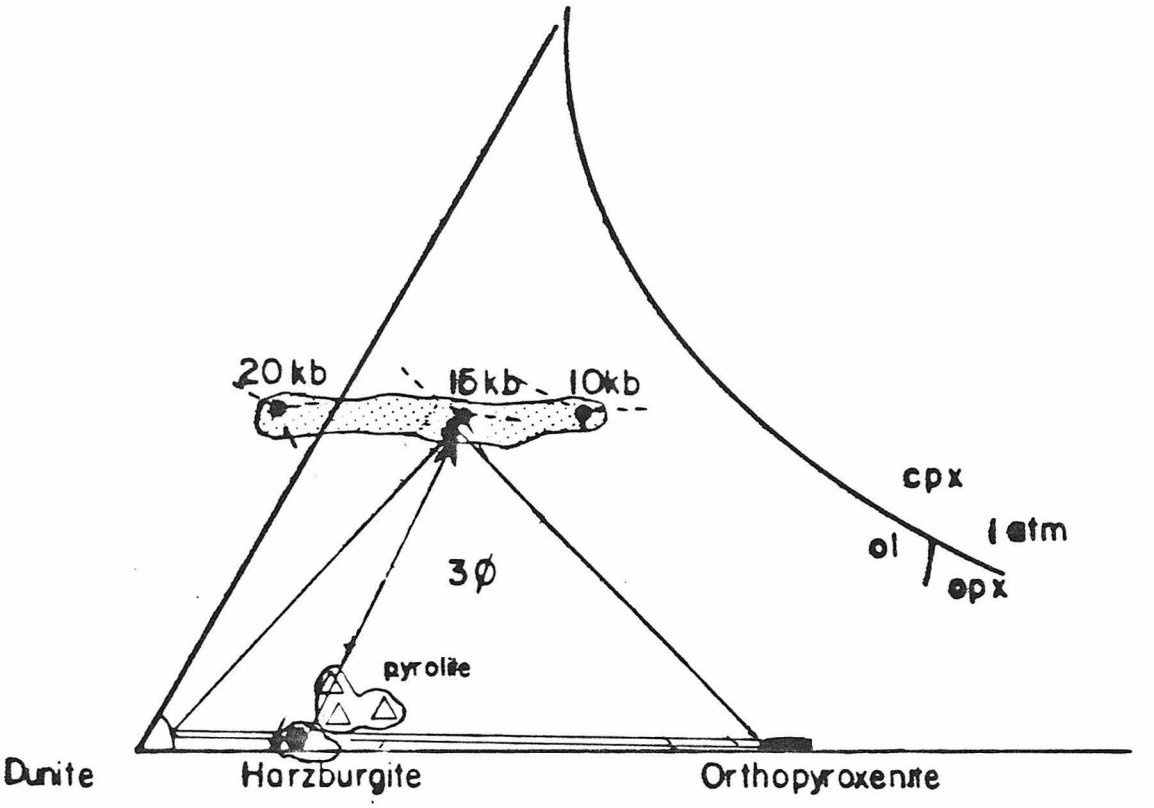
20 kb
15 kb
10 kb
cpx
1 atm
ol
opx
3ϕ
pyrolite
Dunite
Harzburgite
Orthopyroxenite

proportion of enstatite (Fig. 3-8). The cm scale and mineralogy of these structures is suggestive of a regime with a small melt-rock ratio. In contrast, the concordant dunites are generally much larger features (up to several meters thick) and represent a much larger melt-rock ratio. The concordant dunites are interpreted as folded dikes which served as early conduits through which ascending melts traveled. Because the flow rate was high, crystallization of olivine and some reaction at the dike boundaries insulated the melt from the harzburgite and the melt never reached the olivine-orthopyroxene or olivine-clinopyroxene cotectics. The scale and concordant nature of these dunites and orthopyroxenites, and their occurrence within the same outcrops suggest that their origin is most easily explained by this diking mechanism invoking differing melt-rock ratios. Inasmuch as the crystallization occurred during the early stages of the tectonite history, the initial diking relationship has been transposed by the subsequent deformation.

The occurrence of similar concordant dunite and orthopyroxene-layers has been extensively documented in other peridotite bodies such as the Trinity peridotite [Quick, 1981], the Lanzo Massif [Boudier, 1978], the Rhonda Massif [Obata, 1977], and the Beni-Bouchera peridotite [Kornprobst, 1969]. Phase chemistry from all of these bodies suggests an origin deep within the mantle in the garnet-to-spinel lherzolite facies, at depths that may have exceeded 60 km. By analogy, it is concluded that the concordant features within the Samail ophiolite above the basal harzburgite-dunite zone also all formed at depths probably greater than 20 km (the depth reached by present-day exposure) and possibly much deeper. The scale and timing of these features rule

Figure 3-8.

a) The olivine corner of the plane olivine-diopside-silica is used to illustrate paths of the melt and harzburgite under different reaction regimes. In a regime of high melt-rock ratio, the melt remains in the olivine field and crystallization of olivine causes movement directly away from the olivine corner. If reaction occurs with the harzburgite, the wall-rocks move toward the dunite corner while the melt moves toward the olivine-orthopyroxene cotectic. The actual direction the melt takes will be related to the amount of heat available from the crystallization of olivine and the contrast in temperature between the harzburgite and melt.

b) Once the melt reaches the olivine-orthopyroxene cotectic, upon cooling all of these two-phase cumulates will be very rich in modal orthopyroxene. A combination of the paths shown in (a) with crystal fractionation along cotectics indicates that the whole MORB suite can be generated by different reaction crystallization paths of ascending picritic liquids--a conclusion reached by Stolper [1980].

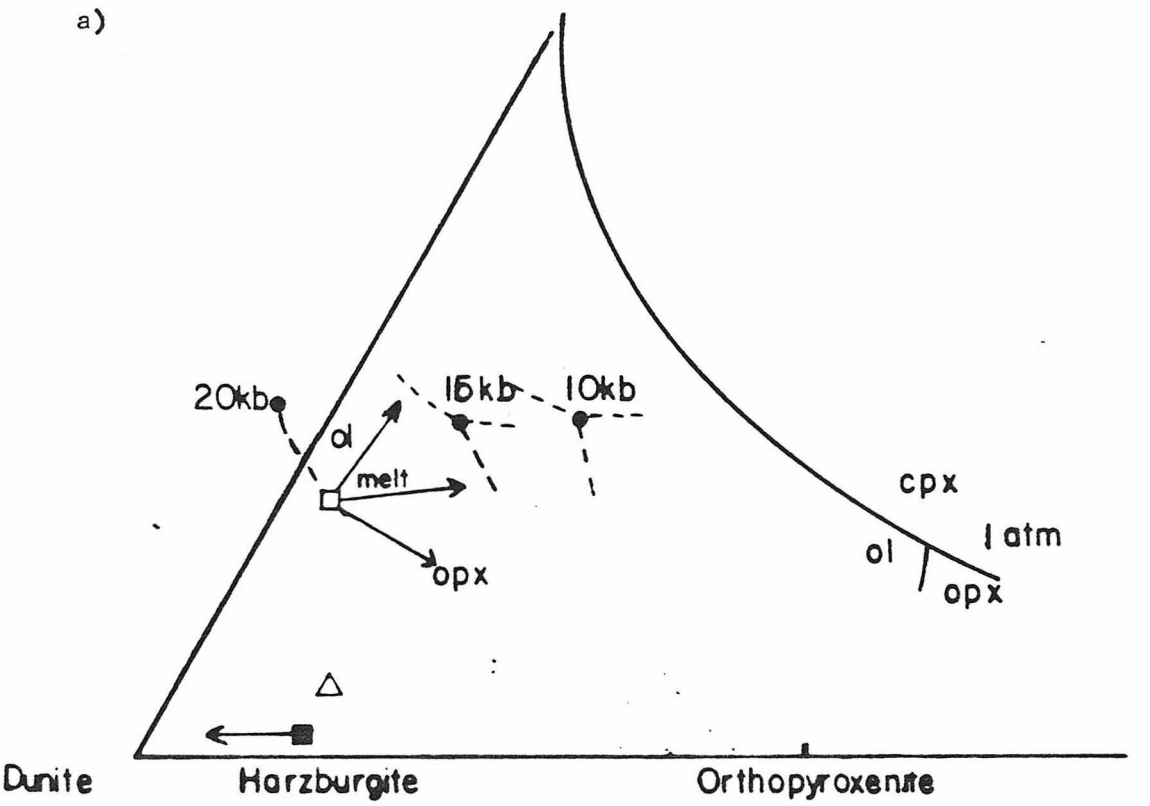
a)
20kb
15kb
10kb
ol
melt
opx
cpx
1 atm
ol
opx
Dunite
Harzburgite
Orthopyroxenite

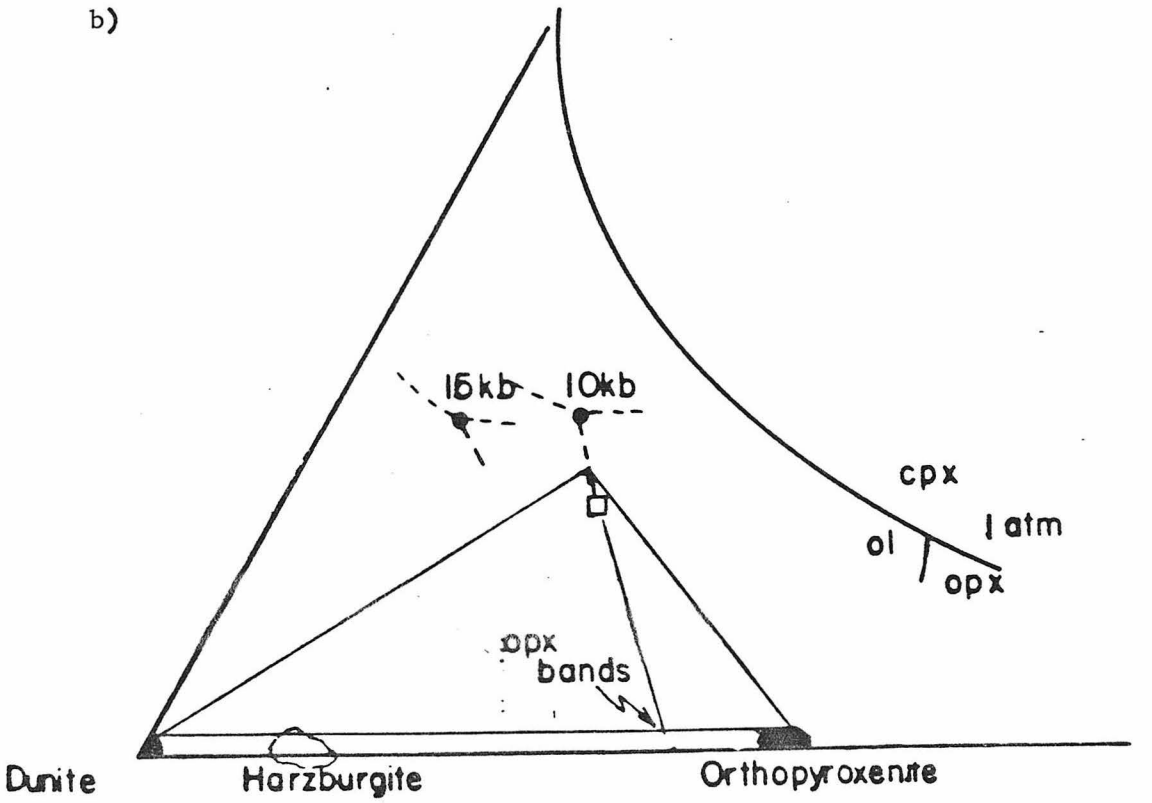
b)
15kb
10kb
cpx
1 atm
ol
opx
opx
bands
Dunite
Harzburgite
Orthopyroxenite

out the general classes of hypotheses concerning origin by metamorphic differentiation [Himmelburg and Loney, 1973] and hydrothermal alteration [Dungan and Ave Lallemont, 1977] for these concordant features.

3.3.4 Discordant bodies (shallow-level features)

The above explanation can readily be applied to all of the dunite bodies throughout the harzburgite section, with the largest and least deformed dunites occupying the last conduits through which melts passed. Support of this interpretation comes from the field occurrences of chromite. Spinel occurs as an accessory mineral in both harzburgite and dunite. Spinel from the dunites occurs as chromite, and the association of dunite and chromite has been recognized the world over in ophiolitic peridotites [Thayer, 1964]. Thayer originally recognized the cumulate textures in chromites and concluded that all of the dunites and harzburgites associated with chromite deposits were crystal cumulates in his mafic-magma stem hypothesis [Thayer, 1963]. Recently Cassard et al. [in press], in a study of New Zealand chromite deposits, have shown a correlation between chromite composition and concordancy of dunite bodies (Figure 3-9). High Cr/Al chromites go hand-in-hand with concordant dunite bodies, with the lowest Cr/Al content in undeformed chromites from crystal cumulates of associated stratiform layered intrusions. The more primitive characteristics in the concordant bodies again suggests the existence of a time-depth-composition relationship in the peridotite.

Moving upward in the section, larger discordant dunite bodies are observed which exhibit various degrees of internal deformation or alignment parallel to the regional foliation of spinel in the harzburgite.

Figure 3-9. The relationship between chromite composition in dunites and concordancy to the regional harzburgite foliation. Notice the more primitive chromites are generally found in the concordant dunites. The diagram is from Cassard *et al.* [in press].

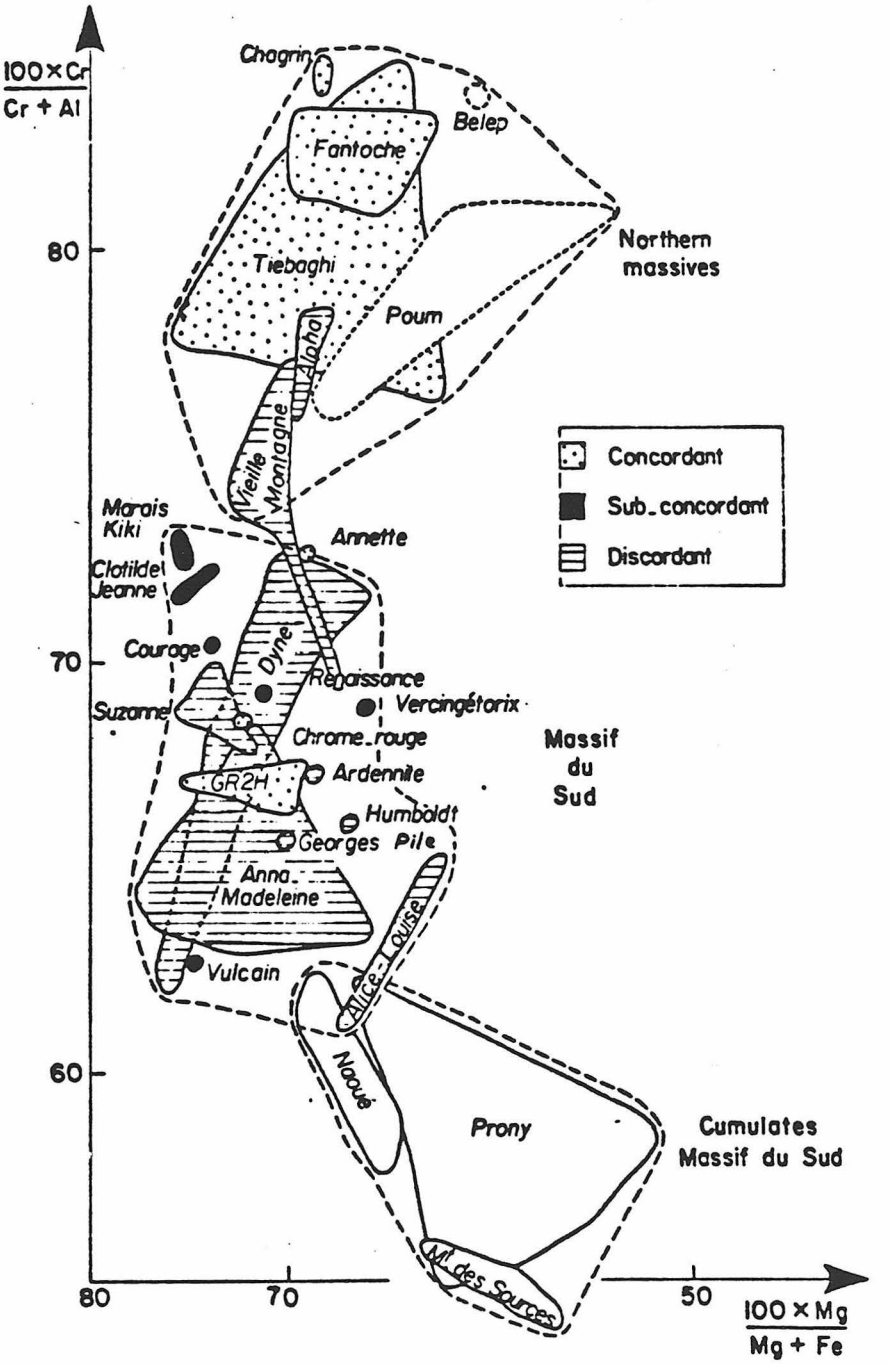
100 × Cr / Cr + Al
80
70
60
80
70
50
100 × Mg / Mg + Fe
Chagrin
Belep
Fantoche
Tiebaghi
Poum
Northern massives
Mt Aloha
Vieille Montagne
Marais Kiki
Clotilde/ Jeanne
Annette
Courage
Dyne
Renaissance
Vercingétorix
Suzanne
Chrome rouge
Ardennite
GR2H
Humboldt
Georges Pile
Anna Madeleine
Massif du Sud
Vulcain
Alice Louise
Nouvé
Prony
Cumulates Massif du Sud
Mt des Sources
Concordant
Sub-concordant
Discordant

Crosscutting these dunite bodies, and sometimes also crosscut by other dunites, are gabbro and websterite dikes that commonly occur as conjugate sets on scales less than 0.5 meters. In Table 3-1, these structures are interpreted to have virtually the same age as the discordant dunites. The gabbro dikes, which also contain inclusions of harzburgite, are most abundant in the upper two-thirds of the Samail peridotite section. Plagioclases in the gabbros are extremely calcic (An_{90}) and (Mg/Mg+Fe)100 for these dikes clusters around 85. Boudier and Coleman [1981] suggest that these dikes are also formed as crystal accumulates from melts moving up through the peridotite. Once again, because these structures occur on cm scales, the liquids in these dikes "see" more harzburgite wall-rock and hence are driven to more fractionated compositions.

The field evidence suggests that at any given time in the history of the peridotite (recorded by the degree of deformation or parallelism with the spinel foliation) small scale features (<1 m) generally exhibit a more fractionated composition and tend to lie along multi-phase saturation surfaces. The orthopyroxene-rich harzburgite bands, the websterites, and the gabbro dikes all represent small melt/rock ratio regimes; these systems are driven out of the olivine field by reaction with the adjacent harzburgites [Figure 3-8]. Larger features, such as the dunite bodies, represent conduits where the local melt-rock ratio was large; therefore the melt remained in the olivine field throughout its entire ascent through the upper mantle.

The presence of discordant dunite, websterite, and gabbro and concordant dunite, websterite, and orthopyroxenite illustrates the myriad of possible paths that primary melts may follow and still deliver MOR tholeiites to the crustal magma chamber or to the ocean

Figure 3-10. The possible crystallization reaction paths are illustrated for two cases: first for a high melt/rock regime where the liquids are effectively insulated from the wall-rocks with the melt remaining entirely in olivine field until it reaches the 1 atmosphere cotectic. If we accept the topology of the cotectics as mapped by Stolper in reconnaisance fashion [1980], then at shallow-levels in the mantle, the melts would be more likely to reach the olivine-clinopyroxene cotectic. In the field, no conjugate orthopyroxenite dikes are observed. However at high pressures and low melt/rock regimes, the orthopyroxene-olivine cotectic is reached. Combining these two regimes indicates that an infinite number of crystallization-reaction paths are possible.

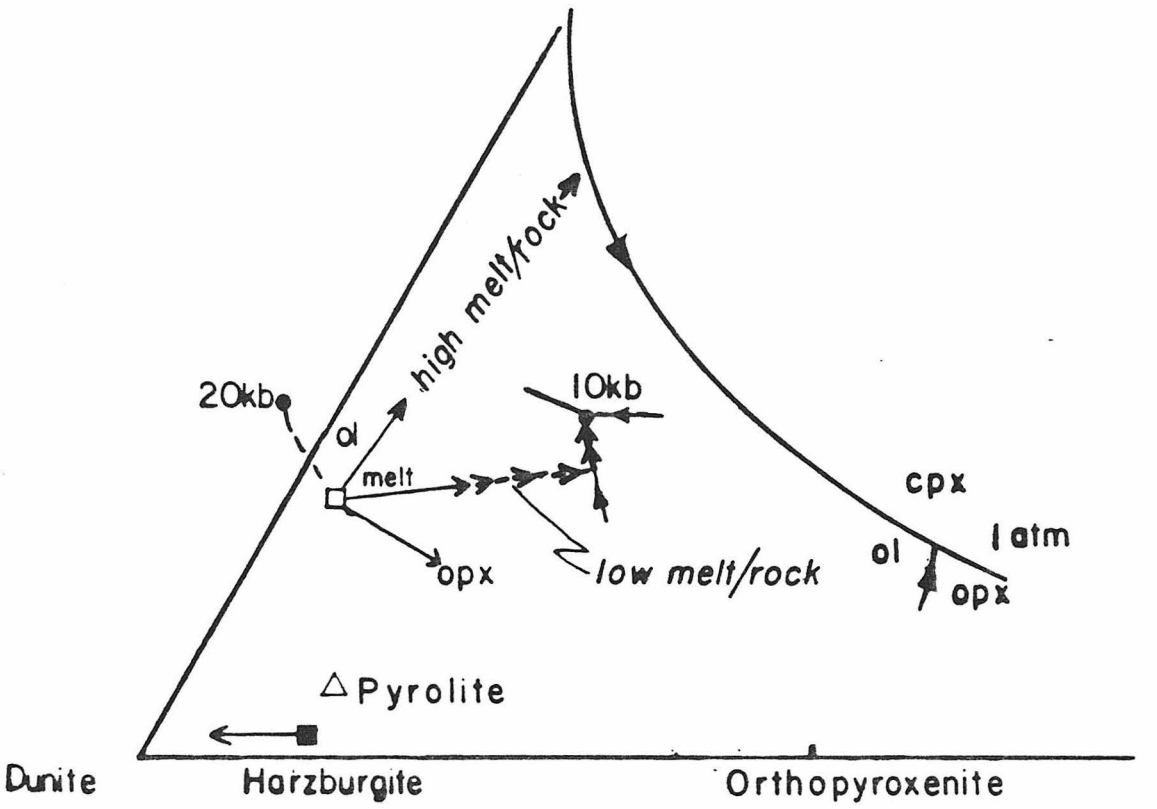
20kb
ol
high melt/rock
melt
10kb
cpx
1 atm
ol
opx
opx
low melt/rock
△ Pyrolite
Dunite
Harzburgite
Orthopyroxenite

floor. Except for the harzburgite, by far the most abundant rock type in the peridotite is dunite. The abundance of dunite suggests that most of the melts resided in the olivine field (Figure 3-10) during their rise to the surface. In Figure 3-10, it is suggested that the whole range of tholeiite compositions (in terms of major elements) observed on the seafloor can be generated from a primitive picrite magma. This picrite is allowed to follow a variety of reaction and crystallization paths during its ascent to the surface, without the presence of a persistent seafloor magma chamber.

In the absence of other criteria for the existence of a crustal magma chamber, such as distribution of trace-elements [O'Hara, 1977], anomalous crystallization sequence [Walker et al., 1979], or the presence of a cumulate gabbro section in ophiolites [Coleman, 1977], major element compositions of abyssal tholeiites cannot be used by themselves to prove or disprove the existence of a magma chamber. However, in Oman, the existence of picrite, dunite, and wehrlite at high stratigraphic levels within the gabbro section (<500 m from the diabase-gabbro contact) suggests that magma mixing in a shallow-level magma chamber was more important in producing variability in the liquid compositions delivered to the surface than the mantle phenomena. The dominance in the Samail ophiolite of near-surface magma mixing is also supported by trace element studies [McCulloch et al., 1980; Pallister and Knight, 1981; and Chen and Pallister, 1981].

3.4 THE SAMAIL OCEANIC CRUST-MANTLE SECTION

3.4.1 Reconstruction of the ophiolite section before detachment

By combining the geology of the gabbro sections discussed in Chapter 2 with the data in this chapter on the peridotite section, a descriptive model can be constructed for the Samail ophiolite at the time of its formation beneath the Hawasina Ocean (Figure 3-11). A key observation in the construction of the model is the presence of both isoclinally folded and conjugate dikes of websterite, which indicates that the low stress mantle deformation of the basal peridotite continued upward to the present level of exposure in the ophiolite. The occurrence of both these concordant and discordant websterite dikes suggests that the isoclinally folded zone may have represented the boundary between rising depleted mantle (the harzburgite) and undepleted mantle not preserved. The interpretation that the basal isoclinally folded zone was the boundary of the original mantle diapir is consistent with the following field observations:

1) Most of the deformation in the basal zone is not directly related to the high stress deformation that produced mylonites at the contact with metamorphic aureole rocks. The mylonitization occurred over a pre-existing zone of weakness where plastic deformation had already occurred.

2) The direction of vergence of isoclinal folds in the section is perpendicular to the dike direction in the Ibra section [Boudier and Coleman, 1981] and in northern Oman [J. Smewing, pers. comm.]. If the dike direction is perpendicular to the spreading direction, then the sense of transport in the basal peridotite tectonite is consistent with spreading in the same direction.

Figure 3-11. Reconstruction of the cross-section through the ridge that produced the Samail ophiolite under the Hawasina Ocean (~100 million years ago). The cartoon is divided into two parts: one half of the ridge shows the orientation of dunite bodies assuming extrusion flow is the mechanism driving the spreading [F. Boudier, pers. com.] and the other half shows the orientation of the dunite bodies assuming gravity flow drives the spreading. In our field area we cannot distinguish which mechanism applied because the direction to the paleoridge is not known. The basal isoclinally-folded zone is interpreted as the boundary of the mantle diapir.

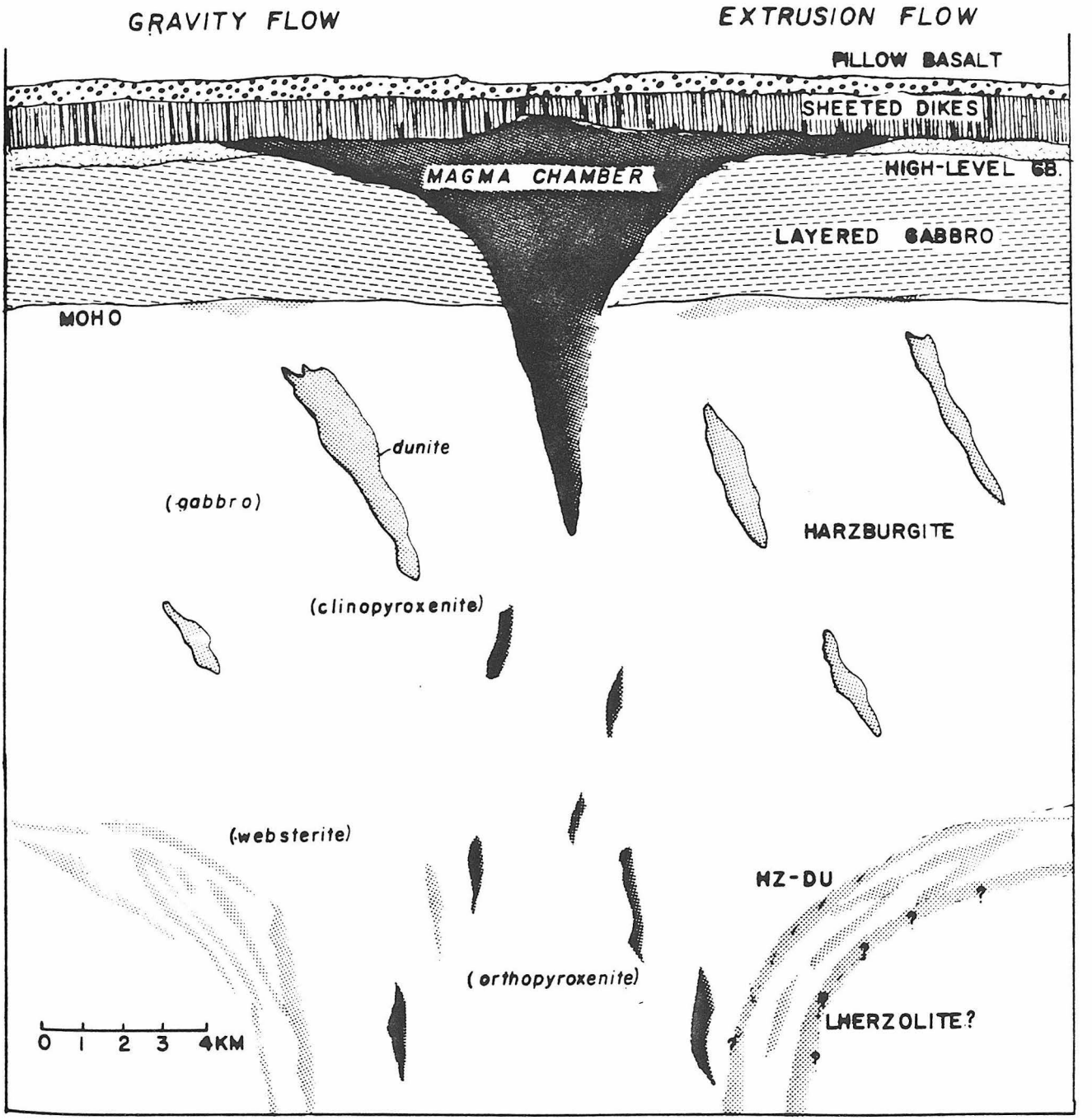
GRAVITY FLOW
EXTRUSION FLOW
PILLOW BASALT
SHEETED DIKES
MAGMA CHAMBER
HIGH-LEVEL GB.
LAYERED GABBRO
MOHO
dunite
(gabbro)
(clinopyroxenite)
HARZBURGITE
(websterite)
HZ-DU
(orthopyroxenite)
LHERZOLITE?
0 1 2 3 4KM

3) In Newfoundland, lherzolite has been observed sandwiched between amphibolites of the contact aureole and a harzburgite-dunite section similar to the section observed in Oman [Malpas and Stevens, 1977]. The lherzolite may represent a fragment of "undepleted" mantle that was welded to the base of the ophiolite during detachment in a fashion similar to that described for amphibolites and phyllites described Chapter 2.

In Figure 3-11, the orientation of the discordant dunites is shown for two different plate-tectonic driving mechanisms -- 1) extrusion flow of the mantle and 2) gravity sliding of the solidified oceanic crust [Nicolas and Poirer, 1976]. The sense of rotation of the discordant bodies is determined by using the sense of shear direction in the peridotite tectonites [Nicolas and Poirer, 1976; Boudier and Coleman, 1981]. If three independent indicators of direction to the paleoridge axis are consistent, then it would be possible to distinguish which of the mechanisms applied to Oman. However, the sheeted dike complex indicates (using chill margin asymmetry [Pallister, 1981]) that the ridge lies to the southwest of the present-day exposure, while data from the cumulate gabbro suggest that the ridge lies in the opposite direction [Pallister and Hopson, 1981]. Unfortunately, no radiometric technique can resolve this discrepancy for rocks of this age since U-Pb dating is probably good to $\pm$ 2 m.y. while Nd-Sm dating is good to $\pm$ 10 m.y. [Tilton et al., 1981; McCulloch et al., 1981]. In addition, both isotopic systems may have been affected by hydrothermal alteration [see below]. In order to resolve the discrepancy, a dating technique capable of discerning age differences in rocks only a few tens of kilometers apart would be required.

Figure 3-12. Photograph of the fossil Moho at the head of Wadi Gideah. The dark layer is cumulate dunite that contains poikilitic clinopyroxene and intercumulus plagioclase. The bottom of the cumulate dunite would be the "petrologic Moho" and the top of the layer would be the "seismic Moho". This dunite layer is only ~100 meters thick. Seismically, these boundaries are at the same depth, because seismic waves cannot resolve the depth to the discontinuity within 100 meters.

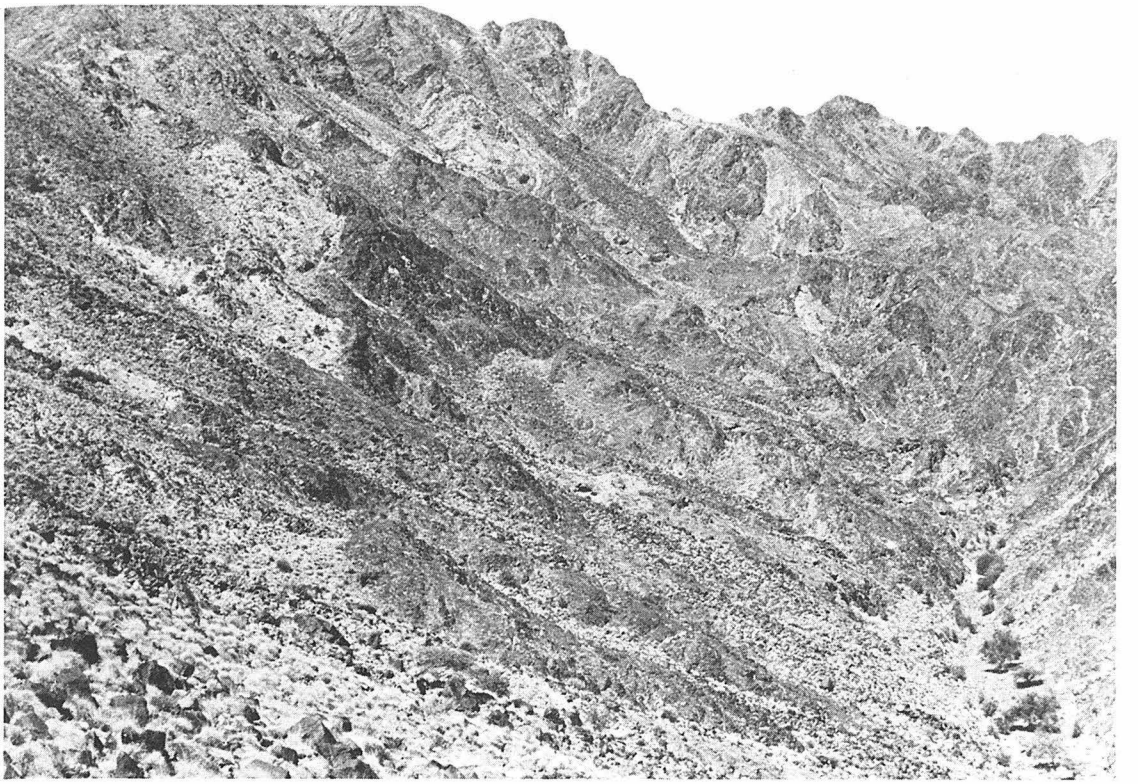

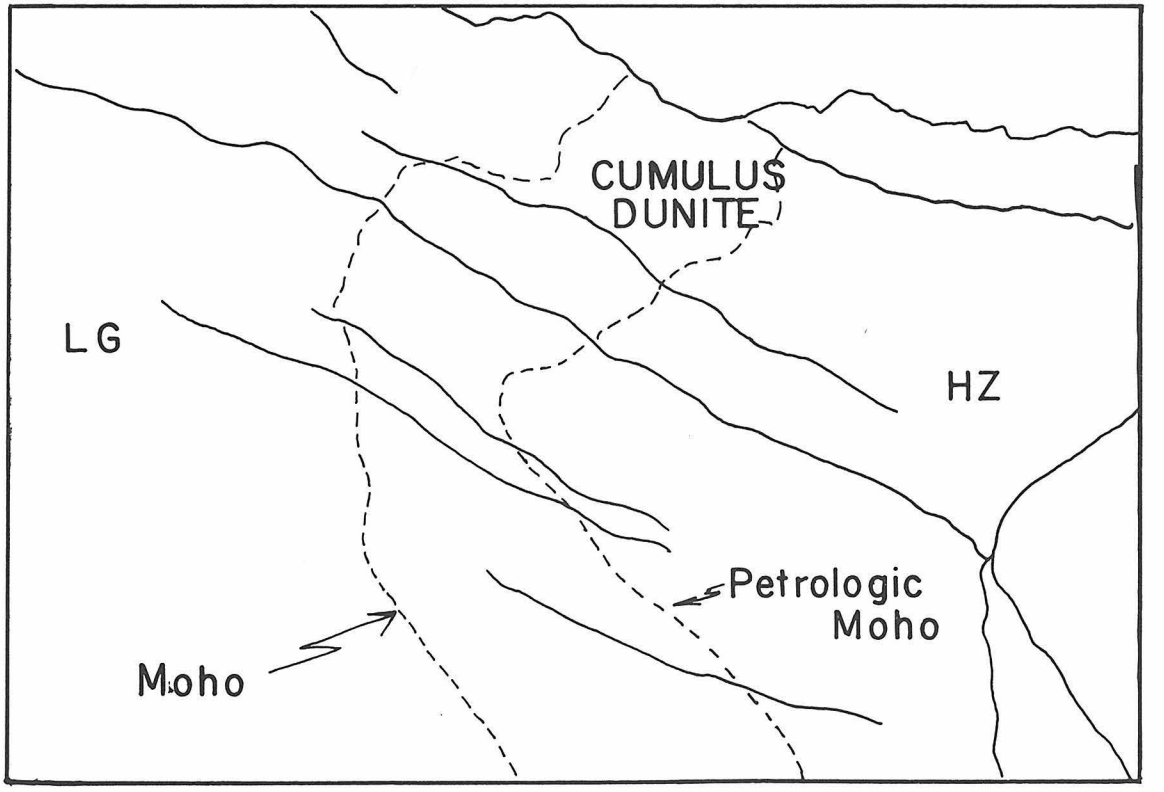
CUMULUS
DUNITE
LG
HZ
Petrologic
Moho
Moho

3.4.2 The gabbro-peridotite contact

The general petrologic description of the peridotite-gabbro transition (Fig. 3-12) is presented in section 2.2.3. In the cartoon reconstruction, large dunite bodies such as the body exposed in Wadi Wushad are rotated back to vertical at the ridge axis and the maximum width of the feeder dike is on the order of 3 km. The actual floor of the magma chamber was not necessarily what is presently the peridotite-gabbro contact, but may have been considerably above or below the contact depending upon the rate of supply of magma. Evidence suggesting that the chamber floor was not at the Petrologic Moho (Fig. 3-11) comes from large breccias consisting of blocks of layered gabbro in a matrix of dunite or wehrlite up to 100 meters thick which occur discontinuously along the peridotite-gabbro contact. This megabreccia probably marks the influx of new pulses of magma into the magma chamber, and combined with the trails of elongated dunites in the tectonite peridotite, suggests that the funnel-shaped cross-section of Figure 3-9 is a reasonable representation of the geometry of the ridge-axis chamber.

3.4.3 The geometry of the crustal chamber

The shape of the ridge-axis magma chamber shown in Figs. 3-11 and 4-15 is modified after the shape originally proposed by Greenbaum [1972] for Troodos, and later proposed by Hopson and Frano [1977] for Point Sal, and for the Samail ophiolite [Pallister and Hopson, 1981; Hopson et al., 1981]. In the first-order model of the Samail gabbro by Pallister and Hopson [1981], once the angle of vergence of cumulate layers to the Moho is known, then presumably the chamber width could be calculated using the thickness of the gabbro section and simple

trigonometry. Estimates of the original chamber width could then be compared to the dimensions of axial valley rifts at active spreading centers in order to estimate paleospreading rates.

The aircraft-carrier shape of the magma chamber is similar in cross section to the geometries observed in the classic continental layered intrusions such as the Skaergaard, Muskox, Great Dyke, and the Bushveld [Wager and Brown, 1968; Irvine, 1970; Worst, 1960; and Jackson, 1970] and the not-so-well-known layered intrusions such as those in Saudi Arabia [Coleman et al., 1972]. The "aircraft-carrier" magma chamber is also consistent with $\partial P/\partial T$ requirements that the crystallization rate in the chamber increases with depth (Figure 3-13). Unfortunately a geometry of this type precludes using the angle of vergence cumulate layers against the fossil Moho and the thickness of the gabbro section to estimate the chamber width as proposed in the first order models of Hopson and Frano [1977] and Pallister and Hopson [1981] (Figure 3-13).

A consequence of the inverted funnel-shaped cross-section, combined with the location in a spreading environment, is that the roof of the chamber is mechanically unstable during the lifetime of the chamber. The unstable roof results in a sandwich horizon, or a thin sheet of late-stage magma, at the diabase-gabbro contact [Hopson et al., 1981; Pallister and Hopson, 1981; Smewing, in press]. As described in Chapter 2, the high-level gabbro represents the heterogeneous remnants of all of the material that crystallized at the roof of the chamber, as well as much material derived by interaction with stoped blocks of the roof rock. In the next section, the problem of the origin and localization of the plagiogranites at this roof contact will be discussed in the context of the framework established thus far.

Figure 3-13. Crystallization rates are contrasted for two different spreading geometries that satisfy the geologic constraints discussed in Chapter 2. The triangular-shaped chamber requires the same rate of crystallization at all depths. In the model of Pallister and Hopson [1981], the angle Θ (the vergence of the cumulate layers upon the Moho) could be used to calculate the width of the chamber. The "aircraft-carrier" shaped chamber satisfies the $\partial P/\partial T$ constraint that the liquidus temperature is mostly likely to be crossed at depth in the chamber, and thus the rate of accumulation is faster near the bottom of the chamber.

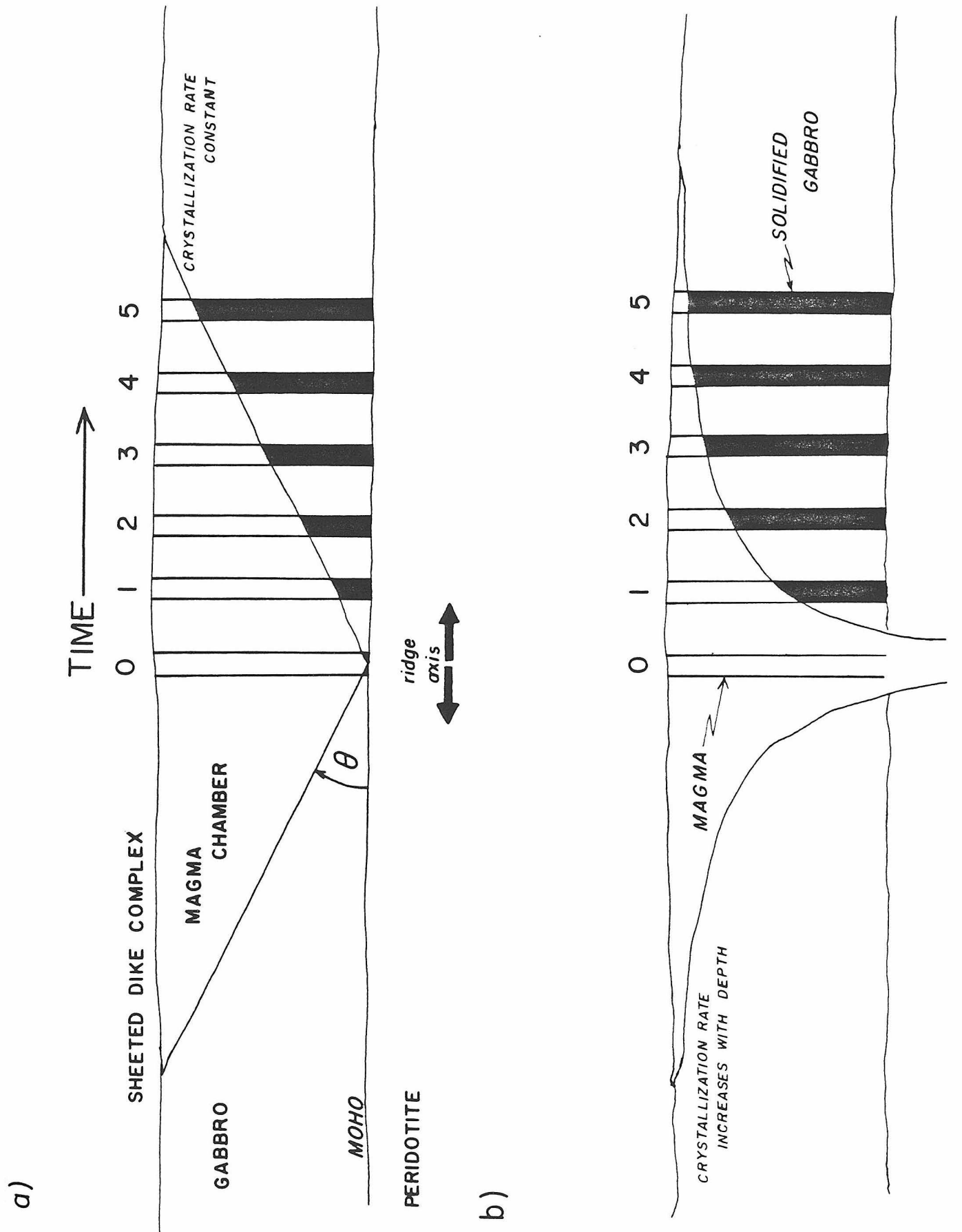
a)
TIME
0
1
2
3
4
5
CRYSTALLIZATION RATE
CONSTANT
SHEETED DIKE COMPLEX
MAGMA
CHAMBER
GABBRO
MOHO
θ
PERIDOTITE
ridge
axis
b)
SOLIDIFIED
GABBRO
MAGMA
CRYSTALLIZATION RATE
INCREASES WITH DEPTH

3.5 THE PLAGIOGRANITES

3.5.1 Previous work on the plagiogranite problem

Since the publication of Coleman and Peterman [1975], where the term plagiogranite was first used to describe oceanic quartz diorites to albite granites with no K-bearing phases (i.e. oceanic "trondjhemites"), numerous articles have addressed the plagiogranite problem, including: Malpas and Stevens, [1977]; Coleman and Donato, [1977]; Spooner et al., [1977]; Stern et al., [1976]; Dixon and Rutherford, [1979]; Brown et al., [1979]; and Aldiss, [1978]. Virtually all of these authors conclude that extreme fractional crystallization of an hydrous tholeiitic melt resulted in plagiogranites. Dixon and Rutherford [1979] proposed liquid immiscibility as a possible mechanism for producing plagiogranite.

Nearly all workers ignore the problem of hydrating a tholeiitic melt at the pressures under which plagiogranite crystallizes (1 to 2 kb). In a review of volatile components in melts, Burnham [1979] showed that dissolution of water into silicate melts was nearly impossible at low pressures. Taylor and Forester [1979] showed that virtually no water diffused directly into the Skaergaard melt during its crystallization history, even though a hydrothermal system was established almost immediately after intrusion, and even though P_{H_2O} was at least as high as 500 bars in the country rock basalts [Norton and Taylor, 1979]. Taylor [1977] proposed that water gained access to these low pressure, shallow-level magma chambers during piecemeal stoping of the chamber roof which was hydrated by hydrothermal

circulation above the cooling intrusion. This mechanism greatly enhances the surface area through which water would diffuse into the melt.

The low K_2O contents of plagiogranites, often lower than those found in their tholeiitic parents [Coleman, 1977], is a problem for all of the models. Secondary, subsolidus enrichment of Na by metasomatism [Gilluly, 1933] has been proposed to explain the low K_2O content; and the universally altered nature of plagiogranite is pointed out by most authors. Transfer of K into an exsolved volatile-rich phase was proposed by Aldiss [1978] in order to explain what he called the potassium problem.

Taylor [1977, 1980] proposed that "late-stage" differentiates of layered intrusions were the result of interactions between hydrothermally altered country rock and the gabbroic melts. Assimilation and/or partial melting of the (meteoric) hydrothermally altered roof-rocks resulted in the K-rich granophyre found in the continental layered intrusions and similar processes involving (marine) hydrothermal alteration resulted in the Na-rich plagiogranite found in ophiolites and on the seafloor [Taylor, 1980]. Wager and Brown [1968] originally proposed that some of the Skaergaard granophyres were the result of partial fusion of stoped blocks of gneiss, and this has recently been supported by oxygen isotope data [Taylor and Forester, 1979] and strontium isotope data [Leeman and Dasch, 1978]. Taylor [1980] suggested that blocks of Na-rich spilitic material are the precursors of plagiogranite in ophiolites and that partial melting of the blocks, or exchange between the late-stage, high-level gabbro magma and such spilitic blocks could produce plagiogranite and keratophyric liquids.

3.5.2 The Dasir Plagiogranite

The purpose of this section is to center the discussion of the plagiogranite problem around the map of the Dasir plagiogranite, which was mapped at ~1:10,000 by R.G. Coleman and myself and over a larger area at 1:60,000 by myself during portions of the 1977, 1978, and 1979 field seasons (Figures 3-14 and 3-16). The Dasir plagiogranite area is special because, unlike the Ibra section [Hopson et al., 1981], large areas of plagiogranite and associated agmatite are exposed and also the underlying cumulate gabbro contains orthopyroxene as an early liquidus phase replacing olivine. Apparently there was a slight difference in the heat budget of the two sections which was enough to "freeze-in" an incomplete stoping event at Dasir while at Ibra only the results of many events are preserved in a much more complex record. In spite of all the discussion concerning plagiogranites, no map of a single plagiogranite body exceeding a size of 1 km^2 has been published to date. Discussion of the oxygen isotopic effects within the plagiogranite will be postponed until the oxygen isotope systematics of the entire oceanic crustal section are presented. However, the oxygen isotope data suggest that the partial melting mechanism of Taylor [1977] must be invoked in the explanation of the heterogeneous $\delta^{18}O$ values of plagiogranite quartz. It is the goal of this chapter to outline field criteria for recognizing this process.

The Dasir area lies at the northeast corner of the Samail Gap about 70 km northwest of Ibra and approximately one-hour's drive from the capital city of Muscat. Plagiogranite crops out in a broad valley that follows the trace of a refolded synclinal axis which trends easterly on the 1:10,000 scale map and swings to the N10E trend of the

Figure 3-14. Map of Dasir plagiogranite area originally mapped at 1:60,000, shown here at 1:100,000.

Map symbols are as follows:

P - tectonite peridotite

G - layered gabbro

HG - high-level gabbro

A - agmatite

Pg - plagiogranite

SD - sheeted dike complex

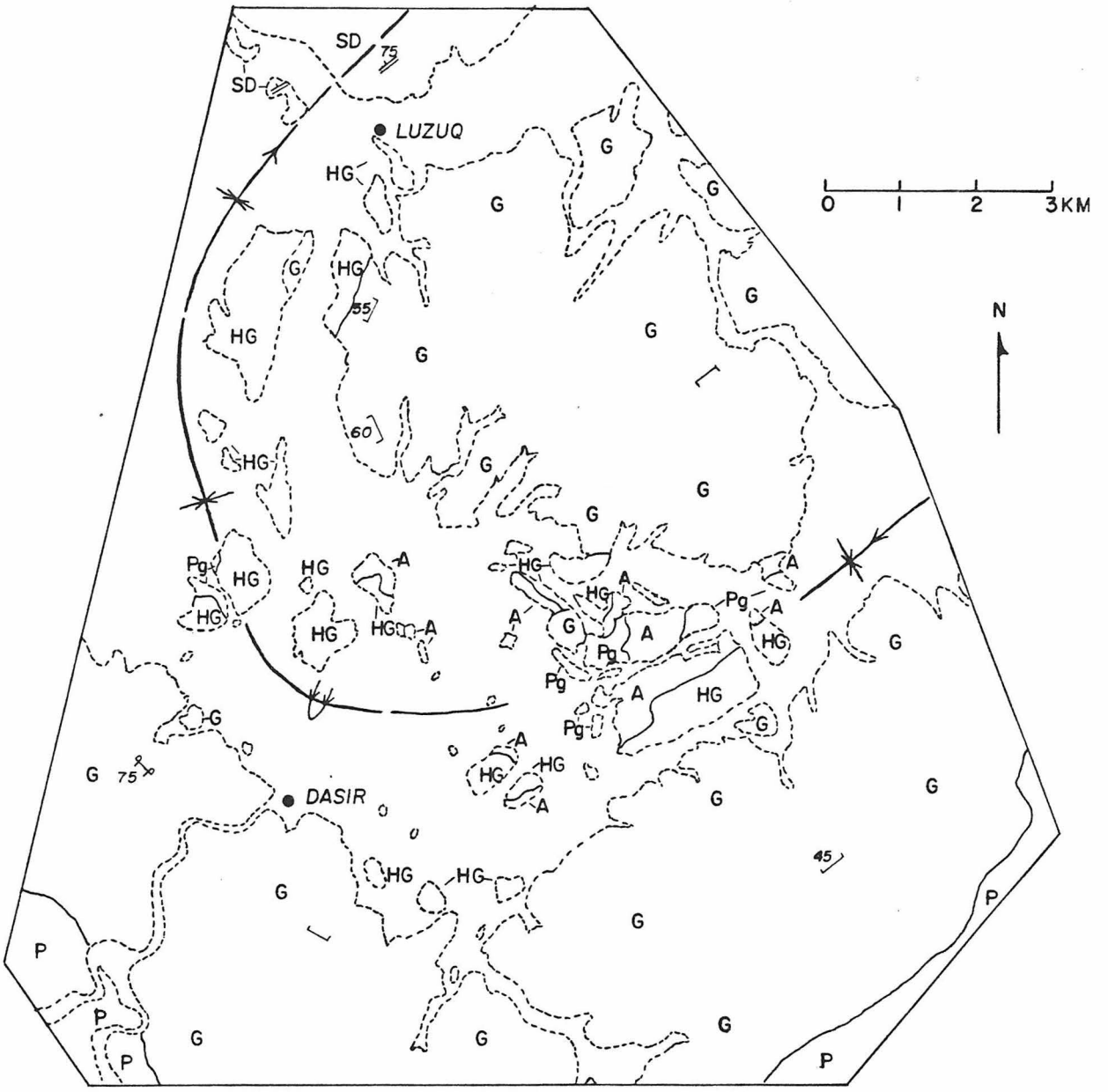
SD
75
SD
LUZUQ
HG
G
0 1 2 3KM
N
55
60
Pg
A
DASIR
45
P

Samail Gap towards the west. If the folding of the Saih Hatat and Jabel Akhdar domes is removed, a large, southward dipping monocline of ophiolite similar to the Jabal Dim'h section is continous from the Ibra area all the way to Nizwa except where interrupted by NNW trending folds and the Dasir section. There are two possibilities which merit further investigation: 1) the Dasir crustal section is typical Samail ophiolite which has been affected by a collapse structure similar to those found east of the Ibra dome, or 2) the Dasir gabbro-plagiogranite represents a crosscutting body similar to those described in northern Oman [J. Smewing, pers. com.]. In either case, the arguments concerning the formation of the plagiogranite body are the same whether the plagiogranite is associated with the magma chamber that formed the oceanic crust or with a later gabbroic magma chamber that formed away from the ridge axis. Without further geologic mapping between Dasir and Ibra this question remains unresolved.

The gabbro section associated with the Dasir plagiogranites is at least 3 km thick (Fig. 3-14) and, in contrast to the Ibra gabbro section, has a considerable thickness of cumulate ultramafics at its base possibly up to 1 km thick. Unfortunately, the peridotite-gabbro transition was not mapped, so the exact nature of the transition from cumulate-ultramafic rocks to tectonite peridotite is not known. Another important difference between the Ibra section and the Dasir section is the several-hundred-meter thick section of two-pyroxene gabbro found at Dasir. The two-pyroxene gabbro cumulates indicate that the Dasir magma chamber received fewer pulses of unfractionated magma than the Ibra chamber, analogous to the differences between the Tortuga and Sarmiento complexes of southern Chile [Stern, 1979].

Figure 3-15. The Dasir plagiogranite (b) is underlain by ~3 km thick section of cumulate rocks (~200m of which is shown) that contains abundant two-pyroxene gabbro (a). The plagiogranite is a composite body composed of agmatite (foreground (b) and (d) and plagiogranite (b).) The plagiogranite (white) on the right-hand side of (b) is about 300 meters long. The agmatite contains abundant hornfelsic amphibolites with cm scale sweatveins of albite granite (c). Overlying the plagiogranite sheet is high-level gabbro; the contact is shown in a 30 meter-high hillside (d).


b


c


a

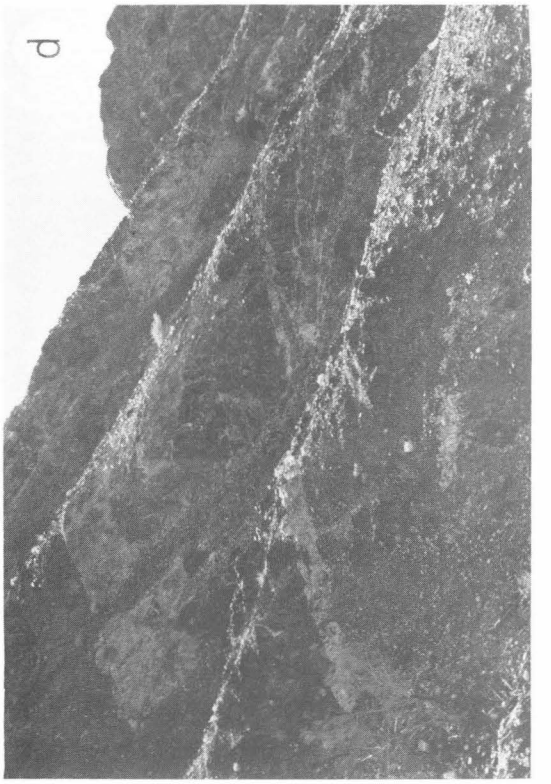
d

The Dasir plagiogranites crop out discontinuously over a broad valley which follows the axis of a syncline. The pure plagiogranite end-member rock is an albite granite with a CI<5 and up to 30 modal percent quartz. The mafic minerals are hornblende>magnetite>biotite (the latter being the only major potassium-bearing phase). However this end-member rock is volumetrically less abundant than inclusion-rich plagiogranite mapped as agmatite in Figures 3-14 and 3-16. The agmatite plus plagiogranite forms a sheet which is sandwiched between layered cumulus gabbro below and non-layered, high-level gabbro above. The composite sheet is less than 500 meters thick and is best exposed in the area covered by the 1:10,000 sheet. The ratio of agmatite to plagiogranite is roughly 3:1, although in places the contact between agmatitic rocks and either high-level gabbro or plagiogranite is gradational and this renders the determination of such a ratio only a crude estimate.

The plagiogranite sheet is floored by interlayered cumulus olivine-clinopyroxene-plagioclase gabbro and two-pyroxene gabbro. Late magmatic brown hornblende is ubiquitous throughout the upper 2 km of the cumulate section, where late-stage poikilitic hornblendes as long as 10 cm also occur. The cumulus gabbro exposed underneath the composite plagiogranite sheet contains inclusions of hornfelsic amphibolite that are cut by sweatveins of albite granite (Figure 3-9). Overlying the plagiogranite sheet is coarse hornblende gabbro (Figure 3-14) which contains microinclusions of hornfels and which also may intrude the agmatite sheet. The coarse hornblende gabbro (equivalent to the high-level gabbro at Ibra but much coarser-grained and richer in hornblende) is overlain by sheeted dike complex near Luzuq (Figure 3-14).

Figure 3-16. 1:10,000 map of part of the Dasir plagiogranite and cross-section.

G - layered, cumulate gabbro with both olivine-clinopyroxene-plagioclase and clinopyroxene-orthopyroxene-plagioclase cumulates present. Hornblende is ubiquitous as a late-stage magmatic phase.

A - Agmatite: an igneous breccia composed of angular fragments of hornfels and metadiabase in a matrix of albite granite.

Pg - Inclusion-free plagiogranite containing sodic plagioclase, quartz, hornblende, magnetite and biotite.

HG - High-level gabbro containing hornblende-plagioclase-magnetite ± clinopyroxene ± orthopyroxene ± olivine.

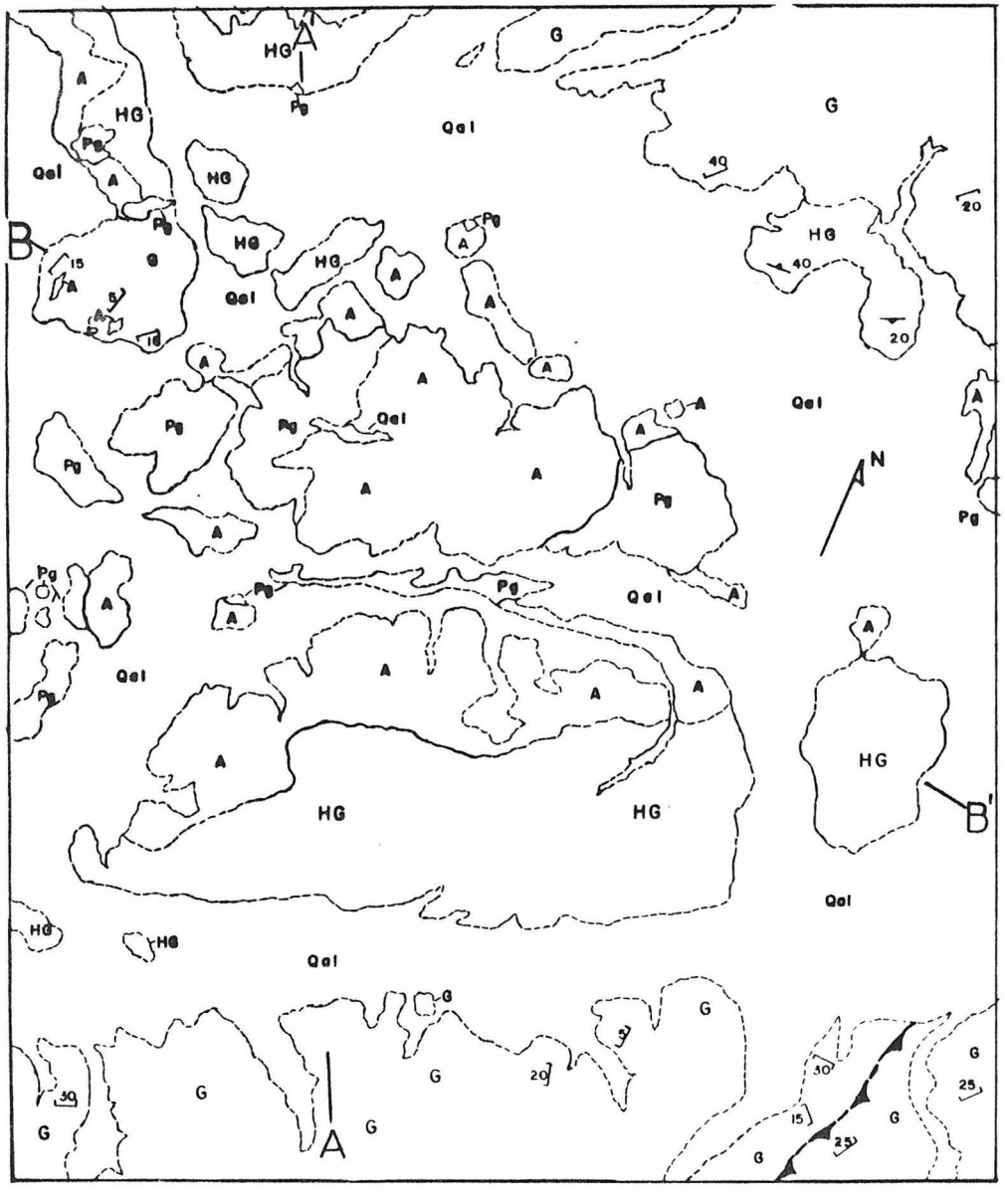

DASIR PLAGIOGRANITE

Qal	ALLUVIUM
HG	HIGH LEVEL GABBRO
A	AGMATITE
Pg	PLAGIOGRANITE
G	CUMULUS GABBRO

0 0.5 1 KM

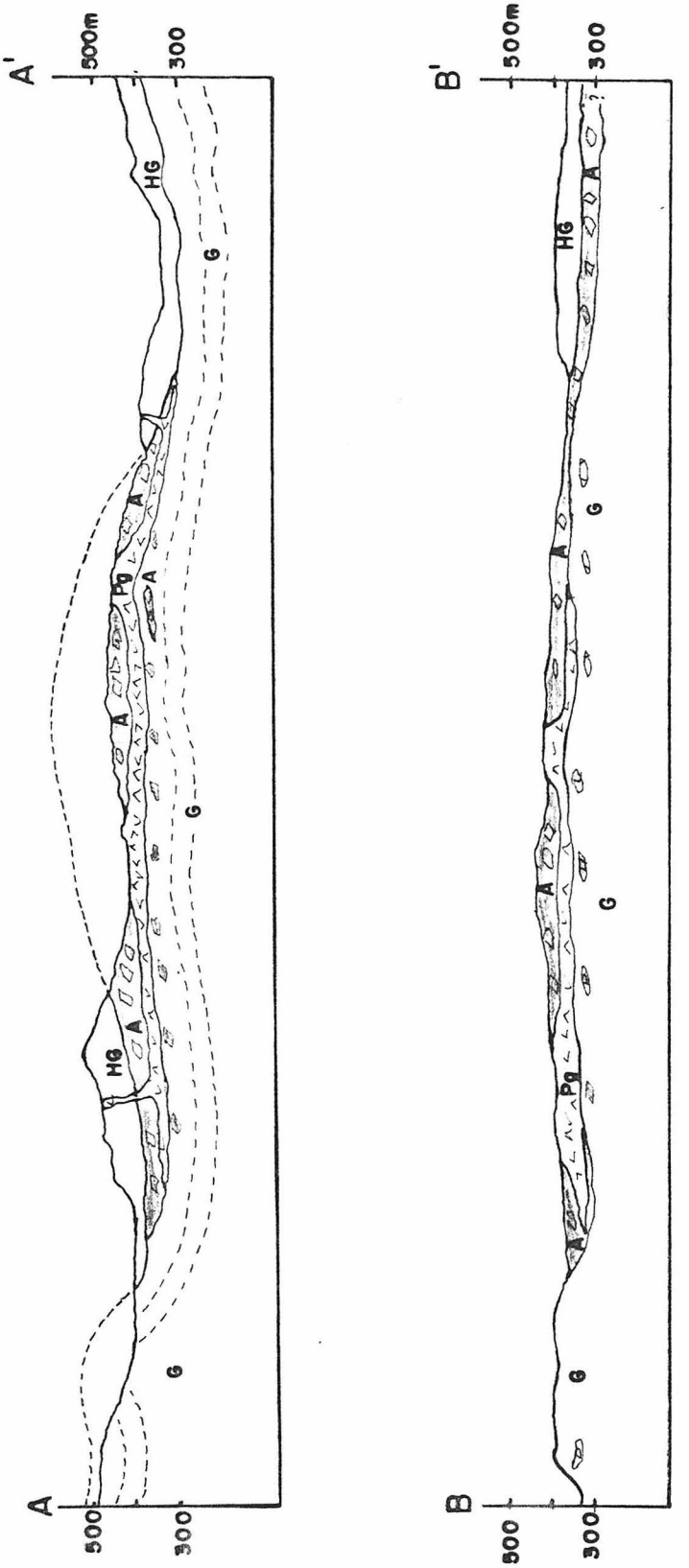

DASIR PLAGIOGRANITE

Figure 3-17.

a) Photograph of inclusion within the layered gabbro (locality G89) that crops out near B in Figure 3-16.

b) Photomicrograph of the host-rock sample G89-1, a layered two-pyroxene gabbro with abundant magmatic hornblende, the large zoned crystal in center of the photograph. The long-axis of the photograph is 3.16 mm. Plagioclase in this sample ranges from An_{40} to An_{55}.

c,d) Photomicrograph (under x-nicols and plane light) of the inclusion in layered gabbro. In the lower right-hand corner is a sweat of albite granite. The hornfelsic portion of the inclusion consists of hornblende, labradorite, magnetite, ± quartz. The long-axis of both photographs is 3.16 mm.

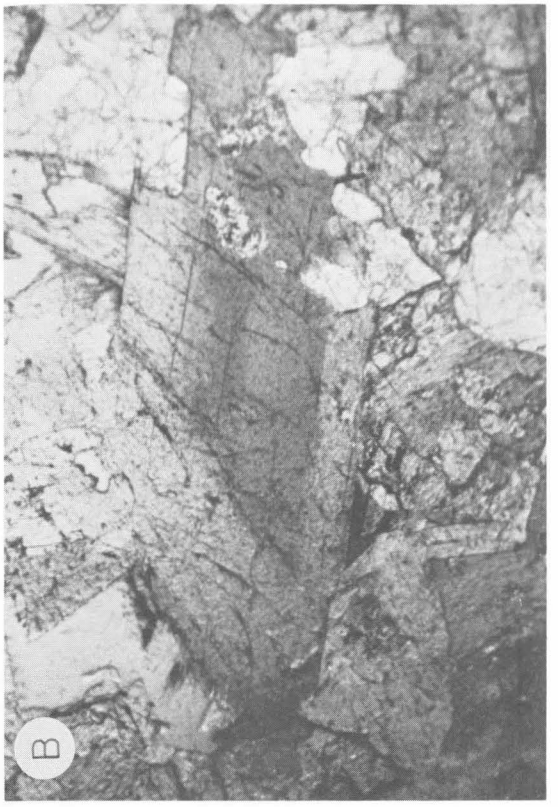
B

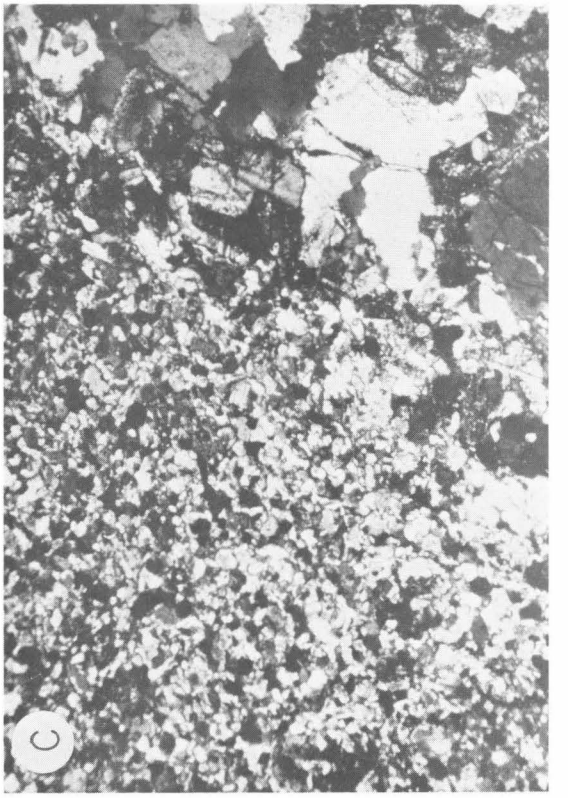
C


A

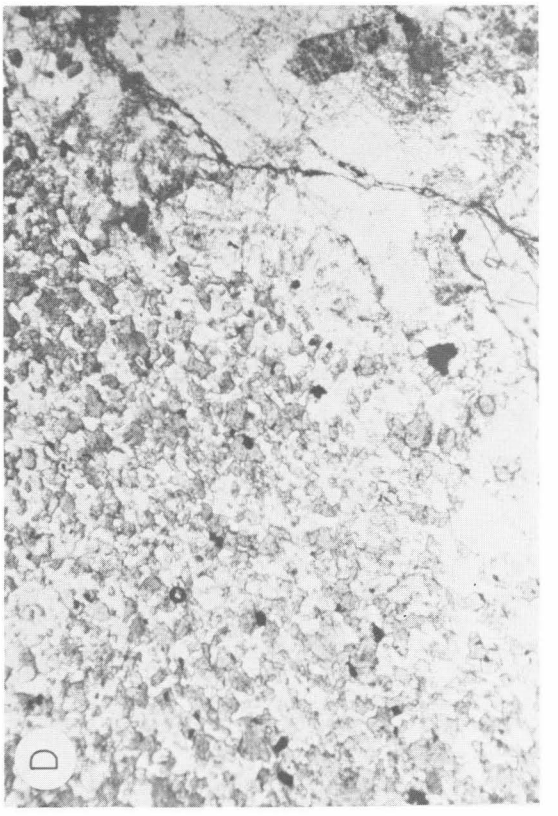
D

Figure 3-18. High-level gabbro overlies agmatite. The arrow at the right-hand corner of (a) points to the outcrop of agmatite shown in (b).


a


b

The composite plagiogranite sheet is composed of two end member rocks, albite granite and mafic hornfels; the latter typically contains 40-50% modal green amphibole, 5-15% magnetite, 25-40% plagioclase, which ranges from labradorite to albite with labradorite as the predominant feldspar, and minor quartz often associated with albite. The color indices of plagiogranites and their inclusions are inversely correlated. The most leucocratic plagiogranites are often inclusion-free or form the leucosome material net-veining the hornfelsic rocks. Plagiogranites which have CI=15-30 often contain schlieren or clots of mafic minerals (hornblende and magnetite) or recrystallized ghosts of xenoliths.

In Fig. 3-16 and 3-14, the plagiogranite end member rock is interpreted, based on the geology, to lie underneath the main mass of the agmatite sheet. However, it locally also intrudes the agmatite sheet along steeply dipping contacts. Dikes of plagiogranite are also found crosscutting the overlying high-level hornblende gabbro (Figure 3-16). The agmatite sheet is an igneous breccia containing abundant angular inclusions of hornfels. The angular shape of the inclusions (Figure 3-19), the fact that in individual outcrops, inclusions can be fit back together, and the flat, sheet-like morphology of the agmatite all indicate that the agmatite was not transported but rather formed in-situ. Therefore, the plagiogranite filling the cracks between inclusions was not intruded as a melt laden with inclusions. The presence of hornfels inclusions within the underlying cumulate gabbro, most of which have petrographic characteristics identical to the hornfels within the agmatite sheet sandwiched between the cumulate gabbro and high-level gabbro, suggests that the plagiogranite-agmatite body does not represent the latest-stage differentiate at a sandwich horizon, but rather must be a

Figure 3-19. In this close-up of the agmatite, the inclusions of meta-diabase can be fit back together suggesting that the agmatite sheet was not formed as an intrusion of inclusion-rich plagiogranite. Instead, the agmatite probably formed in-situ.


b

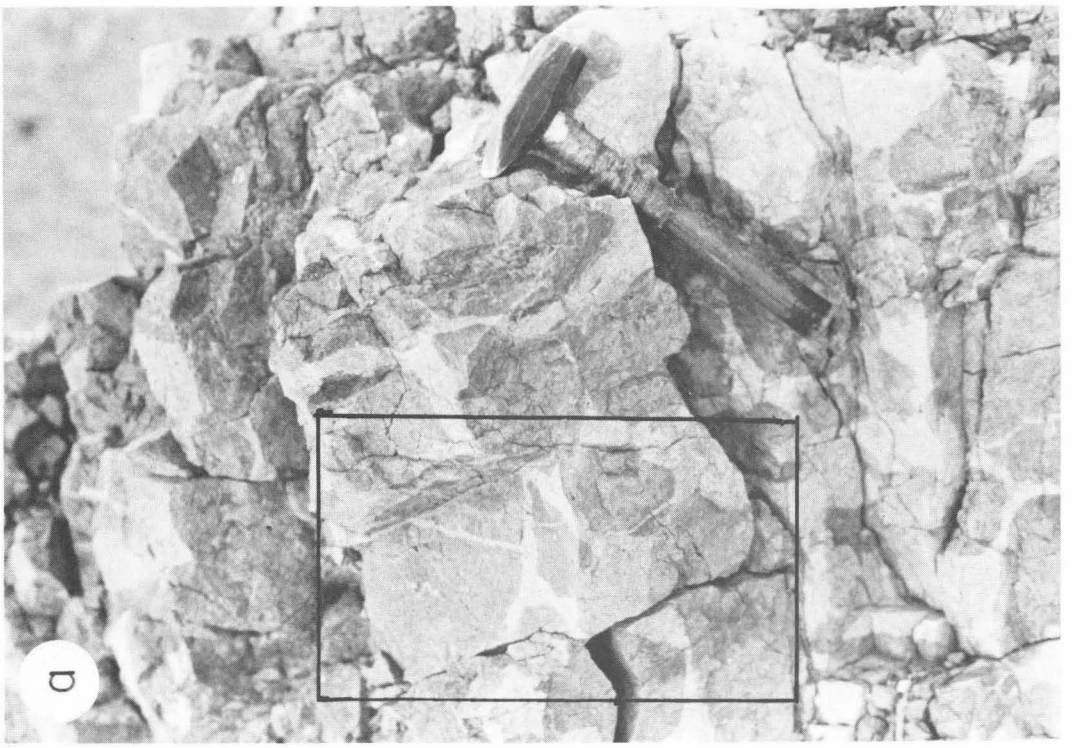
a

partially melted and strongly modified large highly-fractured inclusion or stoped block within the gabbro chamber.

3.5.3 Comparison of the Ibra and Dasir localities

A comparison of the Ibra and Dasir sections of oceanic crust reveals some major differences which are worth emphasizing:

1) The Dasir section has perhaps the best example of a partially melted stoped block of large dimension covering several square kilometers.
2) The cumulates of the Dasir section reached the orthopyroxene-olivine reaction point at a much earlier time (or level within the cumulate section) than the cumulate rocks at Ibra (which virtually did not reach the reaction point).
3) Brown, late-stage magmatic hornblende is much more ubiquitous in the Dasir area and is found at 3-10% levels in the modes of most cumulate rocks.
4) In the high-level gabbro at Dasir, hornblende appears to be a liquidus phase much earlier in the crystallization history (Figure 3-20).
5) Based upon reconnaisance mapping, there appears to be a thicker section of ultramafic cumulates at the base of the Dasir section.

All of these differences indicate that the ridge segments that produced the Ibra and Dasir sections behaved quite differently. The Dasir gabbro section appears to have crystallized under more closed system (fewer pulses of primitive magma) conditions than the Ibra sections. This is the same as inferring that the rate of supply of primitive magma was slower at Dasir allowing the melt to reach the olivine-orthopyroxene reaction. Another possibility is that the Dasir

Figure 3-20. Comparison of the Ibra and Dasir sections.

SD = Sheeted dikes

HG = High-level gabbro

G = Layered cumulate gabbro

D-W = Dunite-wehrlite

H = Harzburgite

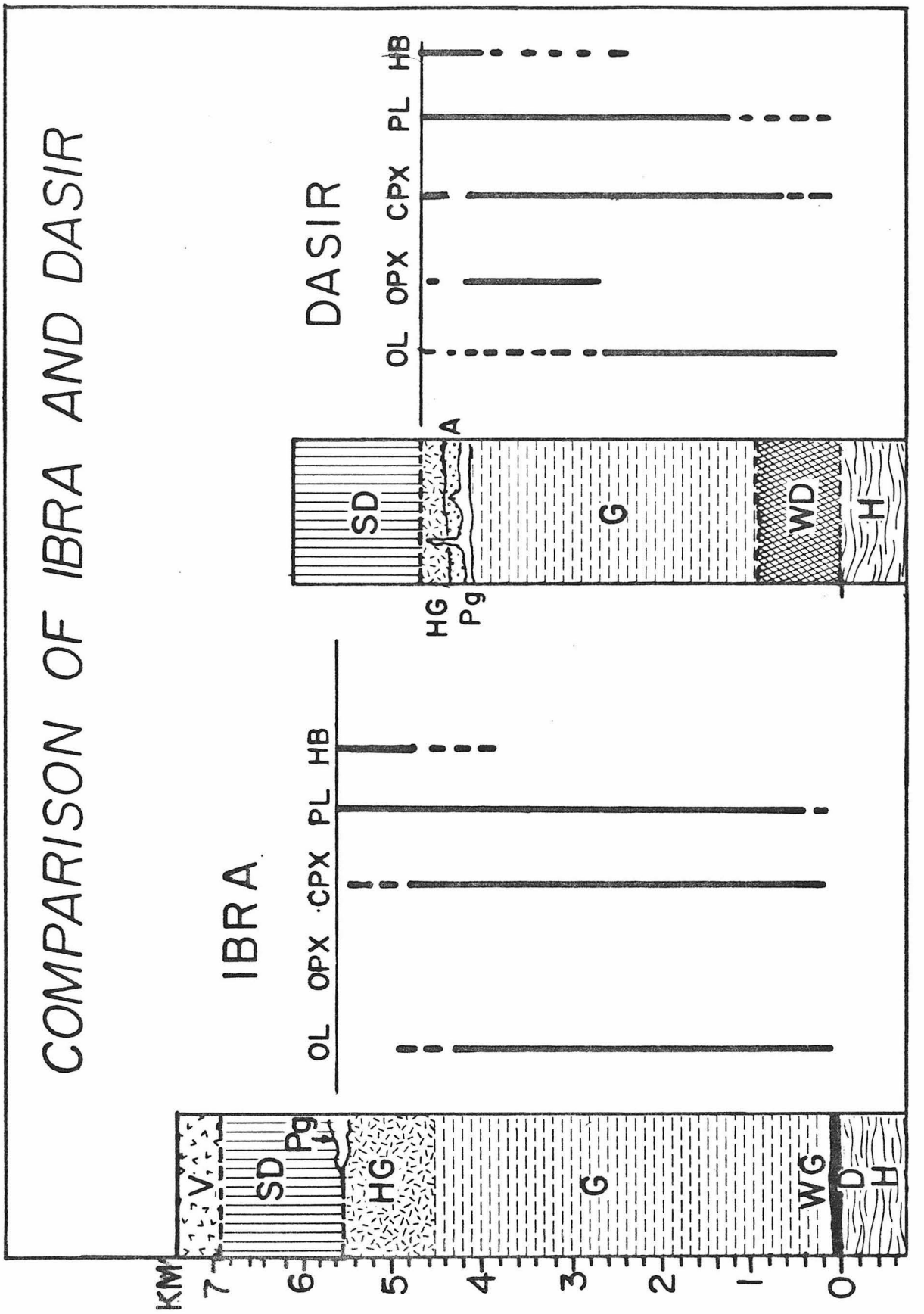
COMPARISON OF IBRA AND DASIR
IBRA
OL OPX CPX PL HB
SD
Pg
HG
G
WG
D
H
V
KM
7
6
5
4
3
2
1
0
DASIR
OL OPX CPX PL HB
A
SD
HG
Pg
G
WD
H

Figure 3-21. A comparison of high-level gabbro sections from Dasir (b) and Ibra (a) on macro- and microscopic scales. In the photomicrograph from Ibra (sample OMG 70), clinopyroxene and olivine are visible with only late-stage hornblende developed (the dark rim around the clinopyroxene grain just left of center). The long dimension in both photomicrographs is 3.16 mm. At Dasir (sample OMG 293-2), the high level gabbro has abundant magmatic hornblende replacing clinopyroxene.

b) DASIR

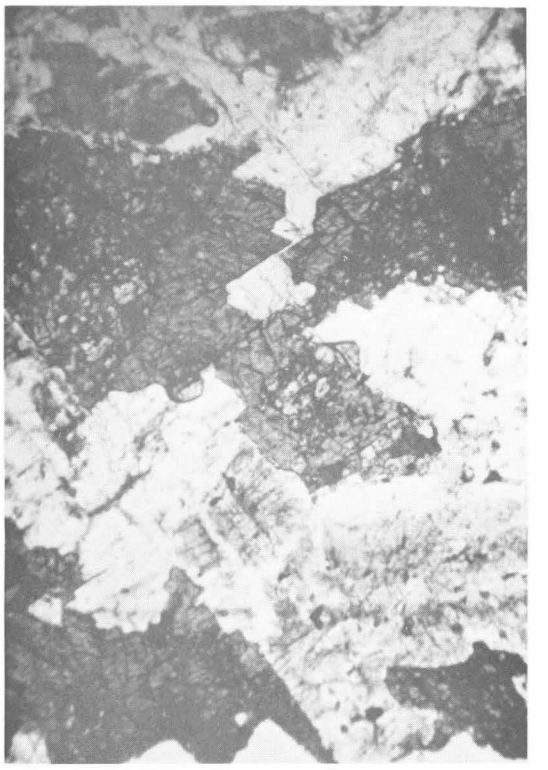

a) IBRA

possibility is that the Dasir area was more tectonically active and that assimilation of the large blocks drove the melt further down the liquid line of descent. Both of these inferences point to the possibility that the Dasir locality may have been close to some type of transform fault boundary which has yet to be recognized in the field.

3.5.4 Origin of the Samail Plagiogranite

The interpretation of the composite plagiogranite body as the remnant of a stoped block is consistent with the following field observations:

1) The underlying cumulate gabbros have labradoritic to bytownitic plagioclase and contain either olivine-clinopyroxene or hypersthene-clinopyroxene assemblages as well as late brown and green magmatic hornblende. The plagiogranites, on the other hand, contain laths of albite indicating a compositional gap inconsistent with simple fractional crystallization.

2) Inclusions of hornfels are found within the cumulate gabbro, and these inclusions are associated with sweats or clots of albite granite. The mineral assemblages in these 5-10 meter-sized inclusions are identical to the assemblages found in the hornfels inclusions in the agmatites.

3) The gabbro structurally above the plagiogranite sheet is coarser-grained than the underlying gabbro, and contains abundant magmatic hornblende, implying that crystallization occurred under much more hydrous conditions than in the cumulate gabbro. This is consistent with a higher concentration of H_2O and other volatiles above the hydrous, stoped block; H_2O would have been absorbed by the overlying

magma during dehydration of the stoped block.

4) The phases within the hornfels are acceptable residual or liquidus phases for the albite granites. Labradorite, hornblende and magnetite are compatible with a minimum melt rich in albite plus quartz.

The following scenario is proposed for the formation of the Dasir plagiogranite. Initially a large block of hydrothermally altered diabase from the sheeted dike complex fell into the magma chamber. The diabase dikes positioned above the magma chamber at the time of foundering were probably at temperatures between 350°-450°C, and would have contained hydrous minerals appropriate for greenschist to amphibilite facies. Upon falling into the chamber filled with gabbroic magma at temperatures exceeding 1000°C, these large foundered blocks suffered thermal shock and fractured. Around each block the gabbro quickly crystallized, effectively sealing off the main mass of basaltic melt from the inclusion. At the base of the block, where temperatures approached the liquidus temperature of the basaltic magma (>1000°C) and significant heat was also available from crystallization of the underlying cumulates, partial melting of the diabase occurred producing hornfels and albite granite. Meanwhile, the upper parts of the stoped inclusion were also recrystallizing and undergoing partial melting but at a slower rate than at the base. The low melting fraction (the albite granite) is concentrated in the fractures created by the thermal shock when the foundered block initially fell into the chamber. This produced the agmatitic texture of the upper parts of the plagiogranite sheet. Albite granite from below intrudes upward into the upper parts of the inclusion and into gabbro that has already crystallized above

the inclusion, and some of the dense restite hornfels blocks sink into the cumulate section. Inasmuch as the solidus temperature of the plagiogranite is lower than that of the surrounding, less-fractionated tholeiitic liquid, the plagiogranite reintrudes the surrounding crystallized gabbro. Upwardly mobile plagiogranites are quenched at the diabase-gabbro contact which constitutes a fairly sharp temperature discontinuity due to more efficient cooling of the diabase dike complex by the still circulating hydrothermal fluids (see below).

The above scenario represents but one stoping event. This scenario can be repeated countless times resulting in the thin heterogeneous high-level gabbro section seen everywhere along the strike of the Samail ophiolite. Plagiogranites produced in this fashion can form at any time in the history of the magma chamber, even right at the ridge axis. This mechanism is one way to explain the common occurrence of diabase dikes crosscutting plagiogranites at the diabase gabbro contact or screens of plagiogranite which occur in the diabase dike complex. In the next chapter, the isotopic characteristics of the Samail ophiolite will be discussed and then the implications of this mechanism for producing plagiogranites will be discussed in terms of the oxygen isotope systematics.

CHAPTER 4

OXYGEN AND HYDROGEN ISOTOPE CHARACTERISTICS OF THE SAMAIL OPHIOLITE

4.1 INTRODUCTION

The main purpose of this chapter is to discuss the oxygen isotope relationships in minerals and rocks throughout a complete section of oceanic crust. Such a characterization is important because of the profound effects that hydrothermal circulation at mid-ocean ridges (MOR) must have upon: (1) the isotopic and chemical composition of ocean water through geologic time; and (2) the isotopic and chemical composition of the oceanic crust that is recycled into the mantle at subduction zones. Oxygen isotope studies of ancient oceanic lithosphere preserved in ophiolite complexes [Coleman, 1977] can provide a framework for studying the time-averaged effects of seawater circulation in "fossil" hydrothermal systems associated with marine spreading centers. Such studies also make it easier to interpret geochemical information gained from dredge samples and from sea-floor hot-spring studies [Muehlenbachs and Clayton, 1972a; Corliss et al., 1979].

Abundant evidence of hydrothermal alteration has now been observed in samples dredged from the sea floor and collected from ophiolite complexes [Coleman, 1977, Wenner and Taylor, 1978; Melson and Van Andel, 1966, Heaton and Sheppard, 1977; Muehlenbachs and Clayton, 1972a]. Heat flow anomalies at mid-ocean ridges also require the existence of such hydrothermal systems, and direct evidence of discharge of thermal waters has now been observed with the ALVIN submersible [Corliss et al. 1979; Edmond et al., 1979].

Previous $^{18}O/^{16}O$ studies of sub-oceanic and ophiolitic terrains indicate the existence of samples that exhibit both ^{18}O enrichments (e.g., pillow lavas) and ^{18}O depletions (e.g., gabbros) relative to the primary magmatic $\delta^{18}O$ values [Heaton and Sheppard, 1977; Magaritz

and Taylor, 1976a; Spooner et al., 1974; Muehlenbachs and Clayton, 1971]. These $\delta^{18}O$ changes have in general all been attributed to subsolidus hydrothermal alteration, respectively, at relatively low temperatures or high temperatures.

Muehlenbachs and Clayton [1976] have proposed that the ^{18}O fluxes into seawater from continental weathering and from dehydration water cycled through subduction zones and outgassed in magmatic arcs are: (1) opposite in sign; (2) roughly equal in magnitude; and (3) a factor of 10 smaller than the potential ^{18}O flux due to marine-hydrothermal interactions at ridges. If these concepts are valid, it is clear that the latter will ultimately determine the $\delta^{18}O$ value of the oceans. Muehlenbachs and Clayton [1976] pointed out that if the ^{18}O fluxes resulting from high-temperature alteration processes (which produce an ^{18}O enrichment of seawater) exactly cancel out the ^{18}O fluxes due to low-temperature interaction (which result in an ^{18}O depletion of seawater), then the average steady-state isotopic fractionation between seawater and oceanic crust would hold seawater at its present-day $\delta^{18}O$ value. Ocean water would be "buffered" at this value as long as extensive hydrothermal circulation at the mid-ocean ridges continued. Perry et al. [1978], however, have proposed that the $\delta^{18}O$ of seawater has changed with time and was controlled by weathering and low-temperature hydrothermal alteration on the sea floor, during most of the Earth's history.

Ophiolite complexes are now generally recognized to represent fragments of ancient oceanic crust and mantle [Coleman, 1977]. $^{18}O/^{16}O$ studies of such complexes thus can provide a test of the Muehlenbachs-Clayton hypothesis [1976]. However, stable isotope studies of ophiolites

have up to now been mainly concerned with the uppermost sections of diabase dikes and pillow lavas, and with the serpentinized peridotites [Wenner and Taylor, 1978; Heaton and Sheppard, 1977; Spooner et al., 1974; Magaritz and Taylor, 1974]. They have generally not addressed the problem of the depth of penetration of marine-hydrothermal ^{18}O effects into the cumulate gabbro sections that are presumably equivalent to oceanic layer three. In order to define the overall average $\delta^{18}O$ value of the oceanic crust it is crucial to determine the volume of ^{18}O-depleted cumulates produced during deep hydrothermal circulation within a typical slice of oceanic crust.

Low-^{18}O basalts and gabbros produced by interaction with low-^{18}O meteoric ground waters have been reported at many continental localities [Taylor, 1968; Taylor and Forester, 1971; Taylor, 1971; Forester and Taylor, 1977]. These low-^{18}O intrusive rocks commonly occur as epizonal intrusions emplaced into highly fractured and permeable volcanic country rocks. The intrusions act as gigantic heat engines which drive hydrothermal circulation of meteoric water through the rocks. Ophiolite gabbro complexes are geologically analogous to some of these ^{18}O-depleted, continental igneous complexes. Examples are sub-volcanic, epizonal layered gabbro bodies intruded into contemporaneous volcanic piles associated with sheeted dike swarms: the Jabal at Tirf complex in the Red Sea rift zone [Taylor and Coleman, 1977]; the Skaergaard intrusion-East Greenland dike swarm [Taylor and Forester, 1979] and the Scottish Hebrides intrusive ring plutons that were emplaced into plateau basalt lavas, both of which are associated with the initial opening of the North Atlantic Ocean [Taylor and Forester, 1971; Forester and Taylor, 1977]; and the present-day, post-glacial basaltic and

rhyolitic volcanism in the Eastern Rift Zone of Iceland [Muehlenbachs et al., 1974]. These all represent classic areas of low-^{18}O igneous rocks produced by interaction with circulating hydrothermal fluids [Taylor, 1980].

The major differences (ignoring scale) between these continental environments and the marine ophiolite complexes are: (1) In the latter, ocean water with a $\delta^{18}O \approx 0$ instead of meteoric water with a $\delta^{18}O \simeq -5$ to -15, is the source of the hydrothermal fluid; and (2) On the sea floor, the spreading rates and rate of production of new crust are typically much more rapid. The difference between hydrothermal fluids derived from seawater or from meteoric water is important, because the contrast in $\delta^{18}O$ between seawater and primary basaltic magma is only about 6 per mil, much less than the contrast between meteoric waters and igneous rocks. The isotopic effects of marine-hydrothermal alteration are therefore much more difficult to detect and interpret, because the "signal-to-noise" ratio is so much smaller. The much more dynamic MOR spreading processes also produce an oceanic crustal ^{18}O profile that represents superposition of various time, space, and temperature regimes. As it moves away from the spreading center into a cooler environment, the oceanic crust experiences an aging process which has no direct counterpart in the continental systems that have been investigated to date. The more active spreading regimes also probably lead to more intense fracturing and collapse features, resulting in higher permeabilities and thus to deeper and more vigorous convective circulation of the hydrothermal fluids.

4.2 GEOLOGICAL RELATIONSHIPS AND SAMPLING

4.2.1 General Features

The Samail Ophiolite, Sultanate of Oman, was selected for this study because it is probably the largest and best exposed ophiolite complex in the world. It crops out in an area of major topographic relief throughout a desert region comparable in size to the Sierra Nevada batholith (Fig. 4-1). Not only is the Samail Ophiolite large and well exposed, in places the thrust slices of oceanic crust are essentially internally undeformed [Coleman, 1977]. Individual members of the ophiolite stratigraphic succession have thicknesses comparable to their typical oceanic counterparts.

The Samail Ophiolite formed in the Hawasina ocean basin, which probably existed as an entity from latest Permian to latest Cretaceous time [Glennie et al., 1974]. The Hawasina Ocean was a portion of the great Tethys seaway, and the Samail Ophiolite apparently formed at a Tethyan mid-ocean ridge during Cretaceous spreading [Reinhardt, 1969; McCulloch et al., 1980; Tilton et al., 1981]. The ophiolite is the highest tectonic member of a series of nappes which were transported southward during late Cretaceous time across the Arabian continental margin [Glennie et al., 1974]. A Maestrichtian-Tertiary shallow water marine limestone unconformably overlies the ophiolite and provides evidence for a minimum emplacement age [Glennie et. al., 1974]. Zircon ages of 95 ± 2 m.y. [Tilton et al., 1981] together with a 90 m.y. K-Ar age from an amphibolite aureole beneath the Samail thrust, bracket the initial detachment age within the interval 95-90 m.y. [Lanphere et al., 1981]. Maestrichtian shales from the

Figure 4-1. Generalized geologic map of the Samail ophiolite, Oman, showing an inset of the Ibra area (after Glennie et al., [1974]).

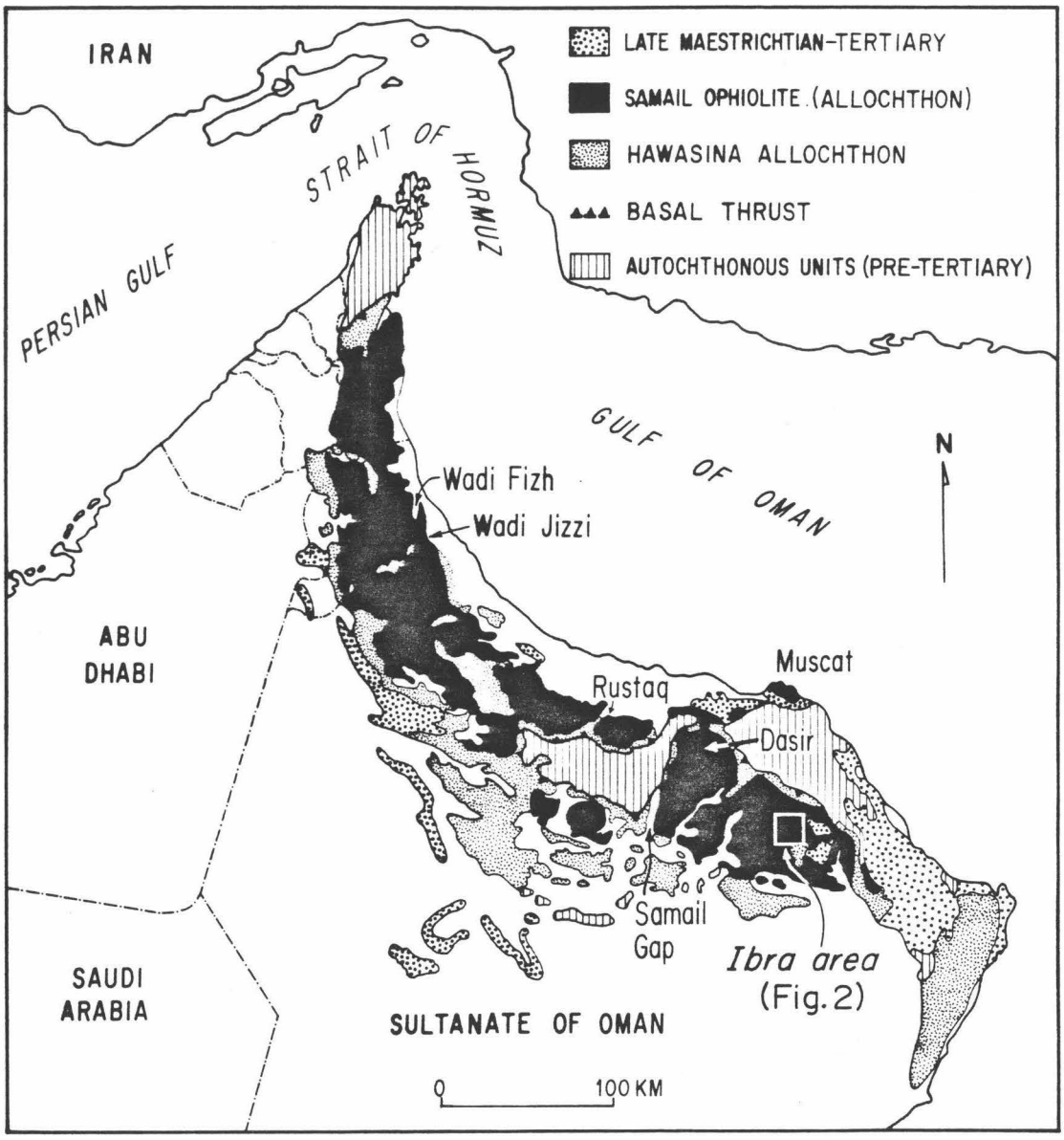
IRAN
STRAIT OF HORMUZ
PERSIAN GULF
GULF OF OMAN
N
LATE MAESTRICHTIAN-TERTIARY
SAMAIL OPHIOLITE (ALLOCHTHON)
HAWASINA ALLOCHTHON
BASAL THRUST
AUTOCHTHONOUS UNITS (PRE-TERTIARY)
Wadi Fizh
Wadi Jizzi
ABU DHABI
Muscat
Rustaq
Dasir
Samail Gap
Ibra area (Fig.2)
SAUDI ARABIA
SULTANATE OF OMAN
0
100 KM

underlying melange require that the last movement of the Samail nappe is probably no older than 65-71 m.y. [Hopson et al., 1981].

The present-day relief of the Oman Mountains is due to a Pliocene folding event contemporaneous with folding in the Zagros belt of Iran. Note that the Samail ophiolite was not emplaced into its present position by subduction followed by buoyant uplift along reverse faults at the front of an andesitic arc [Coleman, 1981]. Basal contact relations prove the existence of an episode of early movement while the lower portion of the Samail nappe was hot enough to produce extensive contact metamorphism, followed by a later movement under much lower temperature conditions. Emplacement was thus a two-stage process that apparently culminated in gravity sliding of the ophiolite mass onto the Arabian continental margin [Coleman, 1981; Boudier and Coleman, 1981].

Except for the basal amphibolite, none of the metamorphic assemblages observed in the oceanic crustal section are due to metamorphism associated with obduction. There is no evidence of any post-emplacement Tertiary igneous activity in the Oman Mountains or along the eastern Arabian continental margin. Rare diabase and gabbro dikes with chilled margins cross-cut the Samail peridotite and the high-temperature contact aureole, but do not cross-cut the allochthonous Hawasina melange, or the autochthonous Hajar group, suggesting a sea-floor, pre-Maestrichtian origin. Therefore, excluding the very low-temperature, late-stage serpentinization of the peridotite, which was apparently caused by meteoric waters [Barnes et al., 1978], all of the hydrothermal metamorphism of the Oman ophiolite oceanic crustal section is attributed to sea floor processes.

4.2.2 Geology and Petrology of the Ibra Section

The samples analyzed in this study come from the Ibra area, south-eastern Oman Mountains (Fig. 4-2). The geology of this area is discussed in detail by Hopson, Coleman, Gregory, Pallister and Bailey [1981], so only those geological relationships necessary for this discussion will be reviewed here.

Samples were collected from two Wadis (Saq and Kadir) which drain the north limb of a syncline (Fig. 4-2). The peridotite-gabbro contact (the fossil "Moho") crops out at the heads of the drainages near the crest of the range. Both wadis empty onto a pediment dotted with low hills of sheeted diabase dikes. The pillow lavas form relatively poor outcrops to the south, near the axis of the syncline.

The Wadi Saq gabbro section is truncated at its base by a late, low-angle fault which results in an atypically thin (3.5 km) gabbro section here [Hopson et al., 1981]. However, this section was picked for study because of the abundant sheeted diabase dikes which form well-exposed outcrops along this traverse. The Wadi Kadir traverse has a complete gabbro section (≈5 km thick), but has limited exposures of sheeted diabase dikes. The combination of the two sections gives a virtually complete cross-section through the oceanic crust.

Samples of gabbro dikes which cross-cut the peridotite but are not chilled against it were collected from a traverse through the peridotite roughly colinear with the east fork of Wadi Kadir, just north of the area shown in Fig. 4-2, in collaboration with R. G. Coleman and F. Boudier. The latter workers are making a detailed structural and petrologic study along this section through the peridotite [Boudier and Coleman, 1981].

Figure 4-2. Geologic map of the Ibra area (after Hopson et al., [1981]), showing the locations of the Wadi Saq, Wadi Kadir, and Wadi Gideah sections, and other samples analyzed in this study and in the study of McCulloch et al., [1981].

P (wavy pattern) = peridotite (tectonized harzburgite and dunite)

G = layered cumulate gabbro

HG = high-level, non-cumulate gabbro

SD = sheeted diabase dike complex; in the Wadi Saw area, the lined pattern is approximately parallel to the strike of the sheeted dikes.

V = pillow basalts

K_h = Hawasina pelagic sediments

Hmel = Hawasina melange

Heavy black lines = faults; dotted contact indicates concealed SD-V contact, which defines the position of the Ibra syncline.

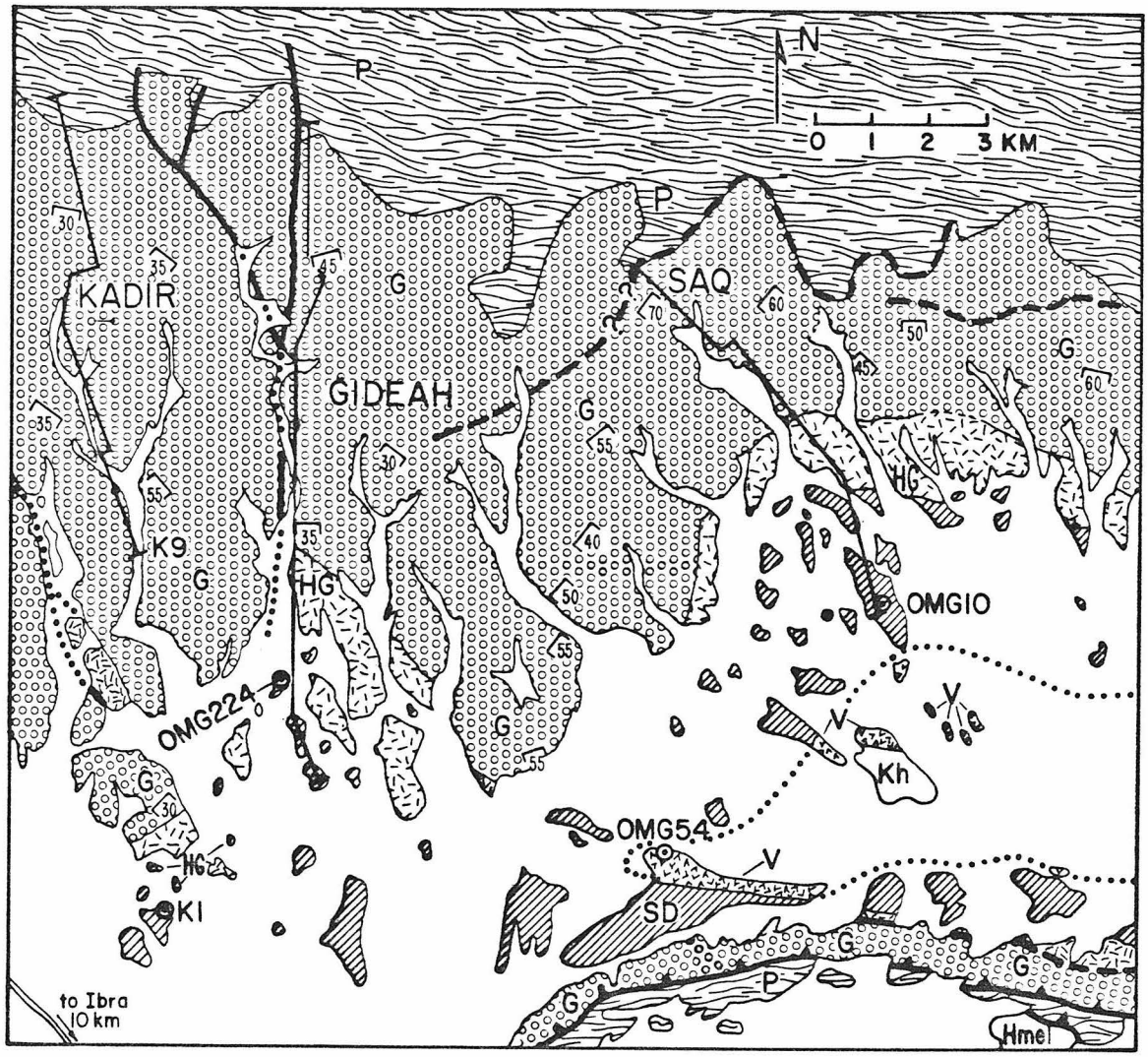
N
0 1 2 3 KM
KADIR
GIDEAH
SAQ
OMG10
OMG224
OMG54
K9
KI
Kh
SD
HG
to Ibra
10 km
Hmel

From bottom to top, a generalized stratigraphic section through the ophiolite in the Ibra area consists of: tectonized harzburgite peridotite; a thin basal zone of olivine-clinopyroxene cumulates (wehrlites); followed by 3-5 km of olivine-clinopyroxene-plagioclase cumulates (layered gabbros); grading into less than 1 km of plagioclase-hornblende ± clinopyroxene ± olivine + magnetite, non-cumulate, high-level gabbro. Over an abrupt transition interval (<10 meters thick), a zone of high-level gabbro with 10% diabase dikes gives way to a 100% sheeted diabase dike complex that is 1 to 2 km thick. Above the diabase dike complex is a relatively thin section of pillow lavas (<700 meters thick), and above the pillow lavas, and in some cases intercalated with the pillow lavas, are rare exposures of red chert.

Alteration minerals are abundant in the pillow basalt section (now altered to zeolite facies), the diabase section (lower greenschist to lower amphibolite facies) and in the high-level gabbro (amphibolite facies). Igneous textures are generally extremely well preserved, indicative of essentially static, hydrothermal metamorphism. The lower cumulates commonly exhibit alteration minerals that are visible only under the microscope, such as very minor talc-magnetite alteration of olivine. The cumulate rocks generally appear to be petrographically unaltered (but they are, in fact, highly altered; see below). The alteration mineral assemblages present in the diabases and pillow lavas are similar to those described in most other ophiolite complexes throughout the world [Coleman, 1977].

4.3 EXPERIMENTAL RESULTS

Oxygen was liberated from silicates using the flourine technique described by Taylor and Epstein, [1962]. The results reported in δ-notation in parts per mil (‰) where:

$$\delta^{18}O_{\text{SAMPLE}} = \left(\frac{^{18}O/^{16}O_{\text{SAMPLE}}}{^{18}O/^{16}O_{\text{STANDARD}}} - 1 \right) 1000$$

Precision is better than 0.2 per mil and raw $\delta^{18}O$ values are corrected to the SMOW scale using Caltech rose quartz $\delta^{18}O = 8.45$. NBS-28 has $\delta^{18}O = +9.60$ on this scale. Hydrogen was liberated from silicates by the technique described by Godfrey [1962], and results are also reported relative to SMOW in per mil.

The $\delta^{18}O$ and δD data are presented in Table 4-1. Plagioclase samples were analyzed in larger numbers than other minerals because feldspar is more sensitive to subsolidus hydrothermal ^{18}O-exchange than any other silicate [Taylor, 1968; Taylor and Forester, 1971]. Therefore, plagioclase was separated from all medium-to-coarse grained intrusive samples either magnetically or by hand picking. Pyroxene and amphibole mineral separates were obtained from magnetic concentrates that were further purified by hand-picking. Quartz from plagiogranites was separated by hand picking and HF treatment.

The $\delta^{18}O$ values of whole-rock samples were either analyzed directly from representative splits made from interior pieces, or they were calculated by material-balance from the $\delta^{18}O$ values of the individual mineral phases in the assemblage. We checked our calculated whole-rock $\delta^{18}O$ values against measured values for samples K9 and OM251, and agreement was well within our experimental precision, <0.1 per mil.

Table 4-1 Oxygen isotope analyses, mineralogy, and calculated values of $\delta^{18}O_{H_2O}$ and water/rock ratio for minerals and rocks of the Samail ophiolite complex, Oman.

Sample*	Mineralogy**	$\delta^{18}O_f$	$\delta^{18}O_{px}$	$\delta^{18}O_{other}$	$\delta^{18}O_{rock}$	$\delta^{18}O$ of H_2O eqt	W/R#
PILLOW BASALT (100°C - 200°C)							
OMG 54 (I)	f,pg,op,z,[ca,sa]				12.7	- 0.6 to 5.8	4.2
OMG 12-1 (J)	f,op,e,z,px				12.5	- 0.8 to 5.6	3.2
L 2.2 125 (J)	f,q,op,c[sp]				10.7	- 2.6 to 3.8	1.2
L.2.2 144 (J)	f,q,op,c,[e,sp]				10.7	- 2.6 to 3.8	1.2
SHEETED DIABASE (250°C to 400°C)							
OMG 6 (S)	f,c,q,e,op,[ca,ℓ]				9.3	4.3 to 7.6	n.d.
OMG 10 (S)	f,a,c,q,e,op,[sp,ca]	11.8			8.5	3.5 to 6.8	n.d.
OMG 8 (S)	f,op,c,e,q				8.2	3.2 to 6.5	n.d.
OMG 7a (S)	f,op,c,e,q				7.9	2.9 to 6.2	n.d.
OMG 7b (S)	f,op,c,e,q				8.3	3.3 to 6.6	n.d.
OMG 5-3 (S)##	f,a,c,op,q,[ca,e]	5.6			4.9	- 0.1 to 3.2	1.2
OMG 5-1 (S)	f,a,e,c,q,op				11.3	6.3 to 9.6	n.d.
K1 (K)	f,a,op,c,q,e				6.8	1.8 to 5.1	n.d.
HIGH LEVEL GABBRO (400°C to 600°C)							
OMG 71-1 (S)##	f,h,a,[px,op,e]	6.8		5.0(a+h)	5.9¢	4.9 to 7.1	n.d.
OMG 70 (S)	f,px,ol[h,op,a,c,t]	6.5				4.9 to 7.0	n.d.
OMG 64 (S)	f,px,h,ol,[op,a,c,t]	4.3				2.4 to 4.6	0.5
OMG 224-2 (K)	f,h,op,a,c,[p]	4.5		2.6(a+h)	3.7	2.2 to 4.5	0.4

CUMULATE GABBRO (400°C to 600°C)								
OMG 66	(S)	f,px,ol,[h,op,a,t,s]	5.8				4.2 to 6.3	0.04
OMG 65	(S)	f,px,ol,[op,t,h]	4.2				2.5 to 4.9	0.6
OMG 63	(S)	f,px,ol,[op,t,h]	4.1	4.3		4.2¢	2.7 to 4.7	0.6
OMG 62	(S)	f,px,ol,[op,t]	4.4			4.5	2.8 to 4.9	0.5
OMG 68	(S)	f,px,ol,[h,t,c,op,s]	3.6	4.1		3.7¢	2.0 to 4.2	0.9
OMG 58	(S)	f,px,ol,[c,s]	5.3	4.9		5.1¢	3.7 to 5.8	0.2
OMG 67	(S)	f,px,ol,[t,op,s,c]	6.0	5.7		6.0¢	4.4 to 6.5	n.d.
OMG 58a	(S)	f,px,ol,[op,s]	4.7			4.5	3.1 to 5.1	0.4
OMG 58b	(S)	f,px,ol,[op,s]	6.0				4.3 to 6.4	n.d.
OMG 57	(S)	f,px,ol,[s,p,hg]	6.6	5.7		6.4	5.1 to 7.2	n.d.
K 13	(K)	f,px,[e,c]	5.5				4.1 to 6.1	0.1
K 13a	(K)	f,px,ol,[c,op,s]				4.4	4.1 to 6.1	0.1
K 9	(K)	f,px,ol[h]	6.0	5.3		5.7,5.8¢	4.3 to 6.4	n.d.
K 16	(K)	f,px,ol,[c,t,op,s]	5.3	5.1		5.2¢	3.6 to 5.7	0.2
OM 251	(F)	f,px,ol,[hg,c,t,s]	6.4	5.8		6.1,6.2¢	4.7 to 6.8	n.d.
OM 28	(R)	f,px,ol,a,[e,t,c,s]	4.7			5.2	3.0 to 5.1	0.4
K 18	(K)	f,px,ol,[a,c,s,t,e]	4.1	4.7		4.3¢	2.4 to 4.5	0.6
OMG 282	(D)##	h			5.4h			
PLAGIOGRANITE (250°C - 400°C)								
OMG 71-2	(S)	f,q,h,a,op,[c,e,p]			4.8q	6.3	3.9 to 6.4	n.d.
OMG 66-3	(S)	f,[e,sp,op,q]				13.6	10.8 to 13.3	n.d.
OMG 66-1	(S)	f,h,[op,e,p,c,a]	8.1		5.6(a+h)		5.8 to 8.1	n.d.
OMG 66-4	(S)	f,p,c,e,op	14.0				11.2 to 13.7	n.d.

OMG 64-3	(S)	f,q,e				9.7	6.7 to 9.4	n.d.
OMG 65-3	(S)	f,[q,op,e]			8.5q	12.4	10.0 to 12.5	n.d.
OMG 224-3	(K)	f,h,q,a,c				5.2	2.3 to 4.8	0.5
GABBRO CUTTING PERIDOTITE (400°C - 600°C)								
K 21a	(K)	f,px,ol,[p,s,hg,op]	7.1	5.9			5.5 to 7.6	n.d.
K 21b	(K)	f,px,ol,[p,s,hg,op]	8.2	6.0			6.6 to 8.7	n.d.
OMG 53	(I)	f,px,ol,[s,hg,op]	9.2	6.4			7.6 to 9.7	n.d.
C 93	(I)	f,px,ol,[s,hg,p]	8.1	6.3			6.5 to 8.6	n.d.
C 204c	(I)	f,px,ol,[s,hg,p]	7.3	5.9			5.7 to 7.8	n.d.
G 141	(I)	f,px,ol,[p,hg,s]	7.8	6.3			6.2 to 8.3	n.d.

* - General geographic location of samples (see Fig. 1): I = Ibra, S = Wadi Saq, K = Wadi Kadir, J = Wadi Jizi, F = Wadi Fizh, R = Rustaq, D = Dasir.

** - Abbreviations: h = hornblende (brown or green), a = actinolite, c = chlorite, ca = calcite, px = clinopyroxene, e = epidote, f = plagioclase, hg = hydrogarnet, ℓ = leucoxene, ol = olivine, op = opaques, p = prehnite, pg = palagonite, q = quartz, s = serpentine, sa = saponite, sp= sphene, t = talc, z = zeolite; underlined symbols = alteration or secondary minerals; brackets [ ] enclose minor minerals (≤ 2% of rock); ¢ = calculated $\delta^{18}O$ of whole rock samples (from mineral ^{18}O data).

- δD values: OMG 5-3 (whole-rock = -53); OMG 71-1 (amphibole = -56); OMG 282f (hornblende = -47).

† - Range of calculated $\delta^{18}O_{H_2O}$ in equilibrium with the rocks using the feldspar geothermometer [O'Neil and Taylor, 1967] & assuming a reasonable range of temperatures, based on the hydrothermal mineral assemblages (given in parentheses for each rock type).

\# - Water/rock ratios (in oxygen units) calculated from the isotopic data, using the lower-temperature limit for each rock type, and the open-system equation $W/R_{open} = \ell n\ (W/R_{closed} + 1)$ for the sheeted diabase and pillow lavas. The closed system equation (see text) was used for the gabbros and plagiogranites. Cretaceous seawater ($\delta^{18}O = -0.5$) was used for the initial H_2O. The abbreviation n.d. means that $\delta^{18}O_{H_2O}{}^{I} = -0.5$ does not yield a valid result using either the closed system or open system calculation.

Table 4-2. Oxygen isotope analyses of whole-rock and mineral samples from the Samail Ophiolite along with location code and mineralogy.**

Sample*		Mineralogy	$\delta^{18}O_f$	$\delta^{18}O_{px}$	$\delta^{18}O_{other}$	$\delta^{18}O_{rock}$
PILLOW LAVAS						
OMG 300-1	(Y)	f,px,op,ca,c				16.0
OMG 301-2	(Y)	f,op,z,sp				16.6
OMG 302	(Y)	f,op,sp,q,z				16.8
OMG 303	(Y)	f,op,c,z				19.6
OMG 36	(B)	f,op,sp,ca				19.6
DIABASE DIKES						
P698-13	(Y)	f,op,a,c,t				4.8
P698-20	(Y)	f,op,c,q,e,a,[ca]				6.4
P698-21	(Y)	f,op,px,c,p,a				8.5
P698-16	(Y)	f,op,a,c,p				5.1
P698-29	(Y)	f,op,h,a,f,l,e				4.5
P698-32	(Y)	f,op,a,c[t,e]				6.5
P684	(Y)	f,op,h,u				2.9
P679-2	(Y)	f,op,a,q,l				8.6

Sample		Mineralogy	$\delta^{18}O_f$	$\delta^{18}O_{px}$	$\delta^{18}O_{other}$	$\delta^{18}O_{rock}$
P697-2	(Y)	f,px,op,c,a,p				8.5
P759-3	(Y)	diabase dike				6.5
P6990	(Y)	f,px,h,op[e]				2.5
HIGH-LEVEL GABBRO						
OMG 20	(G)	f,px,op,c,a	5.3			
OMG 19-5	(G)	f,h,op,a,c,p	5.0		2.1a	
OMG 19-6	(G)	f,h,op,a,sp,p				4.5
OMG 293-2	(D)	f,px,h,op,u	6.4		3.9h	
OMG 283F	(D)	h,f			5.6h	
GE4-6-5	(G)	f,h,q,c,op	6.6		4.9a, 7.5q	
CUMULATE GABBRO						
OMG 45-1	(G)	f,px,ol,[t,s]	5.9			
OMG 47-1	(G)	f,px,ol,[t,s,a]	5.1			
OMG 48-1	(G)	f,px,ol,[t,s,a]	4.6			4.7
OMG 46-1A	(G)	f,a,op,c(vein)	6.4			

Sample		Mineralogy	$\delta^{18}O_f$	$\delta^{18}O_{px}$	$\delta^{18}O_{other}$	$\delta^{18}O_{rock}$
OMG 46-2	(G)	f,px,[h,s]	7.0			
OMG 49-1	(G)	f,px,ol[s]	5.6			
OMG 50-1	(G)	f,px,h[a,c,op]	6.1			
OMG 51-1	(G)	f,px,opx,op[c]	3.9			
OMG 52-2	(G)	f,px,ol,h[c,t]	4.5	5.0		
OMG 235	(K)	f,px,ol				
GE 9	(G)	f,px,ol	5.8			
GE 10	(G)	f,px,ol	6.0	5.5		
GE 7	(G)	f,px,ol	6.1	5.3		
GE 12	(G)	f,px,ol	3.7			
GE 5	(G)	f,px,opx,ol,h,op	6.9	5.2		
K4 G2	(K)	f,px,ol,a	5.4	5.2		
K5 G1	(K)	ol,f,px[s,op]	5.5	4.8		
K6 G2	(K)	f,px,h[a,c,t,s]op	5.2	5.2		
K7 G2	(K)	f,px,ol[t,op,h]	3.7	4.2		
Kf 5-1		f,ol,px,h,op	5.9			

Sample		Mineralogy	$\delta^{18}O_f$	$\delta^{18}O_{px}$	$\delta^{18}O_{other}$	$\delta^{18}O_{rock}$
Kf 6-1		f,ol,px,h,op	5.6			
Kf 7-1		f,ol,px,h	5.3			
Kf 8-1		f,ol,px,h[a]	5.5			
Kf 12-1		f,ol,px,h	6.3	5.9		
Kf 16-1		f,px[h]	3.0	5.2		
Kf 20-1		f,ol,px	5.7	5.8		
OMG 343	(D)	f,ol,px,opx,op	6.5	5.9		
OMG 39-2	(D)	f,px,opx,h,op,h	4.4			
HORNFELS						
OMG 292-2	(D)	h,f,op				3.7
OMG 91-2	(D)	h,f,op				4.3
OMG 89-1	(D)	h,f,op				6.3
OMG 287-3	(D)	h,f,op	5.7		4.1h	4.6
OMG 288-3	(D)	f,h,op				7.4
C 301	(D)	h,f,op				5.6
OMG 286-1	(D)	h,f,op				3.9

Sample		Mineralogy	$\delta^{18}O_f$	$\delta^{18}O_{px}$	$\delta^{18}O_{other}$	$\delta^{18}O_{rock}$
PLAGIOGRANITE						
OMG 293-1	(D)	f,q,h,op,bt,c,e	6.6		6.9q	6.7
C 294	(D)	f,q,h,op	7.1		7.3q	
C 295 A	(D)	f,q,h,op,bt,c	9.00†		7.3q	8.2
OMG 18 b	(D)	f,q,a,e,op,c	11.3		8.1q	
OMG 90-2	(D)	f,q,h,op,e,c,sp	8.6†		7.5q	8.1
OMG 88-4	(D)	f,q,h,op,sp,c,bt,ap	7.0†		7.1q	7.0
OMG 91-3	(D)	f,q,h,op	4.5		7.3q	
OMG 89-1	(D)	f,q,h,op,bt				8.1
C 301	(D)	f,q,h,op			7.8q	
C 291a	(D)	f,q,h,op	10.7		4.1h, 5.4h	
OMG 288-3	(D)	f,q,h,op,sp,c			7.5q, 4.6h	
OMG 297	(D)	f,q,h,op			7.7q	
OMG 206-1	(B)	f,q,op,h,a,c			6.5q	
OMG 25	(B)	f,q,op,h,a,c			4.8q	
OMG 224-3	(K)	f,q,h,op,c,a	5.5		4.0q	5.2

Sample		Mineralogy	$\delta^{18}O_f$	$\delta^{18}O_{px}$	$\delta^{18}O_{other}$	$\delta^{18}O_{rock}$
VEINS						
GE4 G5	(G)	Vein quartz			7.7q	
GE4 Q1	(G)	Vein quartz			9.4q	
GE4 Q2	(G)	Vein quartz			9.0q	

*Location and abbreviation symbols are the same as in Table 4-1, except for bt = biotite, B = Batin, Y = Al Yahamdi, Kf = Wadi Khafifah, G = Wadi Gideah. These place names can be seen on Figure 2-2.

**Table 4-2 includes all the data not reported in Table 4-1.

†$\delta^{18}O$ value calculated by mass balance.

4.4. DISCUSSION OF THE ISOTOPE DATA

4.4.1 General Statement

The main features of the $\delta^{18}O$ data and δD data are presented graphically in Figs. 4-3 and 4-4. The most striking results of this isotopic study are as follows:

(1) Hydrothermal ^{18}O exchange was observed well down into the deeper levels of the cumulate gabbros, and locally was found to penetrate along fractures into the upper mantle peridotites.

(2) Only a few D/H results from the Oman ophiolite are reported in this study, but these are similar to the D/H data from the Troodos ophiolite [Heaton and Sheppard, 1977; Magaritz and Taylor, 1974], and they are compatible with a model of seawater-hydrothermal exchange (Fig. 4-4).

(3) A relatively systematic $^{18}O/^{16}O$ distribution was observed within the pervasively altered section, which includes all the rocks down to about 2 km above the fossil Moho (Fig. 4-3).

(4) Relative to an initial $\delta^{18}O \approx +5.7$, high-T (>350°C) seawater-hydrothermal alteration produced ^{18}O-depleted rocks (down to $\delta^{18}O = +3.5$) throughout the upper cumulate gabbros, as well as locally in the lowest levels of the oceanic crustal section.

(5) ^{18}O-enriched rocks were produced in the higher levels of the oceanic crust, particularly above the contact between high-level gabbro and the sheeted diabase complex.

Figure 4-3a. Oxygen isotope data for the combined Wadi Saq and Wadi Kadir sections. Data below 2 km are from Wadi Kadir. Above 2 km, the data are from Wadi Saq, except where noted by sample number. OMG 10, OMG 54, K 1, K 9, and OMG 224 are samples from the Ibra area analyzed by McCulloch et al., [1981]. Sample L 2.2-125 is from Wadi Jizi. Shaded area represents OMG 65 and OMG 66 outcrops, which are locted at the same structural horizon in Wadi Saq. Dotted line connects analyses of plagioclase separates. Horizontal solid lines connect coexisting minerals from the same hand specimen. Horizontal dashed lines connect data-points from the same outcrop but different hand specimens. Pg = plagiogranite.

Figure 4-3b. Oxygen isotope data for Wadi Saq, Wadi Kadir and Wadi Gideah East traverses. Solid lines connect analyses from the same hand specimen. Dashed lines connect analyses of plagioclase separates. All data not found in Table 4-1 are included in Table 4-2.

a)

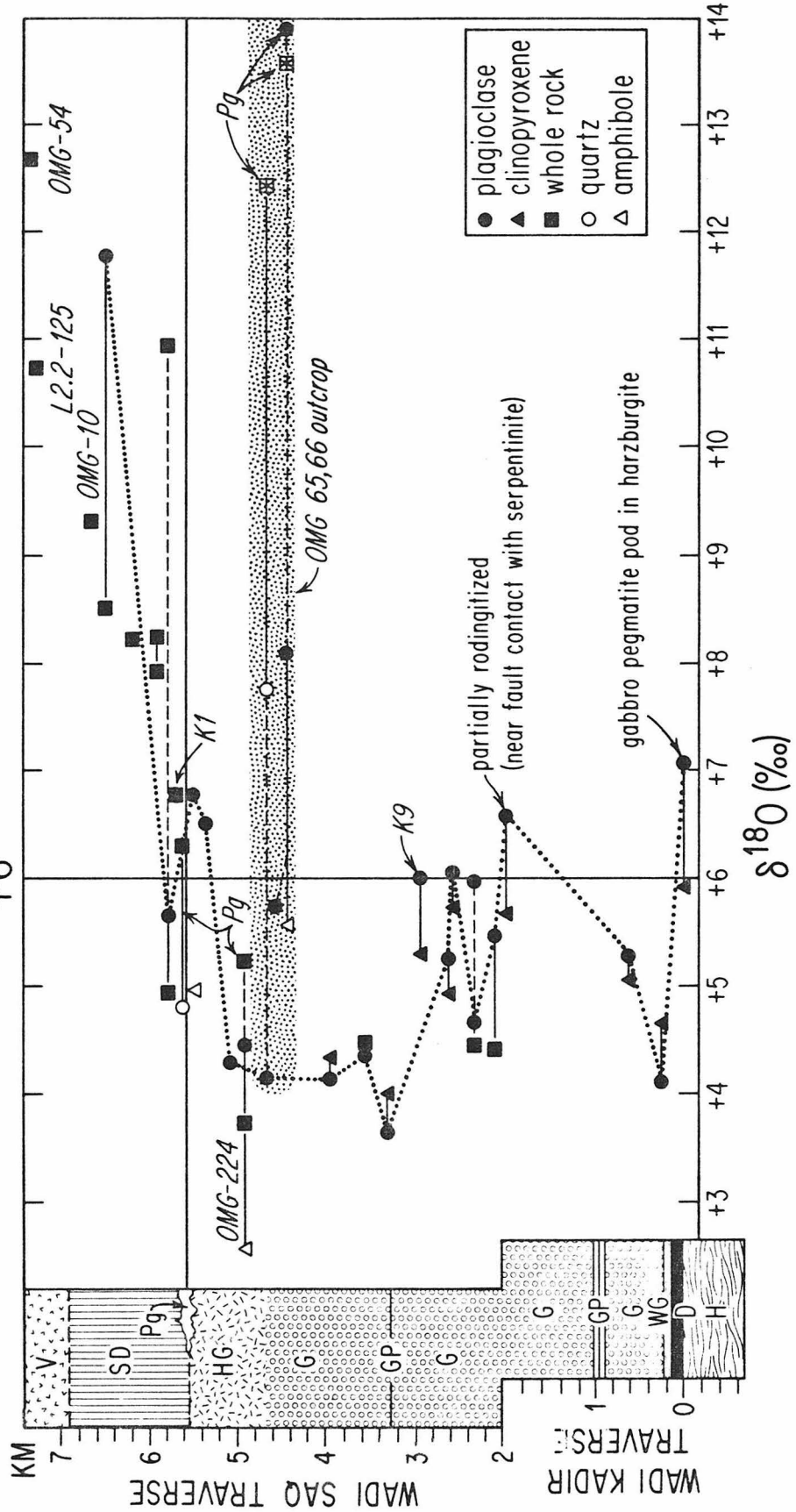
+6
δ18O (‰)
+3
+4
+5
+6
+7
+8
+9
+10
+11
+12
+13
+14
plagioclase
clinopyroxene
whole rock
quartz
amphibole
OMG-54
L2.2-125
OMG-10
OMG-224
K1
K9
Pg
OMG 65,66 outcrop
partially rodingitized
(near fault contact with serpentinite)
gabbro pegmatite pod in harzburgite
KM
WADI SAQ TRAVERSE
WADI KADIR TRAVERSE
V
SD
Pg
HG
G
GP
WG
D
H

b)

WADI SAQ TRAVERSE

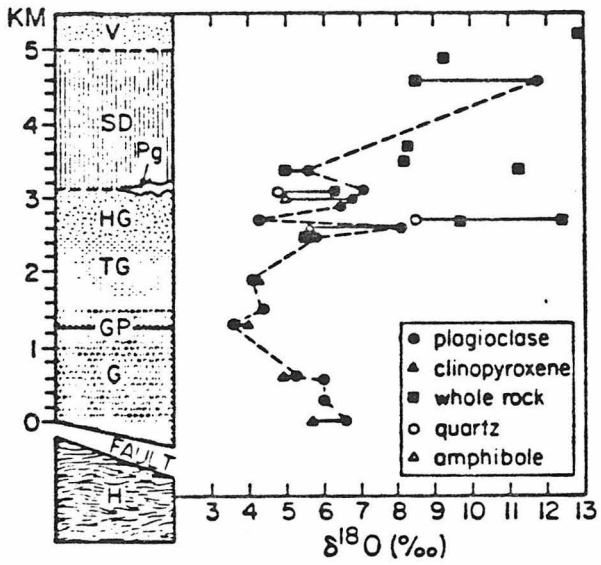

WADI GIDEAH EAST TRAVERSE

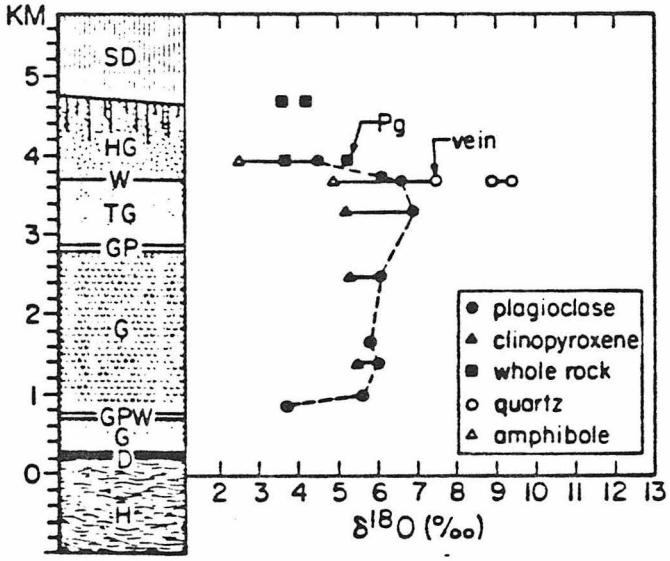

WADI KADIR TRAVERSE

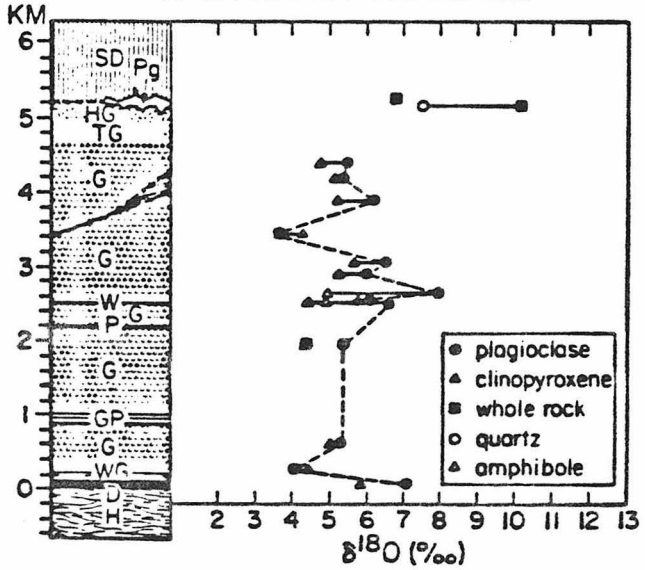

(6) High-temperature ^{18}O exchange with hydrothermal fluids occurred at levels well below the stratigraphic horizon at which secondary hydrothermal OH-bearing minerals disappear in the cumulate gabbros.

4.4.2 Plagioclase-Clinopyroxene Pairs

In addition to the D/H data, evidence for deep circulation of seawater derived hydrothermal fluids comes mainly from data on coexisting plagioclase and pyroxene. Several such mineral pairs were examined from the cumulate gabbros and gabbro dikes and veins which cross-cut the peridotite. This mineral pair is particularly valuable because pyroxene is so much more resistant to hydrothermal ^{18}O-exchange than is plagioclase [Taylor, 1968; Taylor and Forester, 1971; Forester and Taylor, 1977; Taylor and Forester, 1979]. Throughout the gabbro section, this mineral pair exhibits oxygen isotopic disequilibrium; based on analogous results from other localities [Forester and Taylor, 1977; Taylor and Forester, 1979], it is clear that this feature is a result of subsolidus exchange.

Plagioclase-pyroxene pairs analyzed from rapidly quenched gabbroic magmas, such as terrestrial basalts and lunar microgabbros, all have $\Delta^{18}O$ plagioclase-pyroxene $\equiv \delta^{18}O$ plagioclase $- \delta^{18}O$ pyroxene ≈ 0.5, close to the equilibrium fractionation [Taylor, 1968; Anderson et al., 1971; Taylor and Epstein, 1970; Onuma et al., 1970]. Therefore, in normal, mid-ocean ridge tholeiites that have whole-rock $\delta^{18}O = 5.7$, the corresponding primary magmatic $\delta^{18}O$ plagioclase should be +6.0 and the $\delta^{18}O$ pyroxene about +5.5. On a graph of $\delta^{18}O$ plagioclase vs. $\delta^{18}O$ pyroxene (Fig. 4-5), all primary magmatic plagioclase pyroxene pairs from normal tholeiite basalts should therefore

Figure 4-4. Plot of δD vs. $\delta^{18}O$ for rocks analyzed from the Oman ophiolite, showing calculated isotopic compositions of ^{18}O-shifted Cretaceous ocean water and of waters that would be in equilibrium with the Oman samples at T = 300°C and 500°C (for details of calculation, see Heaton and Sheppard, [1977]). Also shown for comparison are data from another Cretaceous Tethyan ophiolite, the Troodos complex, Cyprus, by Heaton and Sheppard [1977] and Magaritz and Taylor [1974].

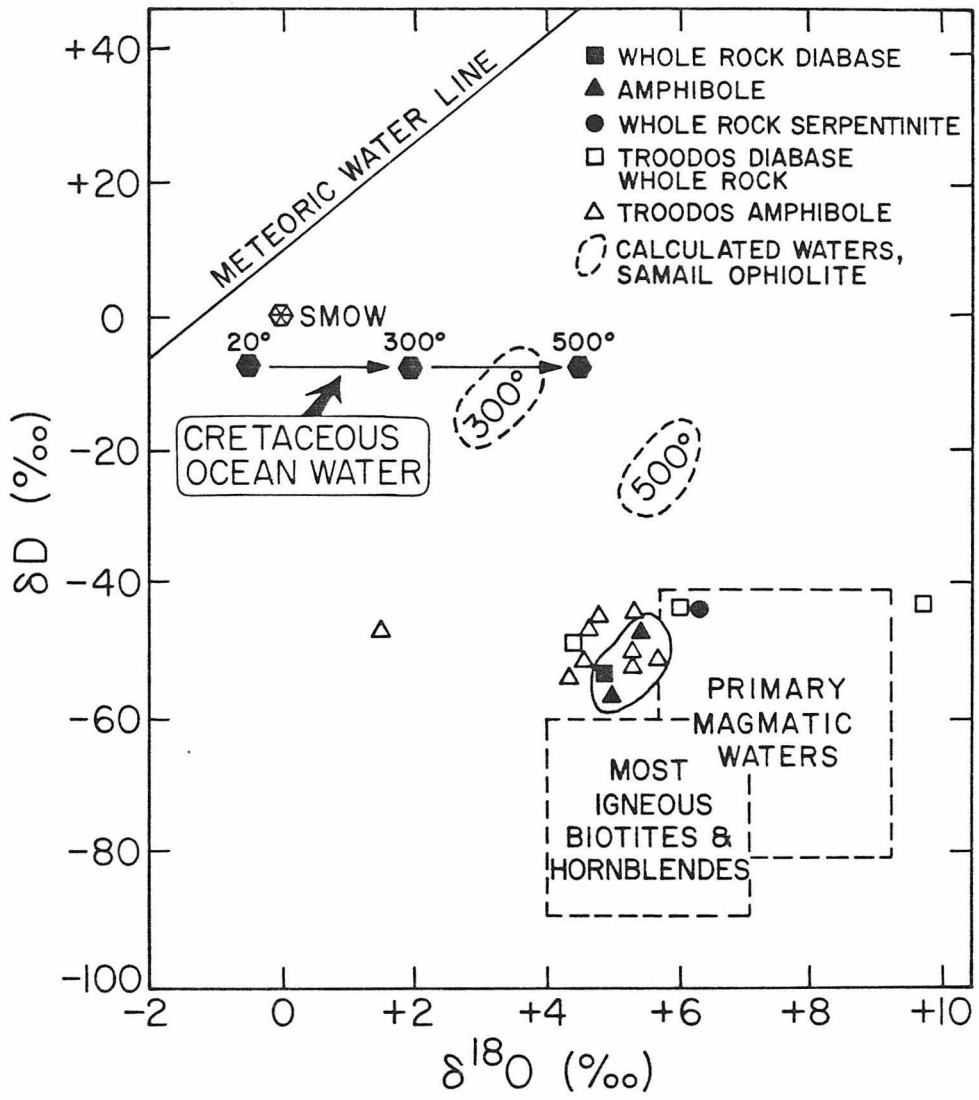
METEORIC WATER LINE
WHOLE ROCK DIABASE
AMPHIBOLE
WHOLE ROCK SERPENTINITE
TROODOS DIABASE WHOLE ROCK
TROODOS AMPHIBOLE
CALCULATED WATERS, SAMAIL OPHIOLITE
SMOW
20°
300°
500°
CRETACEOUS OCEAN WATER
300°
500°
PRIMARY MAGMATIC WATERS
MOST IGNEOUS BIOTITES & HORNBLENDES
+40
+20
0
-20
-40
-60
-80
-100
δD (‰)
-2
0
+2
+4
+6
+8
+10
δ18O (‰)

cluster around a spot having the coordinates (5.5, 6.0). If the bulk $\delta^{18}O$ value of the basaltic liquid differs from +5.7, the plagioclase-pyroxene pairs will map out a straight line of slope 1, the $\Delta = 0.5$ line on Fig. 4-5. If the temperature of final equilibration is higher or lower than the solidus temperature of the basaltic magma, the Δ-values will be respectively, smaller or larger than 0.5. All lines representing constant temperatures of equilibration of pyroxene and plagioclase on Fig. 4-5 will have a slope of 1 and a $\delta^{18}O$ plagioclase intercept equal to $\Delta^{18}O$.

During cooling of the system, plagioclase-pyroxene, $\Delta^{18}O$ will increase. Slowly cooled plutonic gabbros in fact typically exhibit plagioclase-pyroxene Δ-values of 0.8 to 1.3 [Taylor, 1968]. From the original primary magmatic "spot" on Fig. 4-5, rocks undergoing closed-system cooling will map out a series of points that form a right triangle whose sides are the north and west vectors emanating from the "spot" and whose hypotenuse is the line segment with slope = 1 that corresponds to the new temperature of final equilibration (e.g., the $\Delta = 1.5$ line segment on Fig. 4-5). The north vector applies to cumulate layers where modal clinopyroxene >> plagioclase, and the west vector applies to cumulate layers where modal plagioclase >> clinopyroxene. All other intermediate compositions will be within the triangle. This two-component analysis works for the cumulates because the modal abundance of clinopyroxene + plagioclase is much greater than the abundance of olivine, the only other oxygen-bearing cumulus mineral.

In open systems the equilibrium plagioclase-pyroxene pairs are required to lie upon the new "final" temperature line, but not necessarily

Figure 4-5. Plot of $\delta^{18}O$ plagioclase vs. $\delta^{18}O$ clinopyroxene for samples from the cumulate gabbro and from gabbro dikes in the peridotite. These data plot on trends forbidden during closed-system equilibrium cooling (see text).

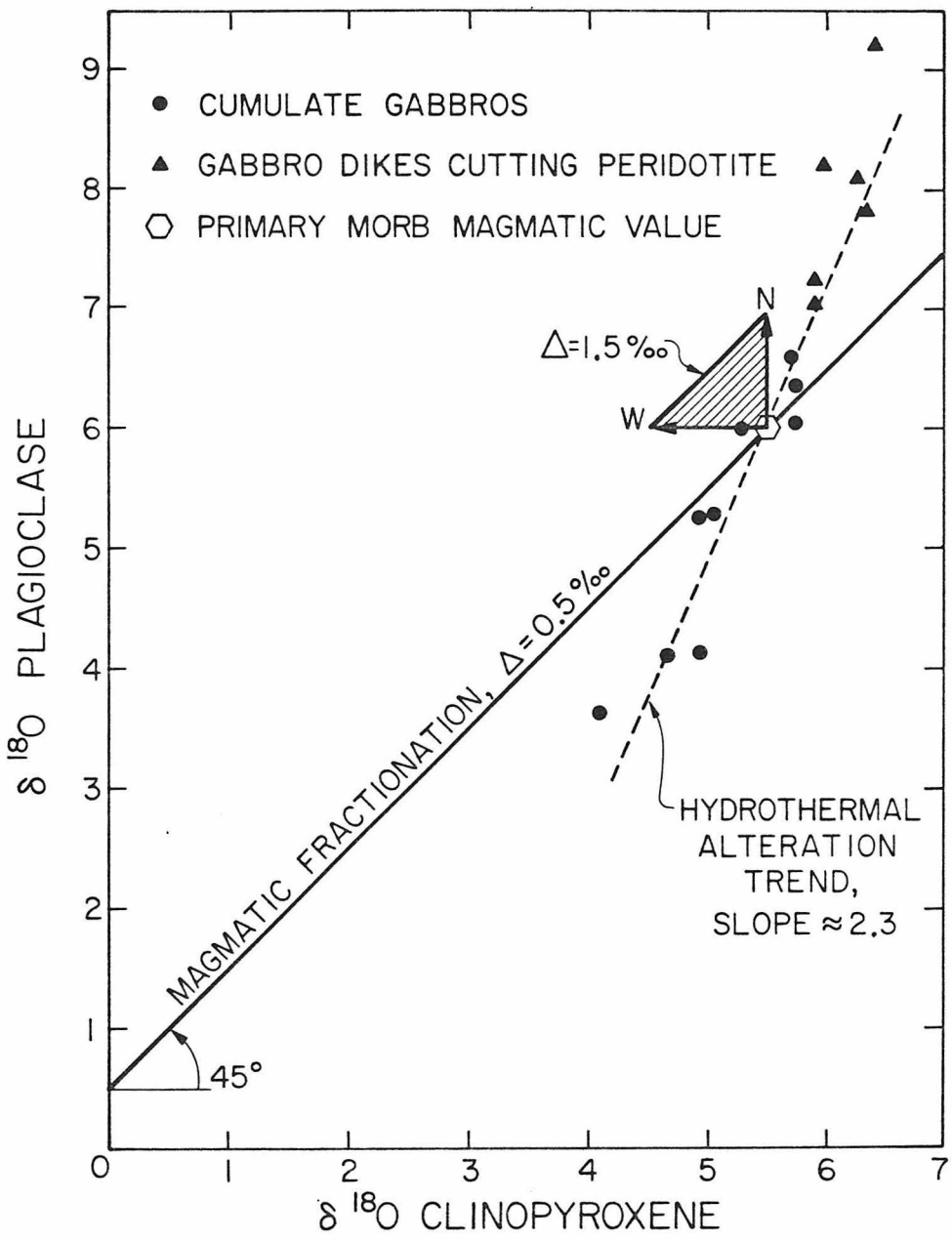
CUMULATE GABBROS
GABBRO DIKES CUTTING PERIDOTITE
PRIMARY MORB MAGMATIC VALUE
N
W
Δ=1.5‰
MAGMATIC FRACTIONATION, Δ=0.5‰
45°
HYDROTHERMAL ALTERATION TREND, SLOPE ≈2.3
δ 18O PLAGIOCLASE
δ 18O CLINOPYROXENE
0
1
2
3
4
5
6
7
8
9

within the closed system "triangle". However, there are no conditions of open- or closed-system equilibrium cooling in which the data points can move below the primary magmatic (Δ = 0.5) line on the plagioclase-pyroxene plot.

Many of the cumulate plagioclase-pyroxene pairs from the Samail ophiolite plot in the field forbidden under equilibrium conditions. In addition, the plagioclase-pyroxene pairs do not plot on an equilibrium trend with slope unity, but instead plot in the vicinity of a least-squares line given by the equation:
$\delta^{18}O$ plagioclase $\approx$ 2.3 $\delta^{18}O$ clinopyroxene - 6.6 (Fig. 4-5).
The $\Delta^{18}O$ values associated with the line of slope 2.3 include some samples that have normal igneous fractionations and in fact this line passes through the primary magmatic "spot". As plagioclase $\delta^{18}O$ values decrease, the $\Delta^{18}O$ values decrease to zero and then become reversed. Since all equilibrium plagioclase-pyroxene $\Delta^{18}O$ values are known to be positive in the temperature range that is geologically reasonable ($T < 1300°C$), the trend of data points in Fig. 4-5 constitutes clearcut evidence for open-system (hydrothermal) sub-solidus exchange. The plagioclase-pyroxene graph is a very sensitive indicator of sub-solidus disequilibrium exchange, as well as testing for open or closed system conditions. Fig. 4-5 shows that virtually all of the plagioclase-pyroxene pairs in the Samail gabbro have exchanged under open system conditions.

Trend lines similar to the one illustrated in Fig. 4-5 have been reported for the Skaergaard intrusion and the Cuillin gabbro of the Isle of Skye [Forester and Taylor, 1977; Taylor and Forester, 1979]. As shown in Fig. 4-6, the slopes of these meteoric-hydrothermal alteration

Figure 4-6. Comparison of $\delta^{18}O$ data on clinopyroxene-plagioclase pairs from Oman (solid dots) with analogous data from the Skaergaard (lined pattern; UBG = Upper Border Group; LS = Layered Series; UZc = Upper Zone c of the Layered Series) and Cuillin gabbros (dashed envelopes); the latter were altered by meteoric-hydrothermal fluids [Taylor and Forester, 1979; Forester and Taylor, 1977]. The Oman data form a more systematic, narrower band which possibly indicates less closed-system, subsolidus cooling prior to interaction with hydrothermal fluids. This may reflect the more tectonically active spreading regime for the ophiolite rocks. The $\Delta = 0.5$ line (45°) represents the accepted ^{18}O fractionation between pyroxene and plagioclase at magmatic temperatures [Anderson et al., 1971].

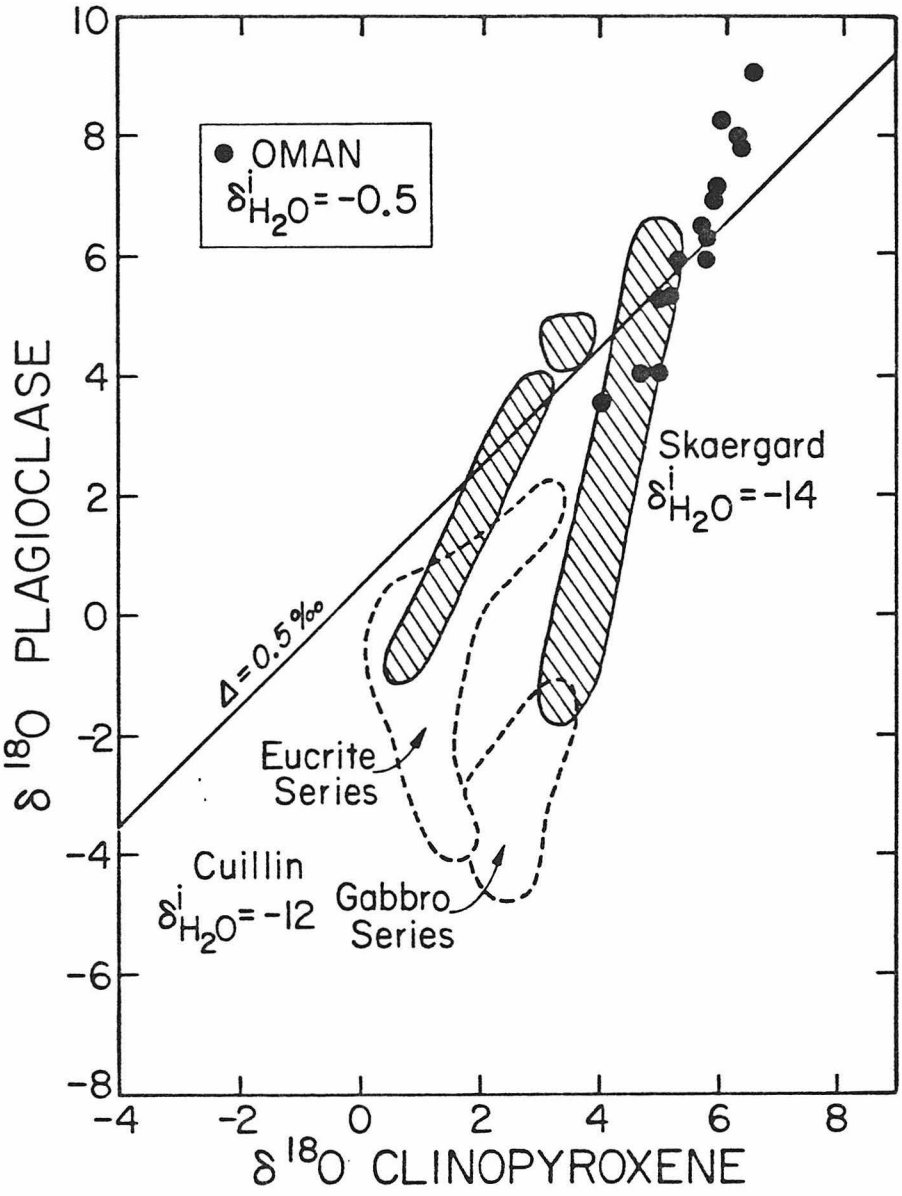
OMAN
$\delta^i_{H_2O} = -0.5$
Skaergard
$\delta^i_{H_2O} = -14$
$\Delta = 0.5‰$
Eucrite
Series
Cuillin
$\delta^i_{H_2O} = -12$
Gabbro
Series
$\delta^{18}O$ PLAGIOCLASE
$\delta^{18}O$ CLINOPYROXENE
10
8
6
4
2
0
-2
-4
-6
-8
-4
-2
0
2
4
6
8

trajectories vary from approximately two to four. These differences in slope are suggestive of differing exchange rates between the various clinopyroxenes and aqueous solutions. Some of the obvious factors that will influence the slope of the alteration trend are grain size, degree of exsolution, fluid-phase composition, $\delta^{18}O$ of the fluid, and perhaps equilibration time. The cumulate plagioclase-pyroxene pairs in Oman display a slope that is less steep than that shown by most of the Skaergaard samples, although they do trend parallel to the UBG, UZc, and Sandwich Horizon pairs from the Skaergaard intrusion, where the effective grain size of the clinopyroxene has been signficantly reduced by sub-solidus recrystallization and inversion from a β-wollastonite precursor [Taylor and Forester, 1979]. Inasmuch as the Oman clinopyroxenes exhibit exsolution features and grain sizes comparable to the rest of the Skaergaard Layered Series, where the alteration slope is approximately four, this raises the question as to which of the other parameters listed above is controlling the slopes.

Let us assume that at a given T, clinopyroxene exchanges with a hydrothermal fluid at a fixed (slower) rate than does plagioclase. This is essentially identical to stating that the effective water/mineral ratio is lower for pyroxene than for plagioclase (i.e. the pyroxene "sees" less H_2O than the adjacent coexisting plagioclase). By setting the water/mineral ratio for plagioclase (An_{75} for the cumulates) equal to a constant times the water/mineral ratio for clinopyroxene, $\delta^{18}O$ trajectories of the plagioclase-pyroxene pairs from the Oman ophiolite and the Skaergaard intrusion can be simulated (Fig. 4-7). In this illustration, the initial Oman $\delta^{18}O_{H_2O}$ is assumed to be -0.5, and the "initial" Skaergaard $\delta^{18}O_{H_2O} \approx -5.0$ [Norton and

Taylor, 1979]. This "initial" Skaergaard fluid composition is an ^{18}O-shifted surface water which originally had a $\delta^{18}O_{H_2O} \approx -14.0$ based on D/H systematics [Taylor and Forrester, 1979]. The boundaries of the fields on Fig. 4-7 are defined arbitrarily by assuming a 500°C exchange temperature, and rate constants for plagioclase that are a factor of two to five times faster than for pyroxene.

The plotted curves bracket the actual data from both the Skaergaard and Oman and suggests the plagioclases exchanged between 3 and 5 times more rapidly than the coexisting clinopyroxenes (the 5x curves on Fig. 4-7). The different slopes, two and four, respectively, for Oman and the Skaergaard are a consequence of the drastically different $\delta^{18}O$ compositions of the hydrothermal fluids. For most mineral-water systems, the first derivative of the hydrothermal exchange curve will equal the rate of constant, if small (open system) water/rock ratios prevail. The larger the difference between initial fluid and initial rock, the more closely will the measured points reflect the rate constant. A second implication of Fig. 4-7 is that the Skaergaard Layered Series and the Samail gabbros both achieved approximately the same water/rock ratio $\approx$ 0.15 (open system mass units). This relatively crude estimate of the water/rock ratio is actually very close to the value ($\approx$ 0.20 for the Layered Series) calculated by Norton and Taylor [1979] in a much more complete numerical modeling study of the Skaergaard intrusion. This suggests that many of the important parameters, such as permeability, porosity, etc., used by Norton and Taylor [1979] in their analysis of the Skaergaard gabbro also would apply to the Samail gabbro and thus to the oceanic crust in general.

Figure 4-7. Plot of $\delta^{18}O$ plagioclase (An_{75}-cumulates; An_{90}-gabbros in the peridotite) vs. $\delta^{18}O$ clinopyroxene for the Oman and Skaergaard mineral-pair trajectories. The curves are calculated in two ways: 1) analytically besetting $W/R_{\text{open system}}^{\text{plagioclase}} = K \times (W/R_{\text{open system}}^{\text{clinopyroxene}})$ or 2) by a finite element technique which allows small but different (by a constant factor) increments of water to equilibrate with plagioclase and as the integrated W/R ratio builds up with each step. Both methods yield the same curves. These paths represent cooling, accompanied by hydrothermal exchange, starting at the magmatic coordinates (5.5, 6.0 Δ =0.5) and proceeding to T ≈ 500°C (Δ =1.67). The initial $\delta^{18}O_{H_2O}$ is assumed to be -5.0 at the Skaergaard [Norton and Taylor, 1979] either -5.0 or +8.9 at Oman; the former value is Cretacious seawater, and the latter value represents magmatic water or strongly ^{18}O-shifted seawater in the deepest parts of the Samail hydrothermal system. Two calculated curves are shown, arbitrarily assuming that plagioclase exchanges with H_2O at a rate either twice (2X) or five times (5X) faster than clinopyroxene. Water/rock ratios of 0.1, 0.25, 0.50, 0.75 and 1.0 (in weight units) are represented by tie-lines connecting the 2X and 5X curves, assuming the rock contains 60% plagioclase and 40% clinopyroxene. The interaction of the exchange curves with the Δ =1.67 line corresponds to an infinite water/rock ratio. The cumulate gabbro trajectories mimic the behavior of the $\delta^{18}O$

Figure 4-7. (cont.)

values of actual mineral assemblages shown in Fig. 4-6, in that the latter do indeed plot on the high-temperature side of the magmatic isotherm (T ≈ 1100°C).

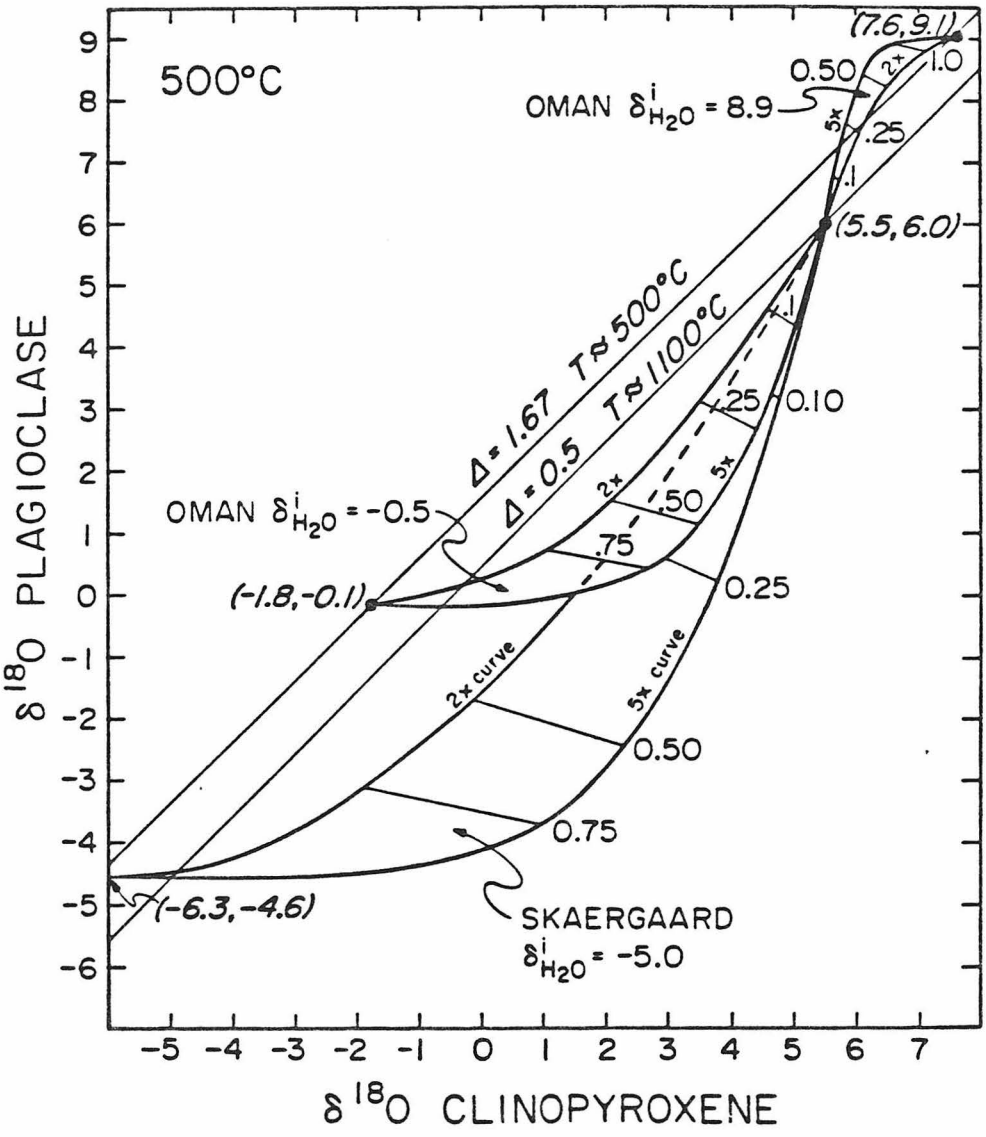
500°C
(7.6,9.1)
0.50
2x
1.0
OMAN $\delta^i_{H_2O}$ = 8.9
5x
.25
.1
(5.5,6.0)
Δ = 1.67 T≈500°C
Δ = 0.5 T≈1100°C
.1
.25
0.10
OMAN $\delta^i_{H_2O}$ = -0.5
2x
5x
.50
.75
(-1.8,-0.1)
0.25
2x curve
5x curve
0.50
0.75
(-6.3,-4.6)
SKAERGAARD
$\delta^i_{H_2O}$ = -5.0
$\delta^{18}O$ PLAGIOCLASE
$\delta^{18}O$ CLINOPYROXENE

The above discussion indicates that the most important factors in fixing the final $\delta^{18}O$ values of mineral pairs affected by hydrothermal alteration are:

(1) The initial $\delta^{18}O_{H_2O}$;

(2) The amount of fluid flushed through the system;

(3) The average temperature of exchange;

(4) Grain size (especially when intense grain-boundary recrystallization or mineral exsolution occurs). Salinity differences in the aqueous fluids appear to be less important, at least at concentrations lower than that exhibited by normal sea water.

4.4.3* General Mineral-Mineral Systematics

In order to test the validity of the conclusions concerning exchange trajectories of mineral pairs in hydrothermal systems, the trajectories were calculated for the ophiolite complex, assuming a wider range of temperatures with differing initial fluid compositions. The results of these calculations (Fig. 4-8) suggest that in the complete open system, as long as the initial fluid is different by several per mil from the initial rock, and the cumulative water/rock ratio is small, the slope of the exchange curve is rather insensitive to temperature. The relationship strictly holds only for exchange processes where no new phases are created. When a new phase is formed during the hydrothermal event, the mineral pairs are more likely to lie on isotherms or approach equilibrium, such as in the Skaergaard Upper Border Group- γ where clinopyroxene inverted from a β -wollastonite precursor or in rocks where secondary amphibole replaces

* Sections 4.4.3 to 4.4.7 are not part of the JGR oxygen isotope article.

Figure 4-8. 2X exchange curves are plotted for various temperature and initial water composition. The heavy solid curves are for T ≈ 600°C and were calculated for $\delta^{i}H_2O$ = -14, -0.5, 1.5, 4.5, 5.5 and 6.5. The arrows on the 600°C isotherm show the direction in which the infinite water/rock point moves as the initial water gets heavier in $\delta^{18}O$. The dot-dash-dot line represents the exchange curve for -0.5 water at 1100°C; the dotted line for -0.5 water at 500°C, and the dashed line represents -0.5 water at 400°C. The calculations show that at the low water/rock end of the curves, virtually all of the trajectories are coincident. Notice that the linear disequilibrium trend can be generated in the gabbro even if the initial fluid composition varies by ~6 per mil, as long as the water/rock ratio is low.

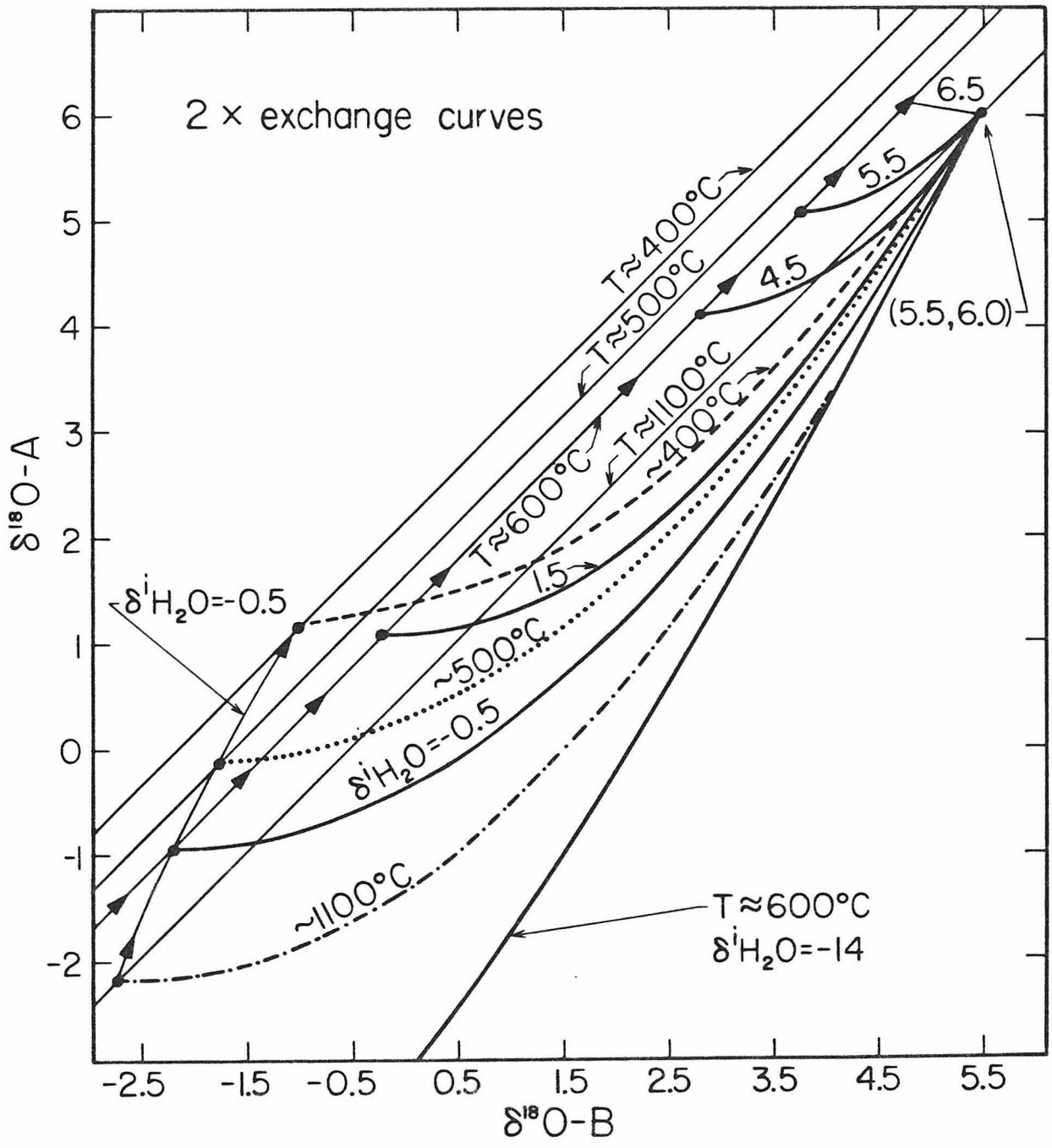
2 × exchange curves
T≈400°C
T≈500°C
T≈600°C
T≈1100°C
~400°C
~500°C
~1100°C
6.5
5.5
4.5
1.5
(5.5,6.0)
δ¹H₂O=-0.5
δ¹H₂O=-0.5
T≈600°C
δ¹H₂O=-14
δ¹⁸O-A
δ¹⁸O-B
6
5
4
3
2
1
0
-1
-2
-2.5
-1.5
-0.5
0.5
1.5
2.5
3.5
4.5
5.5

pyroxene (Fig. 4-6). The slopes of the exchange curves are not insensitive to changes in the initial fluid (Fig. 4-8). This suggests that in principle, by choosing a water which is drastically out of equilibrium with a mineral pair--one mineral that exchanges rapidly and the other that exchanges more slowly--relative exchange rates could be determined in laboratory experiments.

All of the above calculations assumed complete open system conditions which require that each infinitesimal packet of water only reacts with the rock once. The equation governing this "one pass" system is given by:

$$\delta B = (\delta B_i - \delta W - \Delta_B)\left(\frac{\delta A - \delta Wi - \Delta_A}{\delta A_i - \delta Wi - \Delta_A}\right)^K + \delta W_i + \Delta_B$$

where ($\delta A, \delta B, \delta W_i$) are the initial values of the fluid and two minerals; Δ_A, Δ_B are the fractionation factors for mineral A-water and mineral B-water at some specified temperature; the constant K is inversely proportional to the actual rate constant. The exchange trajectories were calculated both analytically using the expression above and by finite element analysis with both procedures yielding the same results. Therefore, the finite element program was utilized in further calculations that were modified to allow for water cycling.

In Figure 4-9, the results of two calculations are presented which allowed each incremental packet of water to mix back into a larger reservoir of fixed value. These calculations show that initially the open and closed systems behave identically. However, as the water continues to react and equilibrate with the minerals the value of the more rapidly exchanging mineral passes through a minimum and begins to increase (for $\delta^{18}O\ H_2O < \delta^{18}O$ bulk system). The exchange curve then

moves towards the new equilibrium value on the new lower temperature isotherm. The final coordinate of the mineral pair is a function of the bulk water/rock ratio and can be calculated by material balance from

$$W \ \delta W_i + a \ \delta A_i + b \ \delta B_i = W \ \delta W_f + a \ \delta A_f + b \ \delta B_f$$

The difference in the trajectories of the open and closed system cases are striking. The mineral-mineral $\delta^{18}O$ data presented thus far, here and elsewhere [Taylor, 1974; Taylor and Forester, 1979; Taylor, 1980; Criss, 1981], show that nearly all of the natural systems contain mineral pairs which lie on either the open system curves or on the beginning portions of the closed system curves (which are essentially open system curves). This suggests that water recirculation or closed system cycling is not an important process in the systems studied thus far, a conclusion also reached by Norton and Taylor [1980] in their numerical analysis of the Skaergaard hydrothermal system.

4.4.4 δ - δ Plots and Mineral Δ Reversals

Recently Kyser [1979] has proposed a reversal in the equilibrium value of $\Delta^{18}O$ clinopyroxene-olivine at high temperatures (>1200°C) in order to explain olivine-clinopyroxene $\delta^{18}O$ values obtained from ultramafic nodules. Using petrologic geothermometers, these workers correlated changes in Δ with increasing temperature. On a plot of $\delta^{18}O$ clinopyroxene vs. Δcpx-ol, a linear array was observed to indeed cross the Δ=0 line. For the Samail ophiolite, the plot Δplag-cpx *vs* $\delta^{18}O$ plag (Fig. 4-10) also produces a linear array which also crosses the Δplag-cpx=0 line. However the latter data clearly cannot be interpreted as evidence for a reversal in the equilibrium value of Δ for the following reasons: 1) Δ is not correlated with depth in the section as Figure 4-3 shows. 2) On the δ-δ plot,

Figure 4-9. Closed and open system exchange curves are compared for minerals A and B (plagioclase and pyroxene). The closed system calculation allows for water recycling, and mimics the open system at the beginning of the calculation. This calculation suggests that all of the natural hydrothermal systems studied to date behaved as open systems, in agreement with Norton and Taylor [1979].

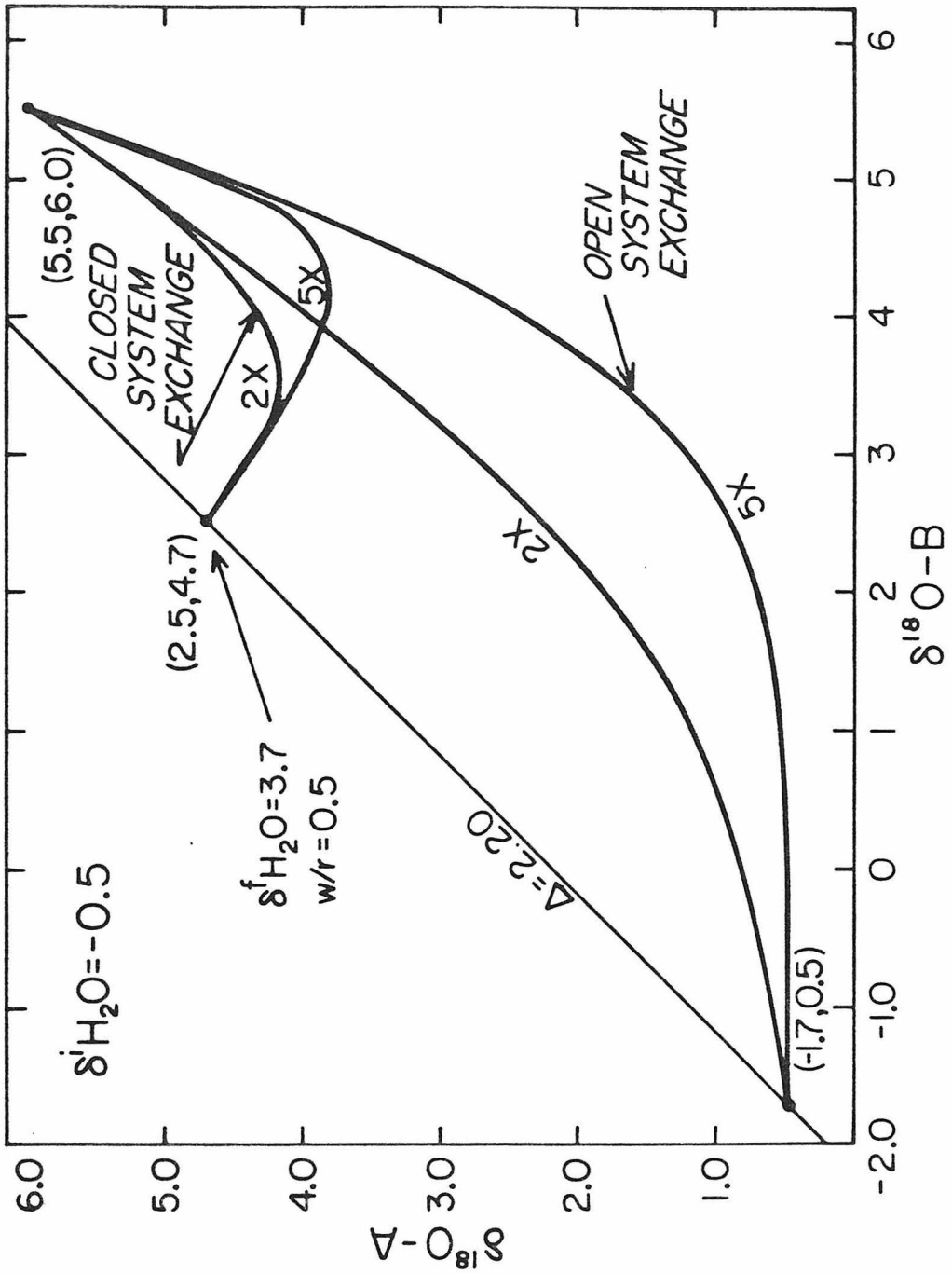
(5.5,6.0)
CLOSED SYSTEM EXCHANGE
5X
2X
OPEN SYSTEM EXCHANGE
5X
2X
(2.5,4.7)
$\delta^f H_2O$=3.7
w/r=0.5
Δ=2.2
$\delta^i H_2O$=-0.5
(-1.7,0.5)
$\delta^{18}O-\Delta$
$\delta^{18}O-B$
6.0
5.0
4.0
3.0
2.0
1.0
-2.0
-1.0
0
1
2
3
4
5
6

Figure 4-10. $\delta^{18}O$ plagioclase versus Δ plagioclase-clinopyroxene for the Samail ophiolite. The area shown by the ruled pattern is the field of closed system exchange assuming a starting coordinate of (6, 0.5). Again, as in the δ-δ diagrams, the Samail data suggest isotopic disequilibrium due to open system exchange between the rocks and an external hydrothermal fluid.

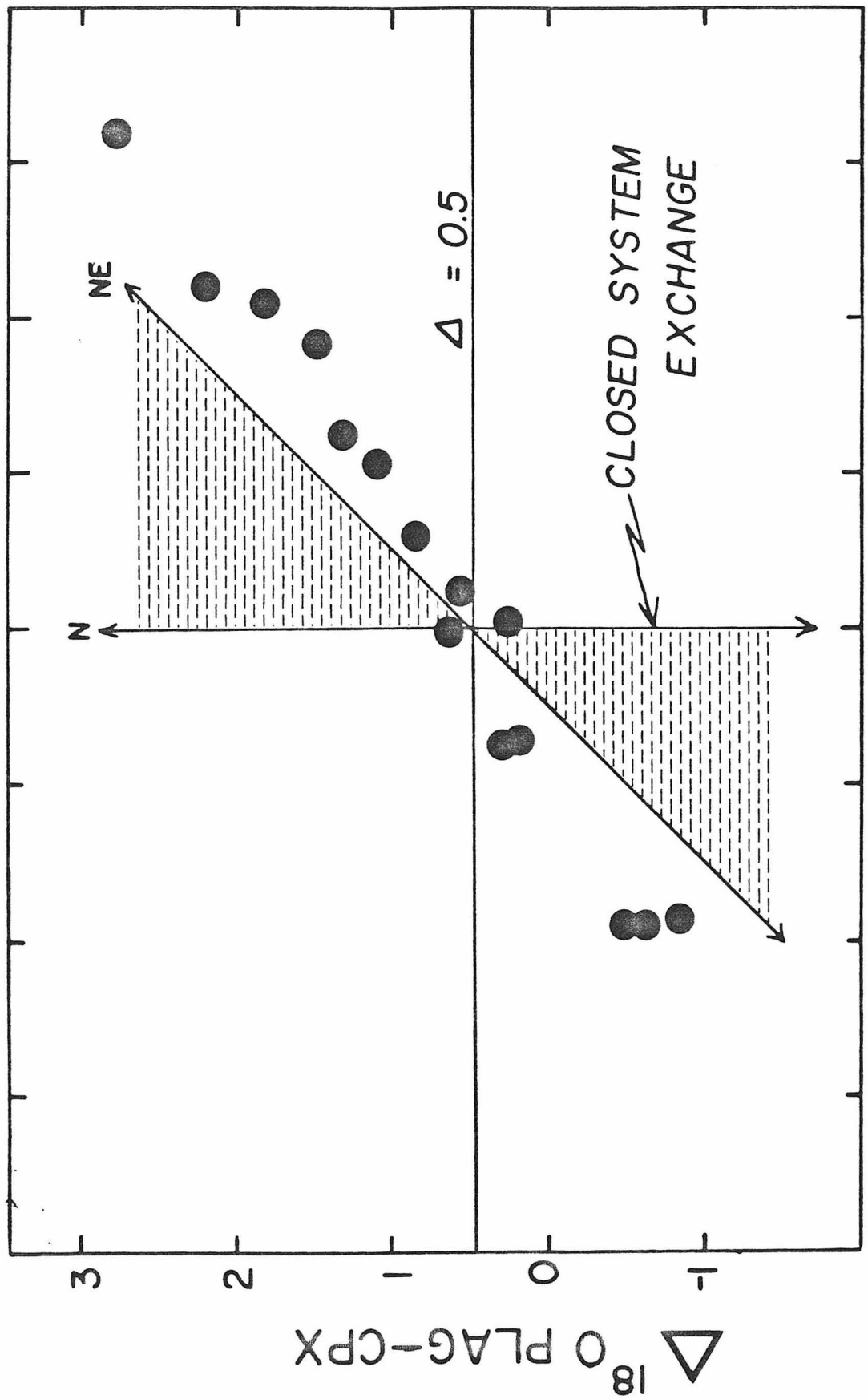
NE
N
Δ = 0.5
CLOSED SYSTEM
EXCHANGE
3
2
1
0
-1
3
4
5
6
7
8
9
Δ 18O PLAG-CPX
δ18O PLAGIOCLASE

slopes of linear arrays consistent with closed system exchange must lie on trends with negative slopes. 3) The array lies outside any of the plausible paths of the closed system exchange on the Δ-^{18}O plot (shaded fields on Fig. 4-10), whether or not a "cross-over" exists and whether the temperature increases or decreases during ^{18}O exchange.

The second point is easily shown either graphically (Fig 4-5) or by considering the following equations:

$$\delta^{18}O \text{ system} = a \quad \delta A + b \quad \delta B$$
$$a+b=1$$
$$\delta^{18}O \text{ system} = a\delta A + (1-a)\delta B;$$

$$\delta A = \frac{a-1}{a} \delta B - \frac{\delta^{18}O \text{ system}}{a}$$

Inasmuch as $(a-1) \leq 0$ the slope of any closed system exchange curve between two minerals must be negative, whereas the actual data from the Samail ophiolite and systems studied elsewhere [Magaritz and Taylor, 1976b; Taylor and Forester, 1979; Wenner and Taylor, 1976; Criss, 1981] have positive slopes.

4.4.5 Quartz-feldspar

All of the principles described above for pyroxene-plagioclase mineral $\delta^{18}O$ diagrams can be applied to granitic rocks using quartz and alkali feldspar. Taylor [1974], and Magaritz and Taylor [1976b] used such diagrams to show that granitic rocks exhibit a wide range of at least 10 per mil in primary magmatic $\delta^{18}O$ and that hydrothermally altered rocks exhibited pronounced oxygen isotopic disequilibrium (Fig. 4-11). This disequilibrium is primarily a result of the resistance of quartz to oxygen exchange recognized by Clayton et al. [1968] and Taylor [1968]; such effects are typically observed in hydrothermal systems associated with intrusive igneous rocks [Taylor and Forester, 1971].

Figure 4-11. $\delta^{18}O$ feldspar versus $\delta^{18}O$ quartz for granitic rocks from all over the world. Data are from: Taylor [1968], Wenner and Taylor [1976], Magaritz and Taylor [1976b], Turi and Taylor [1976], and Taylor [1971].

- ● Rhyolites
- ■ Granophyres for gabbroic complexes
- ▲ Granitic plutons
- ○ Tuscan province
- ▼ Southern California Batholith
- ⬡ St. Francois Granites
- △ St. Francois Rhyolites; Δ_m = matrix
- □ Stono Mountain
- ◉ Cascades Granodiorites

The inset shows how points move during subsolidus hydrothermal alteration. Points lying above the magmatic line were altered by either a high ^{18}O fluid or at low temperature, and points lying below the line by a low ^{18}O fluid.

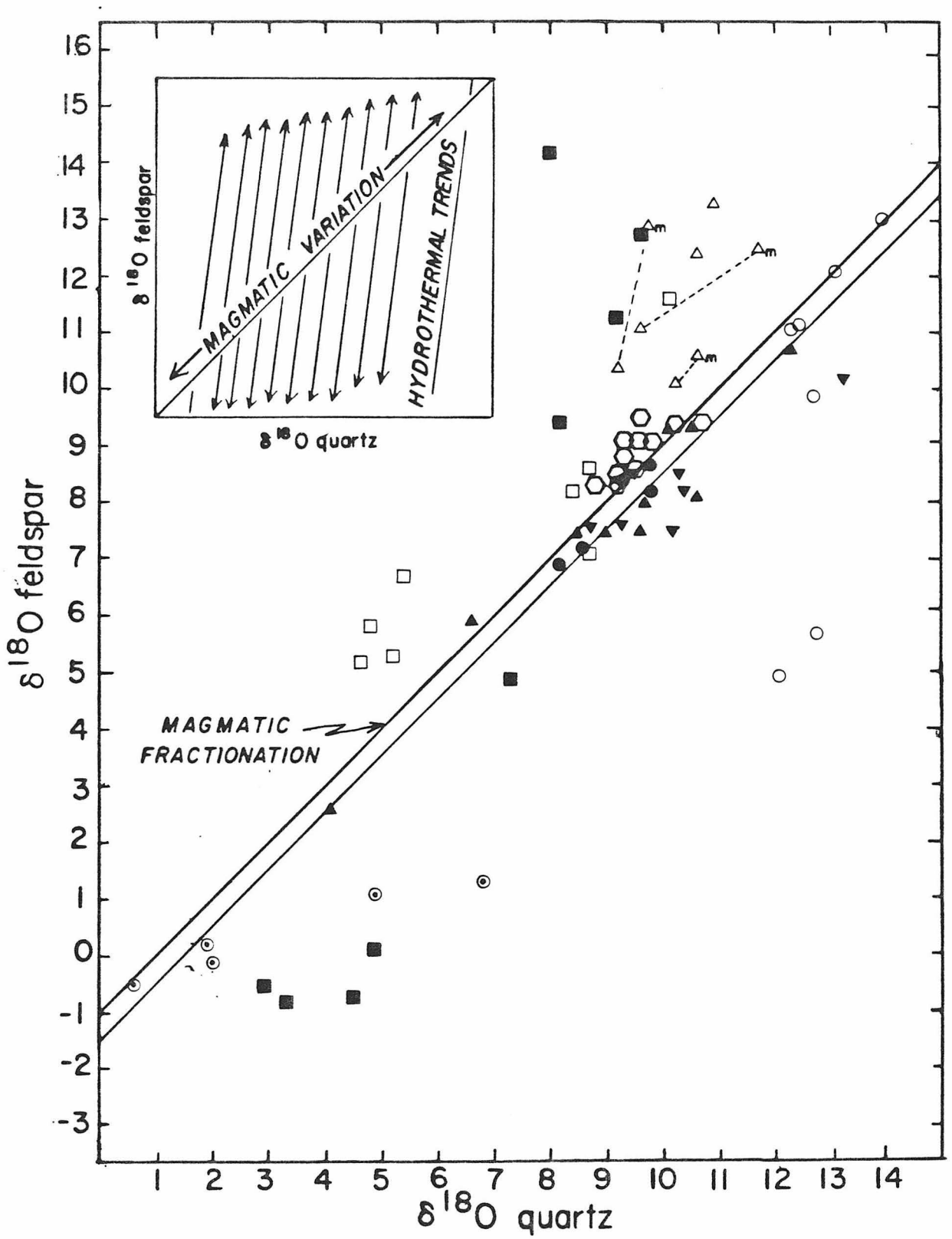
δ18O feldspar
δ18O quartz
MAGMATIC FRACTIONATION
MAGMATIC VARIATION
HYDROTHERMAL TRENDS
δ18O feldspar
δ18O quartz
m
m
m

In the Samail ophiolite, quartz-feldspar pairs from the Dasir area map out a steep hydrothermal trend (Figure 4-12) that projects back to the primary magmatic coordinates of the Dasir plagiogranite (7.1, 5.5), assuming a Δ quartz-feldspar = 1.5. Steep hydrothermal trends such as the Dasir trend were first systematically studied by Criss [1981] for several Eocene plutons in the Idaho batholith. The Tuscan granodiorites in Italy [Taylor and Turi, 1976] also exhibit a steep hydrothermal trend. The recognition of these hydrothermal trends in two continental environments and in an oceanic environment attests to the resistance of quartz to subsolidus hydrothermal exchange. This suggests that the quartz-feldspar points which lie off the equilibrium trend can (with some discretion) be projected back to the primary magmatic line. Such projections for granitic rocks indicate that in general this procedure leads to a correct estimate of the primary $\delta^{18}O$ values of the rocks prior to hydrothermal alteration [Criss, 1981].

In the Samail ophiolite and at Canyon Mountain, Oregon, plagiogranite quartz exhibits a marked dispersion in extrapolated primary $\delta^{18}O$ values ($3.7<\delta^{18}O$ quartz<9.0), suggesting that prior to sub-solidus alteration, the plagiogranites did not form from an isotopically homogeneous reservoir of ^{18}O (Figure 4-13). This is in contrast to the uniform composition of the ^{18}O reservoir from which the gabbros crystallized, as shown by the fact that nearly all of the points on the pyroxene-plagioclase diagram (Figure 4-5) project through the coordinates (5.5, 6.0) to within a half per mil. This suggests a uniform ^{18}O reservoir for the gabbros in spite of field and petrologic evidence that multiple injections of primitive picritic to basaltic melt were

Figure 4-12. $\delta^{18}O$ feldspar versus $\delta^{18}O$ quartz showing steep hydrothermal trajectories for quartz-feldspar pairs analogous to the curves observed for the pyroxene-plagioclase system. This suggests within a single locality the initial $\delta^{18}O$ value of quartz can be quite uniform and its value calculated by projecting the hydrothermal trend back to a magmatic fractionation line. The Eocene pluton data are found in Criss [1981], and the Tuscan granodiorite data come from Taylor and Turi [1976].

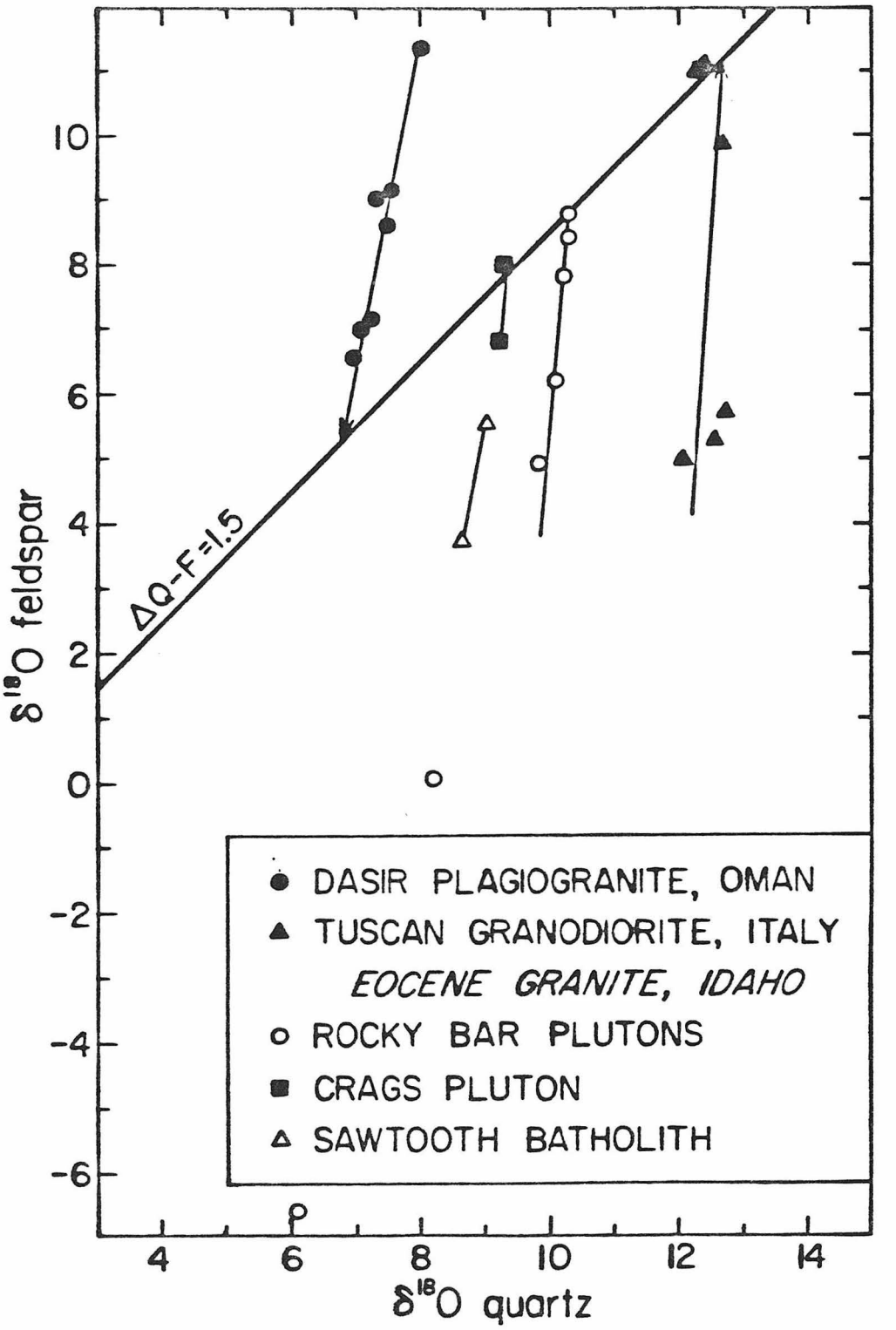
10
8
6
4
2
0
-2
-4
-6
4
6
8
10
12
14
δ18O feldspar
δ18O quartz
ΔQ-F=1.5
DASIR PLAGIOGRANITE, OMAN
TUSCAN GRANODIORITE, ITALY
EOCENE GRANITE, IDAHO
ROCKY BAR PLUTONS
CRAGS PLUTON
SAWTOOTH BATHOLITH

Figure 4-13. $\delta^{18}O$ feldspar versus $\delta^{18}O$ quartz for Canyon Mountain and Dasir plagiogranites. Extrapolating quartz values back to the magmatic line suggests that primary $\delta^{18}O$ quartz varies from 3.7 to 7.8. This suggests that in contrast to the gabbros which crystallized from a uniform reservoir of ^{18}O, the plagiogranites crystallized from a heterogeneous reservoir of ^{18}O. The only source of this heterogeneity is from hydrothermally altered rocks at the roof of the magma chamber. The data suggest that the contaminant was generally lower in ^{18}O than the primary magma implying the existence of a ridge-axis hydrothermal system (see below). The hydrothermal slopes trending north of the magmatic line require a fluid phase strongly enriched in ^{18}O relative to seawater (see Figure 4-8). Because the plagiogranite is found generally at the gabbro-diabase contact, these mineral pairs monitor the fluid composition discharing from the hydrothermal system operating in the layered gabbros.

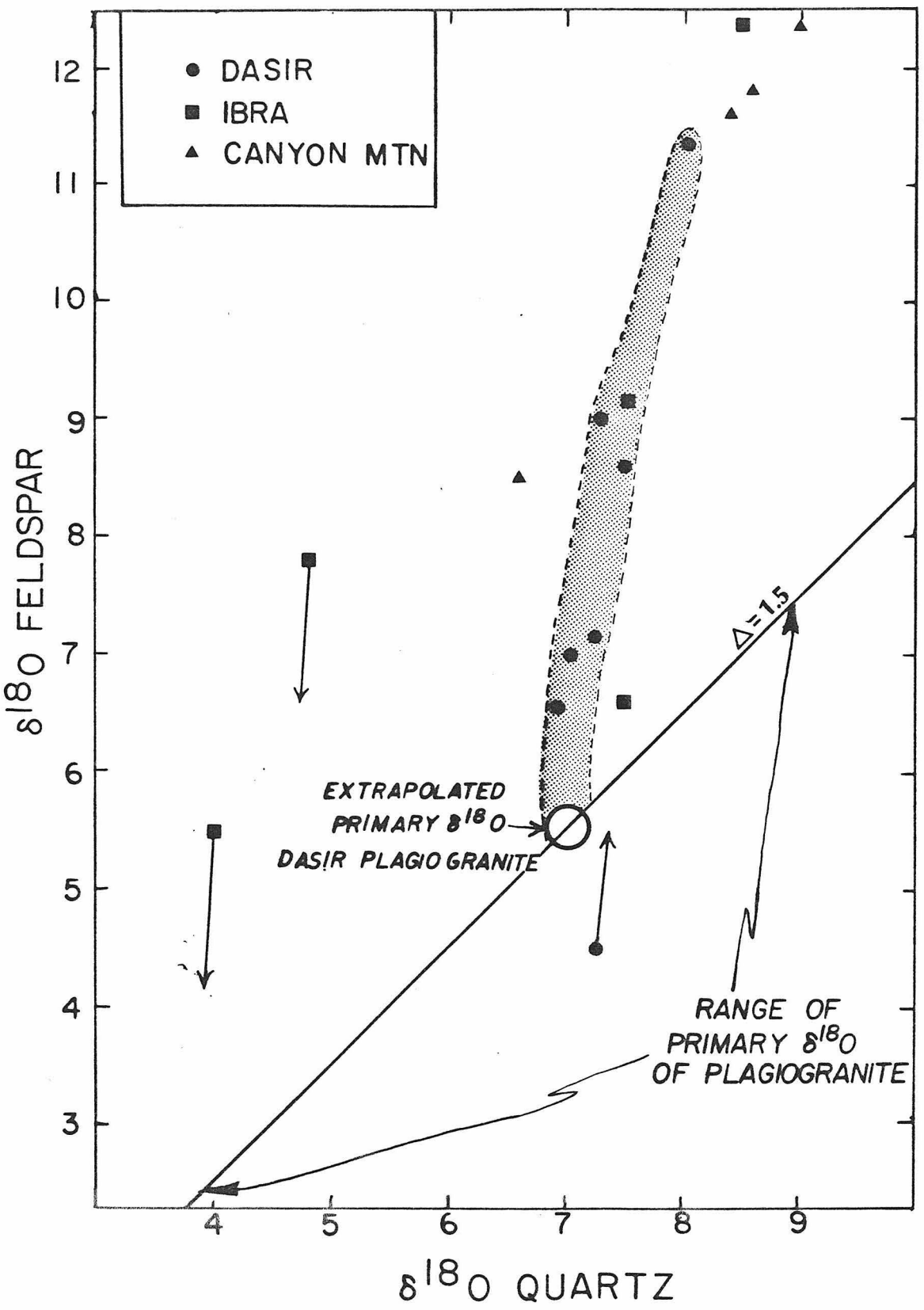
DASIR
IBRA
CANYON MTN
12
11
10
9
8
7
6
5
4
3
$\delta^{18}O$ FELDSPAR
4
5
6
7
8
9
$\delta^{18}O$ QUARTZ
Δ=1.5
EXTRAPOLATED
PRIMARY $\delta^{18}O$
DASIR PLAGIOGRANITE
RANGE OF
PRIMARY $\delta^{18}O$
OF PLAGIOGRANITE

involved in the history of the Samail magma chamber. Combining these two $\delta^{18}O$ "field facts" from the Oman Mtns., this suggests that the isotopically heterogeneous plagiogranites cannot be related (at least in terms of their oxygen isotope characteristics) to the isotopically homogeneous gabbros by any type of simple, single-stage fractional crystallization model. An open system is thus required to explain these isotopic results, all of which can be fitted into the stoping model for plagiogranite genesis described in Sec. 3.5.2. The extreme low $-^{18}O$ quartz values are plausibly explained as a result of partial melting of ^{18}O-depleted blocks of hydrothermally altered diabase derived from the sheeted dike complex just above the roof of the gabbro magma chamber.

4.4.6 Implications of the quartz-feldspar data for the origin of the plagiogranites

The quartz and feldspar $\delta^{18}O$ data suggest that plagiogranites do not crystallize under closed system conditions. An input of ^{18}O from the hydrothermally altered roof rocks must be called upon to explain the spread in the primary magmatic $\delta^{18}O$ values of plagiogranites. In Chapter 3, field evidence in support of direct partial melting of stoped roof blocks was presented. The quartz-feldspar data are consistent with this field interpretation, and thus partial melting of the hydrothermally altered roof must be considered as one mechanism for generating plagiogranites. However, because assimilation and fractional crystallization processes typically go hand-in-hand [Bowen, 1928; Taylor, 1980; McBirney, 1979], generation of plagiogranites by extreme fractional crystallization certainly must occur as well.

If plagiogranites are generated by fractional crystallization driven by assimilation of low-^{18}O hydrothermally altered diabases, then the $\delta^{18}O$ values of the plagiogranite liquids can be crudely calculated [Taylor, 1980; DePaolo, in press]. In order to change the ^{18}O content of the magma, ^{18}O from the roof has to be transferred into the melt and the heat required to do this comes from the crystallizing magma. The assimilated ratio of roof rock to cumulates crystallized directly from the melt determines the curvature of exponential mixing lines. The $\delta^{18}O$ of the remaining liquid is proportional to the fraction of melt remaining raised to an exponent which is a function of the assimilation rate over the crystallization rate [Taylor, 1980; DePaolo, in press].

Considering that there is a small equilibrium fractionation of ^{18}O between quartz and magma, in the most extreme case $\delta^{18}O$ quartz could never be lighter than $\delta^{18}O$ wall-rock + 1. In the Samail ophiolite, if a 1-km thick section of hydrothermally altered diabase with a $\delta^{18}O=2.5$ was assimilated, leaving a plagiogranite liquid representing 2% of the gabbro chamber, the $\delta^{18}O$-quartz of that liquid would be about +3.7 per mil. However, changing the roof-rock $\delta^{18}O$ to 4.0 (a more reasonable value), results in $\delta^{18}O$ quartz $\approx$ 5.6. Inferred plagiogranite primary quartz values range from 3.7 to 7.8 (Fig. 4-13). This suggests that extreme fractional crystallization driven by assimilation could also deliver the observed range of plagiogranite $\delta\ ^{18}O$. Therefore distinguishing between the two mechanisms becomes a difficult exercise in field geology.

Field relations, such as plagiogranite bodies crosscut by diabase dikes, or screens of plagiogranite within the dike complex, may be interpreted as evidence that plagiogranites form during all stages of the

Figure 4-14. Photomicrographs of two plagiogranites, one from Dasir (OMG 293-1) and the other form Wadi Saq, Ibra (OMG 71-2), are shown under both plane- and cross-polarization. (Maximum field of view in all photographs is 3.16 mm). OMG 293-1 (d, c) contains quartz, albite, hornblende, magnetite and biotite. The plagioclase is only slightly turbid. At Ibra (a, b) the feldspar is very turbid. However, Carlsbad-Albite twins are still faintly visible under X-nicols. $\delta^{18}O$ quartz = 6.9 for OMG 293-1 an $\delta^{18}O$ quartz = 4.8 for OMG 71-2. OMG 71-2 crops out at the gabbro-diabase contact, whereas OMG 293-1 crosscuts high-level gabbro at Dasir.

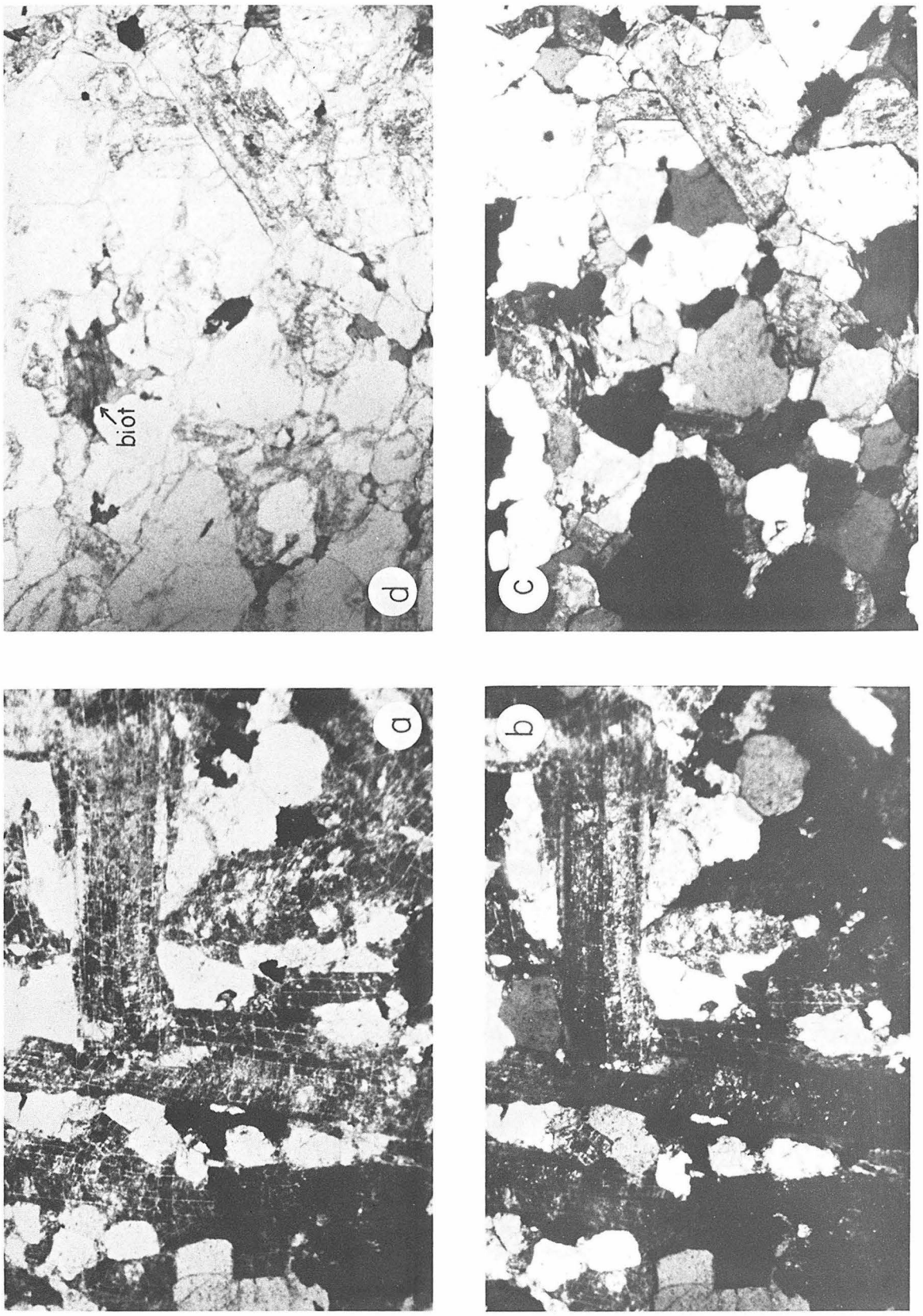
a
b
c
d
biot

magma chamber history. Plagiogranites having low $\delta^{18}O$ quartz (Fig. 4-14a) in these geologic settings almost certainly formed as partial melts of stoped roof-rock blocks. However, as pointed out in Chapter 3, the superposition of many stoping events coupled with extreme fractional crystallization of small patches of magma during each one of these events makes recognition of one model over the other virtually impossible. In effect, the heat required to either partially melt or assimilate the stoped blocks comes from the crystallization of the underlying magma, and thus both mechanisms for producing plagiogranites are a variation on the same theme.

4.4.7 Amphibole-plagioclase

Amphibole-plagioclase $\delta^{18}O$ plots are significant because on petrographic grounds, there are at least two distinct populations of amphibole in the ophiolite. As shown on Figure 4-15, primary (magmatic) amphibole exhibits exchange characteristics similar to clinopyroxene, even though the data are not extensive. The primary amphiboles exhibit a steep disequilibrium hydrothermal trend where mineral pairs lie in the field forbidden under equilibrium conditions.

The secondary amphiboles (uralite or actinolite-tremolite) replace either magmatic pyroxene or amphibole and map out an "equilibrium" trend where the mineral pairs lie along isotherms corresponding crudely to temperatures between 500°-300°C [Javoy, 1977]. In many respects, the secondary amphiboles are analogous to the inverted pyroxenes of the UBG γ and UZc of the Skaergaard intrusion. This suggests that when recrystallization or deposition of a new mineral occurs, the rates of oxygen exchange are dramatically enhanced. The same effect

Figure 4-15. $\delta^{18}O$ plagioclase versus $\delta^{18}O$ amphibole for the Samail ophiolite. Two trends are apparent: 1) a hydrothermal trend with slope ~3 and a recrystallization trend with slope ~1 and T ≈ 300° to 500°C. The large spread along the 1 to 1 line suggests that fluid compositions were highly variable over the life-time of the alteration event. The isotopic changes in the hydrothermal fluid are discussed in section 4.4.8.

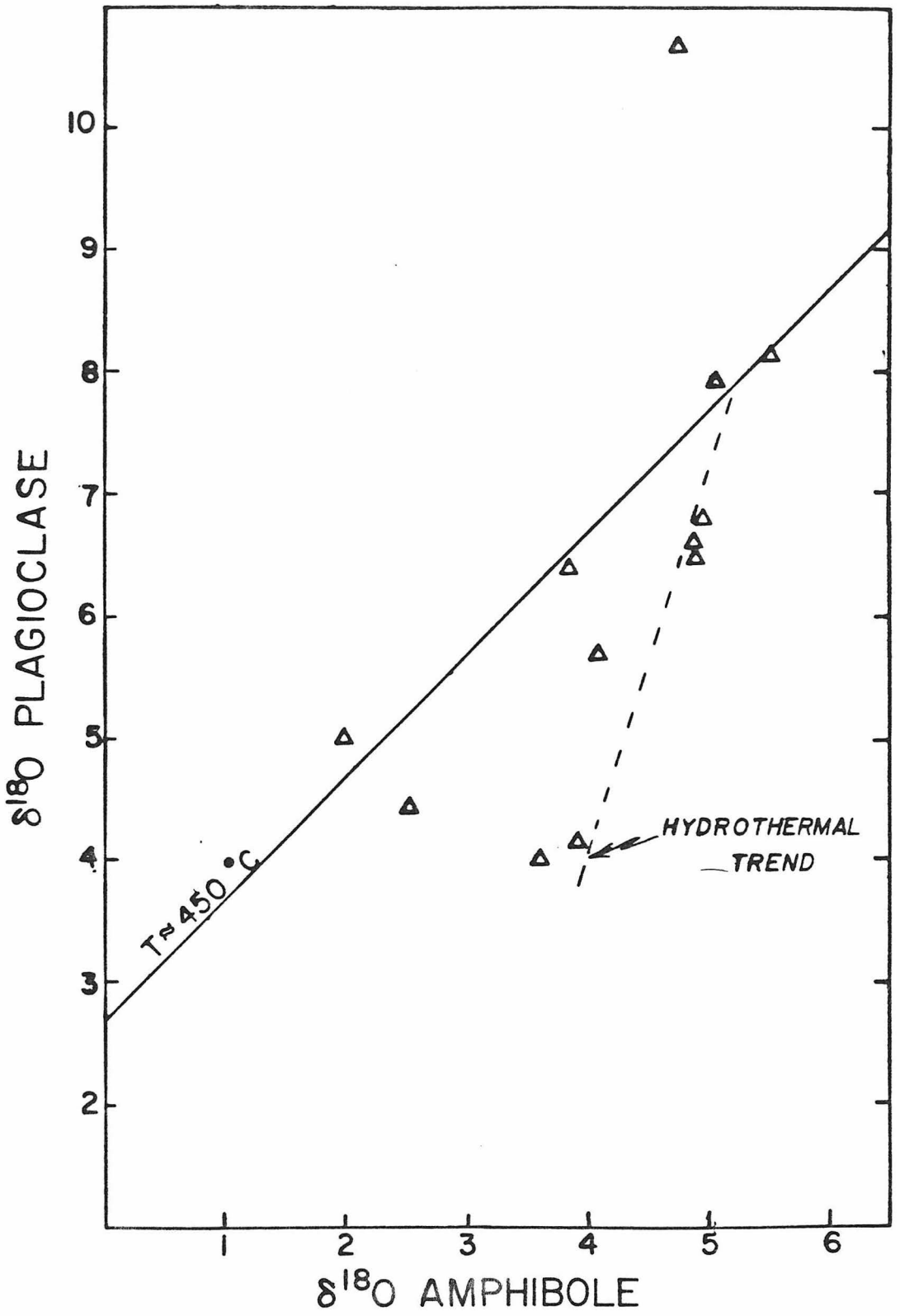
10
9
8
7
6
5
4
3
2
1
2
3
4
5
6
δ18O PLAGIOCLASE
δ18O AMPHIBOLE
T≈450 °C
HYDROTHERMAL
TREND

is observed for strontium isotopes in the Samail ophiolite where rocks that are pervasively recrystallized exhibit the greatest enrichment in $^{87}Sr/^{86}Sr$ ratio (Chapter 5). The transformation from disordered feldspar structure to an ordered structure over a wide range of temperatures may be related to the ease with which feldspar exchanges oxygen with hydrothermal fluids. Thus, the hydrothermally produced order-disorder reactions in feldspars may be analogous to the pyribole reactions but on a scale of unit cell dimension.

4.4.8 Isotopic Changes in the Hydrothermal Fluids

Meteoric-hydrothermal systems associated with the continental intrusions described above (initial $\delta^{18}O_{H_2O} \approx -9$ to -14) invariably result in ^{18}O depletions of the rocks and minerals, whereas in the Samail ophiolite the hydrothermal interaction has produced both ^{18}O depletions and ^{18}O enrichments. This is because the $\delta^{18}O$ of Cretaceous seawater ($\delta^{18}O_{H_2O} \approx -0.1$ to -0.7, see below) is only about 6 per mil lower than that of the inital igneous rock, instead of 15 to 20 per mil lower, as in the subaerial examples. Changes in both temperature and water/rock (w/r) ratio (leading to ^{18}O shifts in the hydrothermal fluid) can result in the observed ^{18}O shifts in the rock either up or down.

Let us consider the plagioclase-water system, whose $\Delta^{18}O$ is given by:

$$\Delta^{18}O_{\text{plagioclase-}H_2O} = \left(\frac{2.91-0.76\beta}{T^2}\right) \times 10^6 - 3.41 - 0.14\beta$$

where β is anorthite content of the plagioclase and T is in °K [O'Neil and Taylor, 1967]. If a packet of seawater with $\delta^{18}O = 0$ equilibrates with cumulate plagioclase (An_{80}, $\delta^{18}O = +6$) at 800°C, the water

will approach a $\delta^{18}O$ value of +7.5. If this strongly ^{18}O-shifted H_2O packet then moves up section and exchanges with plagioclase in the sheeted diabase complex at 350°C, then the feldspar $\delta^{18}O$ value will increase from to +10 (w/r >> 1) or +8 (w/r ≈ 1). If we further lower the temperature of alteration in the diabase, the $\delta^{18}O$ of this plagioclase will become even higher. For example, at 200°C the $\delta^{18}O$ of the feldspar would be about +14 (w/r >> 1) or +10 (w/r ≈ 1). Inasmuch as the upper-level feldspars are typically more Na-rich than An_{80}, the final $\delta^{18}O$ values will actually be even higher (for pure albite, +12 to +9 and +17 to +12, respectively, at 350°C and 200°C).

The final $\delta^{18}O$ of any small volume of rock in the ophiolite will depend strongly upon the previous exchange history or path of the water packets with which it interacts. In a zone where stream lines of fluid circulation are concentrated, as is likely in the sheeted dike complex near the distal edge of the magma chamber (see Fig. 4-15), arguments such as those given above would predict ^{18}O-enrichments in the rocks. In addition, plagioclase is likely to continue to exchange down to temperatures at least as low 150°-200°C as long as it is in contact with hydrothermal fluids. The combination of these processes probably explains the apparent inconsistency between diabase dikes with $\delta^{18}O_{plagioclase}$ = 11.8 and mineral assemblages suggesting T = 300-350°C (i.e. OMG 10). It is clear from this analysis that the hydrothermal fluids in the ophiolite all were strongly modified by exchange, and that none could be considered to be pristine sea water. Assuming plausible temperatures of equilibration for the plagioclase and whole-rock samples given in Table 4-1, the calculated equilibrium $\delta^{18}O_{H_2O}$ values range from -3 to +10.

Gabbro dikes which post-date the peridotite tectonite fabric probably represent crystallization products of melts moving through the peridotite [Boudier and Coleman, 1981]. These dikes line conjugate fracture sets in the tectonites, or occur as local segregations near plagioclase-bearing peridotite. Plagioclase-pyroxene pairs from these gabbros have $\delta^{18}O$ values which plot on the high-^{18}O extension of the disequilibrium least-squares trend line mapped out for the gabbros (Fig. 4-5). For these dike samples, it is important to note that the isotopic analyses were performed upon mineral separates purified to a high degree with heavy liquids to avoid any high-^{18}O rodingite minerals. Even though petrographically unaltered plagioclase and pyroxene were analyzed, the exchange trend extends to approximately a 300°C-400°C isotherm, suggesting the exchange mechanism was similar to that found in the ^{18}O-depleted gabbros higher in the ophiolite section.

A plausible explanation for the high $\delta^{18}O$ values of these dikes and veins is that, because they are the deepest samples, the hydrothermal fluids had previously exchanged with very large amounts of overlying oceanic crustal and/or upper mantle rocks at relatively high temperatures. Thus, these small amounts of deeply circulating H_2O would have become strongly enriched in ^{18}O as they moved down into fractures in the peridotite. Inasmuch as these conjugate dikes post-date the tectonite fabric, their formation and subsequent alteration also must have occurred at a temperature lower than that of the high-temperature regime [Nicolas et al., 1980] in which the tectonite fabric was formed. As the rocks moved away from the ridge axis, the plagioclase-pyroxene pairs in the dikes would have continued to exchange at successively lower temperatures, which may also in part account for the high $\delta^{18}O$

values. The ^{18}O effects are most strongly developed in the dikes and veins because at any given stratigraphic horizon, the water/rock ratios would be expected to be highest along the fractures which are acting as hydrothermal conduits. It is, in fact, very common in plutonic igneous complexes to find unusually large ^{18}O effects in dikes and along fractures [Forester and Taylor, 1977; Taylor and Forester, 1979; Magaritz and Taylor, 1976b].

In Fig. 4-7, the plagioclase-clinopyroxene trajectories for T = 500°C are plotted for a water that had been ^{18}O shifted to $\delta^{18}O = 8.9$, which implies that this water equilibrated with a large amount of gabbro or upper mantle olivine and pyroxene. The trajectories show that exchange with such an ^{18}O-shifted water at temperatures on the order of 500°C is a plausible explanation for the high-^{18}O plagioclase and pyroxene. However, ^{18}O-shifted seawater of +8 composition is essentially indistinguishable in its $\delta^{18}O$ value from magmatic water, so the latter also must be at least considered as a plausible candidate. $^{87}Sr/^{86}Sr$ or D/H studies might possibly help distinguish between magmatic H_2O and ^{18}O-shifted seawater, but no secondary, high-temperature, hydrous minerals are available in these samples, and if the oxygen had shifted to +8, then the Sr isotopes would also probably be buffered by exchange with the rocks. An additional complication is that any late-stage, exsolved magmatic water with $\delta^{18}O \approx +8$ could represent H_2O originally driven into the melt by dehydration of hydrothermally-altered stoped blocks of roof rock [Gregory and Taylor, 1979; Taylor, 1980]. However, neither this type of magmatic water nor a primary magmatic water are deemed to be likely candidates, because the gabbro dikes and veins predominantly occur in conjugate sets which

post-date the peridotite tectonite fabric. This in turn suggests that the alteration probably occurred well out on the flanks of the ridge where ^{18}O-shifted seawater would be the most likely type of hydrothermal fluid (Fig. 4-18).

4.4.9 $\delta\ ^{18}O$ Variations in the Ophiolite Sequence

A few cumulate gabbro samples have been found that have apparently closely preserved their magmatic $\delta^{18}O$ values (samples K9, OMG 67). As might be expected, these are most common in the lower section of cumulates. However, particularly in the vicinity of fractures and prominent veins containing high-T mineral assemblages, low-^{18}O gabbros have been found at very great depths, for example within 250 meters of the tectonite peridotite-gabbro contact. Approximately 2 km above the base of the cumulates, plagioclase $\delta^{18}O$ values decrease to a minimum of 3.6 in the Wadi Saq section (Fig. 4-3b, 4-16). Coexisting pyroxene in this sample has $\delta^{18}O$ equal to 4.1.

Mineralogical evidence for alteration is practically non-existent in all these lower cumulates, even those that are markedly depleted in ^{18}O. Thin reaction rims of talc + magnetite around olivine grains (Fig. 4-16b) occur locally in the low-^{18}O rocks but are not universal. Plagioclase generally appears to be completely unaltered (Fig. 4-17). Pyroxenes, although generally unaltered, may contain minor (<10%) replacement brown amphibole along grain cleavages and fractures (Fig. 4-17). These data indicate that the hydrothermal alteration of most of the gabbro samples occurred at extremely high temperatures, and that subsequently there was only local influx and exchange with low-T waters.

Figure 4-16.

a) Outcrop of cumulate gabbro (OMG 68) from the Wadi Saq traverse exhibiting spectacular cumulate layering. The dark layers are olivine-rich cumulates.

b) Photomicrograph of OMG 68 showing a talc + magnetite reaction rim around the edge of the olivine crystl whch is at extinction in lower right-hand corner of the picture (scale: 3.16 mm long). Plagioclase from this hand specimen has $\delta^{18}O = 3.6$ and coexisting pyroxene has $\delta^{18}O = 4.1$. Both are relatively fresh in thin-section.


a

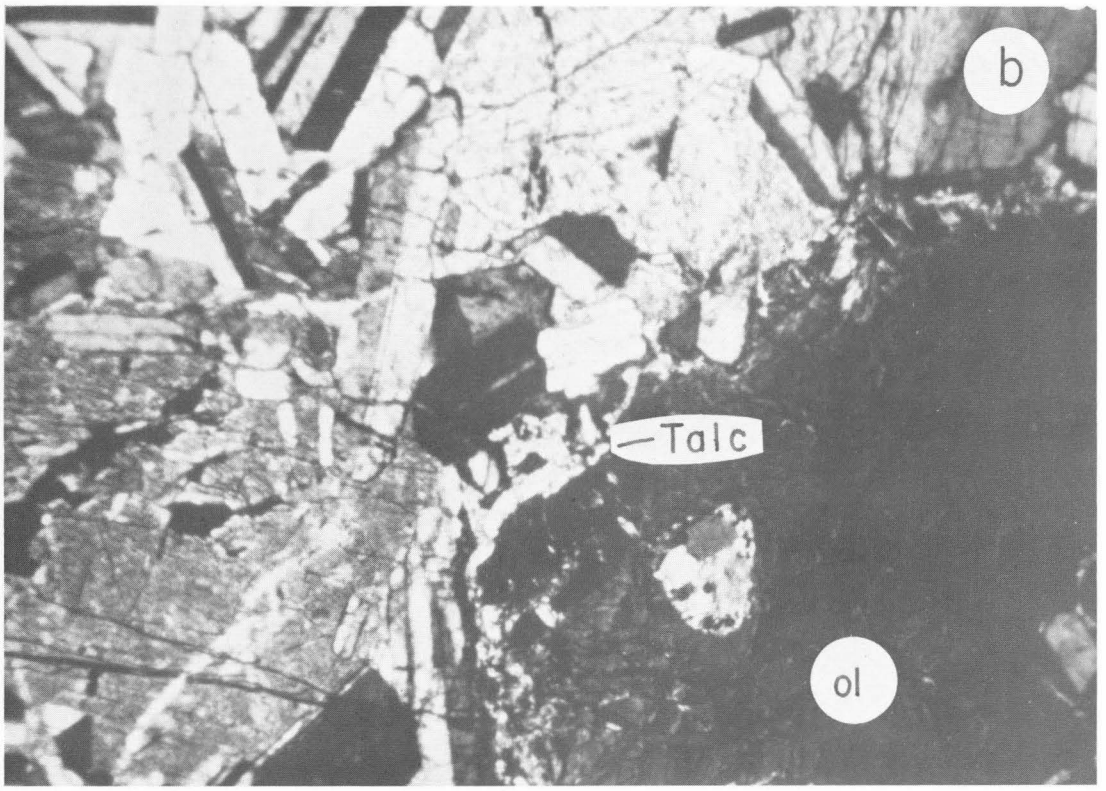
b
Talc
ol

Figure 4-17. a,b) OMG 63--Photomicrograph under plane- and crossed-polarization of cumulate gabbro exhibiting beautiful igneous lamination and adcumulate textures. In this extremely fresh specimen $\delta^{18}O$-plagioclase = 4.1 and $\delta^{18}O$-pyroxene = 4.3.

c, d) Photomicrograph under plane and crossed polarization of OMG 66 cumulate gabbro structurally above OMG 63. Plagioclase, $\delta^{18}O$ = 5.8, is again fresh, yet the clinopyroxenes show overgrowths of green and brown hornblende. The long dimension represented in all photographs of this figure is 3.16 mm.

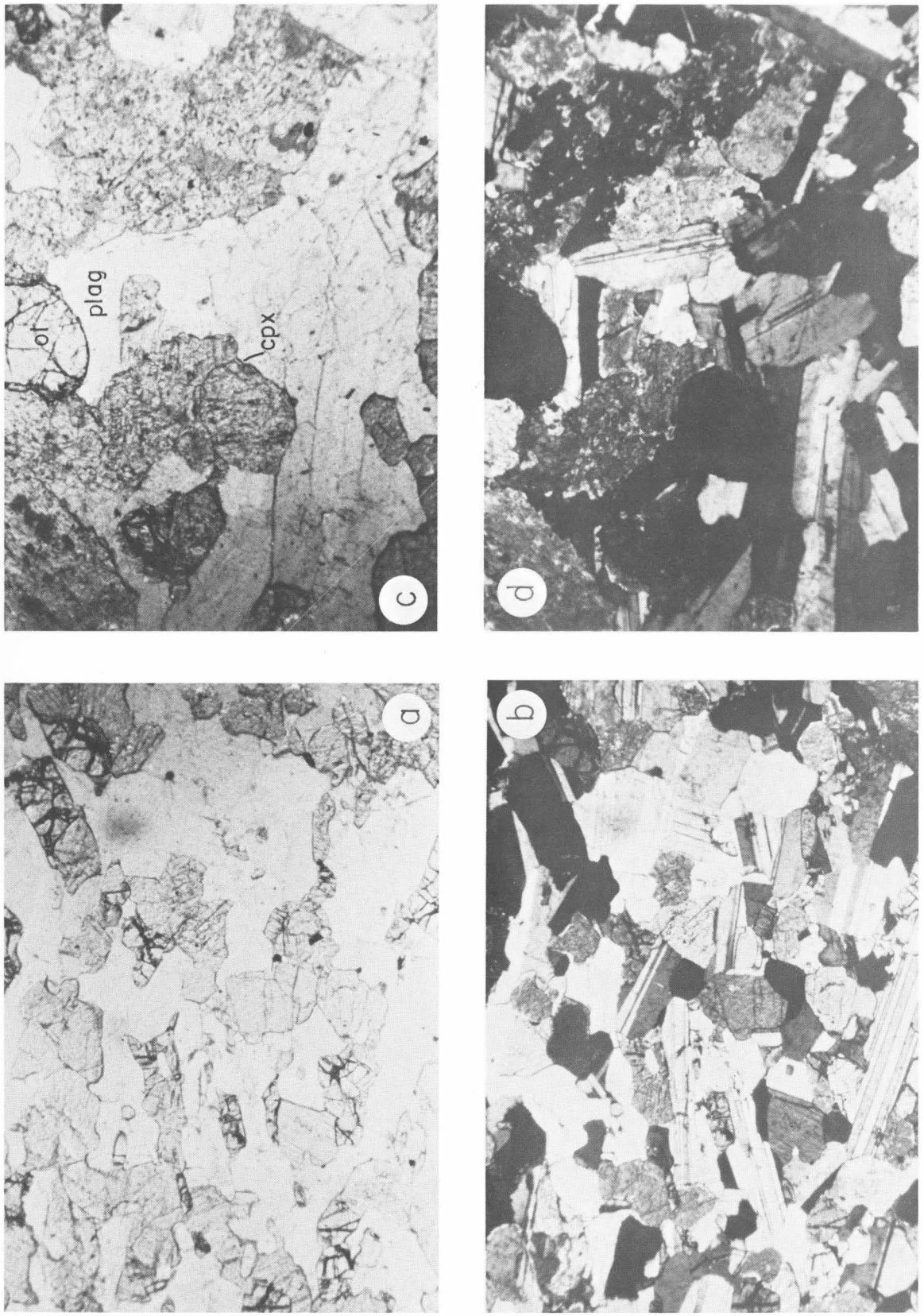
a
b
c
ol
plag
cpx
d

One of the samples studied by McCulloch et al., [1980] is K 9, in which $\delta^{18}O$ plagioclase = 6.0 and $\delta^{18}O$ clinopyroxene = 5.3; during cooling, this sample suffered very little exchange and also it apparently behaved essentially as a closed-system in terms of its oxygen. The plagioclase $\delta^{18}O$ value has remained almost constant, compatible with its large modal abundance (75%) in this specimen. The initial $^{87}Sr/^{86}Sr$ value of the plagioclase also has been almost unaffected, although the $^{87}Sr/^{86}Sr$ of the clinopyroxene was slightly increased, compatible with its lower modal abundance and lower Sr content [McCulloch et al., 1980]. This clinopyroxene also shows a slight overgrowth of brown amphibole, always in optical continuity in each grain. The strontium isotope data demonstrate that small amounts of heated sea water have affected this sample during subsolidus cooling, and together with the ^{18}O data this suggests that the amphibole in K 9 grew at temperatures just below the solidus in communication with small amounts of strongly ^{18}O-shifted, seawater-derived hydrothermal fluid ($\delta^{18}O_{H_2O} \approx +8.1$, $^{87}Sr/^{86}Sr \approx .7044$).

The various isotopic relationships in K 9 were all established or "frozen in" at high temperatures and virtually no exchange occurred at extremely low temperatures. Similar statements can be made about all of the cumulate gabbros, most of which were much more strongly hydrothermally altered at high T than was K 9. The lack of low-temperature retrograde alteration is evidenced by the "unaltered" plagioclase, the unaltered or only slightly amphibolitized clinopyroxene, the absence of serpentine alteration of olivine, and the presence of only minor talc + magnetite. In all these samples the alteration and oxygen exchange must have occurred at temperatures exceeding 400°C, with most

exchange probably at much higher temperature. As the temperature dropped below about 300°C, the water/rock ratio in the main mass of cumulates must have dropped to a value very near zero, except in the immediate vicinity of the vein and fracture systems. The process described above is well-documented in many continental gabbro bodies [Taylor, 1971; Forester and Taylor, 1977; Taylor and Forester, 1979; Taylor and Coleman, 1977] which also were altered at very high temperatures and which exhibit a paucity of OH-bearing hydrothermal minerals. For example, by numerically modelling the Skaergaard hydrothermal system, Norton and Taylor [1979] showed that more than half of the H_2O that was ultimately "pumped" through this gabbro body went through at $T > 480°C$, with maximum fluid flux at around 600°C.

Above the minimum-^{18}O stratigraphic horizon in the cumulate gabbros, the $\delta^{18}O$ values tend to systematically increase upward. These upper cumulates are indistinguishable in hand specimen and in thin section from the low-^{18}O, lower cumulates. In conjunction with this enrichment in ^{18}O, as the gradational contact between the cumulate gabbro and high-level gabbro is approached, OH-bearing alteration minerals become more abundant. Brown amphibole is followed by green amphibole, then chlorite appears, and finally in some rocks rare epidote occurs in the high-level gabbros. The presence of talc + magnetite after olivine (and the lack of serpentine or chlorite) in some high-level gabbros again demonstrates that most of the hydrothermal fluids were flushed through at temperatures exceeding 400°C. $\delta^{18}O$ plagioclase varies from 4.5 to 6.8, generally increasing upward in the high-level gabbros. Whole-rock $\delta^{18}O$ values of the high-level gabbros vary from 3.7 to 6.8, and may coincidentally approximate normal igneous

values. Although absent from meteoric-hydrothermal systems, this "coincidence" phenomenon is a characteristic feature of seawater-hydrothermal systems. Because of the ^{18}O shifts and the relatively high initial $\delta^{18}O$ value of the ocean water, there is a significant range of temperatures over which the whole-rock $\delta^{18}O$ value of a gabbro that has been thoroughly hydrothermally altered in the presence of large amounts of water will, simply by coincidence, be very close to the primary magmatic value of +5.7.

Above the sheeted diabase-gabbro contact, actinolite, chlorite, saussurite, leucoxene, and epidote all become common in the alteration mineral asssemblages. Amphibolite-facies assemblages give way rapidly up section to greenschist assemblages. Feldspar separated from diabase OMG 5c located less than 200 meters above the gabbro contact had a $\delta^{18}O$ = 5.2, while OMG 10 diabase approximately 300 meters below the pillow lava contact has a $\delta^{18}O$ plagioclase = 11.8. The whole-rock $\delta^{18}O$ values are +4.9 and +8.5, respectively. Pillow lava OMG 54 has $\delta^{18}O$ = 12.9, contains plagioclase (An_{25}), palagonitized glass, abundant zeolites and secondary carbonate. Piecing the two stratigraphic columns together, the $\delta^{18}O$ values of whole-rock samples decrease from about +13 in the pillow lavas down to values which approximate normal igneous rocks near the gabbro-sheeted diabase contact. Further down section, $\delta^{18}O$ continues to decrease to a minimum value approximately 1.5 to 2 km below the diabase-gabbro contact. After passing through a minimum value of about 3.8, the whole-rock $\delta^{18}O$ values again tend to increase sporadically down section through to the lowermost gabbros where the exchange effects are localized along fractures and veins.

Neither Wadi Kadir or Wadi Saq represent complete sections through the ophiolite, but where they overlap the agreement between geology, petrography, alteration mineralogy, and the $\delta^{18}O$ profile is very good. The consistency of geology and $\delta^{18}O$ profiles in these two sections separated by a lateral distance of over 15 km, as well as the basically similar geologic sections exposed over several hundred kilometers of the entire Oman mountain belt, both suggest that we are looking at a representative cross section through the Tethyan oceanic crust. It also appears that the physical and chemical processes involved in formation of this oceanic crust had essentially reached steady-state conditions, in the 5-10 m.y. interval after igneous crystallization and before detachment. This steady-state crustal section contains significant volumes of both low-^{18}O (< +6) plutonic rocks and high-^{18}O (> +6) hypabyssal and pillowed volcanic rocks. The upper parts of this mature piece of oceanic crust at Ibra also appear to be very similar to, and representative of, many other ophiolites in terms of both alteration history and $\delta^{18}O$ values [Heaton and Sheppard, 1977; Magaritz and Taylor, 1974; 1976a; Williams and Malpas, 1976; Gregory and Taylor, 1979; Stern et al., 1976].

4.4.10 Isotopic Aging of the Oceanic Crust

The range of whole-rock $\delta^{18}O$ values of diabase dikes from the Wadi Saq and Wadi Kadir sections is +6.8 to +10.9 (one sample of a late, highly chloritized dike has $\delta^{18}O$ = +4.9). However, the range of whole-rock $\delta^{18}O$ values in diabasic xenoliths (now hornfels) associated with plagiogranites from the Dasir area (about 70 km NW of Ibra, see Fig. 4-1) is +3.7 to +7.4 [Gregory and Taylor, 1979]. The Dasir xenoliths represent fragments of diabase dikes from the roof of

the gabbro magma chamber that became incorporated into the magma by piecemeal stoping and foundering of the roof.

The stoped blocks at Dasir record a different, earlier stage of hydrothermal alteration than does the Ibra diabase section. The Dasir xenoliths in part preserved the low-$\delta^{18}O$ values that they had attained just prior to their being stoped into the underlying magma near the ridge axis. In contrast, although the lower parts of the Ibra diabase section probably also underwent a similar high-T, ^{18}O-depletion, they did not preserve these low $\delta^{18}O$ values when they were later subjected to interaction with more ^{18}O-shifted, lower-temperature hydrothermal fluids in the vicinity of the distal portions of the magma chamber as the oceanic crust migrated away from the ridge axis (see Fig. 4-18). The difference in ^{18}O contents can be attributed to the different circulation systems, temperatures, and types of fluid that the two suites of diabases experienced.

The xenolith suite was altered directly above, and virtually in contact with the magma chamber in a region where the hydrothermal circulation system was dominated by high-temperature fluids that circulated to depths of only 2-3 km and interacted only with basalt and diabase. Because of the high water/rock ratios (see below and [McCulloch et al., 1980]), this fluid would not have suffered any large ^{18}O-shifts and thus would be isotopically similar to seawater; the fluid path lines would not take it through the lower portions of the oceanic crust. However, as the crust continues to spread, the diabase section moves beyond the distal edge of the magma chamber (Fig. 4-18) into a regime where the fluids are dominantly moving upward from deep in the cumulate gabbro section. Such fluids may still be at

relatively high temperatures, but because of overall lower water/rock ratios in the less permeable, deeper parts of the ocean crust, they will have suffered much more dramatic ^{18}O shifts because of interactions with the lower cumulates. During continued spreading, the temperatures also continue to decrease, which also leads to ^{18}O-enrichment of the altered rocks. When the high-^{18}O and/or low-T fluids interact with the sheeted diabase complex it becomes enriched in ^{18}O, thus partly masking the earlier low-^{18}O exchange history. Another factor probably involved in the preservation of the low $\delta^{18}O$ values of the Dasir xenoliths is the fact that they were carried down to deeper levels; they now lie approximately 200 m below the diabase-gabbro contact, where they are associated with large masses of plagiogranite.

The type of isotopic aging described above can also be seen on the scale of an individual outcrop. Samples from localities OMG 65 and OMG 66 (see Fig. 4-3a) in Wadi Saq exhibit the same general type of time-$\delta^{18}O$ trends. Samples from the host-rock cumulate gabbros have $\delta^{18}O$ plagioclase = 4.2 to 5.8, whereas the later hornblende-gabbro segregations have $\delta^{18}O$ plagioclase = 8.1, and the still later plagiogranite dikes and veins have $\delta^{18}O$ whole rock = 12.4 to 13.6. The high-^{18}O plagiogranites occupy a prominent fracture system and have sharp non-chilled contacts against the host gabbros. In these fracture-systems the fluids continued to circulate down to relatively low temperatures (as recorded by plagioclase turbidity, and the presence of prehnite, epidote and thullite). The coarser-grained, host gabbros have partially preserved their earlier-formed, lower-^{18}O values, and they also contain only amphibole as a new alteration phase (they have no epidote). The pegmatitic segregations of hornblende

Figure 4-18. Cartoon sketch showing seawater circulation patterns in a cross-section of the Samail ophiolite at the time of its formation. The solid black indicates magma. Note the existence of two essentially isolated circulation regimes, separated by a thin sheet of magma that is essentially impermeable to the fluids in the hydrostatic convective system. One system (the "upper system") extends outward from the ridge axis, and is located directly over the magma chamber, and the other (the "lower system") lies underneath the "wings" of the magma chamber. The two systems interact with one another only at the distal edges of the magma chamber. Also shown is the lateral distance that would be traversed by this oceanic crustal section in 1 m.y., assuming a half-spreading rate of 3 cm/yr. The high-level non-cumulate gabbro is shown as a blank pattern between the sheeted dikes and the layered gabbro. The wavy lined pattern in the peridotite represents the tectonite fabric, and the short, heavy lines schematically indicate gabbro dikes filling conjugate fractures that post-date the tectonite fabric; locally the hydrothermal circulation penetrated these conduits. Note that only one side of the MOR spreading system is illustrated; a mirror-image of the above diagram should exist to the left side of the figure.

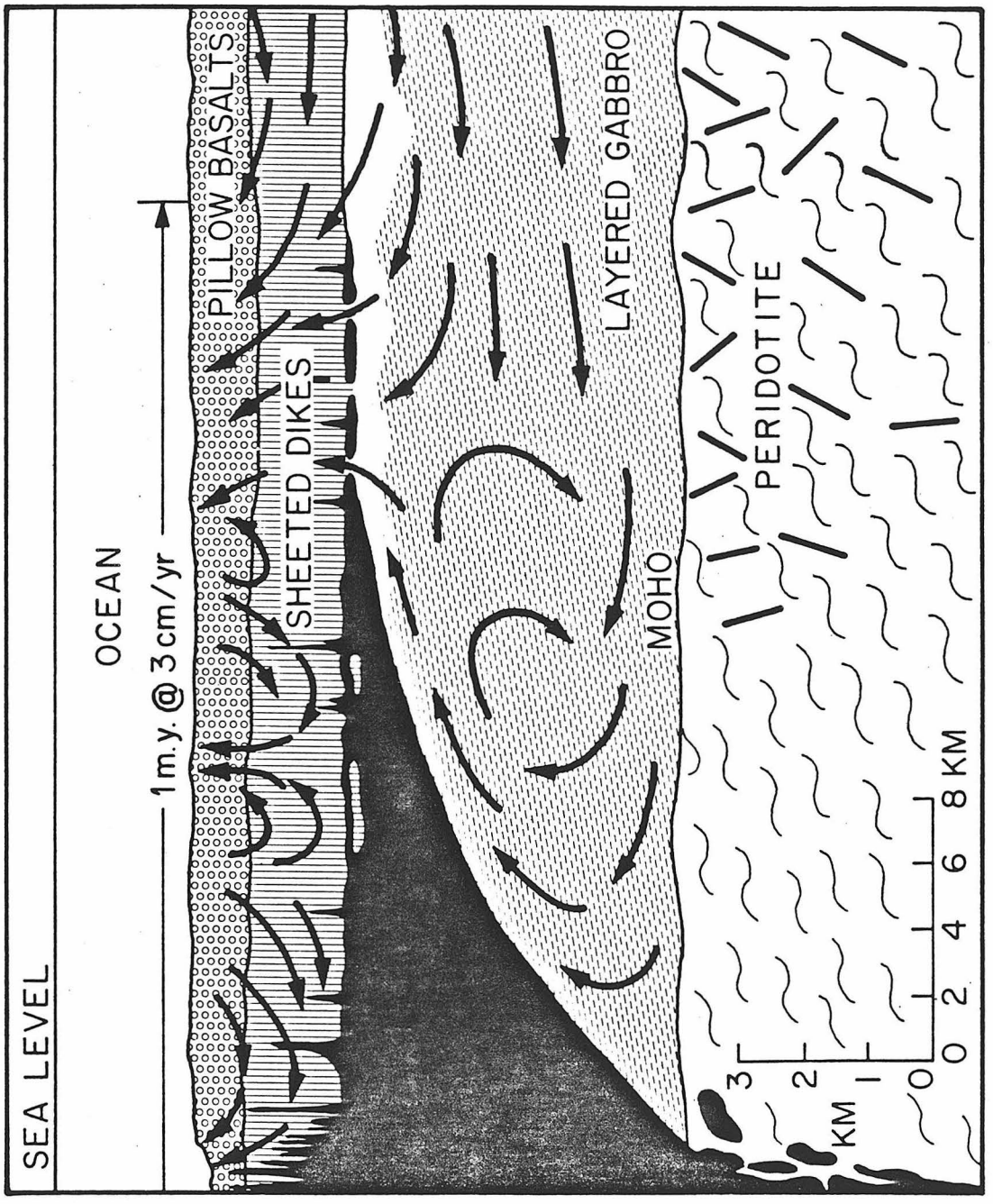
SEA LEVEL
OCEAN
1 m.y. @ 3 cm/yr
PILLOW BASALTS
SHEETED DIKES
LAYERED GABBRO
MOHO
PERIDOTITE
KM
0
1
2
3
0 2 4 6 8 KM

gabbro almost certainly crystallized in the presence of an aqueous fluid phase, but inasmuch as these segregations pre-date the plagiogranites, this was a different, earlier-stage hydrothermal fluid than that which affected the plagiogranite. Thus in this single OMG 65, 66 outcrop we can observe practically the entire range of $\delta^{18}O$ values in the Samail ophiolite, simply by sampling the host rocks as well as the later rock types that occupy the vein and fracture systems.

4.5 SUMMARY

We have shown above that deep hydrothermal circulation of seawater has affected most of the feldspar-bearing rocks of the Samail ophiolite, including a large part of the section that is equivalent to oceanic layer three. The deeper portions are depleted in ^{18}O relative to primary MOR basalts ($\delta^{18}O = +5.7$), whereas the shallower parts are enriched in ^{18}O. However, the final $\delta^{18}O$ profile in the ophiolite is the cumulative result of a long history of hydrothermal alteration, beginning with high-temperature interactions with newly-formed crust at the ridge axis, and continuing for at least several hundred thousand years during spreading away from the ridge axis. The earlier stages tend to produce ^{18}O depletions, whereas the later stages produce ^{18}O enrichments. We have termed the latter process "isotopic aging," and the ^{18}O enrichments are probably a result of two separate effects: (1) Strongly ^{18}O-shifted waters that have circulated deep under the flanks of the magma chambers and then have risen upward just beyond the distal ends of the chamber (Fig. 4-15); (2) Less ^{18}O-shifted waters with much lower temperatures that have circulated downward into the same marginal zone.

We have had some success in defining the isotopic effects produced at various stages of the "isotopic aging" process by looking at veining and dike relationships, and by examining stoped xenoliths in the gabbros in the Samail complex. However, it must be emphasized that the final $\delta^{18}O$ profile in the ophiolite represents the superposition of a very long, complex, and continuously changing, series of events in which the water/rock ratios, temperatures, $\delta^{18}O$ values of the fluids, rock permeabilities, rates of isotopic exchange, and chemical

compositions of the fluids are all varying both with respect to time and with respect to position relative to the ridge axis. Without carrying out a complete numerical analysis of this problem in the manner that was done for the Skaergaard intrusion by Norton and Taylor [1979], we can only describe the observed isotopic effects in semi-quantitative terms.

In spite of the above complexities, it is worthwhile to discuss some implications of the $\delta^{18}O$ data regarding the overall time-temperature history of hydrothermal circulation in the oceanic crust. The proposed style of H_2O circulation is illustrated in cartoon-fashion in Fig. 4-18. On the basis of field mapping, [Hopson et al., 1981; Hopson and Pallister, 1979], the Samail gabbro magma chamber appears to have had a shape similar to that indicated in Fig. 4-18. This is the basic shape proposed for the Troodos [Greenbaum, 1972] and Pt. Sal ophiolites [Hopson and Frano, 1977], and it is similar to the shape of many continental layered gabbro complexes formed in rift environments (e.g. the Muskox [Irvine and Baragar, 1972] and Great Dyke [Worst, 1960]). The floor of the magma chamber thus somewhat resembles the bottom of a wide, very long ship, with the poorly defined feeder dike system representing the keel; in this analogy, the roof of the chamber is the deck of the ship (somewhat analogous to the flight deck of an aircraft carrier). This shape probably closely approximates the geometry of the magma chamber at a fast-spreading ridge. At a slow-spreading ridge the "wings" would be much smaller or non-existent.

The result of this particular geometry is that two decoupled regimes of hydrothermal circulation must exist during most of the history of alteration. The first occurs directly over the magma chamber,

and is continuous across the ridge axis (this is termed the "upper system"). The upper seawater-hydrothermal circulation system lies exclusively within the pillow lavas and the sheeted diabase-dike complex, and the H_2O penetrates downward only as far as the flat roof of the magma chamber. The water cannot penetrate any more deeply than the joint and fracture system will allow, and thus (in geologically reasonable times) the water cannot cross the diabase-magma chamber contact [Taylor and Forester, 1979; Norton and Taylor, 1979]. In fact, some H_2O is undoubtedly added to the magma from the "upper system", but this must come about through dehydration of stoped blocks of hydrothermally-altered roof rocks that should be abundant in such a tectonically active, rifting environment [Taylor, 1977; Taylor and Forester, 1979; Gregory and Taylor, 1979; Taylor; 1980]. Because the stratigraphic thickness of rocks above the roof of the magma chamber is very small compared to the width of the chamber, the upper hydrothermal system probably involves a large number of separate convection cells, perhaps dominated by the ridge-axis system [Corliss et al., 1979]. The upper system therefore must involve very large overall water/rock ratios (> 10, see McCulloch et al. [1981]) and the circulating seawater will be only slightly ^{18}O-shifted away from its initial value.

The isotopic and alteration effects produced by the upper regime are in part destroyed or masked by later alteration effects that come about when fluids from the "lower system" finally are able to penetrate upward into the sheeted diabase complex at the distal edges of the magma chamber. This will happen as soon as the rocks (high-level gabbros and plagiogranites) are consolidated enough to fracture. In the cartoon (Fig. 4-18), this is indicated to occur discontinuously as

small pockets of late-stage magma become isolated from one another due to the vagaries of the crystallization process in such a spreading environment. The seawater circulation system within the layered gabbro cumulates underneath the wings of the magma chamber involves very high temperatures (> 400°C) and low water/rock ratios (closed system) on the order of 0.3-1.0 (weight units).

The fluid involved in the "lower system" is seawater that has moved laterally inward from well beyond the distal ends of the magma chamber. Because this water cannot move upward in any significant quantities directly through the liquid magma, it must either cycle (hence the closed-system characteristic), or escape upward at the distal edge of the chamber when conduits in fractured, solidified rock becomes available at the gabbro-diabase contact (Fig. 4-18). Both processes undoubtedly occur. Therefore, large quantities of this heated and strongly ^{18}O-shifted water ($\delta^{18}O_{H_2O}$ = +4 to +8) will be focused upward along the sloping base of the magma chamber. This H_2O will impose a final alteration event upon the sheeted dike complex, the magnitude of which will depend on the amount of focusing of hydrothermal fluid that occurs at the edge of the chamber. Note that if any water does diffuse directly into the magma from the country rocks, it must be from the "lower system". It is plausible that tiny amounts of the very low density, high-T H_2O in fractures below the "wings" of the magma chamber could diffuse upward into the overlying magma, in the manner proposed for the trough bands of the Skaergaard intrusion [Taylor and Forester, 1979]. The shape of the magma chamber shown in Fig. 4-18 is, in fact, ideal for such a process to operate. The strongly ^{18}O-shifted water of the lower system also locally penetrates down into the peridotite

along conjugate fractures which post-date the tectonite fabric. These waters, whose ^{18}O composition is buffered by a large reservoir of olivine with $\delta^{18}O \approx 5.7$, produce the ^{18}O enrichments of pyroxene-plagioclase pairs in gabbro dikes that were intruded along these fractures (Figs. 4-5 and 4-7).

Strontium isotope data (which are not subject to temperature effects) record open system water-rock ratios (weight units) of approximately 10-30 in the sheeted dike complex [McCulloch et al., 1981]. This represents the integrated effects of hydrothermal fluids of the "upper system", as well as of fluids derived from the "lower" and "marginal" systems. Depending upon the magnitude of the $^{87}Sr/^{86}Sr$ shift in the lower-system fluid, the diabase at the distal edge of the chamber may already be in approximate strontium isotope equilibrium with the fluid discharging upward from the layered gabbros (i.e. $^{87}Sr/^{86}Sr$ in diabase $\approx$ 0.705 [McCulloch et al., 1981]). This suggests that the strontium isotopes may not be recording the final hydrothermal exchange events in the ophiolite, just as the oxygen isotopes do not record (except indirectly) the earlier exchange events in the upper system at the ridge axis. This possibly could be sorted out with more $^{87}Sr/^{86}Sr$ data on certain late-stage features such as veins and plagiogranite dikes. Because of these complex effects, the correlations between $^{87}Sr/^{86}Sr$ and $^{18}O/^{16}O$ suggested by data from Spooner [1977] and McCulloch et al. [1981] are, in some respects, fortuitous.

The style of hydrothermal circulation and the geometry of the magma chamber shown in Fig. 4-18 imply that there should be a dramatic shift or abrupt discontinuity in the isotopic record at the gabbro-

diabase contact (i.e. at the "fossil" roof of the magma chamber). This is, in fact, exactly what is observed, as both the $\delta^{18}O$ (Fig. 4-3) and the $^{87}Sr/^{86}Sr$ values [McCulloch et al., 1981] change very rapidly at this boundary, which must represent a discontinuity in both the average temperature of hydrothermal alteration and in the average, integrated water/rock ratio (see Table 4-1 and Fig. 4-3). Part of the explanation for higher water/rock ratios in the sheeted complex is the long history of hydrothermal exchange that these rocks undergo prior to crystallization of the high-level gabbro (Fig. 4-18). However, in addition, there is almost certainly an abrupt permeability change across the diabase-gabbro contact, as well. The highly jointed dike complex ought to be much more permeable than the gabbros (perhaps by a factor of 10, see Norton and Taylor [1979]). The combination of finer grain size and higher permeability thus also contribute to the much higher effective water/rock ratios in the sheeted complex relative to the gabbros. The variations in these parameters also help to explain the preservation of the high-temperature alteration assemblages and lack of low-temperature ^{18}O-exchange in the gabbros. The finer-grained, more permeable diabase dikes and pillow lavas will undergo ^{18}O-exchange down to much lower temperatures than the coarser-grained, less permeable gabbros. The latter rocks exhibit such effects only along fractures and veins. We do not yet know how far beyond the distal edges of the magma chamber the ^{18}O-exchange effects in the oceanic crustal section proceed at a significant rate.

CHAPTER 5

COMPARISON OF OXYGEN, STRONTIUM, AND NEODYMIUM SYSTEMATICS WITHIN THE SAMAIL OPHIOLITE

5.1 INTRODUCTION

The purpose of this study is to compare the neodymium, strontium, and oxygen isotopic characteristics of the Samail ophiolite, Oman. These rocks are of significance as it is now generally recognized that ophiolites represent transported slabs of oceanic crust and upper mantle emplaced upon continental margins. The Samail ophiolite provides a unique opportunity to study in detail a well exposed and preserved section of oceanic crust. The Samail, unlike most other "dismembered" ophiolites, is remarkably intact with a thickness comparing favorably to geophysical estimates of typical oceanic crustal sections [Coleman, 1977; Christensen and Salisbury, 1975]. Due its enormous size (exposed over most of the 700 km long Oman Mountains), it has been possible to contrast isotopic variations within a single tectonic unit over large distances perpendicular to the presumed paleospreading direction.

The Nd, Sr, and O isotopic characteristics were determined on identical samples from the harzburgite, gabbro, plagiogranite, sheeted dikes, and basalt units. The $^{18}O/^{16}O$ and Rb-Sr isotopic systems are sensitive to hydrothermal exchange with seawater [Taylor, 1968; Muehlenbachs and Clayton, 1972; Peterman et al., 1971; Spooner et al., 1977]. Using $\delta^{18}O$ variations as a criterion, samples were selected for Nd-Sr analyses which exhibited either slight effects of subsolidus hydrothermal exchange or pervasive amounts of high or low temperature exchange. By analyzing both fresh and altered samples as identified by the oxygen and strontium data, the effect of seawater alteration upon the Sm-Nd system could be evaluated.

Sm-Nd isotopic studies of mafic rocks by Lugmair et al. [1976], Nakamura et al. [1976], DePaolo and Wasserburg [1979], and Hamilton et al. [1979] have shown that crystallization ages can in general be obtained from coexisting plagioclase and pyroxene. In addition Nd isotopic studies of young MORB by O'Nions et al. [1977] and DePaolo and Wasserburg [1977] have shown that the Nd isotopic composition is apparently unaffected by hydrothermal interactions. For these reasons the feasibility of obtaining Sm-Nd crystallization ages from the gabbro members of the Samail ophiolite was investigated. The determination of Sm-Nd crystallization ages from ophiolites has many potential applications as most ophiolitic material is unsuitable for isotopic dating by other techniques. An exception is the dating by U-Pb of zircons sometimes found in plagiogranites and in the more differentiated hornblende gabbros [Tilton, Hopson, and Wright, 1981].

A preliminary Nd isotopic study by Richard et al. [1978] of single whole-rock gabbro samples from the Troodos, Samail, and several other ophiolite complexes has shown that the measured $^{143}Nd/^{144}Nd$ ratios are similar to those found in young ocean floor basalts [DePaolo and Wasserburg, 1976a,b; O'Nions et al, 1977]. This study presents a more comprehensive analysis of the results of McCulloch et al. [1980].

5.1.1 Geology and sampling

The Samail ophiolite forms a major part of the 700 km long arcuate Oman Mountains which are on the eastern edge of the Arabian Peninsula (Fig. 4-1). The samples analyzed in this study mainly come from the Ibra ophiolite section of southeastern Oman (see Fig. 4-1). A detailed geologic map of the Ibra section in southeastern Oman is

given by Bailey et al. [1981]. In addition to the samples from Ibra, two cumulate gabbro samples (OM251 and OM28) from the Rustaq and Wadi Fizh localities (Fig. 4-1) were also analyzed to check for regional isotopic and age variations within similar lithologies of the ophiolite on a scale of several hundred kilometers.

A minimum age for the emplacement of the ophiolite is provided by Maestrichtian-Tertiary shallow-water limestones which unconformably overlie parts of the ophiolite. A maximum age is given by K-Ar ages of ~90 m.y. (Turonian) [Lanphere, 1981] from metamorphic biotites in amphibolites from the detachment aureole at base of the Samail thrust sheet. Until now [see also Tilton et al., 1981], evidence for the age of production of the oceanic crust is sparse, although Glennie et al. [1974] estimated a minimum age limit based on middle to late Cretaceous (Cenomanian) sediments which overlie the pillow lavas in northern Oman.

5.1.2 Sample descriptions

The stratigraphic locality of the Ibra samples is shown in Fig. 5-10.

Basalt G54 (Ibra): Microphyric basalt with acicular laths of plagioclase (An25). Groundmass is altered to palagonite, zeolites (?), saponite (?), and calcite. The calcite is present as 1-2 cm amygdules and also as smaller blebs dispersed throughout the rock. A whole rock sample which was free of large amygdules, and calcite from an amygdule were analyzed. The mineralogy and oxygen isotope data (whole rock $\delta^{18}O = 12.7$) are consistent with low temperature alteration (100-200°C).

Diabase Dike G10 (Ibra): Ophitic texture with turbid albitized plagioclase (An20). Alteration products include epidote, chlorite,

actinolite-tremolite pseudomorphs after pyroxene, quartz, carbonate, and leucoxene. The mineralogy indicates alteration in the greenschist facies.

Diabase Dike K1 (Ibra): Ophitic texture with turbid plagioclase (An25), clinopyroxene and opaques. Alteration products include chlorite, uralite, and quartz, and suggest alteration at greenschist facies.

Plagiogranite G224-3 (Ibra): Granophyric texture with zoned plagioclase (core An30, rim An25), hornblende, quartz, magnetite, and trace amounts of apatite. Hornblende is partially altered to uralite. The plagiogranite was collected from a non-chilled dike which cross-cuts uralite gabbro, G224-2, approximately 500 meters below the gabbro-diabase contact.

Uralite Gabbro G224-2 (Ibra): Poikilitic hornblende enclosing zoned plagioclase (core An40, rim An20) and opaques. Alteration products include fibrous amphibole pseudomorphs after hornblende, chlorite, and rare prehnite. The mineralogy and oxygen isotope data (whole rock $\delta^{18}O = 3.7$, plagioclase $\delta^{18}O = 4.5$, and uralite $\delta^{18}O = 2.6$) suggest relatively high temperatures of alteration (>400°C).

Gabbro K9 (Ibra): Adcumulate with igneous lamination; 72% plagioclase (An75), 20% clinopyroxene, 7% olivine, and 1% hornblende. The brown hornblende is a minor alteration product of the clinopyroxene. The mineralogy and oxygen isotope data (whole rock $\delta^{18}O = 5.8$, plagioclase $\delta^{18}O = 6.0$, and clinopyroxene $\delta^{18}O = 5.3$) indicate that this is one of the least altered samples.

Gabbro OM251 (Wadi Fizh, northern Oman): Late cumulate pyroxene poikilitically enclosing plagioclase; 77% plagioclase (An80), 25%

clinopyroxene, and 3% olivine. The olivine has been partially serpentinized. Although the olivine is serpentinized, the oxygen data (plagioclase $\delta^{18}O = 6.4$ and clinopyroxene $\delta^{18}O = 5.8$) indicate that the plagioclase and clinopyroxene have exchanged only slightly with an ^{18}O shifted seawater-derived hydrothermal fluid.

Gabbro OM28 (Rustaq): Adcumulate with igneous lamination; 72% plagioclase (An75), 15% clinopyroxene, 10% amphibole, and 3% serpentine, and/or talc alteration pseudomorphing olivine. In contrast to the other cumulate gabbros, the oxygen isotope data from this sample (plagioclase $\delta^{18}O = 4.7$, and whole rock $\delta^{18}O = 5.2$) indicate significant exchange of plagioclase and pyroxene with a seawater-derived fluid.

Harzburgite K22 (Ibra): Porphyroclastic texture with tectonite fabric; 25% orthopyroxene, 45% olivine, 30% serpentine, and trace amounts of spinel. Serpentine is pseudomorphing olivine.

5.1.2. Experimental procedures

Samples were prepared by removing exterior surfaces with a rock splitter and crushing interior chunks. Only mechanical means were used for mineral separation and involved a combination of handpicking and magnetic separation. These procedures produced high purity (~100%) plagioclase separates and pyroxene separates of greater than 95% purity. The small amount of impurity in the pyroxene separate generally consisted of olivine which is unimportant as it contains extremely low trace element concentrations.

Oxygen was extracted and analyzed from approximately 20 mg of sample using the procedures outlined by Taylor and Epstein [1962]. For Nd and Sr, approximately 200 mg of sample was dissolved using HF and

$HClO_4$. After complete dissolution an aliquot consisting of about 10% of the solution was spiked and concentrations of K, Rb, Sr, Sm, and Nd were determined. From approximately 100 mg of the remaining unspiked solution, Nd and Sr were separated using ion exchange chemistry. For several samples (see Table 5-1) both Sm and Nd concentrations and $^{143}Nd/^{144}Nd$ ratios were obtained from the same spiked sample. For the plagioclase separate from the gabbro K9, the $^{143}Nd/^{144}Nd$ ratio was obtained from both spiked and unspiked samples and was the same within experimental error. The Sr isotopic composition was measured using a single oxidized tantalum filament and typically ~150 ratios were collected. The Nd isotopic composition was determined by measuring NdO^+ on a single rhenium filament and normalized to $^{150}Nd/^{142}Nd = 0.2096$. The 2σ (mean) errors quoted for the $^{143}Nd/^{144}Nd$ ratio were generally obtained from about 250 ratios. For the above procedures the blanks were Rb = 0.01 ng, Sr = 0.1 ng, Sm = 0.006 ng, and Nd = 0.02 ng and are negligible for the data presented here.

For the harzburgite, the lower Sr and Nd concentrations required the use of a slightly modified procedure to enable the precise determination of the isotopic compositions. Approximately 400 mg of the harzburgite was dissolved, and split into three equal portions after removing a 10% aliquot for concentrations. The three portions were passed separately through a cation column, and Sr and rare earths were separated. The rare earth fractions were combined and loaded on the lactic acid column and Nd was separated. Using this procedure, a total of 10 ng of Nd was obtained from the harzburgite K22, with a Nd blank of ~0.06 ng. This blank is less than 0.6% of the total Nd and is therefore still insignificant. For 10 ng of Nd the precision of the $^{143}Nd/^{144}Nd$ ratio is still better than 5 parts in 10^5.

Table 5-1. Nd, Sr, and O isotopic data from the Samail ophiolite.

Samples	$\frac{^{87}Rb}{^{86}Sr}$	$\frac{^{147}Sm}{^{144}Nd}$	$\frac{^{87}Sr}{^{86}Sr}$	$\frac{^{143}Nd}{^{144}Nd}$	ε_{Sr}	ε_{Nd}	$\delta^{18}O$
Basalt							
G54 WR	0.104	0.192	0.70491±4	0.512219±19	5.1±0.6[a]	7.5±0.4[a]	12.7
CALCITE	0.0042	0.209	0.70650±15	0.512265±29	30.5±2.1	8.1±0.6	
Sheeted Dikes							
G10	0.029	0.209	0.70535±4	0.512250±25	13.5±0.6	7.8±0.5	8.5
K1	0.008	0.194	0.70519±4	0.512275±20	11.7±0.6	8.6±0.4	6.8
Plagiogranite							
G224-3	0.035	0.187	0.70362±4	0.512249±18	-11.3±0.6	8.2±0.3	5.2
Gabbros							
G224-2 WR	0.010	0.201	0.70370±3	0.512251±19	-9.5±0.4	8.0±0.4	3.7
PLAG	0.008	0.151	0.70352±4	0.512196±18	-12.5±0.6	7.8±0.3	4.5
URAL	0.014	0.241	0.70426±3	0.512285±19	-1.6±0.4	8.0±0.4	2.6
K9 WR	0.0008	0.271	0.70304±5	0.512310±18	-18.6±0.7	8.0±0.3	5.7
PLAG	0.0005	0.129	0.70296±2	0.512180±25	-19.7±0.3	7.8±0.5	6.0
				0.512181±19[b]		7.8±0.4	
CPX	0.0008	0.322	0.70313±3	0.512341±15	-17.3±0.4	7.7±0.3	5.3
		0.316		0.512332±22[b]		7.7±0.4	
OM251 PLAG	0.0010	0.159	0.70311±5	0.512203±22	-18.0±0.7	7.6±0.4	6.4
CPX	0.0018	0.377	0.70315±5	0.512346±25[b]	-17.5±0.7	7.6±0.5	5.8
OM28 WR	0.0014	0.264	0.70383±5	0.512274±22[b]	-7.8±0.7	7.7±0.4	5.2
Harzburgite							
K22		0.216		0.512278±23		8.3±0.4	

[a] ε_{Sr} and ε_{Nd} values calculated for a cyrstallization age of 130 m.y. except for OM251 and OM28 for which an age of 100 m.y. was used.

[b] $^{143}Nd/^{144}Nd$ determined from spiked sample.

5.1.3 Data representation

The oxygen data are given in the conventional δ-notation of

$$\delta^{18}O = [(^{18}O/^{16}O)_{SAMPLE}/(^{18}O/^{16}O)_{STANDARD} - 1]\ 10^3 \quad .$$

Samples are corrected to the SMOW scale using Caltech rose quartz $\delta^{18}O = 8.45$. Following DePaolo and Wasserburg [1976a] an analogous notation is used for Nd and Sr, with the reference reservoir evolving with time where:

$$\varepsilon_{Nd} = [(^{143}Nd/^{144}Nd)^T_{INIT}/(^{143}Nd/^{144}Nd)^T_{CHUR} - 1]\ 10^4$$

and

$$\varepsilon_{Sr} = [(^{87}Sr/^{86}Sr)^T_{INIT}/(^{87}Sr/^{86}Sr)^T_{UR} - 1]\ 10^4 \quad .$$

The $(^{143}Nd/^{144}Nd)^T_{INIT}$ and $(^{87}Sr/^{86}Sr)^T_{INIT}$ are the measured ratios corrected for decay since the time of crystallization T. The $(^{143}Nd/^{144}Nd)^T_{CHUR}$ and $(^{87}Sr/^{86}Sr)^T_{UR}$ ratios are those in the standard reservoirs [DePaolo and Wasserburg, 1976a,b] at the time T.

5.2 RESULTS

5.2.1 Oxygen isotopic characteristics

The oxygen isotopic systematics of the Samail ophiolite are discussed in detail by Gregory and Taylor [1981]. The three general categories of samples are: (1) lower cumulate gabbros which exhibit close to "normal" ^{18}O characteristics (K9, OM251), (2) rocks below the diabase-gabbro contact which exhibit ^{18}O depletions (G224-2, G224-3, OM28), and (3) rocks above the diabase-gabbro contact which exhibit ^{18}O enrichments, relative to a MORB reservoir of $\delta^{18}O = 5.7$ [Muehlenbachs and Clayton, 1976].

The dichotomy between $\delta^{18}O$ values of the rocks above or below the diabase-gabbro contact is a result of differing alteration environments which depend upon temperature, water/rock ratio, and the history of the exchanging fluid.

In order to understand the ^{18}O variation due to temperature effects, let us consider the ^{18}O fractionation between rock and fluid defined as

$$\Delta^{18}O_{rock} = \Delta \equiv \delta^{18}O_{rock} - \delta^{18}O_{water} \qquad (1)$$

which is a function of temperature given by Taylor [1974]:

$$\Delta(T) = \frac{A}{T^2} + B \quad , \qquad (2)$$

where A,B are constants.

In the basalt-seawater system, temperatures of alteration in the vicinity of 250°C to 300°C produce no ^{18}O shifts in the rocks as a result of hydrothermal exchange (i.e., $\Delta \approx 5.7$). The gabbros which are altered at temperatures greater than 400°C are depleted in $\delta^{18}O$ (i.e., $\Delta < 5.7$). The subsolidus alteration event is characterized by isotopic disequilibrium between coexisting plagioclases and clinopyroxenes and water/rock ratios < 1.0 [Gregory and Taylor, 1981]. The Samail gabbro-water interactions are analogous to those observed in continental layered complexes such as the Skaergaard intrusion which have suffered meteoric hydrothermal exchange [Taylor and Forester, 1979]. The major difference between the continental and marine environments is the contrast between the initial compositions of the hydrothermal fluids: meteoric water with an initial $\delta^{18}O \sim -15$ ‰ (e.g., the Skaergaard [Taylor and Forester, 1979]), and seawater with $\delta^{18}O \sim 0$‰ . The contrast between fluid and rock in the subaerial environments is large,

~ 20‰, so that the hydrothermal exchange with meteoric water produces almost exclusively ^{18}O depletions in the intrusion and its surrounding country rock over a wide range of temperatures [Taylor, 1974; Taylor and Forester, 1979]. In the marine case, because seawater is isotopically closer to the initial rock composition, the effects of high temperature alteration in the gabbros are less pronounced with a maximum $\delta^{18}O$ depletion of approximately 3‰, while in subaerial environments hydrothermally altered gabbros often display $\delta^{18}O$ depletions of as much as 5-10‰ [Taylor and Forester, 1979]. Due to the spreading environment of the seafloor the diabases and pillow lavas overlying gabbroic magma chambers "see" a time-temperature superposition of alteration regimes that has no other analog in the subaerial examples described to date [Gregory and Taylor, this volume].

In order to illustrate these points, considering only the effects of temperature, the diabase dikes altered under greenschist to lower amphibolite facies are expected to be depleted in ^{18}O relative to their primary values if pristine seawater with a $\delta^{18}O \approx -0.5$ is the hydrothermal fluid. However, diabases G10 and K1 with $\delta^{18}O = 8.5, 6.8$, respectively, are to the contrary, enriched in ^{18}O. This contradiction requires that these diabases have exchanged with a seawater-derived hydrothermal fluid that has become ^{18}O enriched relative to its initial value. The fluids which have exchanged with the underlying solidified cumulate gabbro are likely candidates as the gabbro section is a region of high temperature (> 400°C) alteration and low water/rock ratio (< 1); this is ideal for producing a fluid phase with ^{18}O enrichments. Fluids discharging from the gabbros into the diabases have a calculated ^{18}O enrichment relative to an initial $\delta^{18}O \simeq -0.5$ from ~ +2 to ~ +9‰ [Gregory and Taylor, 1981]. Since seawater is only ~ 6‰ lighter than the rock, water exhibiting enrichments of this magnitude reacts with the diabases

at lower temperature resulting in greenschist facies rocks ($2 \lesssim \Delta(T) \lesssim 6$) with a $\delta^{18}O > 6$. This suggests that the oxygen isotopes of the diabases are recording a final exchange event as the following discussion will illustrate.

The inferred funnel-shaped geometry of the oceanic crusted magma chamber [Hopson et al., 1981]; Pallister and Hopson, 1981], requires that fluids which exchange with large amounts of solidified gabbro discharge at the distal edge of the chamber away from the ridge-axis [Gregory and Taylor, 1981]. Since thin sheets of magma (inferred from the crystallization of the most fractionated magma at the diabase-gabbro contact [Pallister and Hopson, 1981]; see Fig. 5-11) act as impermeable barriers to fluid circulation [Taylor and Forester, 1979; Norton and Taylor, 1979], two hydrothermal systems exist during the early history of newly created oceanic crust: one affecting the roof-rocks of the gabbroic magma chamber near the ridge axis and the second affecting the gabbros which have crystallized under the wings of the chamber [Gregory and Taylor, 1979]. Waters discharging from the second system react with the diabases which have been already altered by the upper system as they spread away from the ridge axis and thus the diabases are affected by both systems. These geometrical constraints become important when evaluating the combined Sr and O effects discussed below.

5.2.2 Trace element abundances

The K, Rb, Sr, Sm, and Nd abundances are listed in Table 5-2. The most obvious feature is the contrast in K, Rb, Sm, and Nd concentrations between the layered gabbros (K9, OM28, and OM251) which are a factor of ten to one-hundred times lower than those in the upper sequence (plagiogranite,

Table 5-2. Trace element abundances from the Samail ophiolite (ppm)

Samples	K	Rb	Sr	Sm	Nd	$\frac{Sr}{Rb}$	$\frac{K}{Rb}$	$\frac{Sm}{Nd}$
Basalt								
G54 WR	4470	7.16	198	5.03	15.9	28	624	0.316
G54 CALCITE	76	0.009	6.12	0.043	0.126	680	8440	0.341
Sheeted Dikes								
G10	3950	1.63	162	3.85	11.2	99	2420	0.344
K1	2290	1.04	388	4.16	13.0	370	2201	0.320
Plagiogranite								
G224-3	2200	2.31	192	5.36	17.3	83	952	0.310
Gabbros								
G224-2 WR	1320	0.674	196	2.78	8.36	290	1960	0.333
PLAG	1800	0.950	330	0.563	2.25	350	1890	0.250
URAL	740	0.280	58.7	3.79	9.51	210	2640	0.399
K9 WR	117	0.052	188	0.441	0.986	3610	2250	0.447
PLAG	161	0.050	311	0.085	0.399	6220	3220	0.213
CPX	29	0.023	24.8	1.401	2.630	1080	1260	0.533
OM251								
PLAG	77	0.055	156	0.021	0.081	2840	1400	0.259
CPX	20	0.034	54.2	0.256	0.411	1590	588	0.623
OM28 WR	126	0.066	132	0.168	0.385	2000	1910	0.436
Harzburgite								
K22	6	0.023	0.43	0.013	0.035	19	261	0.371
Average MOR[a] Tholeiite	1300	1	130	2.7	8	130	1300	0.34

[a]Data from Engel et al., 1965; Tatsumoto et al., 1965; Kay et al., 1970; Schilling, 1971.

uralite gabbro, sheeted dikes, and basalts). This feature reflects the mineralogy (clinopyroxene, plagioclase, and olivine) and the cumulate origin of the layered gabbros. Since the K, Rb, Sm, and Nd mineral/liquid partition coefficients of the cumulus phases are all less than unity, the gabbro cumulates have much lower concentrations than the melts from which they crystallized. The resulting melt which is enriched in these elements is presumably represented by the overlying more fractionated rocks such as the diabases and pillow basalts. It is therefore unlikely that any particular ophiolite member represents the primitive melt composition. In contrast, the Sr concentration is relatively uniform throughout the layered gabbros and the upper sequence. This is probably due to the high concentration of Sr in plagioclase of the layered gabbro which compensates for the lower concentrations in the other cumulate minerals, olivine and clinopyroxene, leaving Sr in the melt approximately constant.

Significant variations in concentrations also exist within the same lithologic units. The gabbro K9 has approximately a factor of four higher concentration of Sm and Nd and a factor of approximately two higher K and Sr concentrations than the gabbro OM251 (see Table 5-2). Similar variations have also been observed in the gabbros from the Troodos ophiolite [Kay and Senechal, 1976]. The variations in trace element concentration probably reflect the complex crystal fractionation and replenishment history of the magma chamber. In the Samail ophiolite evidence for multiple cycles of primitive magma replenishment has been extensively documented within the gabbro complex by Pallister and Hopson [1981]. This is a common feature of ophiolite complexes [Moores, 1969; Jackson, 1975], as well as of layered gabbro intrusions emplaced in continental environments, such as the Muskox, Bushveld, and Great Dike intrusions [Jackson, 1970, 1971; Irvine, 1970].

Trace element concentration variations of the alkali elements may be due to the effects of seawater alteration. Within the upper sequence, the K concentration decreases systematically from top to bottom. Rb shows a similar trend to K with the exception of the plagiogranite (G224-3). However, the Sr, Sm, and Nd concentrations do not show any similar systematic trends. This suggests that the higher K and Rb concentrations are due to seawater alteration and are not primary. This is consistent with other studies [Hart, 1970; Chapman and Spooner, 1977] and observations of K-rich alteration minerals in oceanic basalts [Seyfried et al., 1978]. The end member (~ 350°C) water issuing from submarine hot springs [Corliss et al., 1979; Edmond et al., 1979] is enriched in K and Rb relative to normal seawater. These data suggest that K and Rb may have been leached from the deeper levels of the ophiolite complex and preferentially fixed in the upper part of the sequence. Despite the effects of alteration, the K and, to a lesser extent, Rb concentrations of the basaltic rocks are still consistent with an oceanic affinity. The K/Rb ratios of 620 to 2420 and Sr/Rb ratios of 27 to 373 of the diabase dikes and basalt in the Samail ophiolite are roughly comparable to the average MOR tholeiite ratios of K/Rb ≃ 1300 and Sr/Rb ≃ 130 [Engel et al., 1965; Tatsumoto et al., 1965]. The Sm/Nd ratios are within the range of typical MOR tholeiites [Kay et al., 1970; Schilling, 1971], while the Sm and Nd concentrations in the Ibra section of the Samail ophiolite are somewhat higher.

The harzburgite, K22, has distinctly lower trace element concentrations than the rest of the ophiolite members (Table 5-2). Extremely low concentrations of incompatible elements are common in

metamorphic peridotites from other ophiolites and are interpreted as evidence that the harzburgite tectonite is a residual fraction of upper mantle left after partial melting. REE data can also be used [Montigny et al., 1973; Allegre et al., 1973; Pallister and Knight, this volume] to test the hypothesis that the harzburgite is a residue cogenetic with the overlying cumulate gabbros and basaltic suites. This type of calculation requires assumptions concerning amount of partial melting, distribution coefficients, and composition of source material, all of which are uncertain. A more definitive constraint is provided by the Nd isotopic data, presented in the following section.

5.2.3 Crystallization age and initial $^{143}Nd/^{144}Nd$

Although current models for the formation of ophiolites at spreading centers indicate that within a single section all the igneous rocks, with perhaps the exception of the basal peridotites, should be of approximately the same age, there may still be significant variations in initial $^{143}Nd/^{144}Nd$ ratios due to mantle source heterogeneities. For this reason, analyses of only whole rock samples from different parts of an ophiolite may have variable initial $^{143}Nd/^{144}Nd$ ratios and may not define an isochron. In addition, the range in Sm/Nd ratios of total rocks may be inadequate to define an age for such young samples. Therefore, crystallization ages and initial ratios were determined using coexisting minerals separated from gabbros.

We obtained Sm-Nd mineral isochrons from three gabbros (K9, G224-2, OM251) using plagioclase, clinopyroxene, and uralite mineral separates. The gabbro K9 from the Ibra section contains plagioclase, clinopyroxene, and olivine and is extremely fresh, with only a minor

Figure 5-1. Sm-Nd evolution diagram for the cumulate gabbro K9, from the Ibra section, Oman. The uncertainty in the age determination is largely controlled by the difference between the $^{147}Sm/^{144}Nd$ ratios of the coexisting clinopyroxene and plagioclase. The $\varepsilon_{Nd}(0)$ values are the deviations in parts in 10^4 of the measured $^{143}Nd/^{144}Nd$ ratio from the value in CHUR today (0:511836).

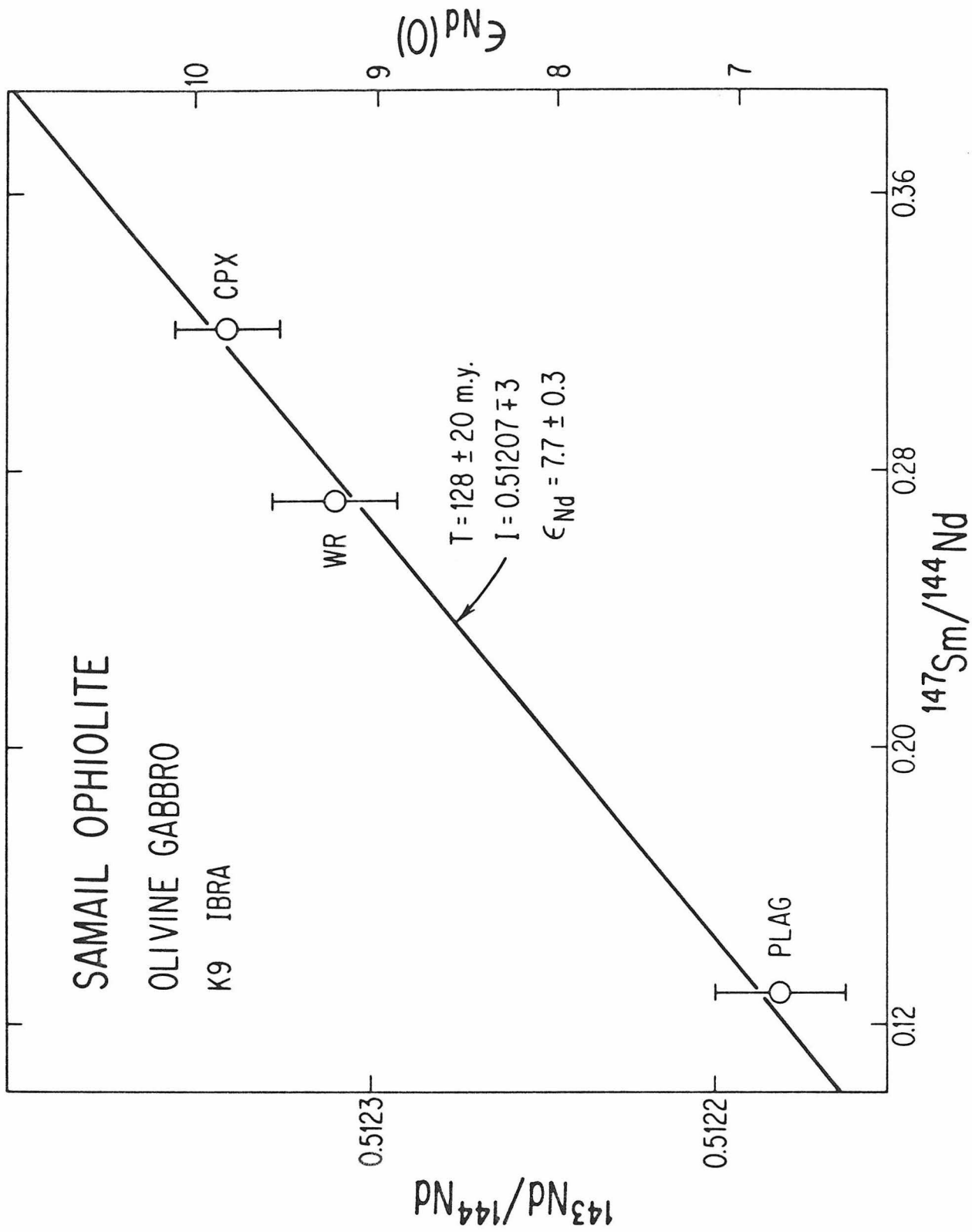
SAMAIL OPHIOLITE
OLIVINE GABBRO
K9 IBRA
CPX
WR
PLAG
T = 128 ± 20 m.y.
I = 0.51207 ∓ 3
ϵ_{Nd} = 7.7 ± 0.3
$^{143}Nd/^{144}Nd$
$^{147}Sm/^{144}Nd$
$\epsilon_{Nd}(0)$
0.5123
0.5122
0.12
0.20
0.28
0.36
10
9
8
7

amount of alteration. It can be seen in Table 5-1 and Fig. 5-1 that the $^{143}Nd/^{144}Nd$ ratio is enriched in the clinopyroxene from K9 by 2 parts in 10^4 relative to the plagioclase. The clinopyroxene also has a higher $^{147}Sm/^{144}Nd$ ratio of 0.320 compared to 0.129 for the plagioclase. Assuming that these minerals and the whole rocks have remained closed systems since crystallizing from an isotopically homogeneous melt, these data indicate a crystallization age of 128±20 m.y. with an initial $^{143}Nd/^{144}Nd$ ratio of $\varepsilon_{Nd} = 7.7\pm0.3$. Since the age and initial ratio for this gabbro are only defined by two independent points, the interpretation of this "two-point isochron" as the time of crystallization is not unique. To eliminate the possibility of two component mixing producing this array, three or more distinct mineral phases would have to be analyzed. This is not possible in this sample, as no other REE bearing mineral phase is present (olivine contains negligible REE).

We analyzed a second gabbro from the upper part of the same gabbro unit as K9. This gabbro (G224-2) contains uralite as a late-stage replacement of pyroxene and primary hornblende. The low $\delta^{18}O$ values for both plagioclase and uralite indicate that this sample has exchanged with seawater at high temperatures (> 400°C). The Sm-Nd data from G224-2 are shown in Table 5-1 and Fig. 5-2. The uralite has the highest $^{147}Sm/^{144}Nd$ and $^{143}Nd/^{144}Nd$ ratios and together with the plagioclase gives an age of 150±40 m.y. and an initial $^{143}Nd/^{144}Nd$ ratio of $\varepsilon_{Nd} = 7.8\pm0.4$. The larger uncertainty in the age compared to K9 is due to the smaller difference between the $^{147}Sm/^{144}Nd$ ratios in the plagioclase and uralite mineral separates. However, within analytical uncertainty, both samples have the same age and initial $^{143}Nd/^{144}Nd$ ratio. In addition, the results

Figure 5-2. Sm-Nd evolution diagram for the high level uralite gabbro G224-2, from the Ibra section, Oman. The larger uncertainty in the age determination compared to the gabbro K9 is due to the smaller spread in $^{147}Sm/^{144}Nd$ ratios of the plagioclase and uralite. The uralitization process must have occurred close to the time of crystallization of the gabbro and does not appear to have disturbed the the Sm-Nd systematics.

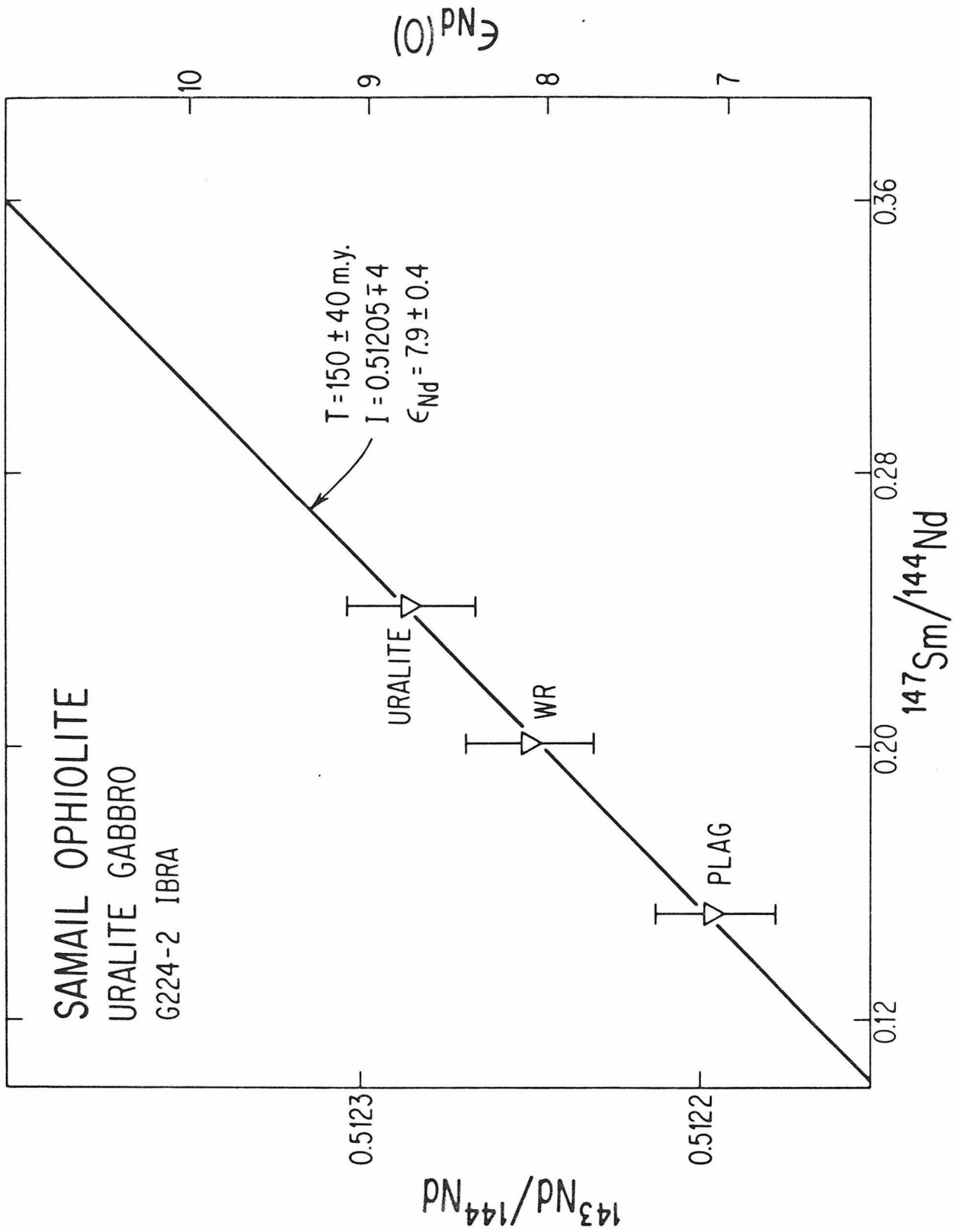
SAMAIL OPHIOLITE
URALITE GABBRO
G224-2 IBRA
T = 150 ± 40 m.y.
I = 0.51205 ± 4
ϵ_{Nd} = 7.9 ± 0.4
URALITE
WR
PLAG
0.5123
0.5122
0.12
0.20
0.28
0.36
10
9
8
7
$^{143}Nd/^{144}Nd$
$^{147}Sm/^{144}Nd$
$\epsilon_{Nd}(0)$

from G224-2 show that the Sm-Nd systematics are not affected by the presence hydrous alteration minerals such as uralite. This is evidence that the correlated variations of $^{143}Nd/^{144}Nd$ and $^{147}Sm/^{144}Nd$ ratios in these minerals represent an isochron rather than an accidental mixing line. The combined Ibra data give an age of 130±12 m.y. and ε_{Nd} = 7.8±0.2. This will be used as a reference isochron for comparison of other data from the Ibra section.

In order to determine whether there exists any variation in either the age or initial $^{143}Nd/^{144}Nd$ ratio, we analyzed the gabbro OM251 which was collected in Wadi Fizh approximately 300 km NW from the Ibra section (see Fig. 4-1). The plagioclase and clinopyroxene data points from this gabbro give an age of 100±20 m.y. and an initial of ε_{Nd} = 7.6±0.3. This initial ratio is slightly lower than that obtained from the Ibra section and the crystallization age appears to be about 30 m.y. younger (note, however, that the error bars on the two isochron ages overlap). This age difference, if substantiated, would imply a tectonic break, for example, a transform fault, with a large lateral offset. Such a structure conceivably might be located in the Samail gap (Fig. 4-1).

Tilton et al. [1981] have dated plagiogranites along the entire length of the Oman Mountains using uranium lead technique on zircons and found U-Pb ages which are virtually constant (94-98 m.y.) for the entire ophiolite. On the basis of these consistent results, Tilton et al. [1981] interpret the zircon ages as the time of igneous crystallization. Sm-Nd ages obtained from north of the Samail gap (Fig. 4-1) agree with the zircon results. However east of the Samail gap, the Sm-Nd data from Ibra give consistently older (~ 30 m.y.) ages than the plagiogranites. Since all Sm/Nd and $^{143}Nd/^{144}Nd$

Figure 5-3. Sm-Nd evolution diagram for the cumulate gabbro OM251, from Wadi Fizh, northern Oman.

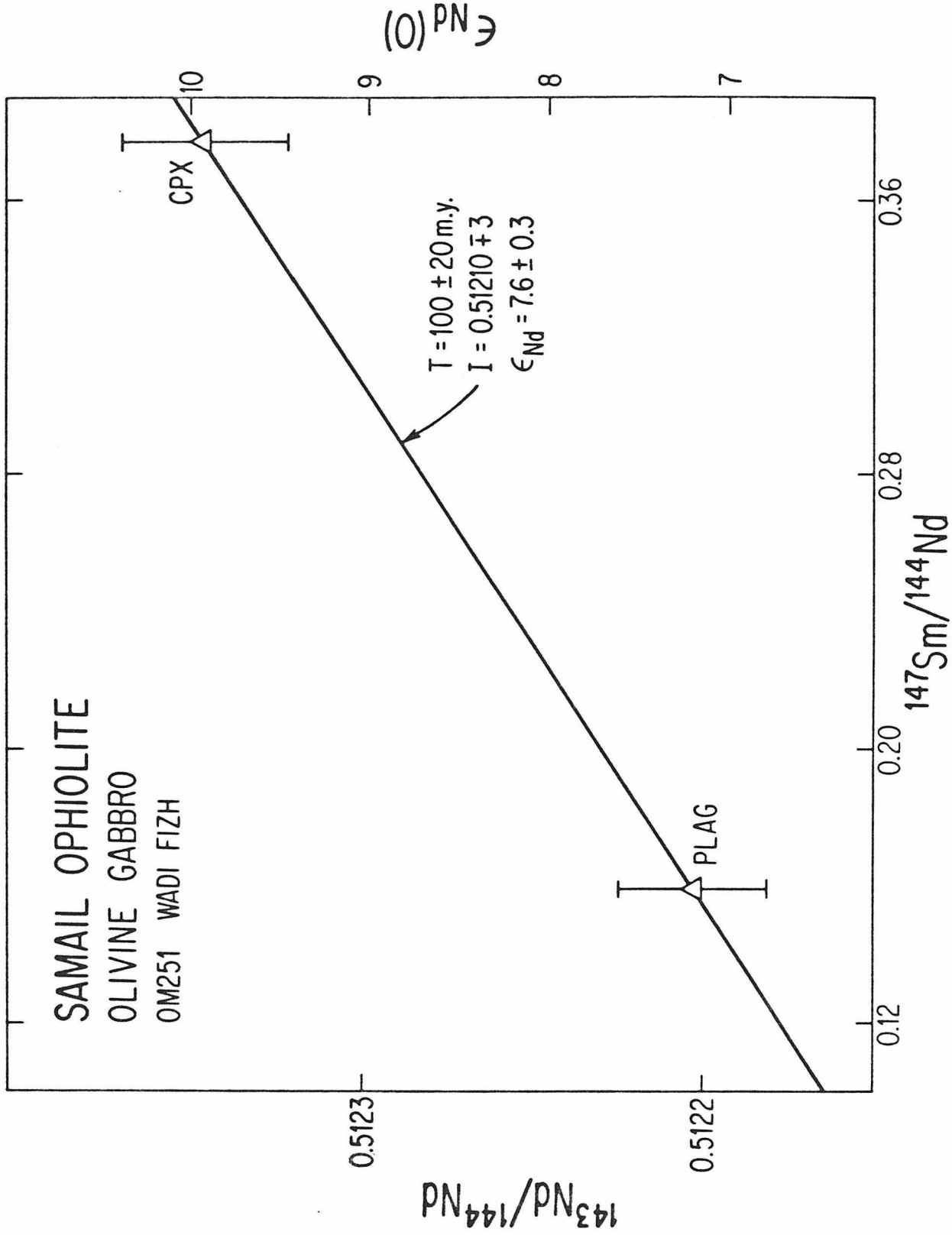
SAMAIL OPHIOLITE
OLIVINE GABBRO
OM251 WADI FIZH
CPX
PLAG
T = 100 ± 20 m.y.
I = 0.51210 ± 3
ϵ_{Nd} = 7.6 ± 0.3
$^{143}Nd/^{144}Nd$
$^{147}Sm/^{144}Nd$
$\epsilon_{Nd}(0)$
0.5123
0.5122
0.12
0.20
0.28
0.36
10
9
8
7

were determined from the same spiked solution for samples northwest of the Samail gap, K9 clinopyroxene was repeated using this same technique. The results of the second run are within experimental error the same as the aliquot data (Table 5-1). Note that the second run was performed on a new mineral separate, yet the Sm-Nd systematics did not change thereby indicating the reliability of the data. The contrast between the two Ibra ages suggests that the U-Pb and Sm-Nd clocks are recording different events southeast of the Samail gap.

The geologic significance of the age discrepancy is not resolved. However, the internal consistency of both the U-Pb [Tilton et al., 1981] and the Sm-Nd data indicates that extreme caution must be exercised when attaching a geologic interpretation to either of the ages. The zircon and Sm-Nd age data from the Blow-Me-Down massif, Bay of Islands, Newfoundland [Mattinson, 1976; Jacobsen and Wasserburg, 1979] illustrate this point. The Sm-Nd internal isochron ages of 508±6 m.y. and 501±13 m.y. for pyroxene gabbro agree with the upper intercept on the U-Pb concordia diagram in a discordia interpretation of the zircon data. Mattinson analyzed three separate zircon fractions (separated using magnetic and size characteristics) from the same plagiogranite and noted that each fraction was concordant within analytical uncertainty. This result is typical for young samples. If only one split from the entire zircon population had been analyzed, the zircon U-Pb age would have been 10-30 m.y. younger than Sm-Nd age from the same section. Due to the low zircon contents of the Oman plagiogranites, it was possible to analyze only one fraction for each plagiogranite. Using this technique on such young samples prevents any assessment of possible dispersion along the concordia in a single plagiogranite, and thus the interpretation of the zircon ages as the time of primary igneous

crystallization may be subject to question.

5.2.4 Sm-Nd whole rock analyses of basalts, sheeted dikes, plagiogranite, and harzburgite

Sm-Nd whole rock analyses were obtained from a plagiogranite (G224-3), sheeted dikes (G10, K1), and a basalt (G54) from the Ibra section. In addition, a calcite amygdule from the basalt G54 was also analyzed for Sm-Nd. From the $\delta^{18}O$ values and petrography, these samples show varying degrees and conditions of alteration and metamorphism ranging from zeolite to greenschist facies. With the exception of the basalt, only a single data point was obtained for each sample and it is therefore not possible to independently calculate both the age and initial ratio for each sample. Therefore, in Fig. 5-4 these data are compared with the mineral isochron defined by the gabbros from Ibra. Apart from the sheeted dike K1, the data all lie within analytical error of the gabbro reference isochron. This is consistent with these samples having the same crystallization age (130 m.y.) and initial $^{143}Nd/^{144}Nd$ ratio. This can be seen from the ε_{Nd} values given in Table 5-1, which for an age of 130 m.y. range from 7.5±0.4 to 8.3±0.3 compared to $\varepsilon_{Nd} = 7.8\pm0.2$ for the two Ibra gabbros. The plagiogranite G224-3, with $\varepsilon_{Nd} = 8.2\pm0.3$ has a clear affinity with these rocks and must represent a later first or second stage differentiate from the same type of oceanic magma source and cannot be a product of melting of any older continental basement.

The tectonized harzburgite K22 with $\varepsilon_{Nd} = 8.3\pm0.4$ is also within analytical uncertainty of the Ibra reference isochron. This suggests that the harzburgite is genetically related to the rest of the ophiolite (i.e.,

Figure 5-4. Sm-Nd evolution diagram showing whole rock data for basalt, sheeted dikes, and plagiogranite from the Ibra section, Oman. With the exception of the sheeted dike K1, the data from the other samples are consistent with the same crystallization age and initial $^{143}Nd/^{144}Nd$ ratio as the gabbros from Ibra. The deviation of K1 indicates the presence of small but significant isotopic heterogeneities in the magma reservoirs. The tectonite harzburgite K22 is within analytical uncertainty of the Ibra reference isochron. This is consistent with the harzburgite being a cogenetic of the partial melting event which produced the rest of the ophiolite.

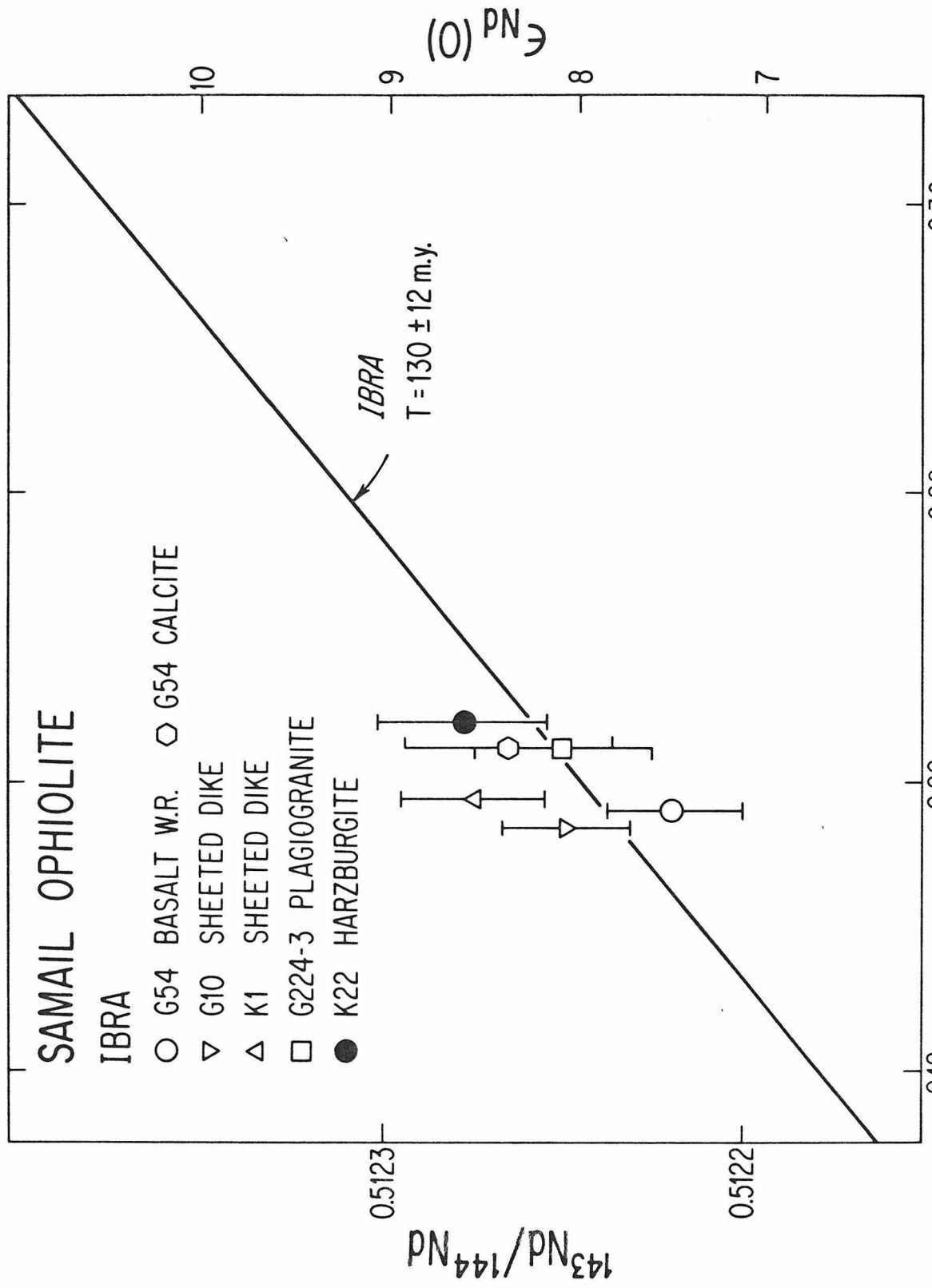
SAMAIL OPHIOLITE
IBRA
G54 BASALT W.R.
G54 CALCITE
G10 SHEETED DIKE
K1 SHEETED DIKE
G224-3 PLAGIOGRANITE
K22 HARZBURGITE
IBRA
T = 130 ± 12 m.y.
0.5123
0.5122
0.12
0.20
0.28
0.36
10
9
8
7
$^{143}Nd/^{144}Nd$
$^{147}Sm/^{144}Nd$
$\varepsilon_{Nd}(0)$

cumulate gabbro and high level volcanics) and that the serpentinization of the harzburgite has not disturbed the Sm-Nd system.

The Sm-Nd analysis of the diabase dike K1 does not overlap with the reference isochron. This cannot be explained by seawater alteration as the more altered samples are consistent with the reference isochron. This small deviation of K1 could be due to variations in both initial $^{143}Nd/^{144}Nd$ ratio and the crystallization age. As it is unlikely that significant age differences exist within the same section, the deviation of K1 is most probably due to a variation in its initial $^{143}Nd/^{144}Nd$ ratio. For an age of 130 m.y. this corresponds to $\varepsilon_{Nd} = 8.6\pm0.4$ for K1 compared to $\varepsilon_{Nd} = 7.8\pm0.2$ for the Ibra gabbros and indicates the presence of small but significant isotopic heterogeneities in the magma reservoirs.

In an attempt to directly ascertain the Nd isotopic characteristics of the interacting fluid, we analyzed a calcite amygdule from the basalt G54. The amygdule has $\varepsilon_{Nd} = 8.1\pm0.6$ which is within error the same as the host basalt. While the solution that deposited the calcite was most likely derived from seawater with an initially negative ε_{Nd} value [O'Nions et al., 1978; Piepgras et al., 1979], the calcite gave an ε_{Nd} value which indicates that the final fluid must have obtained the Nd from the parent rock and not from seawater.

5.3 DISCUSSION

5.3.1 Implications of Sm-Nd

The presence in the Samail ophiolite of only small variations in the initial $^{143}Nd/^{144}Nd$ ratios from different localities and stratigraphic units appears to indicate a relatively uniform isotopic source regions.

It is therefore useful to compare these initial ratios with those found in young ocean ridge, ocean island, island arc, and continental basalts. In Fig. 5-5, ocean ridge and island arc tholeiites have ε_{Nd} values which overlap, with ocean ridge tholeiites having a range of +7 to +13 and island arcs ranging from +7 to +10. These values [DePaolo and Wasserburg, 1976a, 1977; O'Nions et al., 1977; Hawkesworth et al., 1977; Richard et al, 1976] are distinctive from the ocean island range of ~ +4 to +8 [O'Nions et al., 1977; DePaolo and Wasserburg, 1977]. The ε_{Nd} for oceanic rocks is very different from young continental tholeiitic basalts which have $\varepsilon_{Nd} \sim 0$ [DePaolo and Wasserburg, 1976a; Carlson et al., 1978] and older continental crust having $\varepsilon_{Nd}(0) << 0$ [DePaolo and Wasserburg, 1976a; McCulloch and Wasserburg, 1978]. The Samail ophiolite with $\varepsilon_{Nd} = 7.8$ clearly has an oceanic affinity lying in the lower limit of the island arc and ocean ridge basalt range and the uppermost limit of the ocean island range. Due to the overlap of ε_{Nd} values from different tectonic settings shown on Fig. 5-5, the Nd isotopic data cannot distinguish among various possible genetic models such as mid-ocean ridge, back-arc basin, ocean island, or island-arc origin for the Samail ophiolite. However, the lack of light REE enriched samples and alkalic volcanism usually associated with ocean island and island arc environments suggests that the most reasonable scenario for its formation is in an ocean basin.

The value of $\varepsilon_{Nd} = 7.8$ in the Samail ophiolite is somewhat lower than "typical" MORB with $\varepsilon_{Nd} \approx 10$. This may be due to the older age of the Samail ophiolite compared to the zero age basalts plotted in Fig. 6 or it may simply reflect the overall variability present today in ocean ridge basalts. The dispersion in ε_{Nd} of modern-day oceanic basalts is to some extent correlated with chemistry. Alkalic rocks generally have lower ε_{Nd}

Figure 5-5. Histogram comparing ε_{Nd} values from the Samail ophiolite measured in this study with mid-ocean ridge basalts (MORB), marginal basins (Lau, Scotia Sea), island arcs, ocean islands, and continental flood basalts. The Samail ophiolite clearly has an oceanic affinity, although because of the overlap, the Nd isotopic data by themselves cannot definitely distinguish among the various possible oceanic environments. The dashed lines show the ε_{Nd} values of the Samail ophiolite corrected for differential evolution relative to the bulk earth during the past 130 m.y. (see discussion).

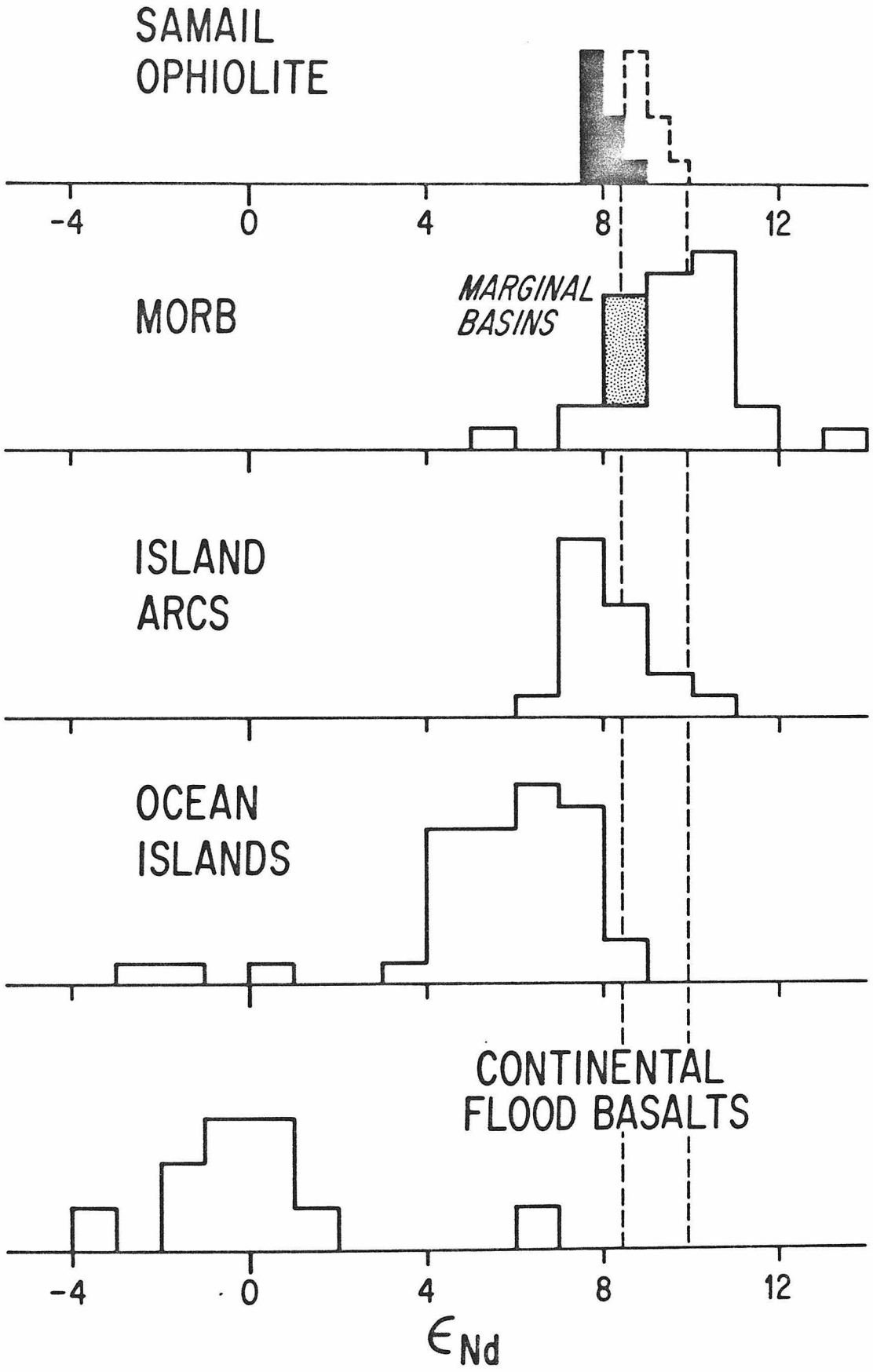
SAMAIL
OPHIOLITE
-4
0
4
8
12
MORB
MARGINAL
BASINS
ISLAND
ARCS
OCEAN
ISLANDS
CONTINENTAL
FLOOD BASALTS
-4
0
4
8
12
ϵ_{Nd}

values than MOR tholeiites [Carlson et al., 1978]. However, several oceanic tholeiites with relatively low ε_{Nd} values in the range of +7.0 to 8.5 have also been found, for example, in the Atlantic (113152 [DePaolo and Wasserburg, 1976b], and ARP75 [Richard et al., 1976]) and Pacific (BD17-1 [DePaolo and Wasserburg, 1976b]) oceans. These samples do not appear to be chemically or tectonically distinctive although the isotopic data indicate an origin from a less depleted source reservoir. Tectonically distinctive oceanic settings which may be modern day analogues of the environment in which the Samail ophiolite was formed are the Lau marginal basin and Scotia Sea back arc. The ε_{Nd} values from these two areas [Hawkesworth et al., 1977; Carlson et al., 1978] are shown in Fig. 5-5 and define a relatively narrow range in ε_{Nd} of from 8.1 to 9.0. These ratios are also somewhat low compared to normal MORB samples and are very similar to the Samail ophiolite.

To some extent the slightly lower ε_{Nd} value of the Samail ophiolite compared to "typical" oceanic crust is due to the evolution of $^{143}Nd/^{144}Nd$ in the oceanic mantle reservoirs during the past 130 m.y. To correct for this evolution an estimate of the $^{147}Sm/^{144}Nd$ ratio in the Samail ophiolite source reservoir is required. This can be obtained by assuming that the composite of the cumulate gabbros, diabase dikes, and pillow basalts represents the primary unfractionated magma. From the Samail ophiolite data we estimate that this magma had Nd ~ 4 ppm and Sm ~ 1.6 ppm. This corresponds to $^{147}Sm/^{144}Nd \sim 0.24 \pm 0.02$. As Nd and Sm are strongly partitioned into the liquid during partial melting, this is also probably a reasonable estimate for the source reservoir. For this value of $^{147}Sm/^{144}Nd$, the Samail source reservoir evolves by ~ 0.6 ε_{Nd} units per 100 m.y. and would

today have $\varepsilon_{Nd} \sim 8.7$. Thus the ε_{Nd} value of the Samail ophiolite would now only be about ~ 1 ε_{Nd} unit below the center of the MORB distribution and is therefore fully consistent with a MORB affinity. It is also noted that for the MORB source reservoir to evolve in a single stage from $\varepsilon_{Nd} = 0$ to the modern day value of $\varepsilon_{Nd} = +10$ requires, for $^{147}Sm/^{144}Nd = 0.24$, a time interval of 1.7 AE. This result is similar to the single stage differentiation ages obtained by Pb-isotope studies [Church and Tatsumoto, 1975; Sun et al., 1975].

The relationship of the basal peridotites to the rest of the ophiolite sequence has been obscure due to the effects of deformation and post-emplacement alteration which have strongly modified the primary geologic structures and relationships. Various hypotheses summarized by Coleman [1977] have considered the harzburgite as a (1) cogenetic lowermost cumulate, (2) older accidental mantle substrate which is not petrogenetically linked to the rest of the ophiolite, or (3) a cogenetic refractory residue remaining from the partial melting which produced the rest of the ophiolite. The initial Nd value of $\varepsilon_{Nd} = 8.3 \pm 0.4$ for the tectonized harzburgite K22 is within error the same as the rest of the ophiolite. This result, together with the low trace element concentrations, supports the third hypothesis.

There is, however, conflicting evidence from the U-shaped (convex downward chondrite normalized) rare earth element (REE) patterns which have been observed in the Samail harzburgite [Pallister and Knight, 1981] and a number of other peridotites [Allegre et al., 1973; Kay and Senechal, 1976; Frey, 1969; Suen et al., 1979]. On the basis of U-shaped REE patterns in harzburgite and dunite from Newfoundland, Suen et al. [1979] have concluded that the tectonite peridotite could not be related to the overlying oceanic

crust by a simple partial melting event. Their argument against a cogenetic origin for the harzburgite is that residues of light REE-depleted MORB should also exhibit LREE depletion. The argument depends upon the choice of crystal-liquid partition coefficients for olivine and orthopyroxene. Natural olivines from meteorites and from peridotite [Schnetzler and Bottino, 1971; Masuda, 1968; Frey, 1969] may exhibit U-shaped REE patterns. Combining natural olivine-orthopyroxene partition coefficient data from Frey [1969] with experimentally determined orthopyroxene-liquid data reviewed by Irving [1978] suggests that residual harzburgites can have U-shaped patterns because olivine dominates the light REE and orthopyroxene dominates the heavy REE. A cumulate dunite measured by Suen et al. [1979] (which on geologic grounds crystallized from the same melts that produced LREE depleted diabases [Malpas, 1978]) has a U-shaped pattern. If we assume that REE partitioning between cumulate and liquid is the same as partitioning between residue and liquid, then a cogenetic residue of harzburgite should also exhibit such a pattern but at lower concentrations.

The harzburgite REE concentrations are lower than expected from simple one stage partial melting and are a consequence of the plumbing system that delivers melts to the surface. Two processes enrich the overall REE contents in ophiolitic diabases and by analogy in seafloor basalts: (1) open system fractionation in crustal magma chambers driven by periodic intrusion and mixing into the chamber of primitive magma [Stern, 1979; Pallister and Knight, this volume], and (2) fractionation of olivine during ascent of the primary melt bodies through the upper mantle [Hopson et al., 1981]. The second process is a consequence of the fact that enstatite is not an early liquidus phrase at low pressure for any MORB compositions--confirmed experimentally by Green et al. [1979] and Stolper [in press] and in the Samail ophiolite [Hopson et al., 1981; Pallister and Hopson, 1981]. The implication of

this relationship is that above depths of 30 km [Stolper, in press] all harzburgite-melt contacts become sites of reaction between ascending melts and their host rocks which are not in magmatic equilibrium. The upward migration and reaction of the melts with the harzburgite is manifested in the Samail peridotite as cross-cutting dunite bodies [Boudier and Coleman, 1981]. Using field estimates of the amount of dunite present in the Samail peridotite, fractionation of olivine during ascent may enrich the REE of the melt by as much as a factor of two.

The former process documented by Pallister and Knight [1981] has enriched the overall REE concentrations of Samail melts by factors up to five. In samples K9 and OM251 a four-fold enrichment is observed. These combined crustal and upper mantle processes may lead to order of magnitude enrichments of overall bulk REE between initial melt segregation and crystallization. Therefore, any trace-element concentration arguments concerning genetic relationships between rocks such as the harzburgites and diabases are subject to post-separation processes which cannot be constrained without other petrologic data (usually not available with seafloor samples). In contrast, the Nd isotope data which are independent of the vagaries of the plumbing system see through this history and thus provide a more straightforward test of the primary relationship between harzburgite and the overlying oceanic crust.

The partial melting event which produced the harzburgite residue is unlikely to be exactly contemporaneous with the crystallization of the immediately overlying pile of cumulate gabbros, sheeted dikes, and pillow lavas. The following sequence is suggested. Partial melting of an already LREE depleted source material (lherzolite) at depths of 60 to 70 km [Green et al., 1979] is followed by melt segregation. The residual harzburgite ascends with a rate constrained by the spreading rate to form the basement

of the cumulate gabbros and basaltic suites. For a half spreading rate of 1 cm/yr, the harzburgite would take ~ 6 m.y. to rise from the partial melting zone. In contrast, the magma produced during this partial melting would rise much more rapidly at a rate of ~ 1 km/yr, otherwise the melt would crystallize before reaching the surface [Marsh, 1979]. Thus for the conservative spreading rate used in this example, the formation of the harzburgite residue probably occurred, at most, 6 m.y. prior to the crystallization of the immediately overlying magmatic suite. This time difference is not resolvable with the present Sm-Nd data. Thus within the analytical uncertainties the harzburgite and overlying magmatic sequences are considered to be cogenetic.

5.3.2 Comparison of Rb-Sr and Sm-Nd

The most obvious contrast between the Sr and Nd isotopic systems is the larger variability of the $^{87}Sr/^{86}Sr$ ratios ranging from 0.70296 (ε_{Sr} = -19.7) to 0.70650 (ε_{Sr} = +30.5) compared to a range in ε_{Nd} of from only 7.5 to 8.6. The lowest $^{87}Sr/^{86}Sr$ ratios are found in the plagioclase separates from the layered cumulate gabbros K9 and OM251. In K9, the plagioclase has an $^{87}Sr/^{86}Sr$ ratio of 0.70296±2. However, the coexisting clinopyroxene has a distinctly higher value of 0.70313±3. In Fig. 5-6 reference isochrons of 130 m.y. and 4550 m.y. are shown. A line connecting the clinopyroxene and plagioclase from K9 gives an impossibly old age of > 4.5 AE. In the high level gabbro G224-2 there is a similar disparity between the plagioclase and uralite. The uralite has an $^{87}Sr/^{86}Sr$ ratio of 0.70426±3 compared to 0.70352±4 for the coexisting plagioclase. These isotopic variations cannot be accounted for by radiogenic decay since crystallization. Instead, this isotopic relationship between

Figure 5-6. Rb-Sr evolution diagram showing whole rock and mineral data from the Samail ophiolite. The near horizontal line is a 130 m.y. isochron and the steeper line is for an isochron of 4550 m.y. The lack of correlation between $^{87}Rb/^{86}Sr$ and $^{87}Sr/^{86}Sr$ and the high $^{87}Sr/^{86}Sr$ is attributed to contamination by seawater.

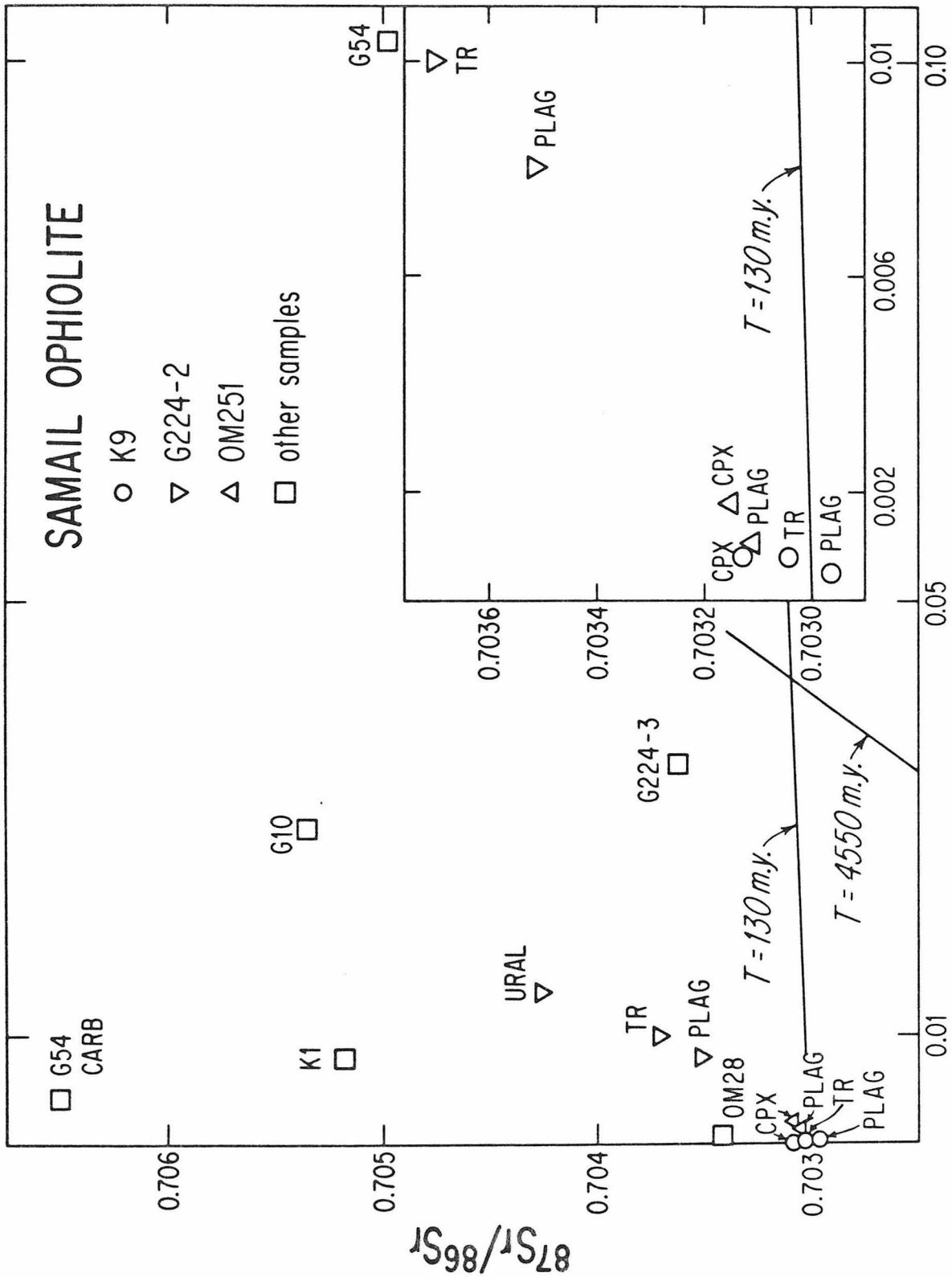
SAMAIL OPHIOLITE
K9
G224-2
OM251
other samples
G54
TR
PLAG
CPX
PLAG
TR
PLAG
G54
CARB
K1
G10
URAL
TR
PLAG
OM28
CPX
PLAG
TR
PLAG
G224-3
T = 130 m.y.
T = 130 m.y.
T = 4550 m.y.
0.706
0.705
0.704
0.703
0.7036
0.7034
0.7032
0.7030
0.01
0.05
0.10
0.002
0.006
0.01
87Sr/86Sr
87Rb/86Sr

the coexisting mineral phases indicates partial exchange with a source of high $^{87}Sr/^{86}Sr$. The enrichment in $^{87}Sr/^{86}Sr$ is more pronounced in the clinopyroxene and uralite and is anticipated as they have a factor of five lower Sr concentration than the plagioclase. This enrichment is also consistent with the petrography as the uralite is clearly an alteration product and the clinopyroxene contains ~ 5% secondary hornblende. These results are in distinct contrast to Sm-Nd, where all mineral phases plot on a 130 m.y. isochron.

The highest $^{87}Sr/^{86}Sr$ ratios found in the Samail ophiolite are in the upper sequences consisting of basalts, sheeted dikes, and plagiogranites. The higher $^{87}Sr/^{86}Sr$ ratios in these rocks is consistent with a greater degree of exchange with seawater having a high $^{87}Sr/^{86}Sr$ ratio. In an attempt to determine the $^{87}Sr/^{86}Sr$ ratio in seawater, we analyzed a calcite amygdule from the basalt OMG54. This has $^{87}Sr/^{86}Sr = 0.7065$ which is significantly higher than that found for any of the igneous rocks and may be compared to 0.7076 estimated for Cretaceous seawater [Peterman et al., 1970; Veizer and Compston, 1974]. These observations are clearly consistent with hydrothermal interaction with seawater. The slightly lower ratio in the carbonate amygdule compared to Cretaceous seawater is probably due to the lowering of $^{87}Sr/^{86}Sr$ in the fluid by interaction with the rock. There is also an approximate correlation between high $^{87}Sr/^{86}Sr$ and stratigraphic height (see Fig. 5-1-) which suggests that water/rock ratios increased upward in the section.

Due to the overprinting of rock Sr with seawater Sr, it is not possible to unambiguously determine the primary magmatic $^{87}Sr/^{86}Sr$ ratio in these rocks. An upper limit is given by the lowest $^{87}Sr/^{86}Sr$ value of

0.70296 found in the plagioclase from the gabbro K9. This may be close to its magmatic value as the coexisting clinopyroxene with a lower Sr concentration has only a slightly greater $^{87}Sr/^{86}Sr$ ratio. The $^{87}Sr/^{86}Sr$ ratios in the clinopyroxene and plagioclase from the gabbro OM251 also have very different Sr concentrations but have the same $^{87}Sr/^{86}Sr$ ratio within error and should thus also represent a primary value. The difference between the plagioclase separates from K9 and OM251 of 0.70296±2 and 0.70311±5 could therefore indicate a small but real difference in the $^{87}Sr/^{86}Sr$ ratios of these samples and apparently of the original magmas from which they crystallized. This suggests that small $^{87}Sr/^{86}Sr$ mantle isotopic heterogeneities may have been preserved during the formation of the Samail ophiolite, because the same effect is also apparent in the Nd isotopic data (Table 5-1). In fact these two samples OM251 and K9 plot right on the MOR correlation line in the ε_{Sr}-ε_{Nd} diagram of Fig. 5-7.

The importance of distinguishing between seawater alteration effects and mantle isotopic variations is illustrated in the Rb-Sr isochron diagram of Fig. 5-6. In this figure, seawater alteration has produced an approximate correlation between Rb/Sr and $^{87}Sr/^{86}Sr$. If interpreted literally, this correlation would imply that Rb/Sr heterogeneities have existed for at least several billion years in the mantle reservoirs of the Samail ophiolite. Similar correlations and interpretations have been suggested in other ophiolites [Peterman et al., 1971], oceanic basalts [Brooks et al., 1976; Hedge, 1978], and ocean islands [Sun and Hanson, 1975; Duncan and Compston, 1976; Whitford et al., 1977]. Although some of these correlations are undoubtedly due to mantle features, the ^{18}O and Sr data from the Samail

Figure 5-7. ε_{Nd} and ε_{Sr} values for the Samail ophiolite (solid). The arrows indicate the effect of contamination with Cretaceous seawater for different water/rock ratios and show that $W/R > 10^5$ is required before ε_{Nd} values are affected. The ε_{Nd} and ε_{Sr} values of uncontaminated samples plot within the "mantle array" and are consistent with derivation from a MORB source region.

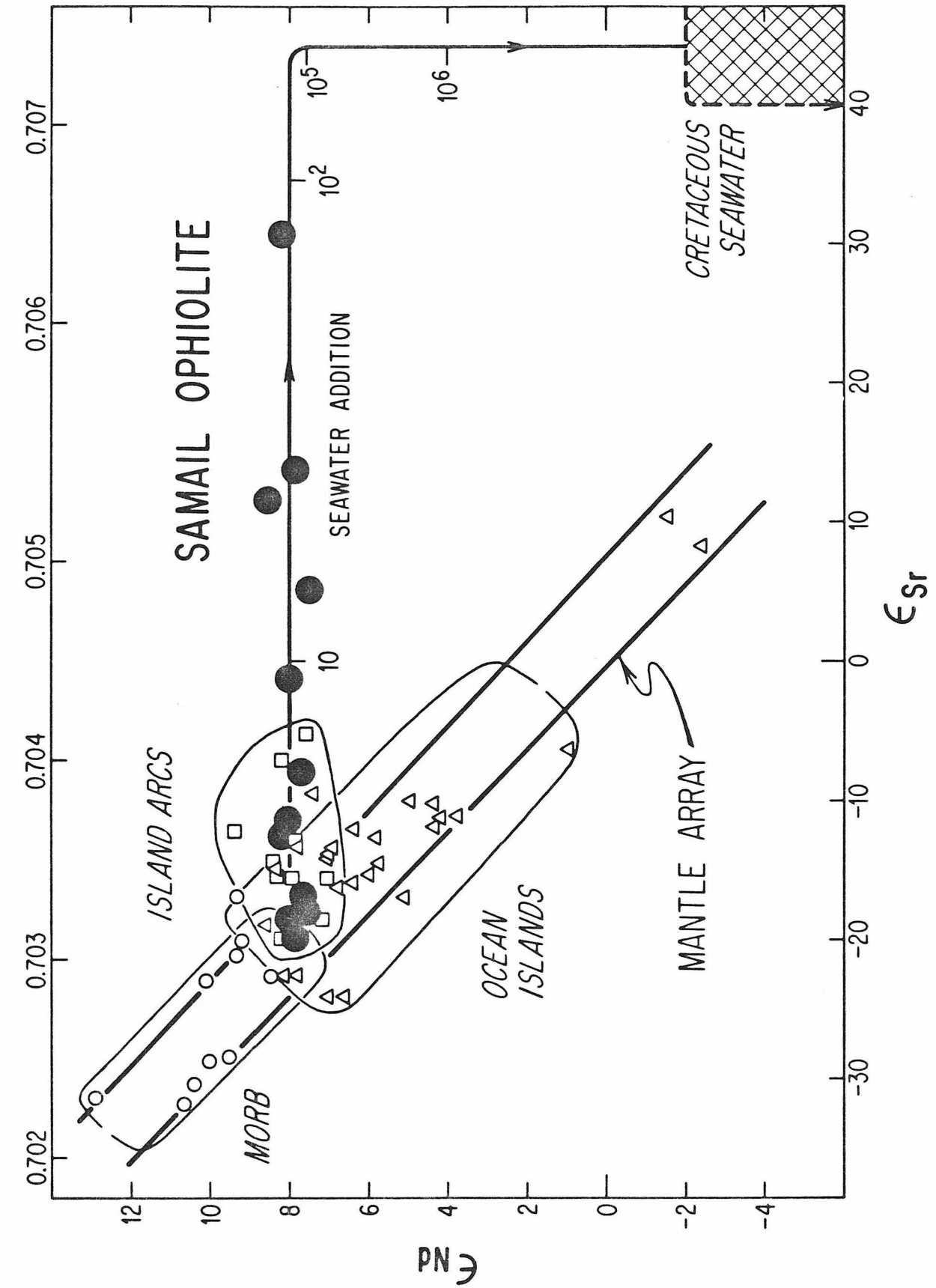
SAMAIL OPHIOLITE
SEAWATER ADDITION
CRETACEOUS SEAWATER
ISLAND ARCS
MORB
OCEAN ISLANDS
MANTLE ARRAY
ϵ_{Nd}
ϵ_{Sr}
0.702
0.703
0.704
0.705
0.706
0.707
12
10
8
6
4
2
0
-2
-4
40
30
20
10
0
-10
-20
-30
10
10^2
10^5
10^6

ophiolite indicate that in this case the Rb/Sr-$^{87}Sr/^{86}Sr$ correlation is clearly an artifact of seawater alteration.

A useful criterion to distinguish between isotopic variations due to either primary magmatic or seawater alteration effects is the ε_{Nd},ε_{Sr} diagram. In Fig. 5-7 the ε_{Nd} and ε_{Sr} values from the Samail ophiolite are shown. They have an origin at the mantle correlation line [DePaolo and Wasserburg, 1976b; O'Nions et al., 1977] and form a horizontal trajectory to the higher ε_{Sr} values. Although this general effect has been observed by previous workers [DePaolo and Wasserburg, 1977; O'Nions et al., 1977], the present results provide a spectacular example of how the Nd isotopic composition is unaffected by seawater contamination while the Sr composition is shifted drastically. It is illustrative to compare the observed ε_{Nd},ε_{Sr} values, with those calculated for contamination of oceanic crust by Cretaceous seawater. Assuming a simple closed system model for mixing of Sr and Nd in seawater with oceanic crust, mass balance between the initial and final products gives:

$$w\,\varepsilon^{i}_{water} + r\,\varepsilon^{i}_{rock} = w\,\varepsilon^{f}_{water} + r\,\varepsilon^{f}_{rock} \qquad (3)$$

where w and r are the atomic proportions of Nd or Sr in the water and rock systems respectively and ε^{i}_{rock} = initial ε_{Nd} or ε_{Sr} value in rock before exchange; ε^{f}_{rock} = final modified rock ε_{Nd} or ε_{Sr} value; ε^{i}_{water} = initial ε_{Nd} or ε_{Sr} value in water before exchange; and ε^{f}_{water} = final modified water ε_{Nd} or ε_{Sr} value. For equilibrium exchange of water and rock, $\varepsilon^{f}_{water} = \varepsilon^{f}_{rock}$ and from equation (3) the water/rock ratio by weight is given by

$$\frac{W}{R} = \frac{\varepsilon^f_{rock} - \varepsilon^i_{rock}}{\varepsilon^i_{water} - \varepsilon^f_{rock}} \left(\frac{C^i_{rock}}{C^i_{water}} \right) \quad (4)$$

where C^i_{rock} = concentration of Sr or Nd in initial rock and C^i_{water} = concentration of Sr or Nd in seawater.

For Sr, the parameters used in this equation are $\varepsilon^i_{rock} = -20$, $\varepsilon^i_{water} = +47$ [Peterman et al., 1970], and $C^i_{water} = 8$ ppm [Goldberg, 1965]. ε^f_{rock} values are given in Table 5-1. It is assumed that the initial Sr concentration in the rock (C^i_{rock}) is the same as the final measured concentration (Table 5-2). For Nd the parameters used in equation (4) are $\varepsilon^i_{rock} = +8.0$, $\varepsilon^i_{water} = -7$, and $C^i_{water} = 2.8 \times 10^{-6}$ ppm [Piepgras et al., 1979]. The C^i_{rock} and ε^f_{rock} values are given in Tables 5-1 and 5-2.

Using equation (4) and the Sr and Nd parameters, the ε_{Nd} and ε_{Sr} values in the rock resulting from mixing of different proportions of seawater with oceanic crust have been calculated. The ε_{Nd}-ε_{Sr} mixing line is shown in Fig. 5-7, together with the water/rock ratios calculated for rock Sr and Nd concentrations of 180 ppm and 10 ppm, respectively. From Fig. 5-8, it can be seen that the ε_{Nd} values are far less sensitive to seawater contamination than the ε_{Sr} values. This is due to the significantly lower concentration of Nd in seawater of 2.8×10^{-6} ppm compared to 8 ppm for Sr. For example, the Sr data indicate that the sample with the highest water/rock ratio is the diabase dike K1 with W/R = 43 (Table 5-3). Using the Sr water/rock ratio for K1, and solving for ε^i_{rock}, shows that a W/R = 43 causes an insignificant change of $\varepsilon_{Nd} = -0.0001$. To produce a measurable

shift in ε_{Nd} of 0.5, a water/rock ratio of W/R = 1.6 x 10^5 would be required. Thus, relative to the most altered rock, an increase in the water/rock ratio of ~ 4 x 10^3 would be required before seawater contamination would measurably change the ε_{Nd} values. A detailed analysis of the effects of seawater interaction using ε_{Sr} and $\delta^{18}O$ variations will be given in the following section.

5.3.3 Comparison of $^{87}Sr/^{86}Sr$ and $\delta^{18}O$

It has already been shown that $^{87}Sr/^{86}Sr$ and $\delta^{18}O$ values are sensitive to hydrothermal alteration. The effects of alteration on both these systems is shown in the initial $^{87}Sr/^{86}Sr$, $\delta^{18}O$ diagram of Fig. 5-8. In this figure there appears to be at least two distinct trends which are centered about the primary values of $\delta^{18}O \approx +6$ and $^{87}Sr/^{86}Sr \approx 0.7030$. The most obvious trend is the approximate inverse correlation corresponding to depleted $\delta^{18}O$ and high $^{87}Sr/^{86}Sr$ ratios. The second, less distinctive, feature is the association of heavy $\delta^{18}O$ values with high $^{87}Sr/^{86}Sr$ ratios in the sheeted dikes and basalt. In an attempt to understand these features, we will now consider simple models for the exchange of Sr and O with seawater.

Let us consider a simple closed system model for the exchange of Sr and O with seawater as has already been discussed for Sr and Nd. Using this model, the water/rock ratio (by weight) calculated using $\delta^{18}O$ variations is given by Taylor [1974]:

$$\frac{W}{R} = \left(\frac{\delta^{f}_{rock} - \delta^{i}_{rock}}{\delta^{i}_{water} - \delta^{f}_{rock} - \Delta)} \right) \left(\frac{C^{i}O_{rock}}{C^{i}O_{water}} \right) \qquad (5)$$

Figure 5-8. Initial $^{87}Sr/^{86}Sr$ versus $\delta^{18}O$ values of whole rocks (solid symbols) and minerals from the Samail ophiolite. The lack of any simple correlation between $^{87}Sr/^{86}Sr$ and $\delta^{18}O$ indicates different temperatures (see Fig. 10) of hydrothermal interaction of seawater and a complex history for the seawater derived fluid. W/R ratios are calculated assuming initial Cretaceous seawater had $^{87}Sr/^{86}Sr = 0.7076$; Sr = 8 ppm, and the initial rocks had $^{87}Sr/^{86}Sr = 0.703$; Sr = 160 ppm.

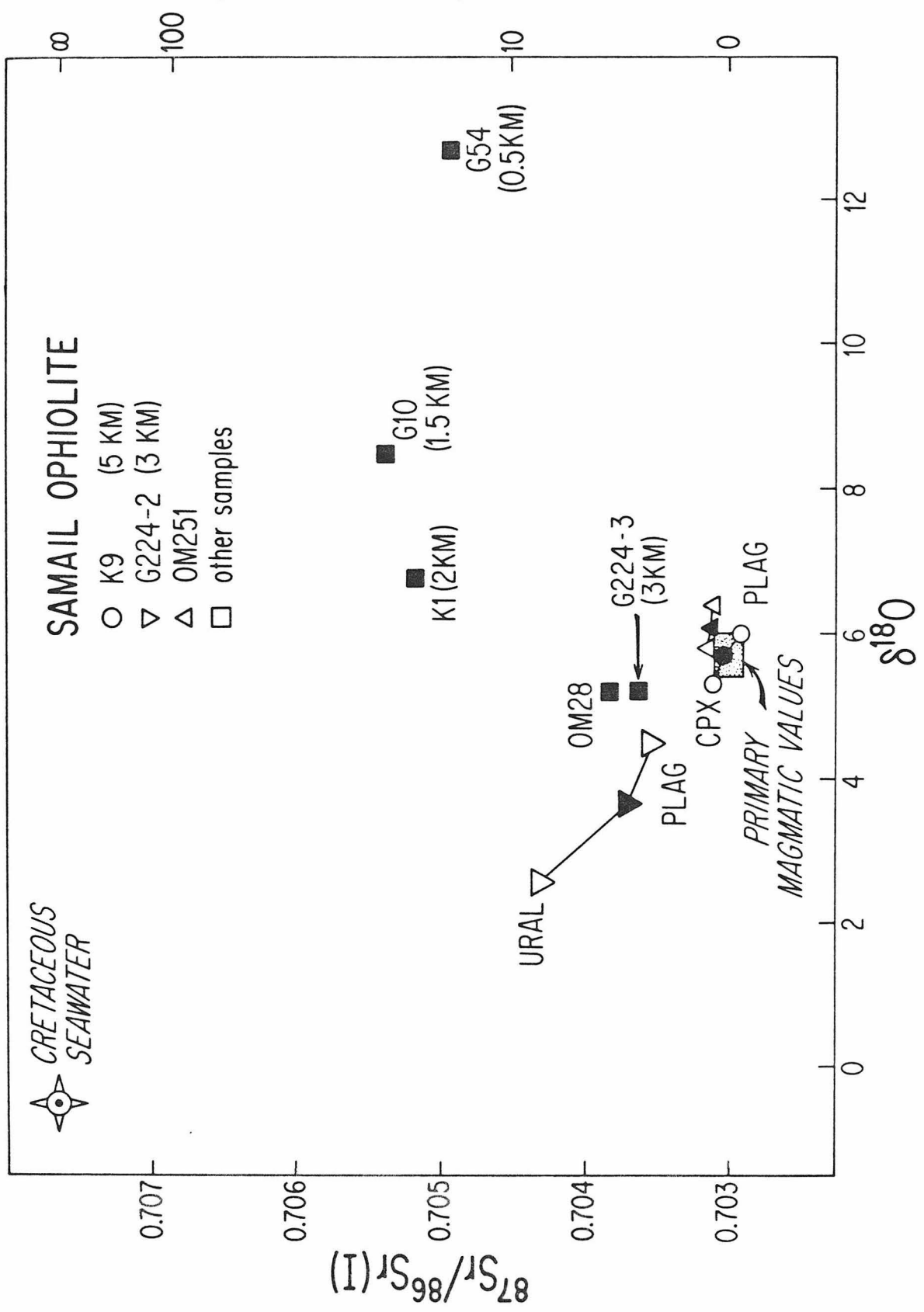
WATER/ROCK (closed system)
∞
100
10
0
SAMAIL OPHIOLITE
K9 (5 KM)
G224-2 (3 KM)
OM251
other samples
G54 (0.5KM)
G10 (1.5 KM)
K1(2KM)
G224-3 (3KM)
OM28
PLAG
URAL
CPX
PLAG
PRIMARY MAGMATIC VALUES
CRETACEOUS SEAWATER
0.707
0.706
0.705
0.704
0.703
87Sr/86Sr (I)
0
2
4
6
8
10
12
δ18O

This equation is identical to that used for Sr, apart from the temperature dependent fractionation factor Δ. Let us now assume that only a particular fraction of the rock exchanges oxygen with seawater. This may, for example, be the case for rocks with different model proportions of easily exchanged minerals such as feldspar. The effective water/rock ratio (W/R(effective)) is then given by

$$\frac{W}{R}(\text{effective}) = \frac{W}{R} \times \frac{1}{q} \tag{6}$$

where q is the fraction (by weight) of rock that exchanged with seawater. A similar equation can also be written for the Sr water/rock ratio, where in this case let us assume that different fractions of the rock, q' exchanged with seawater. Therefore the relationship between the Sr and O water/rock ratios is given by

$$\frac{W}{R}(\text{Sr})\frac{1}{q'} = \frac{W}{R}(\text{oxygen})\frac{1}{q} \tag{7}$$

Using this relationship, equations (4) and (5) can now be combined to give

$$\frac{\varepsilon^f_{rock} - \varepsilon^i_{rock}}{\delta^f_{rock} - \delta^i_{rock}} = \left(\frac{\varepsilon^i_{water} - \varepsilon^f_{rock}}{\delta^i_{water} - (\delta^f_{rock} - \Delta)} \right) \times C \tag{8}$$

where

$$C = \frac{C^i Sr_{water}/C^i O_{water} \times q'/q}{C^i Sr_{rock}/C^i O_{rock}}$$

An example of a mixing line using equation (7) is shown in Fig. 5-9 for $\Delta = 0$. It can be seen that the mixing line is a hyperbola with the

Figure 5-9.a. ε_{Sr} and $\delta^{18}O$ mixing lines for $\Delta = 0$ and C = 0.22. The closed system curve is calculated using equation 8 and maps out the locus of ($\delta^{18}O$, ε_{Sr}) for systems with fixed W/R and water recirculation. The open system curve allows each packet of water to pass through the rock only once; thus no recirculation is permitted. In areas where hot spring activity occurs, such as the Galapagos rift [Corliss et al, 1979], the open system equation applies. The "one pass" curve is calculated by substituting the expression for open system water/rock (equation 9) into equation 7. For Δ and C fixed the natural systems lie between the two curves.

b. ε_{Sr} and $\delta^{18}O$ values in the rock for C = 0.022 and $\Delta = 2$ (line A), $\Delta = 6$ (line C), and $\Delta = 8$ (line B). For $\Delta = 6$ which corresponds to a temperature of ~ 300°C, there can be shifts in ε_{Sr} without any change in $\delta^{18}O$.

c. ε_{Sr} and $\delta^{18}O$ values in water for $\Delta = 2$, $\Delta = 6$, and $\Delta = 8$ (solid lines) are given by $\delta^{18}O^{f}_{water} = \delta^{18}O^{f}_{rock} - \Delta$ and ε^{f}_{roc} For $\Delta < 6$ which corresponds to temperature > 300°C, seawater will be enriched in ^{18}O as long as the water/rock ratio is small. For $\Delta > 6$ (< 300°C) ^{18}O-depleted waters will be produced. The dashed lines show the ε_{Sr} and $\delta^{18}O$ values in the rock (from Fig. 10b). The horizontal dashed line illustrates how the combined strontium and oxygen data can be used as a geothermometer for hydrothermal interactions if the W/R obtained from the $^{87}Sr/^{86}Sr$ ratios is used to solve the oxygen W/R equation for $\Delta(T)$.

d. Example of mixing lines consistent with ε_{Sr} and $\delta^{18}O$ values in the uralite gabbro.

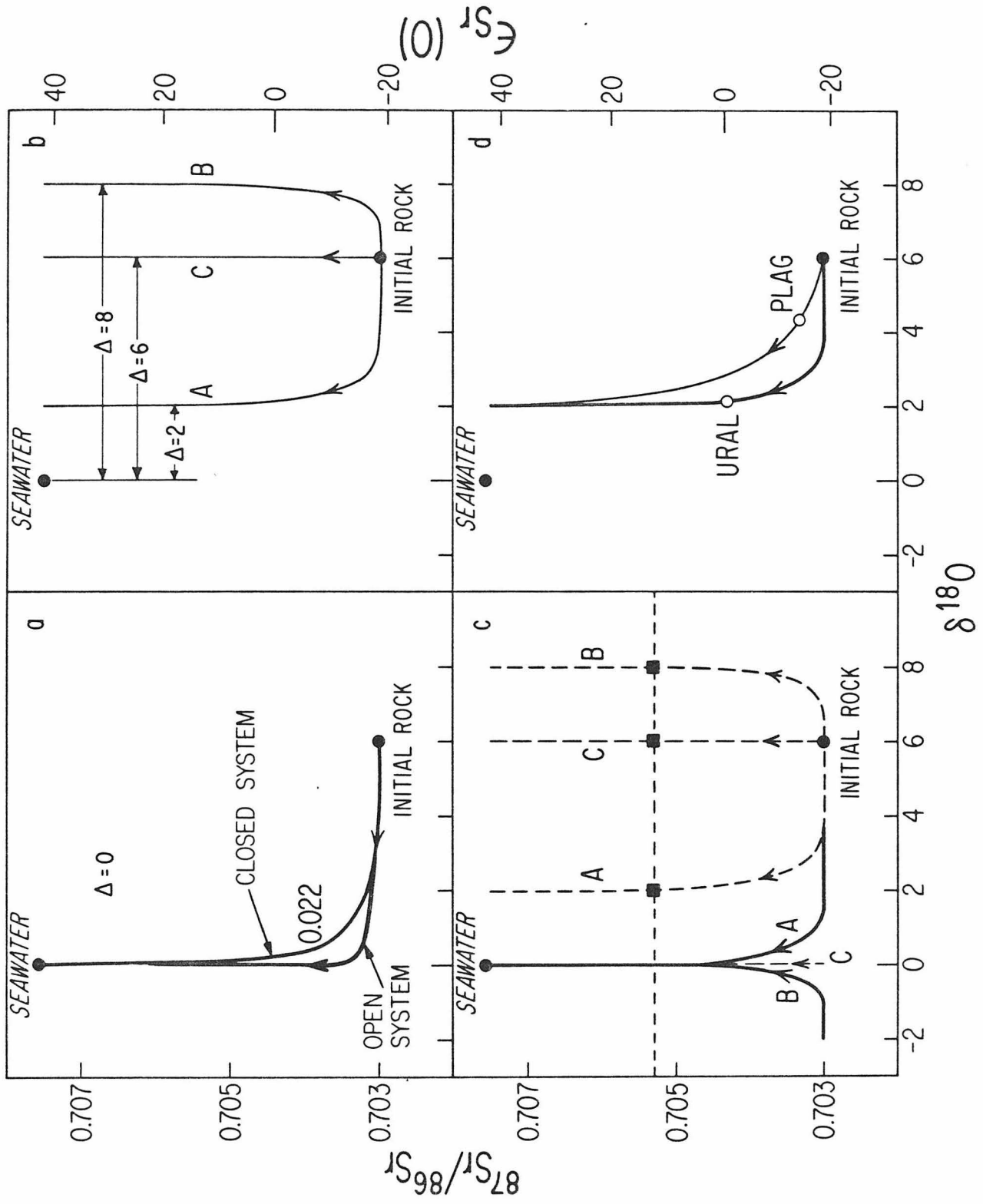
a
b
c
d
SEAWATER
INITIAL ROCK
Δ=0
CLOSED SYSTEM
0.022
OPEN SYSTEM
Δ=8
Δ=6
Δ=2
A
B
C
PLAG
URAL
0.707
0.705
0.703
40
20
0
-20
-2
0
2
4
6
8
$\varepsilon_{Sr}(0)$
$^{87}Sr/^{86}Sr$
$\delta^{18}O$

curvature determined by the constant C. For $q'/q = 1$ and using average concentrations of Sr and O in the rock and seawater, C = 0.022 in both the closed and open system curves shown in Fig. 5-9. Using this arbitrary value of C, the effect of changing the oxygen water-rock fractionation factor from $\Delta = +2$ to $\Delta = +6$ or +8 is shown in Fig. 5-9. The value of Δ depends on the temperature of exchange and is given by equation (2). Thus in an environment with changing exchange temperatures no simple correlation of $\delta^{18}O$ and $^{87}Sr/^{86}Sr$ would be expected. In fact, for $\Delta = 6$ corresponding to a temperature of $\sim 250°C$ there can be changes in $^{87}Sr/^{86}Sr$ without any change in the $\delta^{18}O$ (Fig. 5-9).

For $\Delta \neq 0$ the $\delta^{18}O$ value of the water is different from the $\delta^{18}O$ value of the rock, being related by $\Delta = \delta^{f}_{rock} - \delta^{f}_{water}$. The curves which map the water compositions are shown in Fig. 5-9 for the different Δ values. In Fig. 5-9, for small W/R ratios (< 3) when $\Delta < 6$, the final water which equilibrates with rock will be enriched in $\delta^{18}O$ (i.e., $\delta^{18}O^{final}_{water} > 0$ and for $\Delta > 6$, the water will be depleted. Subsequent interaction of this exchanged water will result in another set of mixing curves. Also, in Fig. 5-9 the $^{87}Sr/^{86}Sr$ value can be used independently to assess the water/rock ratio. Then, either the temperature of equilibration or the final fluid composition can be in principle calculated from equation (8). Using this reasoning on sample G10 (Fig. 5-8) exhibiting a greenschist assemblage suggests that diabase G10 equilibrated with a seawater-derived fluid which had been exchanged and enriched by at least 2‰ over its initial value. Evidence has been found in the diabase dikes for exchange with ^{18}O-enriched water [Gregory and Taylor, 1981], indicating that this water has had a history of high temperature (> 300°C) exchange.

In Fig. 5-9, mixing lines are shown which could account for the

Sr isotopic disequilibrium observed for example between the plagioclase and uralite in the gabbro G224-2. The mixing lines are different for each mineral as they have different Sr concentrations and presumably different exchange rates (i.e., different values of q'/q). As the factor q'/q is unknown, the mixing lines that are shown are arbitrary, but they qualitatively account for the observed $^{87}Sr/^{86}Sr$ and $\delta^{18}O$ values in the minerals of G224-2.

The above calculations were based on a closed system model which assumes continuous recirculation and cyclic re-equilibration of the water with the rock. However, some of the heated water will be lost from the system, for example by escape to the ocean. In the extreme open system case in which each increment of water makes only a single pass through the system, the integrated water/rock ratio is given by the equation from Taylor [1977]:

$$\frac{W}{R}\left(\begin{matrix}\text{open}\\ \text{system}\end{matrix}\right) = \frac{C^i_{rock}}{C^i_{water}} \ln\left[\frac{C^i_{water}}{C^i_{rock}} \frac{W}{R}\left(\begin{matrix}\text{closed}\\ \text{system}\end{matrix}\right) + 1\right] \qquad (9)$$

Water/rock ratios calculated from the Sr data and using both open and closed system models are tabulated in Table 5-3. The W/R ratios are lower in the gabbros than in the upper sequence. In addition, inasmuch as the concentration constant in equation (9) is $<<1$, both the open and the closed system models give similar results (Table 5-3 and Fig. 5-9) except for large values of W/R. However, both of these models only give minimum values of W/R because an appreciable volume of water may move through fractures in the rocks without exchanging.

From this discussion it is apparent that the production of water with $\delta^{18}O > 0$ results from fluid-rock interaction at high temperatures (i.e., with $\Delta < 6$) in an environment with a low water-rock ratio such as in

Table 5-3. Sr water/rock ratios for closed and open systems, Ibra section.

Sample	$\frac{W}{R}$ (open system)	$\frac{W}{R}$ (closed system)
G54	11.6	14.8
G10	14.0	20.2
K1	31.1	43.5
G224-3	3.3	3.6
G224-2	4.2	4.5
K9	0.5	0.5

the gabbro section. This implies that the $\delta^{18}O$ effects in the sheeted dikes were produced by reaction with seawater already enriched in ^{18}O, by exchange with the underlying gabbros at higher temperature as suggested by Gregory and Taylor [1981]. This ^{18}O-shifted fluid would also presumably be shifted in $^{87}Sr/^{86}Sr$ (~ 0.704 indicated by uralite from G224-2) and may not have affected the diabases already enriched in ^{87}Sr during alteration over the ridge axis. As stated above, this implies that there are at least two temperature and spatial regimes where exchange of oxygen and Sr occurs. The first is at the ridge axis above the magma chamber where fluid path lines do not cross the diabase-magma contact. It is in this environment that ^{18}O-depleted rocks and $^{87}Sr/^{86}Sr$ enriched rocks would be produced during reaction and exchange with large volumes of seawater. Subsequently, with continued production of oceanic crust, these rocks are transported away from the ridge into a cooler regime at the distal edges of the magma chamber where interaction between isotopically shifted fluids and the diabases occurs. A high ^{18}O fluid discharges from a second hydrothermal system which operates under the wings of the ridge magma chamber. This fluid imposes an ^{18}O enrichment upon the diabases which masks the earlier ridge-axis oxygen exchange without appreciably affecting the Sr isotope ratios. This "hydrothermal reworking" of oceanic crust may also explain the generally more altered nature of ophiolite pillow basalts and diabases compared to those dredged from ocean ridges.

5.4 SUMMARY

(1) In this study we have established the crystallization age of the Samail ophiolite by obtaining Sm-Nd mineral isochrons from gabbros. The gabbros from the southern part of the ophiolite in Ibra give an age of 128±20 m.y. and 150±40 m.y., while a gabbro from Wadi Fizh in the northern part of Oman gives a somewhat younger age of 100±20 m.y. These results show that the Sm-Nd technique can be used to determine crystallization ages of relatively young mafic rocks.

(2) The initial $^{143}Nd/^{144}Nd$ ratio of gabbros, plagiogranite, diabase dikes, and a basalt from the Samail ophiolite have a narrow range in ε_{Nd} of from 7.5 to 8.6 (Fig. 5-10). This indicates derivation from a relatively uniform reservoir that has been depleted in the LREE for at least a billion years or more. The Samail ophiolite ε_{Nd} values are also within the range expected for Cretaceous MORB, and therefore clearly indicate an oceanic affinity. An oceanic origin is also indicated by the lead isotopic studies of Chen and Pallister [1981].

(3) The tectonized harzburgite has $\varepsilon_{Nd} = 8.3$ which is the same as the overlying cumulate gabbros, sheeted dikes, and pillow basalts. This result, together with its low trace element concentrations, is consistent with the harzburgite being a cogenetic residue from partial melting event which produced the overlying magmatic sequences. However, considering the complexity and heterogeneous character of the peridotite in the Samail ophiolite [Boudier and Coleman, 1981], generalization of this result must await a more complete characterization of the peridotite.

(4) In contrast to the initial $^{143}Nd/^{144}Nd$ ratios, the initial

Figure 5-10. $\delta^{18}O$, ε_{Sr}, and ε_{Nd} values from a composite profile through the Samail ophiolite, Ibra section. The ophiolite section was compiled from the geologic map of Bailey et al. [1981]. The symbol V = pillowed volcanic, SD = sheeted dikes, Pg = plagiogranite, HG = high-level gabbro, G = cumulate gabbro, WG = interlayered wehrlite and gabbro, D = dunite, and H = harzburgite. The plagiogranites and differentiated high-level gabbros are the last intrusive rocks to crystallize. It can be seen that the ε_{Nd} values are in general within error of the primary magmatic value of $\varepsilon_{Nd} = 7.8$. In contrast, the $\delta^{18}O$ [from Gregory and Taylor, 1981] and ε_{Sr} values show large deviations from their primary magmatic values of $\delta^{18}O = 5.7$ and $\varepsilon_{Sr} = -19.5$. These large variations in $\delta^{18}O$ and ε_{Sr} are a consequence of hydrothermal interaction of seawater. The isotopic characteristics of the Samail ophiolite may be similar to those in oceanic crust undergoing subduction in present-day ocean basins.

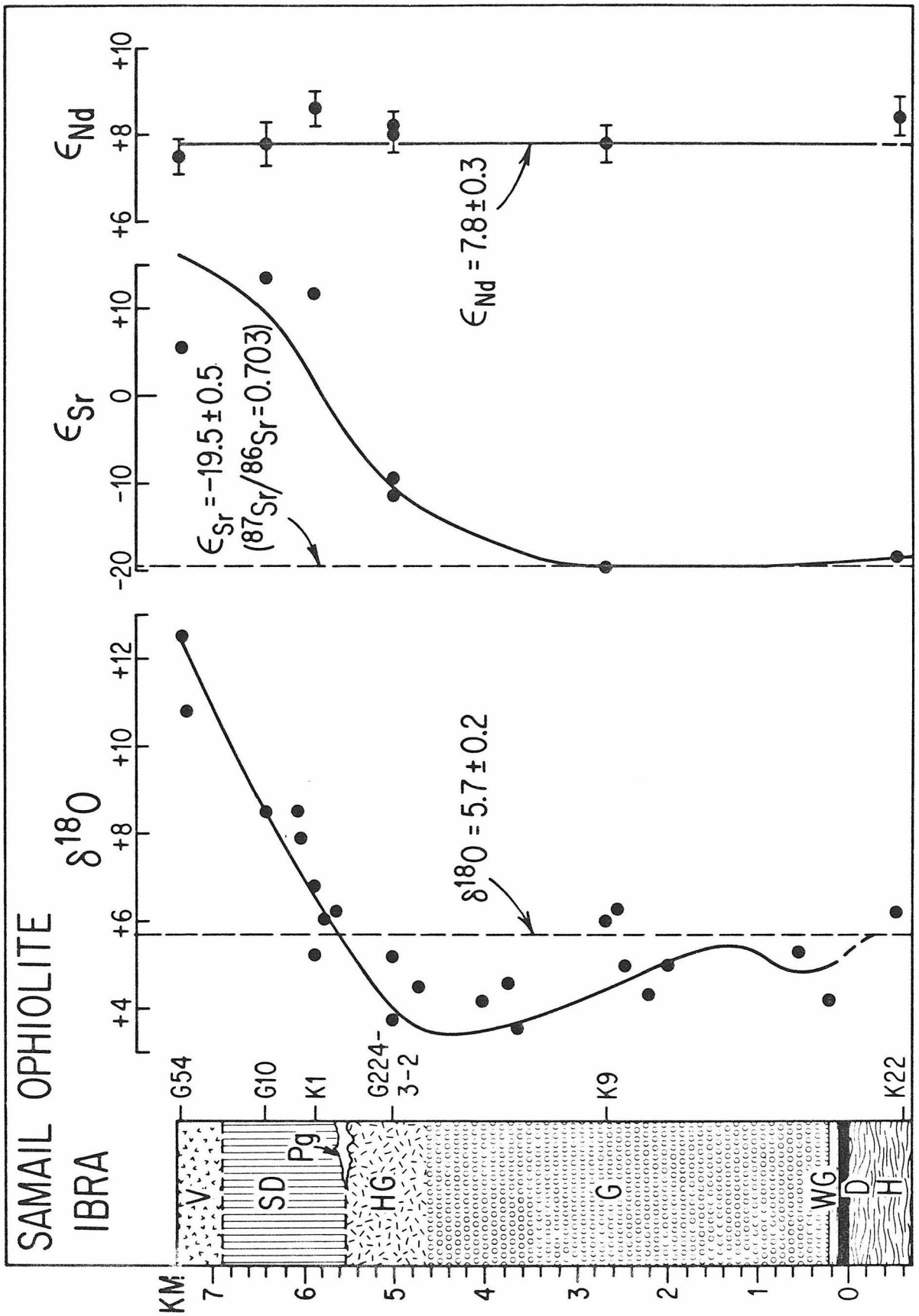
SAMAIL OPHIOLITE
IBRA
KM
7
6
5
4
3
2
1
0
V
SD
Pg
HG
G
WG
D
H
G54
G10
K1
G224-3-2
K9
K22
$\delta^{18}O$
+4
+6
+8
+10
+12
$\delta^{18}O = 5.7 \pm 0.2$
ϵ_{Sr}
-20
-10
0
+10
$\epsilon_{Sr} = -19.5 \pm 0.5$
$(^{87}Sr/^{86}Sr = 0.703)$
ϵ_{Nd}
+6
+8
+10
$\epsilon_{Nd} = 7.8 \pm 0.3$

$^{87}Sr/^{86}Sr$ ratios have an extremely large range of from 0.7030 to 0.7065. This large variation is consistent with hydrothermal interaction of seawater with oceanic crust. In addition, the $^{87}Sr/^{86}Sr$ ratios generally decrease downwards (Fig. 5-10), suggesting downwardly decreasing water/rock ratios. These results indicate extreme caution must be employed before variations in initial $^{87}Sr/^{86}Sr$ ratios of ophiolitic rocks can be attributed to primary magmatic variations. In this study we have in fact found small variations in initial $^{87}Sr/^{86}Sr$ of gabbro plagioclase separates of from 0.70296±2 to 0.70311±5 which we have attributed to primary magmatic variations. However, this interpretation is supported by corresponding variations in the initial $^{143}Nd/^{144}Nd$ ratios and by analysis of coexisting pyroxenes and plagioclases.

(5) The complete ^{18}O profile from Gregory and Taylor [1981] is also shown in Fig. 5-10. With respect to the "normal" value of $\delta^{18}O = 5.7$ there are both ^{18}O-depleted and enriched rocks. The depletions are a result of high temperature hydrothermal alteration whereas the ^{18}O enrichments are due to hydrothermal exchange with either strongly ^{18}O-shifted waters at high temperature or less ^{18}O-shifted waters at much lower temperatures.

(6) In Fig. 5-10, there is approximate linear correlation between high ^{18}O and high $^{87}Sr/^{86}Sr$ ratios above the diabase-gabbro contact. Below this contact, the correlation is approximately inverse, corresponding to depleted ^{18}O and high $^{87}Sr/^{86}Sr$ ratios. These relationships are primarily due to the temperature dependence of the oxygen water-rock interactions. Due to this temperature effect, it has been shown that in general no simple relationship between ^{18}O and $^{87}Sr/^{86}Sr$ variations would be expected for the entire ophiolite section. In fact at the appropriate temperature of hydrothermal interaction with pristine seawater (200-250°C) it is possible to have $^{87}Sr/^{86}Sr$ enrichments

while retaining apparently normal ^{18}O values.

CHAPTER 6

IMPLICATIONS FOR THE OXYGEN ISOTOPIC HISTORY OF THE OCEANS

6.1 AVERAGE $\delta^{18}O$ VALUE OF A SECTION THROUGH THE OCEANIC CRUST

The completeness of the Ibra section, together with the consistency of the geology and the relative simplicity of the mineralogic and isotopic alteration patterns, makes the Samail ophiolite an ideal place to calculate the average $\delta^{18}O$ value of mature, altered oceanic crust. For this purpose, we have combined the Wadi Kadir and Wadi Saq sections. Inasmuch as the pillow lavas are not very well represented in the Ibra section, we also have added analyses of three samples from Wadi Jizi, where pillowed volcanic rocks are abundant. All these data are plotted on Fig. 6-1. For a few of the coarser-grained gabbro samples, the whole-rock $\delta^{18}O$ values plotted on Fig. 6-1 were calculated by material-balance from the modes and the mineral $\delta^{18}O$ values.

The pillow lavas ($\delta^{18}O$ = +12.7 at Ibra; +10.7 to +12.5 at Wadi Jizi) are the most poorly characterized portion of the Ibra section, but this is also volumetrically the smallest unit (<10% of the total column), and thus the least critical in the overall material-balance calculation. Also, it should be noted that many pillow lavas have been analyzed from other ophiolites and they consistently define a range of about +10 to +14 [Heaton and Sheppard, 1977; Magaritz and Taylor, 1976a; Spooner et al., 1974].

When a $\delta^{18}O$ integration (material-balance calculation) is done for the entire Ibra section, it is seen that the contribution of ^{18}O-depleted rocks in the lower sequence do indeed almost exactly cancel out the contribution of the ^{18}O-enriched rocks in the upper sequence, thus strongly supporting the Muehlenbachs-Clayton hypothesis

Figure 6-1. Material-balance calculation for the generalized $\delta^{18}O$ profile displayed by the Ibra section (solid curve fitted to the data by inspection), based on the combined Wadi Saq and Wadi Kadir traverses. Data-points are all whole-rock values; samples exhibiting anomalous $\delta^{18}O$ at a single outcrop such as plagiogranite dikes and hornblende pegmatite segregations cutting massive gabbro (OMG 65-66), and samples adjacent to veins are volumetrically insignificant and thus were not used in this calculation. Samples from Wadi Kadir that lie above the 2 km level are labeled and added to the diagram approximately at their correct stratigraphic positions, assuming that the gabbro sections were initially the same thickness, measuring downward from the diabase-gabbro contact. The stippled areas shown in the diagram are equal in size, and the average $\delta^{18}O$ of this section of altered oceanic crust is 5.8 ± 0.3.

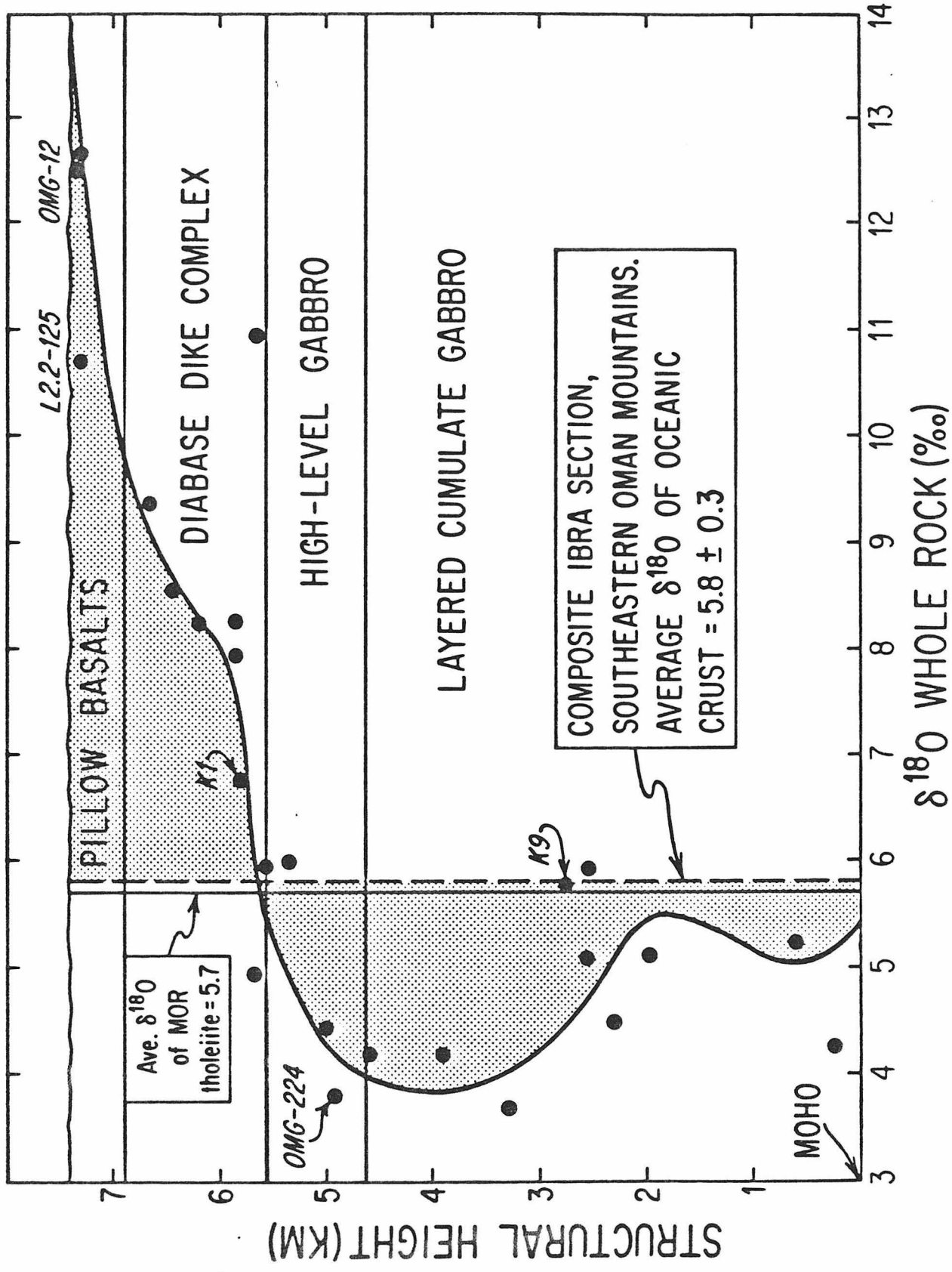
PILLOW BASALTS
DIABASE DIKE COMPLEX
HIGH-LEVEL GABBRO
LAYERED CUMULATE GABBRO
L2.2-125
OMG-12
K1
K9
OMG-224
MOHO
Ave. δ18O of MOR tholeiite = 5.7
COMPOSITE IBRA SECTION, SOUTHEASTERN OMAN MOUNTAINS. AVERAGE δ18O OF OCEANIC CRUST = 5.8 ± 0.3
STRUCTURAL HEIGHT (KM)
δ18O WHOLE ROCK (‰)
1
2
3
4
5
6
7
3
4
5
6
7
8
9
10
11
12
13
14

FIGURE 6-1

(Fig. 6-1). The net change in ^{18}O content of the entire oceanic crust produced by the long history of hydrothermal alteration and isotopic aging of the Ibra section appears to be essentially zero. Our calculated average $\delta^{18}O = 5.8 \pm 0.3$ is, within experimental and geologic error, identical to the average $\delta^{18}O$ of MOR basalts (+5.7), which is accepted to be the primary magmatic $^{18}O/^{16}O$ ratio of the oceanic crust, as well as the overall Earth-Moon system [Muehlenbachs and Clayton, 1972; Taylor, 1968; Taylor and Epstein, 1970].

If there has been no net change in $\delta^{18}O$ of the oceanic crust, there obviously cannot have been any net ^{18}O flux either into or out of seawater as a result of interactions at MOR spreading centers. If we extrapolate the relationship discovered in the Samail ophiolite to all oceanic spreading centers, it is clear that seawater must have been in steady-state isotopic balance, with a $\delta^{18}O$ close to zero during the Cretaceous. However, it is instructive to inquire in more detail exactly what was the buffered $\delta^{18}O$ value of Cretaceous seawater? The overall, average, steady-state $\Delta^{18}O$ fractionation between oceanic crust and seawater is defined as $\Delta = +5.7 - \delta^{18}O_{SW}$, where $\delta^{18}O_{SW}$ is the buffered value of (Cretaceous) seawater.

The <u>exact</u> $\delta^{18}O$ value of Cretaceous seawater is not known, but we can place certain limits upon it. The Cretaceous is widely thought to represent a time period when there was little or no continental glaciation on Earth [Steiner and Grillman, 1973]. We know that rapid melting of all of the present-day ice sheets, which have an average $\delta^{18}O$ of about -35, would only lower the $\delta^{18}O$ value of seawater by about 0.3 to 0.9 per mil [Dansgaard and Tauber, 1969], and certainly by no more than 1.5 per mil. However, because of the cycling of seawater

through the oceanic crust, it is obvious that we cannot calculate the $\delta^{18}O$ of Cretaceous seawater in this simple fashion, as the following discussion will demonstrate.

6.2 Calculation of $^{18}O/^{16}O$ Mass-Balance During Cycling of Seawater through the Oceanic Crust

Inasmuch as we are only concerned with ^{18}O balance, in the following discussion, all mass units or amounts are given in grams of oxygen:

W = mass of the oceans.

R = spreading rate in km^2/year, roughly equivalent to half-spreading rates in cm/yr for the present-day mid-ocean ridge systems.

cR = mass of oceanic crust created and matured each year (eventually almost all of this is subducted); c is a constant determined by the depth of exchange in the oceanic crust, and by the need to convert spreading rates to grams of oxygen.

w = total amount of water that circulates through and exchanges with the oceanic crust to achieve maturity ($= \int_0^{t_m} \bar{w}\, dt$, where $\bar{w}$ is the average amount of water circulated per unit time, and t_m is the time taken to reach maturity or a steady-state profile).

r = total amount of new oceanic crust that exchanged with w amount of seawater $= \int_0^{t_m} \bar{r}\, dt$, where $\bar{r}$ is the amount of rock exchanged with w per unit time; if unit time is expressed in years, $\bar{r} = cR$.

ϕ = w/r, the actual water/rock ratio in oxygen units for the ridge system.

δW = the $\delta^{18}O$ of the oceans (assumed to be well-mixed).

δrock final = δ_{rf} = the final average $\delta^{18}O$ of the mature oceanic crust as it is subducted.

δrock initial = δ_{ri} = +5.7 = $\delta^{18}O_{MORB}$.

δwater final = δ_{wf} = $\delta^{18}O$ value of water that has actually circulated through the oceanic crust and discharged back into the oceans, neglecting H_2O added to the crust by hydration reactions.

Δ ^{18}O crust-seawater $\equiv \delta r_i - \delta^{18}O_{SW}$ (steady-state) $\equiv \Delta$.

Assuming conservation of mass, one may readily derive the following expression which relates the change in ^{18}O content of the oceans to the amount of water circulated through the oceanic spreading centers, and to the ^{18}O change in that fluid as a result of its exchange with the oceanic crust:

(1) $W\, d(\delta W) = (\delta_{wf} - \delta W)\, dw = -(\delta_{rf} - \delta_{ri})\, \bar{r}\, dt$

Using the closed-system water-rock equation [Taylor, 1971], we can solve for δw_f:

$$w/r = \phi = \frac{\delta_{rf} - \delta_{ri}}{\delta W - \delta_{wf}} \quad ; \quad \delta_{rf} = \Delta + \delta_{wf}$$

$$(2)\quad \delta_{wf} = \frac{\phi\, \delta W - \Delta + \delta_{ri}}{\phi + 1} \quad ; \text{ also } \delta_{rf} = \frac{\phi\, \delta W + \phi\, \Delta + \delta_{ri}}{\phi + 1}$$

By substitution, equation 1 becomes

$$(3)\quad W\, d\,(\delta W) = \frac{-\Delta + \delta_{ri} - \delta W}{\phi + 1} \qquad dw = \frac{\phi\,(-\Delta + \delta_{ri} - \delta W)\, r\, dt}{\phi + 1}$$

Rearranging terms

$$(4) \qquad \frac{d\,(\delta W)}{\delta W + \Delta - \delta_{ri}} = - \frac{dw}{W\,(\phi+1)} = - \frac{\phi\,\bar{r}\,t}{W\,(\phi+1)}$$

Integration of equation (4) with ϕ held constant yields:

$$(5) \qquad \ln \left[\frac{\delta W + \Delta - \delta_{ri}}{\delta W_o + \delta - \delta_{ri}}\right] = \frac{-w}{W\,(\phi + 1)} = \frac{-\phi\,\bar{r}\,t}{w\,(\phi + 1)}$$

where δW_o equals the initial $\delta^{18}O$ value of seawater either (1) before any sea-floor spreading begins, or directly after any instantaneous excursion in the $\delta^{18}O$ of the oceans from its steady-state (buffered) value. In equation 5, note that the time, t (in years), is implicit in w, as $w = \phi r = \phi Rct$ where R is the spreading rate in km^2/yr and c is a conversion constant derived from setting a particular value for the depth of exchange (conservatively taken to be 6 km); this equation converts km^3 of rock into grams of oxygen. Exponentiating (5) and substituting ϕRct for w we obtain:

$$(6) \qquad \delta W = (\delta W_o + \Delta - \delta_{ri}) \exp\left[-\left(\frac{\phi}{\phi + 1}\right)\frac{Rct}{W}\right] + (\delta_{ri} - \Delta)$$

where $\delta_{ri} - \Delta \equiv$ the steady-state buffered $\delta^{18}O$ value of seawater. If Δ is exactly +5.7, then the buffered value of seawater is its present-day value, $\delta\,^{18}O_{SW} \equiv 0$, and equation (6) becomes:

$$(6a) \qquad \delta W = \delta W_o \exp\left[-\left(\frac{\phi}{\phi+1}\right)\frac{Rct}{W}\right]$$

A result similar to that given above can be derived in a different manner by again considering the closed-system water/rock equation for very large water/rock ratios (large ϕ values):

$$(7) \quad \frac{W}{cR} = \frac{\delta_{rf} - 5.7}{\delta W_o - \delta W_f}$$

Inasmuch as the mass of the oceans greatly exceeds the mass of rock created in a single year, if we set $\Delta = 5.7$, we have $\delta_{rf} = 5.7 + \delta W_f \approx 5.7 + \delta W_o$. Then the closed-system water/rock equation becomes

$$(8) \quad \delta W_1 = \delta W_o \, (1 - cR/W)$$

which describes the change in the initial $\delta W_o \neq 0$ seawater after one year's worth of aging.

After two years:

$$(9a) \quad \delta W_2 = \delta W_1 \, (1 - cR/W)$$
$$= \delta W_o \, (1 - cR/W)^2.$$

For N years the equation becomes

$$(9b) \quad \delta W_N = \delta W_o \, (1 - cR/W)^N.$$

Remembering that R is the spreading rate in years, we can perform the calculation as many times (n) per year as we wish:

$$(10) \quad \delta W_f = \delta W_o \, (1 - cR/nW)^{nt}$$

with t in years. As $n \to \infty$ this becomes

$$(11)\quad \delta W = \delta W_o \exp\left[-\frac{cRt}{W}\right]$$

which is exactly the same equation (6a) for large ϕ. This represents the fastest rate at which seawater can be brought down to a steady-state value of zero.

In Fig. 6-2, we plot equation (6) for various spreading rates assuming $\Delta = 5.7$, which is the same as assuming a $\delta^{18}O_{SW} = 0$ for the steady-state value. The shaded area represents the average spreading rate for the last 20 m.y. [Berger and Winterer, 1974] for two different values of the water/rock ratio ($\phi = 1$ or 20). The $\phi = 20$ curve represents a plausible maximum water/rock ratio for the mid-ocean ridge systems, as deduced from heat-flow arguments and conservation of energy [Wolery and Sleep, 1976]. The $\phi = 1$ curve is probably close to the slowest plausible decay rate, assuming a simple, one-pulse injection of basaltic magma analogous to the Skaergaard hydrothermal system, where the overall water/rock ratio was about 0.5 to 1.5 [Norton and Taylor, 1979]. The other trajectories on Fig. 6-2 represent transient decay for various assumed spreading rates, remembering that for today's oceans, km^2 spreading rates are roughly equivalent to half spreading rates in cm/year. A rate of 12 km^2/year is used as the most plausible upper limit on the spreading rate; rates this fast have been proposed on some ridge segments during the middle Cretaceous for the period 85-115 m.y. b.p. [Larson and Pitman, 1972]. Such a rate is based upon extrapolating rates determined on small segments of preserved sea-floor to the entire ridge system, as well as assuming that the overall length is equivalent to the present-day value; thus 12 km^2/yr may be

Figure 6-2. Seawater isotopic evolution diagram, showing the effect of the length of time after spreading begins (t, in years) on the $\delta^{18}O$ of seawater. These curves also apply equally well to rapid perturbations or excursions in the $\delta^{18}O$ of seawater, holding world-wide spreading rates constant. ϕ is the w/r ratio (in oxygen units) for the bulk system, deduced from heat-flow arguments, and 12 km^2/yr is chosen as a plausible upper limit for spreading rates. Although the latter rate has been proposed for some portions of Cretaceous ocean floor, extrapolation of such high rates to a world-wide rate is very controversial [Baldwin, et al., 1974]. However, a rate approaching this magnitude conceivably could apply to the Archean.

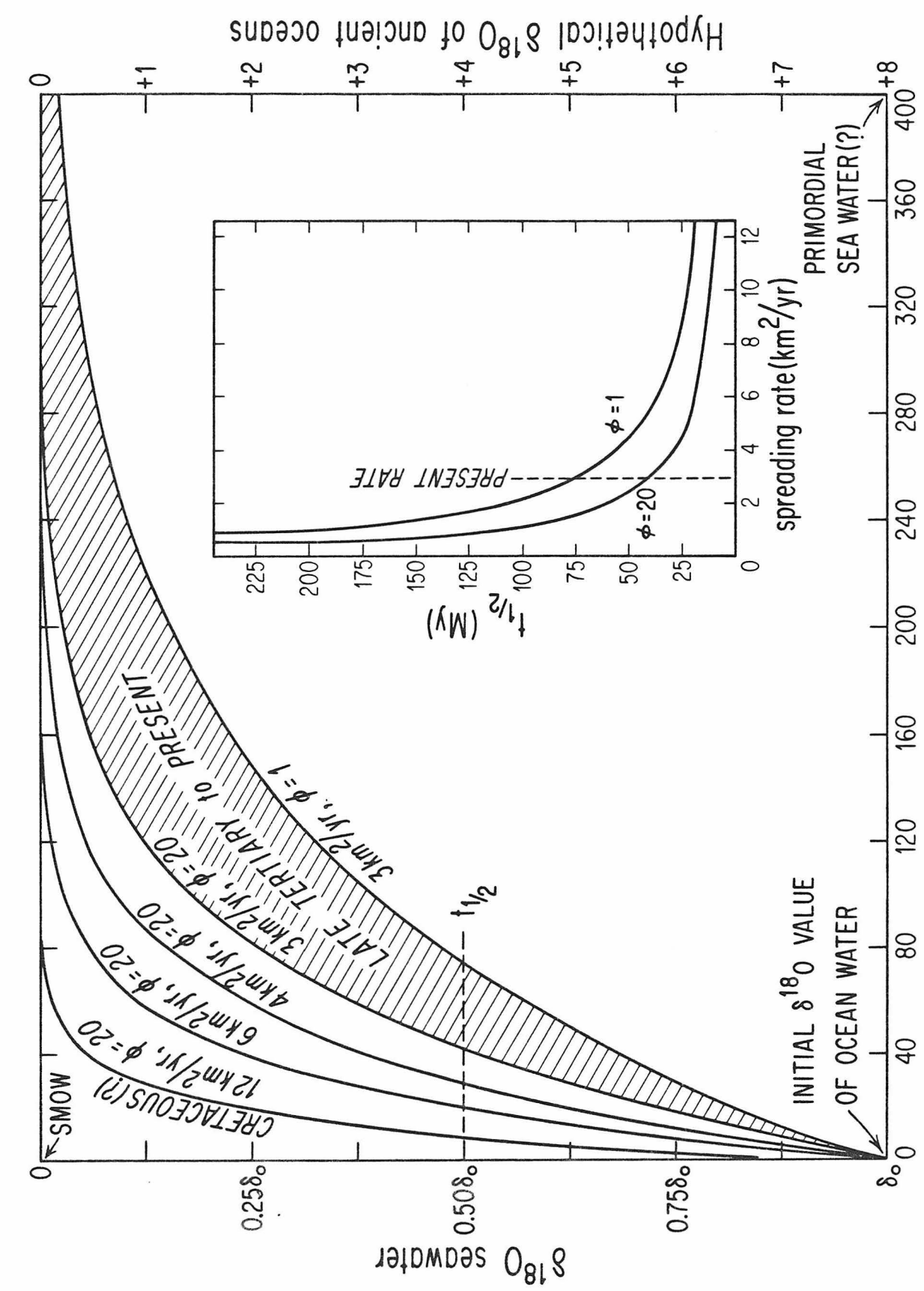
δ18O seawater
0
0.25δo
0.50δo
0.75δo
δo
SMOW
CRETACEOUS(?)
12km2/yr, φ=20
6km2/yr, φ=20
4km2/yr, φ=20
3km2/yr, φ=20
LATE TERTIARY to PRESENT
3km2/yr, φ=1
t1/2
INITIAL δ18O VALUE
OF OCEAN WATER
0
40
80
120
160
200
240
280
320
360
400
time after onset of spreading (My)
Hypothetical δ18O of ancient oceans
0
+1
+2
+3
+4
+5
+6
+7
+8
PRIMORDIAL
SEA WATER(?)
t1/2 (My)
225
200
175
150
125
100
75
50
25
0
2
4
6
8
10
12
spreading rate(km2/yr)
φ=1
φ=20
PRESENT RATE

too high for any reasonable Phanerozoic worldwide rate [Baldwin et al., 1974; Berger and Winterer, 1974].

In order to understand how increasing the spreading rate affects the buffering system, we use a plot of spreading rate vs. $t_{1/2}$, the time it takes for seawater to move half-way from its initial $\delta^{18}O$ value toward its final steady-state $\delta^{18}O$ value. In the insert of Fig. 6-2, the $\phi = 1$ and $\phi = 20$ values bracket the geologically reasonable water/rock ratios for the overall system. If the spreading ratio drops below about 1 to 1.5 km^2/year then the buffering process would break down, and hydrothermal circulation no longer would buffer seawater. Increasing the spreading rate beyond 4-5 km^2/year (or keeping the linear, half-spreading rate constant, while increasing the number of plates) does not appreciably affect the $t_{1/2}$ value.

6.3 The Steady-State (Buffered) $\delta^{18}O$ Value of the Oceans

Using the model described above, we can now make some estimates of the true steady-state $\delta^{18}O$ value of the oceans, and also estimate the average value of Δ for the seawater-crust system. The biggest obstacle in exactly determining these values is the transient effect that late Cenozoic glaciation has had upon the $\delta^{18}O$ contents of seawater. The Pleistocene paleotemperature curves of Emiliani [1966] are interpreted as a combination of temperature effects and isotopic shifts in seawater due to ice storage on the continents [Dansgaard and Tauber, 1969]. From Emiliani's data, the present-day interglacial seawater isotopic composition reflects a minimum value of ice storage for the Pleistocene. During this glacial minimum, Antarctica remained covered by ice. The magnitude of the ^{18}O-shift due to ice storage in Antarctica, and the duration of the glaciation, become the deciding

factors in determining the value of Δ at times when the Earth lacked any continental ice sheets. Estimates of the ^{18}O change in the oceans due to instantaneous Antarctic ice sheet formation are about $+0.53 \pm 0.26$, based on volume estimates of 15 to 30 x 10^6 km^3 of ice having an average $\delta^{18}O$ of -33 ± 4 [Denton et al., 1971; Dansgaard and Tauber, 1969]. This large range of estimates of ice volume and $\delta^{18}O$ compositions comes about because, during the Cenozoic, geologic evidence [Hollister et al., 1976; Hayes et al., 1975; Denton et al., 1971; Barker et al., 1976] for glaciation in Antarctica only suggests when ice sheets were present but does not record volumes. Deep Sea Drilling Project data [Hollister et al., 1976] and other studies [Denton et al., 1971] suggest that although minor glaciation occurred as early as the Eocene, the Antarctic continental ice sheet did not develop until the late Oligocene to middle Miocene, and did not reach its present extent until late Miocene. These time constraints, together with the water/rock (ϕ) limits, fix the exponential factor in equation (6) at 0.76 ± 0.11 for worldwide spreading at 3 km^2/yr for the last 20 m.y. [Berger and Winterer, 1974]. Plugging this value into equation (6) we have:

$$\delta^{18}O^{today}_{seawater} = \delta^{18}O_{SMOW} = 0 = (0.53 \pm 0.26)\ (0.76 \pm 0.11) + (5.7 \pm 0.2) - \Delta.$$

Hence, $\Delta = 6.1 \pm 0.3$

and at steady state the $\delta^{18}O_{seawater} = -0.40 \pm 0.3$.

The above values represent our best estimates of these important parameters based on available information. Note, however, that the value of Δ conceivably could have been different from 6.1, if at certain time periods plate tectonic regimes were markedly different from the

Phanerozoic (i.e the Archean?). Considering another case, if the Antarctic ice sheets have existed since late Eocene, then $\Delta \approx 6.0$ and $\delta^{18}O^{\text{steady-state}}_{\text{seawater}} = -0.3$. Neither this value nor the above value of -0.4 is markedly different from the value of -0.53 ± 0.26 that would be obtained by simply adding back to the oceans all of the present-day ice on Earth. The point of the calculation is that the present-day $\delta^{18}O$ value of zero for mean ocean water is clearly not the steady-state value. Also, simply melting all of the ice sheets and taking into account the $^{18}O/^{16}O$ effect of transferring that water back into the oceans will not necessarily give the true steady-state $\delta^{18}O$ value (depending upon the duration of the glaciation). Note that it makes no difference to the buffered $\delta^{18}O$ value of ocean water whether or not the ice sheets are totally absent or even more abundant by a factor of 100 than they are today; the only consideration is whether they are waxing or waning on a scale of less than a few tens of millions of years. Because of the uncertainties in duration and particularly the magnitude of the Antarctic continental glaciation, the type of analysis outlined above probably cannot deduce the true steady-state $\delta^{18}O$ value of ocean water to better than $\pm$ 0.3 per mil. This is unfortunate as the uncertainty in seawater composition also limits the ultimate resolution of paleotemperature techniques to $\approx$ 3°C for the Mesozoic (ignoring other problems such as preservation of the isotopic record during diagenesis).

6.4 The Significance of Δ, and the $\delta^{18}O$ of Precambrian Oceans

The quantity Δ represents the average ^{18}O fractionation between oceanic crust and seawater. It therefore basically reflects a

weighted-average temperature of alteration of the entire section of oceanic crust, and thus is related to the difference between the ambient temperature of seawater and the liquidus temperatures of the MOR magmas. The final $\delta^{18}O$ profile in the crust, which fixes the value of Δ, probably depends to a lesser extent on a number of other factors, including the geometry of the MOR magma chambers, kinetic effects, and the rates of convective circulation. However, as long as T_{magmas} and $T_{seawater}$ are fixed, and new crust is created by simple sea floor spreading (i.e., a ridge-axis magma chamber capped by a roof of sheeted diabase and pillow lavas), then Δ should also remain essentially fixed.

The existence of ophiolites with similar structure and stratigraphy throughout the Phanerozoic [Coleman, 1977] supports the idea that oceanic crust was created by practically identical processes throughout the last 0.6 AE. Preliminary evidence from the Canyon Mountain ophiolite (Permian), $4.7 < \delta^{18}O_{\text{whole-rock}} < 11.0$, and the Bay of Islands ophiolite (Cambro-Ordovician), $4.5 < \delta^{18}O_{\text{whole-rock}} < 10.9$ [Gregory, unpublished data], compared to the more extensive data-set reported here from Oman ($3.8 < \delta^{18}O_{\text{whole-rock}} < 12.7$), clearly indicates that the Paleozoic Δ value must have been very similar to the Cretaceous value, and thus that seawater has been within ± 1 of its steady-state value at least as far back as the Cambrian. Ophiolites and/or ophiolite-like rocks of late Proterozoic age have been reported from China [Xuchang, 1979] and the Red Sea region [Engel et al., 1978], suggesting that this statement is also probably valid as far back as 1.0 - 1.5 AE. However, in the ancient Precambrian record there are no reported ophiolites or preserved slices of modern types of oceanic crust.

Perry et al., [1978] have proposed that MOR hydrothermal circulation was not as important in the Precambrian as it is today. These conclusions are not reasonable in light of the evidence for deep circulation in the present study. During the early Precambrian, there was a great deal more heat production from radioactive decay, as well as more volcanism, indicating that overall heat loss to the world ocean was greater than at present, either as a result of faster spreading or because there was a much larger number of plates [McKenzie and Weiss, 1975]. Given our knowledge of the permeabilities of recently erupted volcanic piles [Norton and Taylor, 1979], it is certain that convective circulation of surface waters would have occurred on a large scale. However, because of possible differences in style of spreading, it is less certain exactly what the values of Δ and $\delta^{18}O_{SW}$ were during the early Precambrian.

Isotopic data from Precambrian cherts [Perry, et al., 1978; Knauth and Epstein, 1976; Yeh and Epstein, 1978] establish an upper limit for Archean ocean temperatures at less than 75-90°C. Atmosphere models for the Precambrian [Sagen and Mullen, 1972] independently suggest that surface temperatures would not have been drastically higher than present-day temperatures. Volcanic rocks preserved in the Archean greenstone belts range from komatiites to rhyolites, with tholeiitic basalt as the predominant rock type [Naldrett and Goodwin, 1977]. This implies that the temperature difference between ocean water and submarine magmas during formation of the Archean oceanic crust should have been within ± 50 to 100°C of the present-day value (which is about 1100°C). If true, this would require that both the average temperature and the average temperature range (but not the gradient!)

within the hydrothermally altered oceanic crust be almost identical to the present-day value. Irrespective of the thickness of that crust, the proportions of low-T and high-T alteration assemblages thus ought to be constant, as long as seawater circulates downward to within close proximity of the submarine magma chambers. However, because of overall higher temperatures that might have prevailed during hydrosphere-crust interaction in the Archean, there probably would have been less ^{18}O enrichment in the upper portion of the oceanic crust than at present (and thus there would also have to have been a concomitant smaller volume of ^{18}O-depleted rocks in the deeper parts of the oceanic crust). These effects taken together would produce a smaller Δ -value. Nevertheless, Δ would have to be either very close to the present-day value or only slightly lower ($\Delta \approx 5$?), implying that ocean water probably had a constant $\delta^{18}O$ value of about -1.0 to +1.0 during almost all of Earth's history.

In support of the above conclusion, ^{18}O evidence and alteration mineral assemblages from the Archean Abitibi greenstone belt (Beaty and Taylor, 1979) suggest that the seawater that interacted with the Archean pillow lavas had $\delta^{18}O = 0 \pm 2$. Studies of granitic rocks that were isotopically exchanged with Precambrian meteoric-hydrothermal fluids at 1.4 to 1.5 AE (St. Francois Mtns. [Wenner and Taylor, 1976]) and at 2.6 to 3.3 AE (Swaziland and Barberton areas, South Africa [Taylor and Magaritz, 1975]) suggest that Precambrian meteoric waters (and thus by inference the Precambrian oceans, as well) also had $\delta^{18}O$ values similar to those of the present day.

The above interpretation, suggesting relative constancy of the $\delta^{18}O$ of seawater, is in conflict with the conclusions of Perry

and Chase [1972] and Perry et al. (Case 1, their Fig. 4 [1978]). These workers proposed that the $\delta^{18}O$ content of the oceans has steadily increased since ≈ 2.5 AE. However, their hypothesis is not valid because they dismissed the effects of deep, high-T, hydrothermal convective circulation at spreading centers.

CHAPTER 7

CONCLUSIONS

The results of this thesis are relevant to a wide variety of problems associated with the origin of the oceanic crust. Two classes of problems have been discussed: 1) problems which relate to the formation of the oceanic crust in terms of the characteristics of primary melts, structure of the oceanic crust, isotopic constraints on the origin of the plutonic section, and evidence for modification of the primary melts by shallow-level crustal and upper mantle processes, and 2) problems which relate to seafloor hydrothermal alteration in terms of depth of circulation within the oceanic crust, temperature and water/rock regimes in different parts of the crust, the effect of hydrothermal exchange with the oceanic crust on the $\delta^{18}O$ composition of seawater, and the final isotopic profile imposed upon the oceanic crust as the result of oxygen and strontium exchange between circulating seawater and rock.

The major conclusion coming out of the Samail ophiolite with respect to the nature of the primary source of MORB is that no melt reached the seafloor unfractionated. This suggests that it is unlikely that any MORB represents a primary unfractionated melt of the upper mantle, in agreement with the conclusions of O'Hara [1968], Green et al. [1979], and Stolper [1980]. Furthermore, crosscutting relations within the Samail peridotite suggest that the primary melt can be related to the MORB cluster [Walker et al. 1979] by some combination of picritic liquid, olivine, and orthopyroxene. At the depth of the present-day exposure, these primary melts are not cogenetic with the upper mantle harzburgite, inasmuch as the oceanic crustal rocks are not saturated with enstatite. Thus, the field data suggest that melt separation occurred at depths greater than 6 kb. Phase diagram analysis of possible fractional crystallization-assimilation

paths of the ascending melts indicate that primary melts may have separated from the mantle over a wide range of pressures. Nd and Sr isotopic evidence (chapter 5) suggest that at depths greater than 6 kb, the tectonite harzburgite could have been the residue of the partial melting event that produced the overlying oceanic crust. However this inference is based upon a single isotopic determination on the Samail harzburgite, and thus, is preliminary. This conclusion must be further tested in light of the results of chapter 3 which suggest that the Samail harzburgite may have suffered interaction with the ascending melts in a regime of melt/rock ratio of 0.3-0.5. In such a situation, exchange between harzburgite and melt may have obscured any primary isotopic relationships.

Mineral $\delta^{18}O$ data from the plutonic section indicate that the primary ^{18}O reservoir of the gabbroic rocks and by inference the basaltic section was very uniform in $\delta^{18}O$ coming from a reservoir ≈ 5.7. In contrast, the ^{18}O reservoir from which the high-level gabbro and plagiogranites crystallized was contaminated with a hydrothermally altered component introduced into the magma chamber by roof-rock assimilation. The ^{18}O data suggest that the crustal magma chamber was zoned in ^{18}O. This may be analogous (on a different scale) to the zoning postulated for magma chambers associated with bimodal volcanism in extensional tectonic environments [Hildreth,1980]. The differentiated low-^{18}O roof zone of the Samail gabbro section usually represents less than 10 percent of the total plutonic section, and apparently the contamination occurring in this thin roof-zone was not transmitted to the underlying more mafic magma.

Mineral $\delta^{18}O$ data from the layered gabbro (pyroxene-plagioclase), the plagiogranite (quartz-feldspar), and the high-level gabbro (amphibole-

plagioclase) indicate that pervasive subsolidus exchange with a seawater-derived hydrothermal fluid occurred throughout the plutonic section all the way down to the Moho. The pyroxene-plagioclase pairs from the layered gabbro monitor the deeper levels of the crustal hydrothermal system and indicate that the hydrothermal exchange in the layered gabbro was analogous to that of the Skaergaard intrusion [Taylor and Forester,1979; Norton and Taylor, 1979]. Water/rock ratios in the layered gabbros were less than 0.5 and temperature of exchange was high ($T>500°C$). Modeling of the mineral-pair $\delta^{18}O$ indicates that this deep, oceanic crustal, hydrothermal system was: 1) an open system with no recycling of hydrothermal fluid or where each water packet passes through the system once, and 2) involved fluids that were initially isotopically similar to seawater.

The plagiogranite because of its position at the gabbro-diabase contact, monitors the $\delta^{18}O$ composition of the fluids escaping from the lower hydrothermal system operating in the gabbro. Two major conclusions come from the plagiogranite quartz-feldspar pairs: 1) the fluids discharging from the lower hydrothermal system were strongly enriched in $\delta^{18}O$ relative to pristine seawater, and 2) the plagiogranite crystallized from a heterogenous reservoir of $\delta^{18}O$ (generally depleted in ^{18}O relative to 5.7), and which implies the existence of a separate hydrothermal system operating over the roof of the magma chamber. This second upper system resulted in ^{18}O-depleted diabases, some of which were stoped into the magma chamber. The record of the stoping events is reflected in the primary isotopic compositon of the plagiogranite. As spreading progressed, the hydrothermally altered diabases ($\delta^{18}O<5.7$) interacted with fluid discharging from the gabbro section. This high-^{18}O fluid imposed the

final, ^{18}O-enriched ($\delta^{18}O > 5.7$) signature upon the diabase dike complex, generally obliterating the record of the upper hydrothermal system.

In chapters 3 and 4, a cartoon reconstruction of the MOR magma chamber was presented which plausibly, but not uniquely accounts for the petrologic and ^{18}O data. This cartoon represents a simplified attempt at reconstructing the events occurring at a ridge-axis, and does not take into account some factors which may considerably complicate the picture such as: 1) possible picritic magma chambers sitting below the Moho which can be inferred from the existence of the large dunite bodies both as trails extending down into the peridotite and as concentrations below the petrologic Moho [Bailey et al. 1981], 2) possible interfingering multiple chambers inferred from sills of crosscutting dunite at all levels within the plutonic section, and 3) possible stacked chambers such as a gabbroic crustal chamber separated from a subcrustal picritic chamber by layers of solidified cumulates as inferred by the existence of discontinous gabbroic breccia zones at the base of the crust formed when these chambers merge. Future work in Oman may eludicate the nature of some of these complicating factors.

Finally, the new data presented in this thesis allows for the first field test of the Muehlenbachs and Clayton hypothesis that hydrothermal circulation at midocean ridges buffers the $\delta^{18}O$ composition of seawater at its present-day composition. The results of the Oman work strongly support the buffering hypothesis. Mass balance calculations using the new parameters determined in this work suggest that the $\delta^{18}O$ of seawater will be within 1 per mil of the steady-state value of -0.4 ± 0.3 as long as world-wide spreading rates exceed 1 km^2/yr.

REFERENCES

Alabaster, T., J.A. Pearce, and I. Elboushi, The volcanic stratigraphy and location of massive sulfide deposits in the Oman Ophiolite, International Ophiolite symposium, Nicosia, Cyprus [in press].

Aldiss, D.T., Granitic rocks of ophiolites, Ph.D. thesis, the Open University, 1978.

Allegre, C.J., J. Montigny, and Y. Bottinga, Cortege ophiolitique et cortege oceanique, geochimie comparee et mode degenese, Bull. Soc. Geol. France, 15, 471-477, 1973.

Alleman, F. and T. Peters, The ophiolite-radiolarite belt of the North Oman Mountains, Ecolage. geol. Helv., 65, 657-697, 1972.

Anderson, A.T., R.N. Clayton, and T.K. Mayeda, Oxygen isotope geothermometry of mafic igneous rocks, J. Geol., 79, 715-279, 1971.

Bailey, E.H., compiler, Geologic map of Muscat-Ibra area, Sultanate of Oman, Jour. Geophys. Res., in press, 1981.

Bailey, E.H., R.G. Coleman, C.A. Hopson, J.S. Pallister, and R.T. Gregory, Geologic section through the Samail ophiolite in the Ibra region, southeastern Oman Mountains, J. Geophys. Res., in press, 1981.

Baldwin, B., P.J. Coney, and W. R. Dickinson, Dilemma of a Cretaceous time scale and rates of sea-floor spreading, Geology, 2, 267-270, 1974.

Ballard, R.D., and J.G. Moore, Photographic Atlas of the Mid-Atlantic Ridge, 114 pp., Springer, New York, 1977.

Barker, P.F. and I.W.D. Dalziel, Initial reports of Deep Sea Drilling Project, Leg 36, U.S. Government Printing Office, Washington, D.C., 1080, 1976.

Barnes, I., and J.R. O'Neil, The relationship between fluids in some fresh Alpine-type ultramafics and possible modern serpentinization, western United States, Bull. Geol. Soc. Amer., 80, 1947-1960, 1971.

Barnes, I., J.R. O'Neil, and J.J. Trescases, Present day serpentinization in New Caledonia, Oman and Yugoslavia, Geochim. Cosmochim. Acta, 42, 144-145, 1978.

Beaty, D.W. and H.P. Taylor, Jr., Oxygen isotope geochemistry of the Abitibi greenstone belt, Ontario: Evidence for seawater/rock interaction and implications regarding the isotopic composition and evolution of the ocean and oceanic crust, Geol. Soc. Am. Abstr. Progr., 11, 386, 1979.

Berger, W.H. and E.L. Winterer, Plate stratigraphy and the fluctuating carbonate line, in Pelagic sediments on land and under the sea, K.J. Hsu and H.C. Jenkyns, eds., Internat. Assoc. Sedimentologists Spec. Pub. 1, 11-48, 1974.

Bott, M.H.P. and F. Tuson, Deep structure beneath the Tertiary volcanic regions of Skye, Mull and Ardnamurchan, northwest Scotland, Nature, Phys. Sci. 242, 114-116, 1973.

Boudier, F., Structure and petrology of the Lanzo peridotite massif (Piedmont Alps), Geol. Soc. Amer. Bull. 89, 1564-1591, 1978.

Boudier, F. and R.G. Coleman, Cross section through the peridotite in the Samail ophiolite, Oman, Southeastern Oman Mountains, J. Geophys. Res., in press, 1981.

Bowen, N.L. Evolution of the Igneous Rocks, Princeton University Press, 1928, 332.

Brooks, C., S.R. Hart, A. Hoffmann, and D.E. James, Rb-Sr mantle isochrons from oceanic regions, Earth Planet. Sci. Lett., 32, 51-61, 1976.

Brown, E.H., J.Y. Bradshaw, and G.E. Mustoe, Plagiogranite and Keratophyre in ophiolite on Fidalgo Island, Washington, Geol. Soc. Amer. Bull. 90, 493-507, 1979.

Burnham, C.W., The importance of volatile constituents in Evolution of Igneous Rocks; Fiftieth Anniversary Perspectives, J.S. Yoder, Jr., ed., Princeton University Press, Princeton, 1979, 439-482.

Cakir, V., T. Juteau, and H. Whitechurch, Nouvelles preuves de l'ecaillage intra-oceanique precoce des ophiolites tethisieenes: les roches metamorphiques infra-peridotitiques du massif de Poz-anti-Karsanti (Turquie), Bull. Soc. Geol. France, 7, 61-70, 1978.

Carlson, R.W., J.D. Macdougall, and G.W. Lugmair, Differential Sm/Nd evolution in oceanic basalts, Geophys. Res. Lett., 5, 229-232, 1978.

Cassard, D., M. Rabinovitch, A. Nicolas, J. Moutte, M. Leblanc, and A. Prinzhofer, Structural classification of chromite pods in southern New Caledonia (pre-print.)

Chapman, H.J., and E.T.C. Spooner, ^{87}Sr enrichment of ophiolitic sulphide deposits in Cyprus confirms ore formation by circulating seawater, Earth Planet. Sci. Lett., 35, 71-78, 1977.

Chase, C.G. and E.C. Perry, Jr., The oceans: Growth and oxygen isotope evolution, Science, 177, 992-994, 1972.

Chen, J.H., and J.S. Pallister, Lead isotopic studies of the Samail ophiolite, Oman, J. Geophys. Res., in press, 1981.

Christensen, N.I., and M.H. Salisbury, Structure and constitution of the lower oceanic crust, Rev. Geophys. Space Physics, 13, 57-86, 1975.

Church, S.E., and M. Tatsumoto, Lead isotope relations in oceanic ridge basalts from the Juan de Fuca-Gorda Ridge area, N.E. Pacific Ocean, Contrib. Mineral Petrol., 53, 253-279, 1975.

Clayton, R.N., L.J.P. Muffler and D.E. White, Oxygen isotope study of calcite and silicates of the River Ranch No. 1 Well, Salton Sea geothermal field, California, Am. J. Sci., 266, 968-979, 1968.

Coleman, R.G., Tectonic setting for ophiolite obduction in Oman, Jour. Geophys. Res., in press, 1981.

Coleman, R.G., Ophiolites: ancient oceanic lithosphere?, Springer Verlag, New York, N.Y., 1977.

Coleman, R.G., G.F. Brown and T.E.C. Keith, Layered gabbros in southwest Saudi Arabia, U.S. Geol. Survey Prof. Paper 800-D, D143-D150, 1972.

Coleman, R.G., and M.M. Donato, Oceanic plagiogranite revisited, in Trondhjemites, Dacites, and Related Rocks, Elsevier, p. 149-168, 1977.

Coleman, R.G., and Z.E. Peterman, Oceanic plagiogranite, Jour. Geophys. Res. 80, 1099-1108, 1975.

Corliss, J.B., J. Dymond, L.J. Gordon, J.M. Edmond, R.P. von Herzen, R.D. Ballard, K. Green, D. Williams, A. Bainbridge, K. Crane, and T.H. Van Andel, Submarine thermal springs on the Galapagos Rift, Science, 203, 1073-1083, 1979.

Criss, R.E., AN $^{18}O/^{16}O$, D/H and K-Ar Study of the Southern Half of the Idaho Batholith, Ph.D. Thesis, Calif. Inst. Tech., 1981.

Dansgaard, W. and H. Tauber, Glacier oxygen-18 content and Pleistocene ocean temperatures, Science, 166, 499-502, 1969.

Davies, H.L., Papuan ultramafic belt, 23rd Intern. Geol. Congr. Sect. 1, 209-220, 1968.

Denton, G.H., R.L. Armstrong and M. Stuiver, The late Cenozoic glacial history of Antarctica, in The late Cenozoic glacial ages, K.K. Turekian, ed., Yale Univ. Press, New Haven, 267-304, 1971.

DePaolo, D.J., and G.J. Wasserburg, Nd isotopic variations and petrogenetic models, Geophys. Res. Lett., 3, 249-252, 1976a.

DePaolo, D.J., and G.J. Wasserburg, Inferences about magma sources and mantle structure from variations of $^{143}Nd/^{144}Nd$, Geophys. Res. Lett. 3, 743-746, 1976b.

DePaolo, D.J., and G.J. Wasserburg, The sources of island arcs as indicated by Nd and Sr isotopic studies, Geophys. Res. Lett. 4, 465-468, 1977.

DePaolo, D.J., and G.J. Wasserburg, Sm-Nd age of the Stillwater complex and the mantle evolution curve for neodymium, Geochim. Cosmochim. Acta, 43, 999-1008, 1979.

Dixon, S., and M.J. Rutherford, Plagiogranites as late-stage immiscible liquids in ophiolite and mid-ocean ridge suites: an experimental study, Earth and Planet. Sci. Lett. 45, 45-60, 1979.

Donato, M.M., and R.G. Coleman, Sub-sea floor metamorphism pf Saudi Arabian and Oman ophiolite, Amer. Geophys. Union Trans., 57, 1022, 1976.

Duncan, R.A., and W. Compston, Sr-isotopic evidence for an old mantle source region for French Polynesian volcanism, Geology, 4, 728-732, 1976.

Dungan, M.A., and H.G. Ave Lallemant, Formation of small dunite bodies by metasomatic transformation of harzburgite in the Canyon Mountain ophiolite, northeast Oregon, Ore. Dept. Geol. Min. Ind. Bull. 96, 109-128, 1977.

Edmond, J.M., C. Measures, R.E. McDuff, L.H. Chan, R. Collier, B. Grant, L.I. Gordon, and J.G. Corliss, Ridge crest hydrothermal activity and the balances of the major and minor elements in the ocean: The Galapagos data, Earth Planet, Sci. Let., 46, 1-18, 1979.

Edmond, J.M., H. Craig, L.I. Gordon, and H.D. Holland, Chemistry of hydrothermal waters at 21°N on the East Pacific Rise, Trans. Amer. Geophys. U., 60, 864, 1979.

Emiliani, C., Isotopic paleotemperatures, Science, 154, 851-857, 1966.

Engel, A.E.J. T.H. Dixon, R.J. Stern, E.M. El Shazly and A. Abdullah, Geologic evolution of northeast Africa, Geol. Soc. Am. Abstr. Progr., 10, 396, 1978.

Engel, A.E.J., C.G. Engel, and R.G. Havens, Chemical characteristics of oceanic basalts and the upper mantle, Geol. Soc. Am. Bull., 76, 719-734, 1965.

Forester, R.W. and H.P. Taylor, Jr., $^{18}O/^{16}O$, D/H, and $^{13}C/^{12}C$ studies of the Tertiary igneous complex of Skye, Scotland, Amer. J. Sci., 277, 136-177, 1977.

Frey, F.A., Rare earth abundances in a high temperature peridotite intrusion, Geochim. Cosmochim. Acta, 33, 1429-1447, 1969.

Gansser, A., The ophiolitic melange, a world-wide problem on Tethyan examples, Eclogae Geol. Helv 67, 479-507, 1974.

Gass, I.G., and J.D. Smewing, Intrusion, extrusion and metamorphism at constructive margins: evidence from the Troodos massif, Cyprus, Nature (London), 242, 26-29, 1973.

Ghent, E.D., and M.Z. Stout, Metamorphism at the base of Samail ophiolite, southeastern Oman Mountains, Jour. Geophys. Res., in press, 1981.

Gilluly, J., Replacement origin of the albite granite near Sparta, Oregon, U.S. Geol. Survey Prof. Paper 175-C, 65-81, 1933.

Glennie, K.W., M.G.A. Boeuf, M.W. Hughes-Clarke, M. Moody-Stuart, W.F.H. Pilaar, B.M. Reinhardt, Late Cretaceous nappes in the Oman Mountains and their geologic evolution, Amer. Assoc. Petroleum Geol. Bull., 57, 5-27, 1973.

Glennie, K.W., M.G.A. Boeuf, M.W. Hughes-Clark, M. Moody-Stuart, W.F.H. Pilaar, and B.M. Reinhardt, Geology of the Oman Mountains, Transactions of the Royal Dutch Geological and Mining Society, 423, 1974.

Glennie, K.W., M.G.A. Boeuf, M.W. Hughes-Clark, M.W. Moody-Stuart, W.F.H. Pilaar, and B.M. Reinhardt, Geology of the Oman Mountains, Part One (text), Part Two (Tables and illustrations), Part Three (Enclosures), Konink-Nederlandsch Geol. Mijnhoukundig Genootschap Verh., 31, 423 p., 1974.

Godfrey, J.D., The deuterium content of hydrous minerals from the east-central Sierra Nevada, and Yosemite National Park, Geochim. Cosmochim. Acta, 26, 1215-45, 1962.

Goldberg, E.D., Minor elements in sea water, in: J.P. Riley, G. Skirrow, (eds.), Chemical Oceanography, vol. 1, New York, Academic Press, 1965.

Green, D.H., W.O. Hibberson, and A.L. Jaques, Petrogenesis of Mid-Ocean Ridge basalts, in The Earth: Its origin, structure and evolution (ed. M.W. McElhinney), Academic Press, London, 265-299, 1979.

Greenbaum, D., Magmatic processes at ocean ridges: Evidence from the Troodos Massif, Cyprus, Nature, 238, 18-21, 1972.

Greenwood, J.E.G.W., and P.E. Loney, 1968, Geology and mineral resources of the Trucial Oman Range, Great Britain Inst. Geological Sci. Overseas Div., 108, 1968.

Gregory, R.T., and H.P. Taylor, Jr., An oxygen isotope study of the Cretaceous Samail ophiolite, Oman, evidence for deep seawater-hydrothermal circulation and implication for spreading center geometry and $\delta^{18}O$ of seawater, Trans. Am. Geophys. U., 60, 963, 1979.

Gregory, R.T., and H.P. Taylor, Jr., An oxygen isotope profile in a section of Cretaceous oceanic crust, Samail Ophiolite, Oman: evidence for $\delta^{18}O$-buffering of the oceans by deep (> 5 km) seawater-hydrothermal circulation at mid-ocean ridges, J. Geophys. Res., in press, 1981.

Gregory, R.T. and H.P. Taylor, Jr., Oxygen isotope and field studies applied to the origin of oceanic plagiogranites, Abstracts International Ophiolite Symposium, Geol. Survey Dept. Cyprus, 117-118, 1979.

Hamilton, P.J., N.M. Evensen, R.K. O'Nions, H.S. Smith, and A.J. Erlank, Sm-Nd dating of Onverwacht Group volcanics, southern Africa, Nature, 279, 298-300, 1979.

Hart, R.A., Chemical exchange between seawater and deep ocean basalts, Earth Planet. Sci. Lett., 9, 269-279, 1970.

Hart, S.R., A.J. Erlank, and E.J.D. Kable, Sea floor basalt alteration: some chemical and Sr-isotopic effedts, Contrib. Mineral. Petrol., 44, 219-230, 1974.

Hawkesworth, C.J., R.K. O'Nions, R.J. Pankhurst, P.J. Hamilton, and N.M. Evensen, A geochemical study of island-arc and back-arc tholeiites from the Scotia Sea, Earth Planet. Sci Lett., 36, 253-262, 1977.

Hayes, D.E., L.A. Frakes, et al., Initial Reports of Deep Sea Drilling Project Leg 28, U.S. Government Printing Office, Washington, D.C., 1975.

Heaton, T.H.E. and S.M.F. Sheppard, Hydrogen and oxygen isotope evidence for seawater hydrothermal alteration and ore deposition, Troodos complex, Cyprus, in: Volcanic Processes in Ore Genesis, Spec. Paper No. 7, Geol. Soc. London, 42-57, 1977.

Hedge, C.E., Strontium isotopes in basalts from the Pacific Ocean basin, Earth Planet. Sci. Lett., 38, 88-94, 1978.

Hildreth, W., The Bishop tuff: evidence for the origin of compositional zonation in silicic magma chambers, Geol. Soc. Amer. Spec. Paper, 180 43-75, 1979.

Himmelburg, G.R. and R.A. Loney, Petrology of the Vulcan Peak Alpine-type peridotite, southwestern Oregon, Geol. Soc. Amer. Bull. 84, 1585-1600, 1973.

Hollister, C.D., C. Craddock et al., Initial Reports of Deep Sea Drilling Project 35, U.S. Government Printing Office, Washington, D.C., 930, 1976.

Hopson, C.A., R.G. Coleman, R.T. Gregory, J.S. Pallister, and E.H. Bailey, Geologic section through the Samail ophiolite and associated rocks along a Muscat-Ibra transect, southeastern Oman Mountains, J. Geophys. Res., in press, 1981.

Hopson, C.A. and C.J. Frano, Igneous history of the Point Sal ophiolite, southern California, in North American Ophiolites, R.G. Coleman and W.P. Irwin, eds., Oregon Dept. Geol. and Min. Resources Bull., 95, 161-183, 1977.

Hopson, C.A. and J.S. Pallister, Gabbro sections in Samail Ophiolite, southeastern Oman Mountains, Geol. Soc. Amer. abstracts with programs. 10, 424, 1978.

Hopson, C.A. and J.S. Pallister, Samail ophiolite magma chamber: 1, evidence from gabbro phase variation, internal structure and layering, Abstracts International Ophiolite Symposium, Geol. Survey Dept. Cyprus, 37, 1979.

Hudson, R.G.S., The Permian and Trias of the Oman Peninsula, Arabia, Geol. Mag., 97, 4, 299-308, 1960.

Hudson, R.G.S., A. McGugan, and D.M. Morton, The structure of the Jebel Hagab area, Trucial Oman, Geol. Soc. London, Quart. Jour., 110, pt. 1, 438, 121-152, 1954.

Hudson, R.G.S., and M. Chatton, The Musandam limestone (Jurassic to Lower Cretaceous) of Oman, Arabia, Mus. Nat. d'Histoire Naturelle Notes et Memoires Moyen-Orient, (Paris) 7, 69-93, 1959.

Irvine, T.N., Crystallization sequences in the Muskox intrusion and other layered intrusions, I. Olivine-pyroxene-plagioclase relations, Spec. Publs. Geol. Soc. So. Africa, 1, 444-476, 1970.

Irvine, T.N. and W.R.A. Baragar, Muskox intrusion and Coppermine River lavas Northwest Territories, Internat. Geol. Cong. 24, Field Excursion A29 Guidebook 70, 1972.

Irving, A.J., A review of experimental studies of crystal/liquid trace element partitioning, Geochim. Cosmochim. Acta, 42, 743-770, 1978.

Jackson, E.D., The cyclic unit in layered intrusions, Geol. Soc. South Africa Spec. Pub., 1, 391-424, 1970.

Jackson, E.D., Ultramafic cumulates in the Stillwater, Great Dyke, and Bushveld intrusion, in P.J. Wyllie (ed.), Ultramafic and related rocks, New York, John Wiley and Sons, Inc., 2038, 1971.

Jackson, E.D., H.W. Green II, and E.M. Moores, The Vourinos ophiolite, Greece: cyclic units of lineated cumulates overlying harzburgite tectonite, Geol. Soc. Amer. Bull., 86, 390-398, 1975.

Jacobsen, S.B., and G.J. Wasserburg, Nd and Sr isotopic study of the Bay of Islands ophiolite complex and the evolution of the source of mid-ocean ridge basalts, J. Geophys. Res., 84, 7429-7445, 1979.

Javoy, M., Stable isotopes and geothermometry, J. Geol. Soc. Lond. 133, 609-636, 1977.

Kay, R.W., N.J. Hubbard, and P.W. Gast, Chemical characteristics and origin of ocean ridge volcanic rocks, J. Geophys. Res., 75, 1585-1613, 1970.

Kay, R.W., and R.G. Senechal, The rare earth geochemistry of the

Troodos ophiolite complex, J. Geophys. Res., 81, 964-970, 1976.

Kornprobst, J., Le massif ultrabasique des Beni Bouchern (Riv Interne, Maroc): etude des peridotites de haute temperature et de haute pression, et des pyroxenolites a grenat qui leur sont associees, Contrib. Mineral. Petrol. 23, 283-322, 1969.

Knauth, L.P. and S. Epstein, Hydrogen and oxygen isotope ratios in nodular and bedded cherts, Geochim. Cosmochim. Acta, 40, 1095-1108, 1976.

Kushiro, I., Fractional crystallization of basaltic magma, in Evolution of Igneous Rocks; Fiftieth Anniversary Perpectives, J.S. Yoder,ed., Princeton University Press, Princeton, 1979, 171-203.

Kyser, T. Kurtis, The temperature dependence of oxygen isotope distributions and the origins of basalts and ultramafic nodules, Geol. Soc. America Abstracts with Programs 11, 462, 1979.

Lanphere, M.A., K-Ar ages of metamorphic rocks at the base of the Samail ophiolite, Oman, J. of Geophys. Res., in press, 1981.

Larson, R.L. and W.L. Pitmann, III, Worldwide correlation of Mesozoic magnetic anomalies, and its implications, Geol. Soc. Am. Bull., 83, 3645-3662, 1972.

Leeman, W.P. and E.J. Dasch, Strontium, lead, and oxygen isotopic investigation of the Skaergaard intrusion, East Greenland, Earth Planet. Sci. Lett. 43, 47-59, 1978.

Lees, G.M., The geology and tectonics of Oman and parts of Southeastern Arabia, Geol. Soc. London Quart. Jour., 84, pt. 4, 585-670, 1928.

Loney, R.A., G.R. Himmelburg and R.G. Coleman, Structure and petrology of the Alpine-type peridotite at Burro Mountain, California, U.S.A. J. Petro., 12, 245-309, 1971.

Lugmair, G.W., K. Marti, J.P. Kurtz, and N.B. Scheinin, History and genesis of lunar troctolite 76535 or: How old is old?, Proc. Lunar Sci. Conf., 7th, 2009-2033, 1976.

Magaritz, M. and H.P. Taylor, Jr., Oxygen and hydrogen isotope studies of serpentinization in the Troodos ophiolite complex, Cyprus, Earth Planet. Sci. Lett., 23, 8-14, 1974.

Magaritz, M. and H.P. Taylor, Jr., Oxygen, hydrogen and carbon isotope studies of the Franciscan formation, Coast Ranges, California, Geochim. Cosmochim. Acta, 40, 215-234, 1976a.

Magaritz, M. and H.P. Taylor, Jr., $^{18}O/^{16}O$ and D/H studies along a 500 km traverse across the Coast Range batholith and its country rocks, central British Columbia, Can. J. Earth Sci., 13, 1514-1536, 1976b.

Malpas, L., Magma generation in the upper mantle, field evidence from ophiolite suites and application to the generation of oceanic litho-

sphere, Philos. Trans. R. Soc. London, Ser. A, 288, 527-546, 1978.

Malpas, J., Two contrasting trondhjemite associations from transported ophiolites in western Newfoundland: Initial report, in Trondhjemites, Dacites, and Related Rocks, Elsevier, Amsterdam, 465-487, 1977.

Malpas, J. and R.K. Stevens, The origin and emplacement of the ophiolite suite with examples from western Newfoundland, Geotectonics, II, 453-466, 1977.

Marsh, B.D., Island-arc volcanism, Am. Scientist, 67, 161-172, 1979.

Masuda, A., Lanthanide concentrations in the olivine phase of the Brenham pallasite, Earth Planet. Sci. Lett., 5, 59-62, 1968.

Mattinson, J.M., Early Paleozoic ophiolite complexes of Newfoundland: Isotopic ages of zircons, Geology, 4, 393-394, 1976.

McBirney, A.R., Effect of Assimilation, in Evolution of Igneous Rocks: Fiftieth Anniversary Perspectives, J.S. Yoder, Jr., ed., Princeton University Press, Princeton, 307-338, 1979.

McCulloch, M.T., R.T. Gregory, G.J. Wasserburg, and H.P. Taylor, Jr., Sm-Nd, Rb-Sr, and $^{18}O/^{16}O$ isotopic systematics in an oceanic crustal section: evidence from the Samail ophiolite, Jour. Geophys. Res., in press, 1981.

McCulloch, M.T., R.T. Gregory, G.J. Wasserburg and H.P. Taylor, Jr., A neodymium, strontium, and oxygen isotopic study of the cretaceous Samail ophiolite and implications for the petrogenesis and seawater-hydrothermal alteration of oceanic crust, Earth and Planetary Science Letters, 46, 201-211, 1980.

McCulloch, M.T., and G.J. Wassserburg, Sm-Nd and Rb-Sr chronology of continental crust formation, Science, 200, 1003-1011, 1978.

McKenzie, D.P. and N. Weiss, Speculations on the thermal and tectonic history of the Earth, Geophys. J.R. Astro. Soc., 42, 131, 1975.

Melson, W.G. and T.H. Van Andel, Metamorphism in the Mid-Atlantic ridge 22°N latitude, Marine Geol., 4, 165-186, 1966.

Montigny, R., H. Bougault, Y. Bottinga, and C.J. Allegre, Trace element geochemistry and genesis of the Pindos ophiolite suite, Geochim. Cosmochim. Acta, 37, 2135-2147, 1973.

Moore, J.G., Mechanism of formation of pillow lavas, Amer. Jour. Sci., 63, 269-277, 1975.

Moore, J.G., and J.G. Schilling, Vesicles, water, and sulfur in Reykjanes Ridge basalts, Contr. Mineral. and Petrol., 41, 105-118, 1973.

Moores, E.M., Petrology and structure of the Vourinos ophiolite complex, northern Greece, Geol. Soc. America Spec. Paper, 118, 1969.

Morton, D.D., The geology of Oman, 5th World Petroleum Cong. Proc., New York, Sec. 1, 277-294, 1959.

Muehlenbachs, K., A.T. Anderson, and G.E. Sigvaldason, Low-^{18}O basalts from Iceland, Geochim. Cosmochim. Acta, 38, 577-588, 1974.

Muehlenbachs, K. and R.N. Clayton, Oxygen isotope ratios of submarine diorites and their constituent minerals. Can. J. Earth Sci., 8, 1591-1595, 1971.

Muehlenbachs, K. and R.N. Clayton, Oxygen isotope studies of fresh and weathered submarine basalts, Can. J. Earth Sci., 9, 172-184, 1972a.

Muehlenbachs and R.N. Clayton, Oxygen isotope geochemistry of submarine Greenstones, Can. J. Earth Sci., 9, 471-478, 1972b.

Muehlenbachs, K. and R.N. Clayton, Oxygen isotope composition of the oceanic crust and its bearing on seawater. J. Geophys. Res., 81, 4365-4369, 1976.

Nakamura, N., M. Tatsumoto, P.D. Nunes, D.M. Unruh, A.P. Schwab, and T.R. Wildeman, 4.4 b.y.-old clast in Boulder 7, Apollo 17: A comprehensive chronological study by U-Pb, Rb-Sr, and Sm-Nd methods, Proc. Lunar Sci. Conf., 7th, 2309-2333, 1976.

Naldrett, A.J. and A.M. Goodwin, Volcanic rocks of the Blake River Group, Abitibi greenstone belt, Ontario, and their sulfur content, Can. J. Earth Sci., 14, 539-550, 1977.

Nicolas, A., F. Boudier, and J-L Bouchez, Interpretation of peridotite structures from ophiolitic and oceanic environments, Am. J. Sci., in press.

Nicolas, A. and J.P. Poirier, Crystalline plasticity and solid state flow in metamorphic rocks, Wiley Interscience, London, 444, 1976.

Norton, D. and H.P. Taylor, Jr., Quantitative simulation of the hydrothermal systems of crystallizing magmas on the basis of transport theory and oxygen isotope data: An analysis of the Skaergaard intrusion, J. Petrology, 20, 421-486, 1979.

Obata, M., Petrology and Petrogenesis of a High-Temperature Peridotite Intrusion: Serrania de la Ronda, southern Spain, Ph.D. Thesis, Massachusetts Institute of Technology, 1977.

O'Hara, M.J., The bearing of phase equilibria studies in synthetic and natural systems on the origin and evolutions of basic and ultrabasic rocks, Earth-Sci. Rev. 4, 69-133, 1968.

O'Hara, M.J., Geochemical evolution during fractional crystallization of a periodically refilled magma chamber, Nature, 266, 503-507, 1977.

O'Neil, J.R. and H.P. Taylor, Jr., The oxygen isotope cation exchange chemistry of feldspars, Am. Miner., 52, 1414-1437, 1967.

O'Nions, R.K., P.J. Hamilton, and N.M. Evensen, Variations in $^{143}Nd/^{144}Nd$ and $^{87}Sr/^{86}Sr$ ratios in oceanic basalts, Earth and Planet. Sci. Lett., 34, 13-22, 1977.

Onuma, N., R.N. Clayton, and T.K. Mayeda, Apollo 11 rocks: oxygen isotope fractionation between minerals and an estimate of the temperature of formation, Proc. Apollo 11 Lunar Sci. Conf., Geochim. Cosmochim. Acta Suppl. 1, vol. 2, 1429-1434, 1970.

Pallister, J.S., Sheeted dike complex of the Samail ophiolite near Ibra, Oman: An initial report, J. Geophys. Res., in press, 1981.

Pallister, J.S., and C.A. Hopson, Samail ophiolite plutonic suite: Field relations, phase variation, cryptic variation and layering; and a model at a spreading-ridge magma chamber, Jour. Geophys. Res., in press, 1981.

Pallister, J.S., and R.J. Knight, REE geochemistry of the Samail ophiolite, J. Geophys. Res., in press, 1981.

Perry, Jr., E.C., S.N. Ahmad and T.M. Swulius, The oxygen isotope composition of 3,800 m.y. old metamorphosed chert and iron formation from Isukasia, West Greenland, J. Geol., 86, 223-239, 1978.

Peterman, Z.E., R.G. Coleman, and R.A. Hildreth, $^{87}Sr/^{86}Sr$ in mafic rocks of the Troodos massif, Cyprus, U.S. Geol. Surv. Prof. Pap., 750, 157D-161D, 1971

Peterman, Z.E., C.E. Hedge, and H. Tourtelot, Isotopic composition of Sr in seawater throughout Phanerozoic time, Geochim. Cosmochim. Acta, 34, 105-120, 1970.

Piepgras, D.J., G.J. Wasserburg, and E.J. Dasch, The isotopic composition of Nd in different ocean masses, Earth Planet. Sci. Lett., 45, 223-236, 1979.

Quick, J., Part I: Petrology and Petrogenesis of the Trinity Peridotite, Northern California, Ph.D. Thesis, Calif. Inst. Tech., 1981.

Reinhardt, B.M., On the genesis and emplacement of ophiolites in the Oman Mountains geosyncline, Schweiz. Min. Petrog. Mitt., 49, 1-30, 1969.

Richard, P., N. Shimizu, and C.J. Allegre, $^{143}Nd/^{146}Nd$, a natural tracer: An application to oceanic basalts, Earth Planet Sci. Lett., 31, 269-278, 1976.

Richard, P., D. Rousseau, and C.J. Allegre, Nd and Sr systematics in ophiolites, Short papers of the 4th Internat. Conf. Geochron. Cosmochron. Isotope Geol., Geol. Surv. Open-File report, 78-701, 350, 1978.

Sagan, C. and Mullen, G., Earth and Mars: evolution of atmospheric and surface temperatures, Science, 177, 52-56, 1972.

Saleeby, J., Fracture zone tectonics, continental margin fragmentation and emplacement of the Kings-Kaweah ophiolite belt, southwest Sierra Nevada, California, Oregon Dept. Geol. Min. Res., 95, 141-161, 1977.

Schilling, J.G., Sea-floor evolution: Rare-earth evidence, Phil. Trans. Roy. Soc. Lond. A., 268, 663-706, 1971.

Schnetzler, C.C., and M.L. Bottino, Some alkali, alkaline earth, and rare earth element concentrations and the Rb-Sr age of the Lost City meteorite and separated phases, J. Geophys. Res., 76, 4061-4066.

Seyfried, W.E., W.C. Shanks, and W.E. Dibble, Clay mineral formation in DSDP leg 34 basalt, Earth Planet. Sci. Lett., 41, 265-276, 1978.

Smewing, J.D., Regional setting and petrological characteristics of the Oman ophiolite in North Oman, Tethyan Ophiolite volume, 26th International Geol. Congress, Paris, 1980 (in press).

Smith, C.H., Bay of Islands igneous complex, western Newfoundland, Geol. Survey Can. Mem. 290, 1-132. 1958.

Spooner, E.T.C., Hydrodynamic model for the origin of the ophiolitic cupriferous pyrite ore deposits of Cyprus, Geol. Soc. Lond. Spec. Pub. 7, 58-72, 1977.

Spooner, E.T.C., R.D. Beckinsale, W.S. Fyfe and J.D. Smewing, ^{18}O-enriched ophiolitic metabasic rocks from E. Liguria, Pindos and Troodos, Contrib. Mineral. Petrol., 47, 41-62, 1974.

Spooner, E.T.C., H.J. Chapman, and J.D. Smewing, Strontium isotopic contamination and oxidation during ocean floor hydrothermal metamorphism of the ophiolitic rocks of the Troodos, Cyprus, Geochim. Cosmochim. Acta, 41, 873-890, 1977.

Steiner, J. and E. Grillman, Possible galactic causes for periodic and episodic glaciations, Geol. Soc. Am. Bull., 84, 1003-1018, 1973.

Stern, C., Open and closed system igneous fractionation within two Chilean ophiolites and the tectonic implication, Contrib. Mineral. Petrol., 68, 243-258, 1979.

Stern, C., M.J. de Wit and J.R. Lawrence, Igneous and metamorphic processes associated with the formation of Chilean ophiolites and their implication for ocean floor metamorphism, seismic layering and magnetism, J. Geophys. Res., 81, 4370-4380, 1976.

Stolper, E., A phase diagram for mid-ocean ridge basalts: preliminary results and implications for petrogenesis, Contrib. Mineral. Petrol., in press.

Suen, C.J., F.A. Frey, and J. Malpas, Bay of Islands ophiolite suite, Newfoundland: petrologic and geochemical characteristics with emphasis on rare earth element geochemistry, Earth Planet. Sci. Lett., 45, 337-348, 1979.

Sun, S.S., M. Tatsumoto, and J.G. Schilling, Mantle plume mixing along the Reykjanes Ridge axis: Lead isotopic evidence, Science, 190, 143-147, 1975

Sun, S.S., and G.N. Hanson, Evolution of the mantle: Geochemical evidence from alkali basalt, Geology, 3, 297-302, 1975.

Tatsumoto, M., C.E. Hedge, and A.E.J. Engel, Potassium, rubidium, strontium, thorium, uranium, and the ratio of Sr-87 to Sr-86 in oceanic tholeiitic basalt, Science, 150, 886-888, 1965.

Taylor, H.P., Jr., The application of oxygen and hydrogen isotope studies to problems of hydrothermal alteration and ore deposition, Econ. Geol., 69, 843-883, 1974.

Taylor, H.P., Jr., The oxygen isotope geochemistry of igneous rocks, Contrib. Mineral. Petrol., 19, 1-71, 1968.

Taylor, H.P., Jr., Oxygen isotope evidence for large-scale interaction between meteoric ground waters and Tertiary granodiorite intrusions, western Cascade Range, Oregon, J. Geophys. Res., 76, 7855-74, 1971.

Taylor, H.P., Jr., Oxygen and hydrogen isotope evidence for large-scale circulation and interaction between ground waters and igneous intrusions, with particular reference to the San Juan volcanic field. Colorado, Geochemical Transport and Kinetics, Hofmann, et al. eds., Carnegie Inst. Wash. Publ. 299-324, 1974.

Taylor, H.P., Jr., Stable isotope studies of spreading centers and their bearing on the origin of granophyres and plagiogranites, Proc. International Meeting of Mafic-Ultramafic Association in Orogenic Belts, C. Allegre, ed., in press, 1980.

Taylor, H.P., Jr., The effects of assimilation of country rocks by magmas on $^{18}O/^{16}O$ and $^{87}Sr/^{86}Sr$ systematics in igneous rocks, EPSL, 47, 243-254, 1980.

Taylor, H.P., Jr., Water/rock interactions and the origin of H_2O in granitic batholiths, J. Geol. Soc. Lond., 133, 509-558, 1977.

Taylor, H.P., Jr., and R.G. Coleman, Oxygen isotopic evidence for meteoric-hydrothermal alteration of the Jabal at Tirf complex, Saudi Arabia, EOS Trans. Amer. Geophys. Union, 58, 516, 1977.

Taylor, H.P., Jr., and S. Epstein, Relationships between $^{18}O/^{16}O$ ratios in coexisting minerals of igneous and metamorphic rocks, Geol. Soc. Am. Bull., 73, 461-480, 675-694, 1962.

Taylor, H.P., Jr., and S. Epstein, $^{18}O/^{16}O$ ratios of Apollo 11 lunar rocks and minerals, Apollo 11 Lunar Sci. Conf., Geochim. Cosmochim. Acta Suppl. 1, vol. 2, 1613-1626, 1970.

Taylor, H.P., Jr., and R.W. Forester, An oxygen and hydrogen isotope study of the Skaergaard intrusion and its country rocks: A description of a 55-m.y. old fossil hydrothermal system, J. Petrology, 20, 355-419, 1979.

Taylor, H.P., Jr., and R.W. Forester, Low-^{18}O igneous rocks from the intrusive complexes of Skye, Mull, and Ardnamurchan, western Scotland. J. Petrol., 12, 465-497, 1971.

Taylor, H.P., Jr., and M. Magaritz, Oxygen and hydrogen isotope studies of 2.6 3.4 b.y. old granites from the Barberton Mountain Land, Swaziland, and the Rhodesian cration, Southern Africa, Geol. Soc. Am. Abstr. Progr., 7, 1293, 1975.

Taylor, H.P., Jr., and B. Turi, High ^{18}O igneous rocks from the Tuscan magmatic province, Italy, Contrib. Mineral. Petrol. 55, 33-54, 1976.

Thayer, T.P., Principle features and the origin of podiform chromite deposits and some observations on the Guleman-Soridag District, Turkey, Econ. Geol., 59, 1497, 1964.

Thayer, T.P., The Canyon Mountain Complex, Oregon, and the Alpine mafic magma stem, U.S. Geol. Sur. Prof. Paper 475-C, C82-C85, 1963.

Tilton, G.R., C.A. Hopson, and J.E. Wright, Uranium-lead isotopic ages of the Samail ophiolite, Oman, with applications to Tethyan ocean ridge tectonics, J. Geophys. Res., in press, 1981.

Tippit, P.R., and E.A. Pessagno, Jr., Age of the Samail ophiolite based on radiolarian biostratigraphy, Trans. Amer. Geophys. Union, 60, 962, 1979.

Tschopp, R.H., The general geology of Oman, 7th World Petroleum, Cong. Proc., Mexico, 2, 231-242, 1967.

Veizer, J., and W. Compston, $^{87}Sr/^{86}Sr$ composition of seawater during the Phanerozoic, Geochim. Cosmochim, Acta, 38, 1461-1484, 1974.

Wager, L.R., and G.M. Brown, Layered Igneous Rocks, Oliver and Boyd, Edinburgh, 588 p., 1968.

Walker, D., T. Shibata, S.E. Delong, Abyssal tholeiites from the Oceanographer Fracture Zone II, Phase equilibria and mixing, Contrib. Mineral. Petrol., 70, 111-125, 1979.

Wenner, D.B. and H.P. Taylor, Jr., Oxygen and hydrogen isotope studies of a Precambrian granite-rhyolite terrain, St. Francois Mountains, southeastern Missouri, Geol. Soc. Am. Bull., 87, 1587-1598, 1976.

Wenner, D.B. and H.P. Taylor, Jr., Oxygen and hydrogen isotope studies of the serpentinization of ultramafic rocks in oceanic environments and continental ophiolite complexes, Am. J. Sci., 273, 207-239, 1978.

Whitford, D.J., W. Compston, I.A. Nichols, and M.J. Abbott, Geochemistry of late Cenozoic lavas from eastern Indonesia, Role of subducted sediments in petrogenesis, Geology, 5, 571-575, 1977.

Williams, H. and J. Malpas, Sheeted dikes and brecciated dike rocks within transported igneous complex, Bay of Islands, western Newfoundland, Can. J. Earth Sci., 9, 1216-1229, 1976.

Wilson, J.J., Late Cretaceous eugeosynclinal sedimentation, gravity, tectonics, and ophiolite emplacement in Oman mountains, southeast Arabia, Amer. Assoc. Petroleum Geologists Bull., 53, 626-761, 1969.

Wolery, T.J. and N.H. Sleep, Hydrothermal circulation and geochemical flux at mid-ocean ridges, J. Geol., 84, 249-275, 1976.

APPENDIX 1

GEOLOGIC SECTION THROUGH THE SAMAIL OPHIOLITE AND ASSOCIATED ROCKS ALONG A MUSCAT-IBRA TRANSECT, SOUTHEASTERN OMAN MOUNTAINS

Running Title - Muscat-Ibra Geologic Transect, Samail Ophiolite

C.A. Hopson, University of California, Santa Barbara, CA

R.G. Coleman, U.S. Geological Survey, Menlo Park, CA

R.T. Gregory, California Institute of Technology, Pasadena, CA

J.S. Pallister, University of California, Santa Barbara, CA

E.H. Bailey, U.S. Geological Survey, Menlo Park, CA

ABSTRACT

Regional mapping at 1:60,000 of a 30-km strip from the Gulf of Oman (Muscat) across the Oman Mountains, 130 km to the south, provides the geologic setting for the (~95 m.y.) Ibra section of the Samail ophiolite. Where best preserved, the Ibra ophiolite section is an ~8 km-thick oceanic crustal section consisting of ~0.5 km of pillow lavas; 1.2 to 1.6 km of sheeted diabase dike complex; 0.2 to 1.0 km of high-level noncumulate gabbro, and 3.0 to 5.0 km of cumulate gabbro that is underlain by tectonite peridotite 9 to 12 km thick. The Ibra section is found on the southward dipping limb of the Sayah Hatat antiform. The tectonite peridotite represents uniformly depleted harzburgite and dunite that have been deformed by high-temperature low-stress asthenospheric flow. Discordant dunites within the tectonite peridotite appear to represent either flow crystallization products from primary picritic liquids or reaction products of these liquids with the harzburgite. The structural base of the tectonite peridotite is overprinted by a high-stress low-temperature deformation that can be related to its oceanic detachment. The layered gabbros are predominantly olivine-clinopyroxene-plagioclase cumulates, and orthopyroxene does not occur as a cumulus phase. Occurrence of cumulate wehrlites and picrites at high stratigraphic levels within the layered gabbros is evidence that the gabbroic section crystallized predominantly from the bottom upwards in a periodically replenished magma chamber. High-level gabbro represents remnants of crystallization at the roof of the magma chamber and intrudes most overlying diabase dikes.

Both the diabase dike complex and pillow lavas are hydrothermally altered and alteration and metamorphism increase downward (zeolite (?) to epidote-amphibolite facies). In spite of pervasive alteration, relict primary mineralogy and bulk chemistry suggest that the diabase dikes and pillow lavas are cogenetic with the underlying gabbros.

The present-day Samail thrust surface truncates ophiolite stratigraphy and puts the Samail ophiolite on top of unmetamorphosed Hawasina melange. Last motion on this surface is probably no older than Maestrichtian (70-65 m.y.). Garnet amphibolites exposed as remnants of earlier thrusting (~90 m.y.) record initial ophiolite detachment at 14-20 km depth within the Tethyan oceanic lithosphere. Underlying the Samail ophiolite is the Hawasina Group, which is a block melange where exposed near Muscat in the north grading into an imbricated broken formation at the southern limit of the map area. The Hawasina group is thrust over Permian to Late Cretaceous shelf carbonates representing autochthonous Arabian continental shelf deposits. Recent (post-Miocene) collapse and dome structures such as the Ibra dome have complicated ophiolite stratigraphy south of Jabal Dimh. Our geologic studies strongly indicate the Samail ophiolite represents a large, coherent slab of transported oceanic lithosphere formed at a Late Cretaceous spreading center in the Tethyan Sea.

ACKNOWLEDGMENTS

The production of this paper was a group effort, and C.A. Hopson was responsible mainly for the sections on the volcanic rocks and Hawasina nappe. J.S. Pallister worked on the sheeted dikes and layered gabbro along with C.A. Hopson. R.T. Gregory put together the sections on the

plagiogranite and Maestrichtian-Tertiary rocks and acted as co-editor. E.H. Bailey developed the structural section, provided the final compilation of the 1:100,000-scale geologic map used as a basis for this discussion, and also worked on the Hawasina and volcanic sections. R.G. Coleman worked on the tectonite peridotite and metamorphic sections, and acted as co-editor for the entire manuscript. F. Boudier, University of Nnates, collaborated on the field mapping of the peridotite. P.R. Tippit and D.L. Jones provided fossil ages from the Hawasina Group.

The project was jointly sponsored by the National Science Foundation and the U.S. Geological Survey. We are indebted to the Ministry of Petroleum and Minerals of the Sultanate of Oman for their generous support and interest in this project. In particular, we would like to thank Mohammed Kassim, Kalifa Al Hina, and Ismail El Boushi.

AN OXYGEN ISOTOPE PROFILE IN A SECTION OF CRETACEOUS OCEANIC CRUST, SAMAIL OPHIOLITE, OMAN: EVIDENCE FOR $\delta^{18}O$-BUFFERING OF THE OCEANS BY DEEP (>5 km) SEAWATER-HYDROTHERMAL CIRCULATION AT MID-OCEAN RIDGES*

By

Robert T. Gregory

and

Hugh P. Taylor, Jr.

Division of Geological and Planetary Sciences
California Institute of Technology
Pasadena, California 91125

*Contribution Number 3284, Division of Geological and Planetary Sciences, California Institute of Technology, Pasadena, California 91125.

ABSTRACT

Isotopic analyses of 75 samples from the Samail Ophiolite indicate that pervasive subsolidus hydrothermal exchange with seawater occurred throughout the upper 75% of this 8-km thick oceanic crustal section; locally, the H_2O even penetrated down into the tectonized peridotite. Pillow lavas ($\delta^{18}O$ = 10.7 to 12.7) and sheeted dikes (4.9 to 11.3) are typically enriched in ^{18}O, and the gabbros (3.7 to 5.9) are depleted in ^{18}O. In the latter rocks, water-rock <0.3, and $\delta^{18}O_{cpx} \approx 2.9 + 0.44\ \delta^{18}O_{feld}$, indicating pronounced isotopic disequilibrium. The mineral $\delta^{18}O$ values approximately follow an exchange (mixing) trajectory which requires that plagioclase must exchange with H_2O about 3 to 5 times faster than clinopyroxene. The minimum $\delta^{18}O_{feld}$ value (3.6) occurs about 2.5 km below the diabase-gabbro contact. Although the gabbro plagioclase appears to be generally petrographically unaltered, its oxygen has been thoroughly exchanged; the absence of hydrous alteration minerals. except for minor talc and/or amphibole, suggests that this exchange occurred at T > 400°-500°C. Plagioclase $\delta^{18}O$ values increase up section from their minimum values, becoming coincident with primary magmatic values near the gabbro-sheeted diabase contact, and reaching 11.8 in the diabase dikes. These ^{18}O-enrichments in greenschist-facies diabases are in part due to exchange with strongly ^{18}O-shifted fluids, in addition to retrograde exchange at much lower temperatures. The $\delta^{18}O$ data and the geometry of the MOR magma chamber require that two decoupled hydrothermal systems must be present during much of the early spreading history of the oceanic crust (~ the first 10^6 yrs.); one system is centered over the ridge axis and probably involves

several convective cells that circulate downward to the roof of the magma chamber, while the other system operates underneath the wings of the chamber, in the layered gabbros. Upward discharge of ^{18}O-shifted water into the altered dikes from the lower system, just beyond the distal edge of the magma chamber, combined with the effects of continued low-T hydrothermal activity, produces the ^{18}O-enrichments in the dike complex. Integrating $\delta^{18}O$ as a function of depth for the entire ophiolite establishes (within geologic and analytical error) that the <u>average</u> $\delta^{18}O$ (5.7 ± 0.2) of the oceanic crust did not change as a result of all these hydrothermal interactions with seawater. Therefore, the net change in $\delta^{18}O$ of seawater was also zero, indicating that seawater is buffered by MOR hydrothermal circulation. Under steady-state conditions, the overall bulk ^{18}O fractionation (Δ) between the oceans and primary MORB magmas is calculated to be +6.1 ± 0.3, implying that seawater has had a constant $\delta^{18}O \approx -0.4$ (in the absence of transient effects such as continental glaciation). Utilizing these new data on the depth of interaction of seawater with the oceanic crust, numerical modeling of the hydrothermal exchange shows that as long as world-wide spreading rates are greater than 1 km^2/year, ^{18}O-buffering of seawater will occur. These conclusions can be extended as far back in time as the Archean (> 2.6 AE) with the proviso that Δ may have been slightly smaller (about 5?) because of the overall higher temperatures that could have prevailed then. Thus, ocean water has probably had a constant $\delta^{18}O$ value of about -1.0 to +1.0 during almost all of the Earth's history.

ACKNOWLEDGEMENTS

We are extremely grateful to Robert G. Coleman of the U.S. Geological Survey who first suggested this study and whose scientific guidance and expertise have been invaluable in the planning, logistics, and field work in Oman in 1977 and 1978. This work is part of a cooperative study carried out with C.A. Hopson, E.H. Bailey and J.S. Pallister, who have also contributed greatly to our understanding of the geology and petrology of the Oman Mountains. A few additional samples were provide by R.G. Coleman. We particularly want to thank R.E. Criss for numerous discussions, including his help in clarifying the nature of the plagioclase-pyroxene $\delta^{18}O$ exchange phenomena. We also thank M.T. McCulloch, D. Beaty and S. Epstein for stimulating discussions of this work. Financial support for this study came from the National Science Foundation, Grants EAR-76-21310 and EAR-7816874, and the Department of Energy Grant EX-76-G-03-1305, to Taylor, as well as a National Science Foudnation Grant to C.A. Hopson for field work in Oman. Additional support for Gregory came from a graduate fellowship from the Continental Oil Company, and a Penrose Grant from the Geological Society of America for field work in 1979. Field vehicles were provided by the California Institute of Technology and by Petroleum Development (Oman) Ltd. We gratefully acknowledge the Ministry of Agriculture, Fisheries, Petroleum, and Minerals and especially the Directorate General of the Petroleum and Minerals, Sultanate of Oman for their help and sponsorship of this study.

Sm-Nd, Rb-Sr, AND $^{18}O/^{16}O$ ISOTOPIC SYSTEMATICS IN AN OCEANIC CRUSTAL SECTION: EVIDENCE FROM THE SAMAIL OPHIOLITE

Malcolm T. McCulloch,[1] Robert T. Gregory
G.J. Wasserburg,[1] and Hugh P. Taylor, Jr.

Division of Geological and Planetary Sciences
California Institute of Technology
Pasadena, California 91125

Division Contribution No. 3303 (317)

[1]Lunatic Asylum of the Charles Arms Laboratory

ABSTRACT

The Sm-Nd, Rb-Sr, and $^{18}O/^{16}O$ isotopic systems have been used to distinguish between the effects of sea floor hydrothermal alteration and primary magmatic isotopic variations. The Sm-Nd isotopic system is essentially unaffected by seawater alteration while the Rb-Sr and $^{18}O/^{16}O$ systems are sensitive to hydrothermal interactions with seawater. Sm-Nd mineral isochrons from the cumulate gabbros of the Samail ophiolite have an initial $^{143}Nd/^{144}Nd$ ratio of ε_{Nd} of from 7.5 to 8.6, indicating that all the lithologies have distinctive oceanic affinities although there is also some evidence for small isotopic heterogeneities in the magma reservoirs. The Sm-Nd mineral isochrons give crystallization ages of 128±20 m.y. and 150±40 m.y. from Ibra and 100±20 m.y. from Wadi Fizh which is approximately 300 km N.W. of Ibra. These crystallization ages are interpreted as the time of formation of the oceanic crust. The $^{87}Sr/^{86}Sr$ initial ratios on the same rocks has an extremely large range of from 0.7030 to 0.7065 and the $\delta^{18}O$ values vary from 2.6 to 12.9. These large variations clearly demonstrate hydrothermal interaction of oceanic crust with seawater.

ACKNOWLEDGEMENTS

We are particularly indebted to R.G. Coleman and C.A. Hopson who conceived and organized the U.S. Geological Survey--National Science Foundation Oman project. Field work was also conducted with E.H. Bailey and J.S. Pallister. The samples from northern Oman were provided by Bob Coleman who also reviewed the manuscript. This work has benefitted from discussion with M.A. Lanphere, S.B. Jacobsen. R.E.

Criss, E. Stolper, and J. Chen. We express our gratitude to the Ministry of Agriculture, Fisheries, Petroleum, and Minerals, Sultanate of Oman, whose hospitality enabled us to conduct field work in Oman. This work has been supported by NSF Grants: PHY 76-83685, EAR 76-21310, EAR 78-16874, and indirectly by a grant to C.A. Hopson.

APPENDIX 2

Abstracts of Papers Submitted to the International Ophiolite Symposium, Nicosia, Cyprus. Geological Survey Department, Nicosia, p. 32-33, 1979.

* $^{18}O/^{16}O$ variations in gabbro, diabase and volcanic sections in Semail ophiolite, southeastern Oman Mountains and the nature of hydrothermal alteration in the oceanic crust

R. T. Gregory, and H. P. Taylor
Division of Geological and Planetary Sciences, California Institute of Technology, Pasadena, California 91125, U.S.A.

Whole rock and mineral $\delta^{18}O$ values have been determined for 75 samples from the Semail Ohiolite complex near Ibra, Sultanate of Oman. The $\delta^{18}O$ data show that pervasive sub-solidus exchange with circulating sea water has affected three quarters of the oceanic crustal section, including the cumulate gabbros to within 2 km of the peridotite-gabbro contact. Basal unaltered cumulate gabbros have $\delta^{18}O$-plagioclase = 6.4 $\pm$ 0.3 and $\delta^{18}O$-clinopyroxene = 5.6 $\pm$ 0.2. Above the unaltered zone, cumulate plagioclase values decrease to a minimum value of 3.6 Rocks with depleted ^{18}O plagioclase have reversed plagioclase-pyroxene fractionations. In most of these rocks no secondary hydrous alteration minerals are observed, indicating that temperatures at the base of the altered zone during hydrothermal exchange exceeded 500°C. Upward in the section secondary(?) brown amphibole becomes stable and temperatures of alteration decrease. Plagioclase $\delta^{18}O$ values increase upward in the section; high level (non-cumulate) gabbro plagioclases have $\delta^{18}O$ = 4.5 to 6.8. High level gabbro amphiboles have $\delta^{18}O$ = 2.1 to 5.6 with actinolites and uralites <5.0 Altered rocks in the transition zone between high level gabbro and sheeted dike complex have whole-rock and plagioclase ^{18}O values which coincidentally approximate normal igneous values (6.0 to 6.8). Diabase dike complex whole-rocks have $\delta^{18}O$ = 4.5 to 11.3 with lower values near the gabbro-sheeted diabase contact. Highest whole-rock $\delta^{18}O$ = 12.5 to 12.9 is found in the volcanic (pillow lava) section. Integration of whole-rock $\delta^{18}O$ values for the entire oceanic crustal igneous section shows (within analytic and volumetric error) that the ^{18}O-depleted rocks cancel out the contribution of ^{18}O-enriched rocks so that the net change in $\delta^{18}O$ due to the alteration is zero. This implies by mass balance that the net change in sea water ^{18}O-composition is also zero and that the isotopic composition of sea water is buffered by circulation at mid-ocean spreading centers. This is in agreement with the hypothesis of Muehlenbachs and Clayton. Assuming a production of 3km^3/yr of oceanic crust, 2 per mil excursions in the ^{18}O composition of sea water will be damped out within 50 m.y. Instantaneous (<5m.y.) excursion in sea water composition such as those produced during ice-ages will be preserved in the geologic record as shifts in the average ^{18}O value of altered oceanic crust.

Abstracts of Papers Submitted to the International Ophiolite Symposium, Nicosia, Cyprus. Geological Survey Department, Nicosia, p. 117-118, 1979.

Oxygen isotope and field studies applied to the origin of oceanic plagiogranites

R. T. Gregory and *H. P. Taylor, Jr,*
Divison of Geological and Planetary Sciences, California Institute of Technology, Pasadena, California 91125, U.S.A.

Two possible origins for oceanic plagiogranites have been proposed: 1) differentiation of basaltic magma and 2) partial melting of hydrothermally altered roof rocks atop mid-ocean ridge magma chambers. In order to test these hypotheses, whole-rock and mineral $\delta^{18}O$ values have been obtained for plagiogranites and host rocks from the Semail Ophiolite, Sultanate of Oman and the Canyon Mountain Ophiolite, southeastern Oregon, U.S.A. More than 50 analyses indicate: 1) All plagiogranites in the sandwich horizon between sheeted diabase and gabbro have disequilibrium Δ quartz-plagioclase; commonly $\Delta < 0$. All sandwich horizon plagiogranites have experienced sub-solidus isotopic exchange with circulating sea water; plagioclases ($\delta^{18}O$ = 4.5 to 14.0) yield no information on the primary ^{18}O composition of plagiogranite magmas. This alteration undoubtedly affects other geochemical parameters (e.g. intial strontium) and obscures the origin of plagiogranite. A rare plagiogranite dike which cross-cuts Oman peridotite beneath the zone of hydrothermal alteration contains K-feldpar and has $\delta^{18}O$ whole-rock = 7.9; $\delta^{18}O$ quartz = 8.3. This suggests that the absence of K-feldspar in plagiogranites may be related to sub-solidus exchange with sea water and solves a major problem (lack of K-feldspar) in the differentiation model. 2) Plagiogranite quartz (grain size >0.75 mm.) have $\delta^{18}O = 4.8$ to 8.5 (Oman) and quartz $\delta^{18}O = 6.6$ to 9.0 (Canyon Mountain). Quartz is virtually inert during sub-solidus isotopic exchange and best preserves its primary igneous $\delta^{18}O$ values. Plagiogranite quartz formed by differentiation of a gabbroic magma has estimated $\delta^{18}O = 7.8 \pm 0.3$. The large spread in $\delta^{18}O$ quartz is inconsistent with a simple fractional crystallization model. Granophyric textured plagiogranites with quartz <7.5 can be explained by equilibration (at the time of crystallization) with a direct mixture of sea water vapor ($-1 < \delta^{18}O < 4.0$) and exsolved magmatic vapor. However, many plagiogranites with quartz <7.5 do not have granophyric textures and quartz values >8.1 are inconsistent with a sea water contaminated vapor. This suggests that these quartz ^{18}O variations reflect silicate melt ^{18}O compositions. Large (> 1km²) plagiogranite bodies (Dasir, Oman and Canyon Mountain) have extensive border facies which are rich in xenoliths (> 75%) of hydrothermally altered diabases ($4.5 < \delta^{18}O < 11.3$), altered fine-grained gabbro, and hornfels ($3.7 < \delta^{18}O < 6.3$). Outcrop ratios of the border facies material to plagiogranite are 2.5 : 1 (Dasir). The large plagiogranite bodies sit in coarse cumulate gabbros (Dasir) and coarse hornblende gabbros. The source of the xenolith material is up-section and suggests that these large plagiogranite bodies formed from large blocks of hydrothermally altered roof rock that have fallen into the magma chamber and have been modified by partial melting. The association of plagiogranite and abundant coarse hornblende gabbro suggests that a water-rich environment is necessary for plagioggranite formation and the source of water is the foundered blocks. Once hornblende becomes stable, the remaining melt will become over-saturated in silica and then moves to a plagiogranite end member. Mixing of assimilated roof material ^{18}O and melt ^{18}O can account for all of the $\delta^{18}O$-quartz variations. Where hydrothermally altered blocks of roof rock have not interacted with the magma chamber, the magma remains anhydrous and little plagiogranite (possibly formed by fractional crystallization) is observed in the field. The field associations and the quartz ^{18}O data indicate that assimilation and partial melting of hydrothermally altered roof rocks are the dominant processes in the origin of plagiogranites.

Submitted for Annual Meeting of the Geological Society of America, Nov. 5-8, 1979.

A PETROLOGIC AND STABLE ISOTOPE STUDY OF THE OMAN OPHIOLITE — IMPLICATIONS FOR ORIGIN AND METAMORPHISM OF THE OCEANIC CRUST

GREGORY, Robert T. and TAYLOR, Hugh P., Jr., Division of Geological and Planetary Sciences, California Institute of Technology, Pasadena, California 91125; COLEMAN, Robert G., U. S. Geological Survey, Menlo Park, California 94025

300 $\delta^{18}O$ analyses from the Samail Ophiolite indicate that pervasive, subsolidus hydrothermal exchange with sea water (water/rock < 1) has affected the upper 75% of this oceanic crustal section. Along fractures, hydrothermal fluids have even penetrated down into the tectonized upper mantle. Primary magmatic plagioclase ($\delta^{18}O \approx 6.0$) and pyroxene ($\delta^{18}O \approx 5.5$) occur locally in the lower gabbro cumulates, but most assemblages exhibit isotopic disequilibrium. The minimum value of $\delta^{18}O$ plag (3.6) occurs about 2 km beneath the gabbro-diabase contact. Overall, 1.8 $\delta^{18}O$ cpx -3.7 $\approx$ $\delta^{18}O$ plag, suggesting that plagioclase exchanged with sea water at a rate about twice that of pyroxene. Except for minor alteration of olivine to talc + magnetite, the lower cumulates contain no hydrous minerals, implying $T > 500^{\circ}C$. Secondary amphibole ($2.0 < \delta^{18}O < 5.5$) is common in high-level, non-cumulate gabbro, suggesting $350^{\circ} < T < 500^{\circ}C$. Plagioclase $\delta^{18}O$ values increase up section from their minimum values, reaching 11.8 in the sheeted dike complex. $\delta^{18}O$ of the pillow lavas is 7.5 to 13.0, increasing upward. Plagiogranites (all of which are altered) occur at the sheeted dike-gabbro contact, have disequilibrium $\Delta^{18}O$ qtz-plag (commonly < 0), $\delta^{18}O$ qtz = 4.8 to 8.5, and $\delta^{18}O$ plag = 4.5 to 14.0. The plagiogranites are late-stage differentiates formed as a result of assimilation and partial melting of hydrothermally altered roof blocks stoped into the magma chamber. The ^{18}O-depleted rocks of the middle part of the section cancel out the contribution of the ^{18}O-enriched rocks of the upper section, giving a mean $\delta^{18}O = 5.7$. Thus, the overall net change in $\delta^{18}O$ of the bulk oceanic crust is zero, implying by mass balance that the net change in sea water is also zero and that sea water is buffered at its $\delta^{18}O = 0$ by hydrothermal circulation at mid-ocean ridges.

Submitted for Annual Meeting of the American Geophysical Union, December 3-7, 1979

AN OXYGEN ISOTOPE STUDY OF THE CRETACEOUS SAMAIL OPHIOLITE, OMAN: EVIDENCE FOR DEEP SEAWATER-HYDROTHERMAL CIRCULATION AND IMPLICATIONS FOR SPREADING CENTER GEOMETRY AND $\delta^{18}O$ OF SEAWATER

R.T. Gregory
H.P. Taylor, Jr. (Div. of Geol. & Planet. Sci., Calif. Inst. of Tech., Pasadena, CA 91125)

$^{18}O/^{16}O$ analyses of 100 samples from 4 traverses through the ophiolite indicate that the upper 3/4 of this oceanic crustal section was affected by pervasive, sub-solidus, seawater-hydrothermal exchange. Pillow lavas ($\delta^{18}O$ = 7.4 to 12.7) and sheeted dikes (4.9 to 11.3) typically exhibit ^{18}O enrichments. However, an abrupt ^{18}O shift occurs at the roof of the "fossil" MOR magma chamber, as the gabbros have $\delta^{18}O$ = 3.7 to 5.9. Minimum values for pyroxene and plagioclase (4.1, 3.6) occur ~2.5 km below the diabase-gabbro contact (primary MORB values are 5.5, 6.0). This indicates the existence of two decoupled hydrothermal systems at this Tethyan spreading center: one relatively shallow system involved several convection cells (water/rock >> 1) near the ridge axis that penetrated 2-3 km down to the wide, flat roof of the magma chamber; the other system involved deep circulation underneath the "wings" of differentiated magma at the top of the chamber (water/rock < 0.3). Strongly ^{18}O-shifted seawater discharged upward from the lower system at the distal edge of the magma chamber, superimposing an ^{18}O enrichment ("isotopic aging") upon the diabases and basalts previously affected by the upper system near the ridge axis. The gabbro plagioclase is petrographically unaltered, and pyroxenes (and olivine) show only minor alteration to amphibole (and talc), indicating lower-system ^{18}O exchange occurred at T > 400°C. The net change in the mean $\delta^{18}O$ of the oceanic crust ($\approx$5.7) due to all of these hydrothermal effects is zero; thus, Cretaceous seawater was buffered at $\delta^{18}O \approx -0.4$. Except during continental glaciation, seawater will remain fixed at this $\delta^{18}O$ value as long as world-wide spreading rates exceed 1 km^2/year.

THE
GEOLOGICAL SOCIETY
OF AMERICA
Telephone (303) 447-8850
Publications Department

PLEASE SUBMIT THIS ORIGINAL AND FOUR COPIES

1980
ABSTRACT FORM

See instruction sheet for deadlines and details

Exact format shown on instruction sheet must be followed. Blue margins below are absolute limits.

THE ORIGIN OF PLAGIOGRANITE BY PARTIAL MELTING OF HYDROTHERMALLY ALTERED STOPED BLOCKS AT THE ROOF OF A CRETACEOUS MIDOCEAN RIDGE MAGMA CHAMBER, THE SAMAIL OPHIOLITE, OMAN

GREGORY, Robert T., and TAYLOR, Hugh P., Jr., Div. of Geological & Planetary Sci. California Institute of Technology, Pasadena, CA 91125. COLEMAN, Robert G., U.S. Geological Survey, 345 Middlefield Rd., Menlo Park, CA 94025

Field, petrologic, and $\delta^{18}O$ studies indicate that plagiogranites form by two mechanisms in the oceanic crust: 1) Extreme fractional crystallization of hydrous tholeiites in isolated thin sheets of melt at the distal edges of the magma chamber; 2) Partial melting of the hydrothermally altered chamber roof in a dynamic environment dominated by piecemeal stopping of roof-rock blocks occurring during all stages of the chamber history. At Dasir, results of this later process are seen over 10 km^2 in a composite plagiogranite sheet (<500 m thick) composed of agmatite(>75%) and albite granite which is floored by cpx+plag±ol±opx±hbl layered cumulus gabbro and overlain by coarse-grained, non-cumulus, hornblende gabbro. Hornfelsic inclusions $3.7 < \delta^{18}O < 7.3$ (hbl>plag>mgt±qtz±biot) in agmatites and gabbro are the residuum left after partial melting of hydrothermally altered diabase $2.5 < \delta^{18}O < 11.3$ to produce plagiogranite (albite>qtz>>hbl>mgt>biot). $\delta^{18}O_{qtz} = 7.1 \pm 0.3$ from Dasir albite granites suggests diabases were ^{18}O-depleted prior to the melting. Heat from the crystallizing gabbro drives partial melting of the blocks; initial Ab-granite minimum melts move into fractures within the inclusions. The surrounding crystallized gabbroic host rocks are intruded by the plagiogranites which have a lower solidus temperature. Upwardly mobile plagiogranites are quenched at the diabase-gabbro contact cooled by vigorous hydrothermal circulation in the more permeable dike complex. Repeated collapse of the chamber roof destroys the original intrusive relationships; only a partial record of each stoping event is preserved in the heterogeneous high-level gabbro. Spreading axis rhyolites, ophiolitic diabase dikes intruding plagiogranites; overall plagiogranite quartz $\delta^{18}O = 4.8\text{-}8.5$ are all more consistent with the partial melting mechanism than with fractional crystallization.

APPENDIX 3

Table A-3-1 $\delta^{18}O$ data from the Canyon Mountain ophiolite complex

Sample and rock type†	Location*	whole-rock	qtz	feld	pyrox
SHEETED DIKES					
093a (keratophyre)	Sec 34 NE1/4SW1/4	11.0	8.5	12.7	
092a	Sec 34 NE1/4NE1/4	8.8			
085	R31 Sec 31 SW1/4NE1/4	8.2			
PLAGIOGRANITE					
082	Sec 27 SE1/4SE1/4	10.7	9.0	12.4	
063a	Sec 34 NE1/4NE1/4	9.3	8.4	11.6	
087a	R31 Sec 34 SW1/4NE1/4	10.0	8.6	11.8	
078b					
GABBRO					
080 (vein)	Sec 34 NE1/4NE1/4		16.9		
061 (vein)	Sec 27 NW1/4SW1/4		15.5		
062b	Sec 27 NW1/4SW1/4	10.2			5.4 (amphibole)
071b	Sec 32 NE1/4NW1/4	6.5			
072a	Sec 32 NE1/4NW1/4	7.1			
072b	"			7.9	
074b	Sec 26 NW1/4SE1/4			7.8	
073b	Sec 26 NE1/4SE1/4			4.8	4.5
076b	Sec 26 SW1/4NW1/4			5.9	5.3
075a	Sec 26 NW1/4NW1/4			6.1	
049	Sec 30 SW1/4SW1/4			6.7	
048b	"			6.4	4.7
038	Sec 30 SE1/4SE1/4				4.8

† Samples are listed in approximate structural order with single-spacing separating those samples which come from a similar structural height and double spacing separating samples from different structural horizons.

* All townships are T14S and all range coordinates are R32E unless shown otherwise. All map coordinates were originally plotted on the U.S. Geological Survey John Day 15° Quadrangle.

Table A-3-2 $\delta^{18}O$ data from the Bay of Islands ophiolite complex

Sample[§]	Rock type	Depth (KM)	$\delta^{18}O_{rock}$
BMD-24	pillow basalt	0.58	10.9
BMD-10	diabase	1.34	4.5
BMD-12	diabase	2.48	5.4
BMD-8	hornblende gabbro	3.45	7.3
BMD-2A	pyroxene gabbro	4.95	6.4
BOI-62B	pyroxene gabbro	6.08	5.9
BMD-7	pyroxene gabbro	6.10	6.8[¶]
BMD-17	orthopyroxenite	6.60	6.5

§ Samples were collected by Stein B. Jacobsen. The Nd-Sr systematics of the ~500 million year old Blow-Me-Down Masssif are discussed in Jacobsen and Wasserburg [1979].

¶ Analysis of cumulus plagioclase. All other analyses are whole-rock determinations.